Probing nano-specific interactions between bacteria and antimicrobial nanoparticles using microbial community changes and gene expression

Submitted in partial fulfillment of the requirements for

the degree of

Doctor of Philosophy

in

Civil and Environmental Engineering

Joe Dallas Moore

B.A., Biology, Wabash College
M.S., Civil Engineering, Carnegie Mellon University

Carnegie Mellon University
Pittsburgh, PA

December, 2017

© Joe D. Moore, 2017
All Rights Reserved

ACKNOWLEDGMENTS

This work has been funded by the following sources: Carnegie Mellon University (CMU) College of Engineering Dean's fellowship; National Science Foundation (NSF) Graduate Research Fellowship Program; the US NSF (DGE-1252522) and the Environmental Protection Agency (EPA) under NSF Cooperative Agreement EF 0830093/1266252, Center for the Environmental Implications of NanoTechnology (CEINT); and from the NSF Nanotechnology Environmental Effects and Policy Integrated Graduate Education and Research Traineeship (DGE-0966227). Portions of this research were carried out at the Stanford Synchrotron Radiation Lightsource (SSRL) beamlines 11-2 and 4-1. SSRL is a national user facility of the Department of Energy, Office of Basic Energy Sciences.

Beyond my funders, innumerable people and institutions enabled the work reported in this dissertation – too many to acknowledge here. I am particularly indebted to my committee members, department and lab colleagues, and, most of all, family.

Ron Ripper, who manages the environmental lab for the department, has been a huge asset. He has always been willing to help – with ordering equipment, with fixing faulty instruments, with grumbling about politics – and always with a smile and hearty laugh. This work would not have been possible without his effective management of the labs.

All of my current and former labmates have also helped in numerous ways through the years. Djuna Gulliver and Arvind Murali Mohan helped me get started doing research. Later, John Stegemeier, Brian Vencalek, and Dan Ross assisted in a variety of ways. Eric McGivney has been a great fellow biology labmate and friend. He has provided eager eyes and ears when I have wanted to discuss lab issues or new data or show him figures or a research poster…or complain. Astrid Avellan has also been an amazing sounding board since she arrived as a postdoctoral scholar one year ago. She has been an eager collaborator, and her contributions have made my research better. Of all of my labmates, Clint Noack has been the most helpful. Even as he has finished his Ph.D. research and embarked on entrepreneurial

pursuits, he has generously assisted with statistics and data visualizations. He has taught me a ton, mostly without even being condescending. Thanks for always being willing to let me bother you, Clint.

My committee consists of Aaron Mitchell, Ph.D., of Carnegie Mellon University (CMU); Ken Urish, M.D., Ph.D., of the University of Pittsburgh and the University of Pittsburgh Medical Center; Kyle Bibby, Ph.D., of the University of Notre Dame; Greg Lowry, Ph.D., of CMU; and Kelvin Gregory, Ph.D., also of CMU. I have been co-advised by Greg and Kelvin. Aaron served on a labmate's proposal committee and provided excellent and thoughtful feedback. When I sought to enlist a bonafide microbiologist with expertise in pathogen research, he was an obvious choice. Though I asked him to be on my committee barely a month prior to my defense, he agreed without hesitation, despite having more than a full plate, including being the Department of Biology department chair. Thank you for being so generous with your time, Aaron. I look forward to working through this with you.

Ken was willing to engage with me when I emailed him out of the blue about his work. He did not hesitate to provide *Staphylococcus aureus* strains isolated during his orthopedic surgery practice. And despite being overbooked with clinical work and research, he has engaged in our research endeavors, sending unprompted emails to check in, passing along advice and protocols, and even agreed to participate in this committee. Thank you, Ken.

Kyle has been an excellent advisor and mentor. From the start, he was generous with his time and advice. For the first project of my Ph.D., he let me work with his Ph.D. student and postdoc to process samples and sequence them. He brainstormed solutions to a reviewer's critique of our first paper. He has met with me on multiple occasions to discuss professional life post-Ph.D. and even introduced me to a potential postdoc advisor. Kyle, I hope I have not taken too much advantage of your generous spirit. Thanks for everything and best of luck in "God's country" (Indiana, of course).

Greg has been an indispensable co-advisor. He is a world-renowned researcher. Having worked with him the past several years, it is clear why. Greg, whose research is typically abiotic or recently with

plants, is curious to learn the details of my microbiology methods and to identify the big picture takeaways from our work. Microbiology has increasingly become the primary focus of my research interests, but Greg has stuck with me despite this and has helped identify important questions about engineered nanomaterials (ENM). He has endured my questions with patience and thoughtfulness, whether they pertain to future professional aspirations or a manuscript. He has been an excellent advisor. Thank you, Greg.

I owe Kelvin, my other co-advisor, for this whole enterprise. He gave me my start in the lab during the summer between my second and third semesters in the M.S. program. I was taking a class at the University of Pittsburgh, and he allowed me the flexibility to do research on the side and gain the confidence that allowed me to start my Ph.D. research in January 2013. Throughout my Ph.D., Kelvin has afforded me great freedom to explore questions of particular personal interest and to self-direct my experiments. As he allowed me to become a (mostly) self-reliant researcher, he remained available to help me overcome inevitable lab struggles. He truly has an open door policy. I hope I have not exploited this policy too much! Thank you for giving me the opportunity that led me down the Ph.D. path, Kelvin, and for sticking with me through the end.

My parents provided me with an amazingly supportive upbringing that fostered independence, questioning (including of them – sorry!), and setting high expectations for myself. They demonstrated the importance of work ethic in their own professional lives and excellently balanced work-life balance, accommodating epic family road trips with some historical site destination in a full-sized van. I would not have been interested in a Ph.D. without that. Thank you, mom and dad. My siblings, Jaci, Jenni, and Jordan, have also been great supports over the years. I am lucky to have them.

My mother- and father-in-law have been incredibly supportive throughout this journey, too. They have taken on childcare duties, provided countless meals, and housed us on numerous occasions. Thank you, Julie and Harold. I could not ask for better in-laws – but I *would* like to ask for flank steak to celebrate this occasion!

Above all, I am indebted to Juleen, my wife, for supporting me through the Ph.D. Her love and support have been monumental. When I expressed interest in going back to school for the M.S. in CEE, she was completely on board. She celebrated my every achievement – M.S. graduation, completing the qualifier exams, the proposal, and now this – selflessly, as if these were truly unique and she had not done the same years prior, without fanfare. She has been an excellent partner beyond work, including an excellent mother to our sons, Quinn and Julian. She has encouraged me to attend conferences and week-long workshops and get exercise despite the burden that places on her. She is the best, and I am lucky to call her my spouse, my partner, my love.

Quinn and Julian have been the lights of our lives, and I am not sure that they know it. They are bundles of joy (most of the time), and great excuses to think of something beyond research and engineering. Quinny and Julian, you guys are the best.

ABSTRACT

Antimicrobial engineered nanomaterials (ENM) are increasingly incorporated into products despite limited understanding of the interactions between ENMs and bacteria that lead to toxic impacts. The hazard posed by increasing environmental release of antimicrobial ENMs is also poorly characterized. The overall objective of this thesis is to inform questions about the types of interactions that lead to an ENM inducing bacterial toxicity. Many antimicrobial ENMs are soluble, and the ion plays an important role in their toxicity. Some believe that, beyond release of ions, ENM toxicity is expected to derive from a nanoparticle (NP)-specific effect. This research compares bacterial responses to ENMs, their metal salts, and/or their transformed species within different experimental settings to improve our understanding of the interactions that enable ENM bacterial toxicity.

The first objective is to characterize the potential hazard posed by pristine and transformed antimicrobial ENMs on microbial communities within a complex environmental system. One pair of ENMs (Ag^0 and Ag_2S) led to differential short-term impacts on surficial sediment microbial communities, while the other did not (CuO and CuS), showing that ENM transformation does not universally lead to distinct impacts. The metal ion (Cu^{2+}) had a more profound microbial community impact than did any of the four ENMs. By 300 days the microbial community structure and composition re-converged, suggesting minimal long-term impacts of high pulse inputs of antimicrobial ENMs on microbial communities within complex environments.

The second objective is to identify NP-specific effects of a common antimicrobial ENM on a model bacterium. Analysis of transcriptional responses identified NP-specific induction of a

membrane stress responsive gene, providing evidence of a NP-specific effect. Otherwise, our results suggest that CuO NP toxicity triggers the same stress responses as does Cu^{2+}, but at more moderate levels. Two ion treatments with the same total Cu input – one with pulse addition and one with gradual addition that was meant to better represent the slow dissolution of the CuO NP – led to temporally distinct responses. This calls for the use of more representative ion controls for comparison against soluble NP impacts in future nanotoxicity studies.

The third objective is to investigate the potential use of CuO ENMs to reduce virulence and growth of an emerging bacterial pathogen. CuO NP exposure led to reduction in relative expression of three *Staphylococcus aureus* virulence factor genes, especially in methicillin-resistant *S. aureus* (MRSA) clinical isolates. Growth was inhibited at high CuO NP concentrations for all four isolates, too. Comparison across all genes assayed showed isolate-specific transcriptional responses, but with NP- and ion-induced responses showing clear differences for each isolate, too. Altogether, this research contributes novel knowledge that will guide efforts to characterize potential hazard from release of ENMs into the environment and to apply ENMs for effective antibacterial treatment.

TABLE OF CONTENTS

LIST OF TABLES

LIST OF FIGURES AND ILLUSTRATIONS

CHAPTER ONE

INTRODUCTION

Engineered nanomaterials (ENM) are being used as antimicrobial agents within commercial products, e.g., within agrochemicals and medical devices.[1–6] As production and use of antimicrobial ENMs increase, so will their prevalence in the environment, raising concern around potential environmental impacts of ENM release. Both the hope surrounding use of ENMs as antimicrobial agents[4,6] and the concern around ENM environmental impact call for improving our understanding of interactions between ENMs and bacteria, which remain poorly elucidated. It remains unclear if an ENM must come into contact with a bacterium to exert its toxicity and what the actual source of that toxicity is – the ENM itself or ion released from it. To fully grasp the potential for ENMs to inhibit microbial growth and the possible environmental impacts of ENM release requires an improved understanding of ENMs and their interactions with microbial life.

ENMs are toxic in laboratory settings over short timespans,[7–9] but whether their toxicity will be evident in environments with greater chemical and biological diversity and endure for longer time periods is unclear. Within complex environmental systems, ENMs are not static; the pristine (as-synthesized) form dissolves, aggregates, gains and loses coatings, and/or transforms, all processes linked to toxicity.[10–14] The microbial communities that ENMs encounter in wastewater treatment plants (WWTP), agricultural soil, and aquatic sediments are complex, too.[15–19] Understanding the long-term effects of antimicrobial ENMs on complex microbial communities in complex environments will improve our understanding of the potential environmental hazard posed by these novel contaminants.

Antimicrobial ENMs are already being applied widely, to textiles, cosmetics, food packaging, toothpaste, etc.,[20] despite limited understanding of the interactions that underpin their bacterial toxicity. It is still unclear, for example, if there is a unique nanoparticle (NP) effect in terms of biological impact or if the toxicity arises from the released ion alone.[21–24] With antibiotics failing and few drugs taking their place,[25–27] there is talk of antimicrobial ENMs being used to help control bacterial growth.[6,28] Understanding the mode of interaction between ENMs and bacteria that best enables toxic impact could help enable more effective antimicrobial ENM applications. Broadly, improving our understanding of the interaction between ENMs and bacteria could inform questions about potential environmental impacts and enable development of more effective antimicrobial ENMs.

1.1 BACKGROUND

1.1.A Interactions between ENMs and bacteria. ENMs are known to associate with biological membranes.[29–31] Many ENMs, and especially soluble metal-based ENMs, are also known to be antimicrobial.[32] What is not clear is exactly what type of interaction between an ENM and a bacterium is necessary for the ENM to have this effect. Does an ENM have to be adsorbed onto a bacterium to exert its toxicity? Or is the toxicity due to ENM release of toxic ion into the bulk liquid phase?

Questions about the interactions of ENMs and bacteria and how ENMs are antimicrobial require an understanding of the dynamic nature of ENMs in biological systems. In abiotic systems, ENMs, and soluble ENMs in particular, are dynamic – dissolving, adding or losing coatings, aggregating, transforming, etc.[14,33,34] Biological systems present ENMs more opportunities to demonstrate their dynamicism,[35] as ENMs have a strong tendency to associate

with bacterial membranes.[30,36] Some have postulated that bacteria can internalize such ENMs, as is widely accepted for eukaryotic cells,[37–39] but a large majority of the ENMs studied have been large enough (>10 nm) that bacterial internalization of ENMs is highly unlikely. The largest molecules that intact *Escherichia coli* and *Bacillus subtilis* can passively uptake are 2 nm,[40] and *E. coli*'s largest known porin for active transport is 6 nm.[41] If not via internalization, how do ENMs exert their bacterial toxicity?

This question has largely been boiled down to an oft-debated question in the literature: Is there a unique "nano effect" (or "NP-specific effect") of ENM exposure or are ENMs' microbial impacts entirely ion-mediated?[21] As the literature around ENM-bacteria interactions has progressed, two camps have arisen, each offering opposing answers to this question. A hybrid understanding has developed, as well.

One camp attributes ENM toxicity to a unique "nano effect" whereby the ENM itself is responsible for the observed toxic effects. Some studies report enhanced effects of equivalent doses of ENMs compared to their dissolved ions,[42–44] supporting the view that an ENM could be exerting some toxicity independent of the ions it releases. How might an ENM be able to exert toxicity beyond the effect of an equivalent ionic dose? One possibility arises from their association with bacterial membranes.[30,31] Many studies have observed via TEM or other methods apparent ENM-induced membrane damage.[45–49] The coupling of dissolution and resultant ion-mediated toxicity and nano-specific membrane damage could explain greater impacts of ENMs versus their dissolved ion.

The other camp considers ENM toxicity to solely be a function of ion release. Work showing similar effects of ENMs and their leachate and/or minimal to no impact of non-dissolving ENMs supports the latter.[22,23] Studies have also shown that sulfidizing ENMs, which can produce less

soluble chemical species, e.g., Ag^0 to Ag_2S, can mitigate negative effects on various biological systems.[24,50–53]

Another addition to this debate is the middle-ground argument that ENMs in suspension can achieve a nano-specific distribution. ENMs preferentially adsorb onto cellular membranes.[30,54] Their toxicity is primarily exerted through ion release, but with preferential collocation with bacteria, the argument goes, ENM dissolution leads to a locally elevated concentration of ion (local to a bacterium) compared to the average concentration in solution.[21,55]

Time is likely a critical variable when it comes to soluble ENMs' biological impacts. In many systems, soluble ENMs' undergo slow dissolution,[56,57] but time can also allow for ENM transformation.[14,58] Properly comparing biological impacts of ionic and soluble nanoparticulate species, thus, requires consideration of time and of ionic input. Much work shows that toxic ENM effects are largely ion-mediated.[23,50] Yet the standard approach for implementing ion controls is to dose a single pulse input of ion at the beginning of an experiment, an approach that contrasts with the slow release of ion expected from ENMs in many systems. Tracking biological impacts of ENMs and ions over time and attempting to more accurately represent ionic exposures from slowly-dissolving ENMs could serve to improve our understanding of the interactions that underpin ENMs' bacterial impacts and their potential for long-term impacts.

1.1.B ENMs' bacterial toxicity mechanisms. Compared to the debate over nano- versus ion-mediated toxicity, the debates surrounding ENM bacterial toxicity have been less contentious. By and large reactive oxygen species (ROS) generation has been construed as the primary mediator of ENM toxicity.[45,59–63] The tendency of ENMs to interact with bacterial outer membranes[64] and the role of those membranes in respiration, i.e., electron transfer, make ROS generation a plausible mechanism of ENM toxicity, at least for aerobic bacteria, which often

accumulate superoxide and peroxide that are the precursors for Fenton chemistry and generation of the most reactive of the ROS, the hydroxyl radical.[65] Many of the metals used for ENMs are redox labile, e.g., Ag, Cu, Zn and Fe, and work with several ENMs has supported a prominent role for ROS – both intra- and extracellular – as a mediator of ENM toxicity.[22,44,45,66,67] Importantly, ROS generation has been implicated as a means by which many of these metal ions are believed to be toxic.[68]

As introduced above, membrane damage is also commonly described as a mode of ENM toxicity.[64,69–71] Potential overlap between these ENM bacterial toxicity mechanisms exists as ROS generation at the bacterial surface could lead to lipid peroxidation and membrane damage.[72] Studies have identified induction of lipid peroxidation with ENM exposure.[6,45]

Neither the interactions of ENMs with bacteria nor the exact mechanisms of ENM bacteria are well understood. Yet ENMs are increasingly being incorporated into commercial products as antimicrobial agents. Only a few efforts have been made to distinguish bacterial toxicity mechanisms of nanoparticulate versus ionic species, and almost all of these studies have been with *E. coli*.[62,68] As the leading cause of urinary tract infections (UTI),[73] *E. coli* is more than just a model bacterium. The goal of the field should be to work with clinically relevant bacteria, *E. coli* and otherwise, against which antimicrobial ENM treatments are hoped to be effective. Improving our understanding of questions around ENM-bacterial interactions and modes of antibacterial ENM action with *E. coli* and other pathogenic bacteria could enable more effective, and longer-lasting ENM application.

One underutilized tool for elucidating ENM-bacteria interactions and toxicity mechanisms is analysis of bacterial gene expression. Well-established methods exist for such analysis, e.g., reverse-transcriptase quantitative polymerase chain reaction (RT-qPCR) and RNA-seq, and these

methods have been used to elucidate mechanisms of bacterial toxicity of a wide range of compounds.[74,75] Annotation of genomes of model organisms and many pathogens has made identification of many of the genes responsive to chemical exposure, e.g., Cu and other metals, and stress responses relatively straightforward.

1.1.C ENMs in the environment. With increasing usage of ENMs, there is greater potential for adverse environmental impacts coming from their release. Environmental fate models for ENMs predict accumulation of ENMs in soil and subaquatic sediments.[13,76] This is a result of ENMs in wastewater effluent and of runoff from agricultural lands that apply biosolids, where the majority of ENMs entering a WWTP accumulate[77] or nano-enabled agrochemicals. With runoff from farmlands, ENMs are expected to enter surface waters, and freshwater and estuarine sediments.[76,78,79] Pristine metal and metal oxide ENMs are known to transform to different species under environmental conditions,[10–12,14] e.g., Ag^0 transforms to Ag_2S [80] and metallic Cu transforms to CuO then CuS.[12,81] Transformation can lessen ENMs' biological impacts.[50,51] Very recent work has begun to consider the effect of environmental transformations when assessing environmental impacts of ENMs, typically observing lesser impacts,[24,52,53] but questions persist around the short- and long-term effects of ENM release into complex environmental matrices. Determining whether antimicrobial ENMs are likely to have a long-term impact in such systems and comparing their effects to that of a dissolved ion and the effects of pristine and transformed ENMs could inform efforts to assess risk posed by release of ENMs into the environment.

One of the primary concerns surrounding ENMs' environmental implications is their potential effect on microbial communities. Microbes provide important ecological services, such as primary production and nutrient cycling, and ENMs have been shown to impact phototrophic bacteria and rhizosphere microbial communities.[82,83] With many ENMs expected to transport

into WWTPs, onto agricultural land in biosolids, and into subaquatic sediments due to run-off,[76,78,79] ENMs will encounter microbial communities actively performing important human health and ecological services. Whether ENM exposure in such complex systems is likely to adversely affect those communities, and the corresponding ecosystem services they provide, is an open question.

1.2 Objectives and Overview of this Thesis

The overall goals of this thesis are to improve our understanding of antimicrobial ENMs':

(1) impacts on microbial communities within complex environmental systems, and

(2) bacterial toxicity mechanisms both in the sense of the source of the ENM's toxicity (ion or NP-specific effect) and the stress responses ENM exposure elicits.

These goals will be accomplished by comparing bacterial responses to ENMs, their metal salts, and/or their transformed species. Three projects comprise this thesis: one investigating microbial community impacts of multiple ENMs and a metal ion, and two characterizing transcriptional responses to a metal ENM and equivalent ionic doses.

Completion of this research agenda will:

(1) improve our understanding of the hazard posed by antimicrobial ENMs to extant microbial communities in chemically and microbiologically complex wetland systems

(2) inform the mechanism of bacterial toxicity of CuO ENMs, including identification of NP-specific impacts

(3) and gauge the potential of an antimicrobial ENM to reduce virulence and growth of pathogenic bacteria

1.2.A Impacts of pristine and transformed Ag and Cu engineered nanomaterials on surficial sediment microbial communities appear short-lived. The main objective of this work was to characterize the potential hazard posed by pristine and transformed antimicrobial ENMs on microbial communities within a complex environmental system. Pristine Ag^0 and CuO NPs and transformed Ag_2S and CuS NPs were dosed into wetland mesocosms at equal as metal concentrations. Measurements of surficial sediment microbial community size, structure, and composition and metal speciation were taken over 300 days. This research demonstrated that within 300 days of exposure to high doses of ENMs microbial communities are similar in terms of community size and composition to undosed controls. It also revealed that ENM transformation does not necessarily lead to distinct, i.e., mitigated, impacts. This work resulted in a peer-reviewed publication in *Environmental Science & Technology*.[84]

1.2.B Time-dependent bacterial transcriptional response to CuO nanoparticles differs from that of Cu^{2+} and provides insights into CuO nanoparticle toxicity mechanisms. The main objective of this work was to identify NP-specific effects of a common antimicrobial ENM on a model bacterium. Sub-objectives included informing the mechanism of CuO ENM bacterial toxicity and comparison of bacterial responses to pulse and gradual addition of Cu^{2+}. This research identified a membrane stress response induced only by CuO ENM exposure. It further found that CuO ENMs lead to similar, but more moderate transcriptional responses than equivalent ion doses, and that those responses pertain to Cu homeostasis and protein damage, and largely not ROS. This work also demonstrated that gradual ion addition leads to a temporally distinct transcriptional response than does pulse ion. This work is currently in revision for publication in *Environmental Science: Nano*.

1.2.C In laboratory and clinical MRSA, CuO nanoparticles reduce virulence factor gene expression and induce transcriptional response distinct from ion. The main objective of this work was to investigate the potential use of CuO ENMs to reduce virulence and growth of a leading bacterial pathogen. Sub-objectives included comparing different *S. aureus* isolates' transcriptional responses, especially their virulence factor gene expression, with the goal of identifying strain- versus treatment-specific responses and informing the mechanism of CuO ENM toxicity on *S. aureus*. Expression of genes involved in Cu homeostasis, metal binding, protein damage, heat shock, and ROS response were investigated, as were virulence factor genes, in a methicillin-susceptible *S. aureus* (MSSA) laboratory strain (SH1000), a methicillin-resistant *S. aureus* (MRSA) laboratory strain (BAA-1556), and two MRSA clinical isolates. This research demonstrated the capacity of CuO NP exposure to lead to reductions in virulence factor gene expression. It further showed that CuO NP interaction and response are largely strain-specific, though within-strain treatment-specific responses are evident. This work will be submitted for peer-reviewed publication shortly after submission of this thesis.

1.3 References for Chapter One

(1) Faunce, T.; Watal, A. Nanosilver and global public health: international regulatory issues. *Nanomedicine (Lond).* **2010**, *5* (4), 617–632.

(2) Anita, S.; Ramachandran, T.; Rajendran, R.; Koushik, C.; Mahalakshmi, M. A study of the antimicrobial property of encapsulated copper oxide nanoparticles on cotton fabric. *Text. Res. J.* **2011**, *81* (10), 1081–1088.

(3) Blaser, S. A.; Scheringer, M.; Macleod, M.; Hungerbühler, K. Estimation of cumulative aquatic exposure and risk due to silver: contribution of nano-functionalized plastics and textiles. *Sci. Total Environ.* **2008**, *390* (2–3), 396–409.

(4) Parani, M.; Lokhande, G.; Singh, A.; Gaharwar, A. K. Engineered Nanomaterials for Infection Control and Healing Acute and Chronic Wounds. *ACS Appl. Mater. Interfaces* **2016**, *8* (16), 10049–10069.

(5) Rodrigues, S. M.; Demokritou, P.; Dokoozlian, N.; Hendren, C. O.; Karn, B.; Mauter, M. S.; Sadik, O. A.; Safarpour, M.; Unrine, J. M.; Viers, J.; et al. Nanotechnology for sustainable food production: promising opportunities and scientific challenges. *Environ. Sci. Nano* **2017**, *4* (4), 767–781.

(6) Wang, L.; Hu, C.; Shao, L. The antimicrobial activity of nanoparticles: present situation and prospects for the future. *Int. J. Nanomedicine* **2017**, *12*, 1227–1249.
(7) Reyes, V. C.; Opot, S. O.; Mahendra, S. Planktonic and biofilm-grown nitrogen-cycling bacteria exhibit different susceptibilities to copper nanoparticles. *Environ. Toxicol. Chem.* **2015**, *34* (4), 887–897.
(8) Beddow, J.; Stolpe, B.; Cole, P.; Lead, J. R.; Sapp, M.; Lyons, B. P.; Colbeck, I.; Whitby, C. Effects of engineered silver nanoparticles on the growth and activity of ecologically important microbes. *Environ. Microbiol. Rep.* **2014**, *6* (5), 448–458.
(9) Yang, Y.; Wang, J.; Xiu, Z.; Alvarez, P. J. J. Impacts of silver nanoparticles on cellular and transcriptional activity of nitrogen-cycling bacteria. *Environ. Toxicol. Chem.* **2013**, *32* (7), 1488–1494.
(10) Khaksar, M.; Jolley, D. F.; Sekine, R.; Vasilev, K.; Johannessen, B.; Donner, E.; Lombi, E. In Situ Chemical Transformations of Silver Nanoparticles along the Water-Sediment Continuum. *Environ. Sci. Technol.* **2014**, *49* (1), 318–325.
(11) Sekine, R.; Brunetti, G.; Donner, E.; Khaksar, M.; Vasilev, K.; Jämting, Å. K.; Scheckel, K. G.; Kappen, P.; Zhang, H.; Lombi, E. Speciation and Lability of Ag-, AgCl-, and Ag2S-Nanoparticles in Soil Determined by X-ray Absorption Spectroscopy and Diffusive Gradients in Thin Films. *Environ. Sci. Technol.* **2014**, *49* (2), 897–905.
(12) Wang, Z.; von dem Bussche, A.; Kabadi, P. K.; Kane, A. B.; Hurt, R. H. Biological and environmental transformations of copper-based nanomaterials. *ACS Nano* **2013**, *7* (10), 8715–8727.
(13) Dale, A. L.; Lowry, G. V; Casman, E. A. Modeling nanosilver transformations in freshwater sediments. *Environ. Sci. Technol.* **2013**, *47* (22), 12920–12928.
(14) Lowry, G. V; Gregory, K. B.; Apte, S. C.; Lead, J. R. Transformations of nanomaterials in the environment. *Environ. Sci. Technol.* **2012**, *46* (13), 6893–6899.
(15) Roesch, L. F. W.; Fulthorpe, R. R.; Riva, A.; Casella, G.; Hadwin, A. K. M.; Kent, A. D.; Daroub, S. H.; Camargo, F. A. O.; Farmerie, W. G.; Triplett, E. W. Pyrosequencing enumerates and contrasts soil microbial diversity. *ISME J.* **2007**, *1* (4), 283–290.
(16) Borneman, J.; Skroch, P. W.; O'Sullivan, K. M.; Palus, J. A.; Rumjanek, N. G.; Jansen, J. L.; Nienhuis, J.; Triplett, E. W. Molecular microbial diversity of an agricultural soil in Wisconsin. *Appl. Environ. Microbiol.* **1996**, *62* (6), 1935–1943.
(17) Kemp, P. F.; Aller, J. Y.; J.W., S.; B.F., M.; F., D.; J.A., C.; G., M.; E.J., V. H.; H.J., G.; H.J., L. Bacterial diversity in aquatic and other environments: what 16S rDNA libraries can tell us. *FEMS Microbiol. Ecol.* **2004**, *47* (2), 161–177.
(18) Liu, W. T.; Marsh, T. L.; Cheng, H.; Forney, L. J. Characterization of microbial diversity by determining terminal restriction fragment length polymorphisms of genes encoding 16S rRNA. *Appl. Environ. Microbiol.* **1997**, *63* (11), 4516–4522.
(19) Wagner, M.; Loy, A.; Nogueira, R.; Purkhold, U.; Lee, N.; Daims, H. Microbial community composition and function in wastewater treatment plants. *Antonie Van Leeuwenhoek* **2002**, *81* (1/4), 665–680.
(20) Nanotechnologies, P. on E. Consumer Products Inventory. *Consumer Products Inventory*. 2015.
(21) Lubick, N. Nanosilver toxicity: ions, nanoparticles--or both? *Environ. Sci. Technol.* **2008**, *42* (23), 8617–8617.
(22) Gunawan, C.; Teoh, W. Y.; Marquis, C. P.; Amal, R. Cytotoxic Origin of Copper (II) Oxide Nanoparticles : Comparative Studies and Metal Salts. *ACS Nano* **2011**, No. 9,

7214–7225.
(23) Xiu, Z.; Zhang, Q.; Puppala, H.; Colvin, V.; Alvarez, P. Negligible particle-specific antibacterial activity of silver nanoparticles. *Nano Lett.* **2012**, 10–14.
(24) Lin, S.; Taylor, A. A.; Ji, Z.; Chang, C. H.; Kinsinger, N. M.; Ueng, W.; Walker, S. L.; Nel, A. E. Understanding the transformation, speciation, and hazard potential of copper particles in a model septic tank system using zebrafish to monitor the effluent. *ACS Nano* **2015**, *9* (2), 2038–2048.
(25) Schäberle, T. F.; Hack, I. M. Overcoming the current deadlock in antibiotic research. *Trends Microbiol.* **2014**, *22* (4), 165–167.
(26) Prevention, C. for D. C. and. *Antibiotic resistance threats in the United States, 2013*; Atlanta, 2013.
(27) Conly, J.; Johnston, B. Where are all the new antibiotics? The new antibiotic paradox. *Can. J. Infect. Dis. Med. Microbiol. = J. Can. des Mal. Infect. la Microbiol. medicale* **2005**, *16* (3), 159–160.
(28) Beyth, N.; Houri-Haddad, Y.; Domb, A.; Khan, W.; Hazan, R. Alternative Antimicrobial Approach: Nano-Antimicrobial Materials. *Evidence-Based Complement. Altern. Med.* **2015**, *2015*, 1–16.
(29) Lesniak, A.; Salvati, A.; Santos-Martinez, M. J.; Radomski, M. W.; Dawson, K. A.; Aberg, C. Nanoparticle Adhesion to the Cell Membrane and Its Eff ect on Nanoparticle Uptake Efficiency. *J. Am. Chem. Soc.* **2012**, *135*, 1438–1444.
(30) Thill, A.; Zeyons, O.; Spalla, O.; Chauvat, F.; Rose, J.; Auffan, M.; Flank, A. M. Cytotoxicity of CeO2 nanoparticles for Escherichia coli. Physico-chemical insight of the cytotoxicity mechanism. *Environ. Sci. Technol.* **2006**, *40* (19), 6151–6156.
(31) Chen, K. L. Nanoparticles Meet Cell Membranes: Probing Nonspeci fi c Interactions using Model Membranes. *Environ. Sci. Technol.* **2014**, *48*, 873–880.
(32) Aruoja, V.; Pokhrel, S.; Sihtmäe, M.; Mortimer, M.; Mädler, L.; Kahru, A. Toxicity of 12 metal-based nanoparticles to algae, bacteria and protozoa. *Environ. Sci. Nano* **2015**, *2* (6), 630–644.
(33) Conway, J. R.; Adeleye, A. S.; Gardea-Torresdey, J.; Keller, A. A. Aggregation, Dissolution, and Transformation of Copper Nanoparticles in Natural Waters. *Environ. Sci. Technol.* **2015**, *49* (5), 2749–2756.
(34) Li, Y.; Zhang, W.; Niu, J.; Chen, Y. Surface-Coating-Dependent Dissolution, Aggregation, and Reactive Oxygen Species (ROS) Generation of Silver Nanoparticles under Different Irradiation Conditions. *Environ. Sci. Technol.* **2013**, *47* (18), 10293–10301.
(35) Nel, A. E.; Mädler, L.; Velegol, D.; Xia, T.; Hoek, E. M. V; Somasundaran, P.; Klaessig, F.; Castranova, V.; Thompson, M. Understanding biophysicochemical interactions at the nano-bio interface. *Nat. Mater.* **2009**, *8* (7), 543–557.
(36) Chen, K. L.; Bothun, G. D. Nanoparticles Meet Cell Membranes: Probing Nonspecific Interactions using Model Membranes. *Environ. Sci. Technol.* **2014**, *48* (2), 873–880.
(37) Catalano, F.; Accomasso, L.; Alberto, G.; Gallina, C.; Raimondo, S.; Geuna, S.; Giachino, C.; Martra, G. Factors Ruling the Uptake of Silica Nanoparticles by Mesenchymal Stem Cells: Agglomeration Versus Dispersions, Absence Versus Presence of Serum Proteins. *Small* **2015**, *11* (24), 2919–2928.
(38) Hsiao, I.-L.; Hsieh, Y.-K.; Wang, C.-F.; Chen, I.-C.; Huang, Y.-J. Trojan-Horse Mechanism in the Cellular Uptake of Silver Nanoparticles Verified by Direct Intra- and

Extracellular Silver Speciation Analysis. *Environ. Sci. Technol.* **2015**, *49* (6), 3813–3821.
(39) Zhao, F.; Zhao, Y.; Liu, Y.; Chang, X.; Chen, C.; Zhao, Y. Cellular Uptake, Intracellular Trafficking, and Cytotoxicity of Nanomaterials. *Small* **2011**, *7* (10), 1322–1337.
(40) Demchick, P.; Koch, A. L. The permeability of the wall fabric of Escherichia coli and Bacillus subtilis. *J. Bacteriol.* **1996**, *178* (3), 768–773.
(41) Wang, H.-W.; Chen, Y.; Yang, H.; Chen, X.; Duan, M.-X.; Tai, P. C.; Sui, S.-F. Ring-like pore structures of SecA: implication for bacterial protein-conducting channels. *Proc. Natl. Acad. Sci. U. S. A.* **2003**, *100* (7), 4221–4226.
(42) Yang, Y.; Quensen, J.; Mathieu, J.; Wang, Q.; Wang, J.; Li, M.; Tiedje, J. M.; Alvarez, P. J. J. Pyrosequencing reveals higher impact of silver nanoparticles than Ag+ on the microbial community structure of activated sludge. *Water Res.* **2014**, *48*, 317–325.
(43) Yin, L.; Cheng, Y.; Espinasse, B.; Colman, B. P.; Auffan, M.; Wiesner, M.; Rose, J.; Liu, J.; Bernhardt, E. S. More than the ions: the effects of silver nanoparticles on Lolium multiflorum. *Environ. Sci. Technol.* **2011**, *45* (6), 2360–2367.
(44) Choi, O.; Hu, Z. Size dependent and reactive oxygen species related nanosilver toxicity to nitrifying bacteria. *Environ. Sci. Technol.* **2008**, *42* (12), 4583–4588.
(45) Applerot, G.; Lellouche, J.; Lipovsky, A.; Nitzan, Y.; Lubart, R.; Gedanken, A.; Banin, E. Understanding the antibacterial mechanism of CuO nanoparticles: revealing the route of induced oxidative stress. *Small* **2012**, *8* (21), 3326–3337.
(46) Meghana, S.; Kabra, P.; Chakraborty, S.; Padmavathy, N. Understanding the pathway of antibacterial activity of copper oxide nanoparticles. *RSC Adv.* **2015**, *5* (16), 12293–12299.
(47) Guo, J.; Gao, S.-H.; Lu, J.; Bond, P. L.; Verstraete, W.; Yuan, Z. Copper Oxide Nanoparticles Induce Lysogenic Bacteriophage and Metal-Resistance Genes in Pseudomonas aeruginosa PAO1. *ACS Appl. Mater. Interfaces* **2017**, in press.
(48) Mathelié-Guinlet, M.; Béven, L.; Moroté, F.; Moynet, D.; Grauby-Heywang, C.; Gammoudi, I.; Delville, M.-H.; Cohen-Bouhacina, T. Probing the threshold of membrane damage and cytotoxicity effects induced by silica nanoparticles in Escherichia coli bacteria. *Adv. Colloid Interface Sci.* **2017**.
(49) Sondi, I.; Salopek-Sondi, B. Silver nanoparticles as antimicrobial agent: a case study on E. coli as a model for Gram-negative bacteria. *J. Colloid Interface Sci.* **2004**, *275* (1), 177–182.
(50) Reinsch, B. C.; Levard, C.; Li, Z.; Ma, R.; Wise, a; Gregory, K. B.; Brown, G. E.; Lowry, G. V. Sulfidation of silver nanoparticles decreases Escherichia coli growth inhibition. *Environ. Sci. Technol.* **2012**, *46* (13), 6992–7000.
(51) Levard, C.; Hotze, E. M.; Colman, B. P.; Dale, A. L.; Truong, L.; Yang, X. Y.; Bone, A. J.; Brown, G. E.; Tanguay, R. L.; Di Giulio, R. T.; et al. Sulfidation of silver nanoparticles: Natural antidote to their toxicity. *Environ. Sci. Technol.* **2013**, *47* (23), 13440–13448.
(52) Judy, J. D.; Kirby, J. K.; Creamer, C.; McLaughlin, M. J.; Fiebiger, C.; Wright, C.; Cavagnaro, T. R.; Bertsch, P. M. Effects of silver sulfide nanomaterials on mycorrhizal colonization of tomato plants and soil microbial communities in biosolid-amended soil. *Environ. Pollut.* **2015**, *206*, 256–263.
(53) Dharsana, U. S.; Sai Varsha, M. K. N.; Khan Behlol, A. A.; Veerappan, A.; Thiagarajan, R. Sulfidation modulates the toxicity of biogenic copper nanoparticles. *RSC Adv.* **2015**, *5* (38), 30248–30259.
(54) Lesniak, A.; Salvati, A.; Santos-Martinez, M. J.; Radomski, M. W.; Dawson, K. A.;

Åberg, C. Nanoparticle Adhesion to the Cell Membrane and Its Effect on Nanoparticle Uptake Efficiency. *J. Am. Chem. Soc.* **2013**, *135* (4), 1438–1444.
(55) Navarro, E.; Piccapietra, F.; Wagner, B.; Marconi, F.; Kaegi, R.; Odzak, N.; Sigg, L.; Behra, R. Toxicity of Silver Nanoparticles to *Chlamydomonas reinhardtii*. *Environ. Sci. Technol.* **2008**, *42* (23), 8959–8964.
(56) Kent, R. D.; Vikesland, P. J. Controlled Evaluation of Silver Nanoparticle Dissolution Using Atomic Force Microscopy. *Environ. Sci. Technol.* **2012**, *46* (13), 6977–6984.
(57) Vencalek, B. E.; Laughton, S. N.; Spielman-Sun, E.; Rodrigues, S. M.; Unrine, J. M.; Lowry, G. V.; Gregory, K. B. In Situ Measurement of CuO and Cu(OH)2 Nanoparticle Dissolution Rates in Quiescent Freshwater Mesocosms. *Environ. Sci. Technol. Lett.* **2016**, *3* (10), 375–380.
(58) Lowry, G. V; Espinasse, B. P.; Badireddy, A. R.; Richardson, C. J.; Reinsch, B. C.; Bryant, L. D.; Bone, A. J.; Deonarine, A.; Chae, S.; Therezien, M.; et al. Long-term transformation and fate of manufactured ag nanoparticles in a simulated large scale freshwater emergent wetland. *Environ. Sci. Technol.* **2012**, *46* (13), 7027–7036.
(59) Shvedova, A.; Pietroiusti, A. Mechanisms of carbon nanotube-induced toxicity: focus on oxidative stress. *Toxicol. Appl. Pharmacol.* **2012**, *261*, 121–133.
(60) Hwang, E. T.; Lee, J. H.; Chae, Y. J.; Kim, Y. S.; Kim, B. C.; Sang, B.-I.; Gu, M. B. Analysis of the toxic mode of action of silver nanoparticles using stress-specific bioluminescent bacteria. *Small* **2008**, *4* (6), 746–750.
(61) Ivask, A.; Juganson, K.; Bondarenko, O.; Mortimer, M.; Aruoja, V.; Kasemets, K.; Blinova, I.; Heinlaan, M.; Slaveykova, V.; Kahru, A. Mechanisms of toxic action of Ag, ZnO and CuO nanoparticles to selected ecotoxicological test organisms and mammalian cells in vitro: A comparative review. *Nanotoxicology* **2013**, *5390* (April 2016), 1–15.
(62) McQuillan, J. S.; Shaw, A. M. Differential gene regulation in the Ag nanoparticle and Ag(+)-induced silver stress response in Escherichia coli: A full transcriptomic profile. *Nanotoxicology* **2014**, *5390* (I), 1–8.
(63) Maurer-Jones, M. A.; Gunsolus, I. L.; Murphy, C. J.; Haynes, C. L. Toxicity of engineered nanoparticles in the environment. *Anal. Chem.* **2013**, *85* (6), 3036–3049.
(64) Neal, A. L. What can be inferred from bacterium-nanoparticle interactions about the potential consequences of environmental exposure to nanoparticles? *Ecotoxicology* **2008**, *17* (5), 362–371.
(65) Imlay, J. A. Cellular defenses against superoxide and hydrogen peroxide. *Annu. Rev. Biochem.* **2008**, *77*, 755–776.
(66) Dimkpa, C. O.; Calder, A.; Britt, D. W.; McLean, J. E.; Anderson, A. J. Responses of a soil bacterium, Pseudomonas chlororaphis O6 to commercial metal oxide nanoparticles compared with responses to metal ions. *Environ. Pollut.* **2011**, *159* (7), 1749–1756.
(67) Aruoja, V.; Pokhrel, S.; Sihtmäe, M.; Mortimer, M.; Mädler, L.; Kahru, A. Toxicity of 12 metal-based nanoparticles to algae, bacteria and protozoa. *Environ. Sci. Nano* **2015**.
(68) Ivask, A.; ElBadawy, A.; Kaweeteerawat, C.; Boren, D.; Fischer, H.; Ji, Z.; Chang, C. H.; Liu, R.; Tolaymat, T.; Telesca, D.; et al. Toxicity Mechanisms in Escherichia coli Vary for Silver Nanoparticles and Differ from Ionic Silver. *ACS Nano* **2014**, *8* (1), 374–386.
(69) Brayner, R.; Ferrari-Iliou, R.; Brivois, N.; Djediat, S.; Benedetti, M. F.; Fiévet, F. Toxicological impact studies based on Escherichia coli bacteria in ultrafine ZnO nanoparticles colloidal medium. *Nano Lett.* **2006**, *6* (4), 866–870.
(70) Fang, J.; Lyon, D. Y.; Wiesner, M. R.; Dong, J. Effect of a Fullerene Water Suspension on

Bacterial Phospholipids and Membrane Phase Behavior. *Environ. Sci. Technol.* **2007**, *41* (7), 2636–2642.
(71) Zhang, L.; Jiang, Y.; Ding, Y.; Povey, M.; York, D. Investigation into the antibacterial behaviour of suspensions of ZnO nanoparticles (ZnO nanofluids). *J. Nanoparticle Res.* **2006**, *9* (3), 479–489.
(72) Pérez, J. M.; Arenas, F. A.; Pradenas, G. A.; Sandoval, J. M.; Vásquez, C. C. Escherichia coli YqhD exhibits aldehyde reductase activity and protects from the harmful effect of lipid peroxidation-derived aldehydes. *J. Biol. Chem.* **2008**, *283* (12), 7346–7353.
(73) Foxman, B. The epidemiology of urinary tract infection. *Nat. Rev. Urol.* **2010**, *7* (12), 653–660.
(74) Vikram, A.; Bomberger, J. M.; Bibby, K. J. Efflux as a glutaraldehyde resistance mechanism in Pseudomonas fluorescens and Pseudomonas aeruginosa biofilms. *Antimicrob. Agents Chemother.* **2015**, *59* (6), 3433–3440.
(75) Krivoshiev, B. V.; Dardenne, F.; Blust, R.; Covaci, A.; Husson, S. J. Elucidating toxicological mechanisms of current flame retardants using a bacterial gene profiling assay. *Toxicol. Vitr.* **2015**, *29* (8), 2124–2132.
(76) Dale, A. L.; Lowry, G. V; Casman, E. A. Stream Dynamics and Chemical Transformations Control the Environmental Fate of Silver and Zinc Oxide Nanoparticles in a Watershed-Scale Model. *Environ. Sci. Technol.* **2015**, *49* (12), 7285–7293.
(77) Kim, B.; Murayama, M.; Colman, B. P.; Hochella, M. F.; Colvin, V. L.; Tomson, M. B.; Engelhard, M.; Wiesner, M. R.; Auffan, M.; Labille, J.; et al. Characterization and environmental implications of nano- and larger TiO2 particles in sewage sludge, and soils amended with sewage sludge. *J. Environ. Monit.* **2012**, *14* (4), 1129.
(78) Petosa, A. R.; Jaisi, D. P.; Quevedo, I. R.; Elimelech, M.; Tufenkji, N. Aggregation and deposition of engineered nanomaterials in aquatic environments: role of physicochemical interactions. *Environ. Sci. Technol.* **2010**, *44* (17), 6532–6549.
(79) Quik, J. T. K.; Stuart, M. C.; Wouterse, M.; Peijnenburg, W.; Hendriks, A. J.; van de Meent, D. Natural colloids are the dominant factor in the sedimentation of nanoparticles. *Environ. Toxicol. Chem.* **2012**, *31* (5), 1019–1022.
(80) Colman, B. P.; Arnaout, C. L.; Anciaux, S.; Gunsch, C. K.; Hochella, M. F.; Kim, B.; Lowry, G. V; McGill, B. M.; Reinsch, B. C.; Richardson, C. J.; et al. Low concentrations of silver nanoparticles in biosolids cause adverse ecosystem responses under realistic field scenario. *PLoS One* **2013**, *8* (2), e57189.
(81) Ma, R.; Stegemeier, J.; Levard, C.; Dale, J. G.; Noack, C. W.; Yang, T.; Brown, G. E.; Lowry, G. V. Sulfidation of copper oxide nanoparticles and properties of resulting copper sulfide. *Environ. Sci. Nano* **2014**, *1* (4), 347–357.
(82) Gil-Allué, C.; Schirmer, K.; Tlili, A.; Gessner, M. O.; Behra, R. Silver Nanoparticle Effects on Stream Periphyton During Short-Term Exposures. *Environ. Sci. Technol.* **2015**, *49* (2), 1165–1172.
(83) Ge, Y.; Priester, J. H.; Van De Werfhorst, L. C.; Walker, S. L.; Nisbet, R. M.; An, Y.-J.; Schimel, J. P.; Gardea-Torresdey, J. L.; Holden, P. A. Soybean Plants Modify Metal Oxide Nanoparticle Effects on Soil Bacterial Communities. *Environ. Sci. Technol.* **2014**, *48* (22), 13489–13496.
(84) Moore, J. D.; Stegemeier, J. P.; Bibby, K.; Marinakos, S. M.; Lowry, G. V; Gregory, K. B. Impacts of Pristine and Transformed Ag and Cu Engineered Nanomaterials on Surficial Sediment Microbial Communities Appear Short-Lived. *Environ. Sci. Technol.* **2016**, *50*

(5), 2641–2651.

CHAPTER TWO:

Impacts of pristine and transformed Ag and Cu engineered nanomaterials on surficial sediment microbial communities appear short-lived

This work has been published:

Moore, J.D., Stegemeier, J.P., Bibby, K., Marinakos, S., Lowry, G.V., Gregory, K.B. "Impacts of pristine and transformed Ag and Cu nanomaterials on surficial sediment microbial communities appear short-lived," *Environmental Science and Technology*, 2016, 50(5): 2641-2651. DOI: 10.1021/acs.est.5b05054

2.1 ABSTRACT

Laboratory-based studies have shown that many soluble metal and metal oxide engineered nanomaterials (ENM) exert strong toxic effects on microorganisms. However, laboratory-based studies lack the complexity of natural systems and often use “as manufactured” ENMs rather than more environmentally relevant transformed ENMs, leaving open the question of whether natural ligands and seasonal variation will mitigate ENM impacts. Because ENMs will accumulate in subaquatic sediments, we examined effects of pristine and transformed Ag and Cu ENMs on surficial sediment microbial communities in simulated freshwater wetlands. Five identical mesocosms were dosed through the water column with either Ag^0, Ag_2S, CuO or CuS ENMs (nominal sizes of 4.67 ± 1.4, 18.1 ± 3.2, 31.1 ± 12 and 12.4 ± 4.1 nm, respectively) or Cu^{2+}. Microbial communities were examined at 0, 7, 30, 90, 180 and 300 d using qPCR and high-throughput 16S rRNA gene sequencing. Results suggest differential short-term impacts of Ag^0 and Ag_2S, similarities between CuO and CuS, and differences between Cu ENMs and Cu^{2+}. PICRUSt-predicted metagenomes displayed differential effects of Ag treatments on photosynthesis and of Cu treatments on methane metabolism. By 300 d all metrics pointed to reconvergence of ENM-dosed mesocosm microbial community structure and composition, suggesting limited long-term microbial community impacts from a pulse of Ag or Cu ENMs.

2.2 INTRODUCTION

Engineered nanomaterials (ENM) are increasingly incorporated into commercial and industrial products.[1] ENMs have already been detected within wastewater streams,[2] and, with increasing usage, their concentration in the environment and potential for environmental impact will rise. While it is known that Ag and Cu ENMs are toxic or inhibitory to pure cultures and communities of microorganisms in the laboratory,[3–6] it is not clear whether, in natural environments, their effects will be mitigated. It is also known that ENMs transform.[7] However, the degree to which transformation will contribute to mitigation of ENM impacts is also an open question. Here we report the findings of a long-term (300 d) study in which we evaluated the magnitude and longevity of the effects of Ag^0 and CuO ENMs, and their sulfidized analogs, on sediment microbial communities in large-scale, outdoor wetland mesocosms.

Metal nanoparticles (NP) are some of the most commonly incorporated ENMs, with silver (Ag) and copper (Cu) being two of the most frequently, and increasingly, used metals.[1] These NPs are often added to commercial products specifically because of their antimicrobial and antifungal properties.[8–10] Applying ENMs to agricultural land within fertilizers is also a developing area of research.[11] With increasing usage, the number of ENM-contaminated environmental compartments and the concentrations of ENMs within those compartments will rise. Ag NPs have already been detected in wastewater treatment plants.[2] Environmental fate models for ENMs predict accumulation of ENMs in subaquatic sediments. This is a result of ENMs in wastewater effluent and of runoff from agricultural lands that apply biosolids.[12,13] With runoff from farmlands, ENMs are expected to enter surface water, and freshwater and estuarine sediments.[14–16] In wastewater treatment plants, and freshwater sediments, on agricultural land and within commercial products, ENMs will encounter diverse microbial communities that perform services important to

human and ecosystem health. Thus, both in terms of the effectiveness of ENM-enabled antimicrobial products and the indirect environmental impacts of ENMs, studies of ENMs' impacts on microbial communities are warranted.

Ag NPs are toxic to microorganisms.[3,17] Though Cu-based NPs are less well studied, comparisons with other ENMs have suggested that Cu-based NPs also have considerable potential for environmental impact,[4,18,19] which is in line with the well-documented antimicrobial nature of Cu.[20] A recent study comparing the toxicity of a variety of ENMs to bacteria and other unicellular organisms found Ag and Cu NPs to be the most toxic to bacteria, yeast, and algae.[21] By studying the impacts of Ag and Cu NPs, we intended to capture the impacts of a worst-case scenario of possible ENM exposures.

Pristine metal and metal oxide ENMs are known to transform to different species under environmental conditions,[7,22–24] e.g. Ag^0 transforms to Ag_2S [25] and metallic Cu transforms to CuO then CuS.[24,26] Recent work comparing effects of pristine and transformed Ag NPs revealed that they disparately inhibit *E. coli*,[27] as well as nematodes, aquatic plants, and several fish species.[28] Dissolved constituents and redox conditions affect ENM transformation, aggregation and bioavailability.[29–31] Very recent work has begun to consider the effect of environmental transformations when assessing environmental impacts of ENMs, typically observing lesser impacts.[32–34] Nevertheless, studies purporting to assess potential ENM environmental toxicity still perform experiments in biological growth media or deionized water using pristine ENMs.[35–38] In this study, we dosed mesocosms with pristine and transformed ENMs to determine if transformation mitigates the impacts of ENMs.

Of the relatively few studies that have investigated impacts of Ag NPs on complex environmental microbial communities, there is little consensus regarding the degree or even the

presence of impacts. Bradford et al. did not detect impacts of Ag NPs on transplanted estuarine sediment microbial communities using denaturing gradient gel electrophoresis (DGGE).[39] Similarly Colman et al. did not observe impacts on terminal restriction fragment length polymorphism (T-RFLP) analysis following Ag NP dosing of sediment slurries.[40] Conversely, very recent work using 16S rRNA gene sequencing to detect impacts of Ag NPs has detected changes in microbial community structure in wastewater sludge[41] and nitrifying batch reactors.[42] Others have observed impacts on rhizosphere microbial communities[43] and microbial photosynthesis and phototrophic bacteria,[44,45] calling into question the effects of Ag NPs on C cycling. The shortest of these studies investigated impacts after only two hours, and the longest was less than two months. In the present study, we opted for high-throughput 16S rRNA gene sequencing to obtain a high resolution view of impacts on microbial communities and embarked on a nearly year-long study to assess the longevity of impacts.

Freshwater wetland microbial communities provide numerous ecosystem services, e.g. primary production, carbon and phosphorus sequestration and water quality improvements through denitrification.[46–48] Ag NPs are likely to accumulate within subaquatic sediments.[39,49] In fact, very recent work tracking the fate of Ag NPs within freshwater lakes showed biofilms within the lake, along with the sediment, to be Ag NP sinks.[50] These results raise concerns around Ag and other antimicrobial metal NPs, specifically whether they will harm extant freshwater wetland microbial communities and the ecosystem services they provide.

The goal of this study was to assess whether Ag and Cu ENMs will have lasting impacts on microbial communities in freshwater wetlands and whether sulfidation and/or environmental resilience will mitigate these impacts. We used large-scale, open air, outdoor mesocosms to capture as much of the natural complexity as possible, e.g. natural ligands, temperature changes,

precipitation influxes, and ecology. We dosed separate mesocosms with Ag^0, Ag_2S, CuO or CuS NPs or with a Cu ion (Cu^{2+}) control. (In a previous study, we included a Ag ion control which was found to transform into Ag_2S,[51] so we did not include a Ag ion control in the present study.) We hypothesized that given our relatively high dosing regimen – representing a worst case release scenario – pristine Ag^0 and CuO NPs would have more pronounced impacts than their sulfidized counterparts, Ag_2S and CuS NPs. We further hypothesized that sulfidation and environmental factors would combine to mitigate impacts of the NPs. To the best of our knowledge, this is the first study to assess long-term (10 months) effects of pristine and transformed metal ENMs on microbial communities under realistic conditions.

2.3 MATERIALS AND METHODS

2.3.A Nanomaterial synthesis, sulfidation, and characterization. For synthesis of pristine, gum arabic (GA)-coated Ag^0 NMs, 1.37 L of ultrapure water (Barnstead Nanopure Diamond, Thermo Fisher Scientific, Waltham, MA), 45 mL of 10 g/L gum Arabic (Thermo Fisher Scientific), and 45 mL of 0.1 M silver nitrate (Sigma Aldrich, St. Louis, MO) were added to an Erlenmeyer flask. The solution was stirred for 5 min. Forty-five mL of 0.1 M ice-cold sodium borohydride (Sigma Aldrich) were added all at once, and stirring was continued for 10 min. Multiple batches were combined, and the NPs were purified and concentrated by dialysis (Optiflux F200NR Fresenius Polysulfone Dialyzer, Fresenius Medical Care, Bad Homburg, Germany). The suspension was diluted in water and concentrated two additional times in order to obtain the final product as has been previously described.[52] To produce transformed, GA-coated Ag_2S NMs, Ag^0 NMs were sulfidized following a modified published procedure (see Supplemental Methods in Supporting Information for more details).[53]

One gram of <50 nm CuO NPs (Sigma Aldrich) was re-suspended and stabilized with 2.5 g GA (Thermo Fisher Scientific) in 900 mL of DI water via a sonicating probe at power level 3 for one minute (Branson Model 250, Branson Ultrasonics, Danbury, CT). To remove excess GA, the suspension was centrifuged, decanted, and re-suspended in DI water with the sonicating probe. This washing process was repeated three times to obtain the final product. The CuO NPs were sulfidized using a direct sulfidation process adapted from a procedure described previously (Supplemental Methods).[26,27]

The initial pristine and transformed ENMs were characterized using dynamic light scattering (DLS) and electrophoretic mobility (EPM) in filtered mesocosm porewater, and by transmission electron microscopy (TEM) (Appendix A Supplemental Methods). Ag and Cu ENMs had hydrodynamic diameters around 100 nm and 200 nm, respectively (**Table 2.1**). In TEM images, both Ag and Cu NPs were seen to have considerably smaller primary particle sizes (**Figure A.1**). TEM of Ag NPs showed monodisperse, largely spherical particles, while Cu NPs were polydisperse spherical and rod-shaped particles (**Figure A.1**). When suspended in filtered mesocosm porewater (pH ~7), all NPs were found to have negative surface charges (**Table 2.1**). Estimates of filtered porewater ionic strength (I) are based on measured specific conductivities (**Table 2.1**).[54]

Table 2.1. ***Nanomaterial suspension in filtered mesocosm porewater characterization and DLS and zeta potential (ZP) characterization.*** *Values are expressed as mean ± one standard deviation (SD). Ionic strength (I) is estimated from specific conductance according to the approach described by Marion & Babcock for mixed salt solutions.[54] ZP was calculated from measured EPM data using the Smoluchowski equation.*

ENM	pH	Specific conductance [µS/cm]	Estimated I [mM]	Primary particle diam. [nm]	Hydrodynamic diam. [nm]	Zeta potential [mV]
Ag^0	7.3	114 ± 1.4	1.6	4.67 ± 1.4	113 ± 9.4	-22.2 ± 1.5
Ag_2S	7.2	101 ± 0.82	1.4	18.1 ± 3.2	61.5 ± 0.37	-25.8 ± 2.5
CuO	7.0	70.8 ± 0.16	1.0	31.1 ± 12	236 ± 11	-25.2 ± 1.4
CuS	7.1	74.8 ± 0.21	1.1	12.4 ± 4.1	185 ± 11	-21.6 ± 0.70

2.3.B Mesocosms. The mesocosms in this study were designed to mimic emergent freshwater wetland systems (**Figure A.2**, **A.7**, and **A.8**). They have been described in detail previously.[55,56] In brief, they are large (3.7 m long by 1.2 m wide by 0.81 m deep), open top, rectangular boxes lined with water-tight 0.45mm-thick polypropylene. The mesocosm bed slopes down (~13º) from a terrestrial half to an aquatic half. Both terrestrial and aquatic plants typical of North Carolina wetlands were added to the mesocosms. A blend of three top soils was used to produce 22 cm of sediment and soil cover. About 400 L of local well water were added to each mesocosm. The mesocosms were planted in Feb 2013 and allowed to stabilize until the experiment began in Oct 2013. In the week prior to the experiment, water was cycled from one box to another in order to homogenize water quality parameters. The system was then allowed to further stabilize before dosing. Mesocosm water column water quality data has been reported in a previous study that used the same source as this study for the mesocosm water and soil.[55]

2.3.C Experimental design. A total of 3 g $[Ag]_T$ or $[Cu]_T$ of Ag or Cu NPs or Cu ion were divided into four equal water column dosing events at day 0, 7, 14 and 21. The 3 g of Ag or Cu was expected to increase the Ag or Cu concentration of the top centimeter of sediment by 100 ppm to allow for X-ray characterization of metal speciation in surficial sediment (see SI for X-ray absorption methods). In each dose, 300 mL of a 2.5 g/L suspension of ENMs or ions were added to the mesocosms. The background mesocosm surficial sediment Cu concentration was 5.07 ± 0.27 (± one standard deviation) mg Cu per kg surficial sediment, and Ag was not detectable (Supplemental Methods).

Subaquatic surficial sediment samples were taken, using sterile sampling techniques, from each dosed mesocosm at 0 (prior to dosing), 7, 30 and approximately 90, 180 and 300 days. Trends observed in a preliminary high-throughput 16S rRNA gene sequencing effort (methods explained

below) after 90 d suggested that microbial communities in ENM-dosed mesocosms might already be converging. As a result, we arranged to sample an undosed control mesocosm at the conclusion of the study (300 d) in addition to the 5 dosed mesocosms. All samples were taken from the submerged, sloped portion of the mesocosm (**Figure A.2**). This area of the mesocosm was submerged, i.e. subaquatic, for the entirety of the study. To limit perturbation and to ensure that samples consisted of intact surficial sediment, duplicate samples consisted of one sample from each side of the box. The surficial sediment layer was sampled using a modified 50 mL centrifuge tube, with two 3.3 m long (4.3 mm diameter) polypropylene tubes fitted into the cap of the centrifuge tube. Negative air pressure was generated using one tube while the surficial sediment sample was lightly vacuumed with the other. By gently dragging the submerged tube over 0.5 to 1 m of sediment surface, we collected 45 mL of solution containing 2 to 3 g of homogenized surficial sediment (henceforth, "sample" and "homogenized sample" will be used interchangeably). Tubes were washed with 70% ethanol after each sample was taken. Two homogenized samples were taken per mesocosm per sampling event. Samples were frozen in the field with ethanol and dry ice and stored on dry ice until they were returned to the laboratory, where they were stored at -80ºC until further processing.

2.3.D DNA extraction and qPCR. Upon thawing, samples were immediately centrifuged at 2,500 X *g* for 5 min to concentrate sediment. DNA extraction was performed using the PowerSoil DNA extraction kit (MoBio, Carlsbad, CA) following the manufacturer's protocol. Molecular biology grade water was used for final elution of DNA. Extracted DNA was stored at -20ºC. Bacterial cell density was estimated by quantitative polymerase chain reaction (qPCR) of 16S rRNA genes, as has been described previously (Supplemental Methods).[57,58] 16S rRNA gene copies were quantitated based on a serial dilution of *E. coli* K-12 genomic DNA (ATCC 10798).

Select samples were analyzed for qPCR inhibition, and no inhibition was observed (Supplemental Methods).

2.3.E 16S rRNA gene sequencing. Polymerase chain reaction (PCR) amplification of the 16S rRNA gene V4 region followed a slightly modified version of that used by Caporaso et al. (Supplemental Methods).[59] Duplicate PCR products were pooled prior to purification. Agencourt AMPure XP (Beckman Coulter, Indianapolis, IN) was used for purification of amplified DNA on a 12-tube magnetic plate with slight modification of the manufacturer's protocol (Supplemental Methods). Elution was performed with 30 µL of molecular biology grade water.

Gel electrophoresis of purified 16S PCR products confirmed that amplicons were of the correct length and that negative (DNA-free) amplification and purification controls showed no signs of DNA. Double-stranded DNA (dsDNA) was quantitated with a Qubit 2.0 fluorometer (Life Technologies, Carlsbad, CA), using high sensitivity standards. All sample DNA was pooled and then diluted, denatured, further diluted and supplemented with PhiX DNA immediately prior to sequencing (Supplemental Methods). Sequencing was performed on an Illumina MiSeq (Illumina, San Diego, CA), using a 2x251 base pair (bp) configuration. Raw reads were submitted to the National Center for Biotechnology Information (NCBI) Sequence Read Archive (SRA) under the accession number SRR2541828.

2.3.F Sequence processing and analysis. PANDASeq was used to assemble paired-end reads.[60] Assembled reads longer than 300bp were discarded and remaining reads were output as a fastq file. Otherwise, default PANDASeq parameters were used.

QIIME (version 1.8.0) was used for demultiplexing, filtering of low quality and chimeric reads, with ChimeraSlayer,[61] operational taxonomic unit picking via uclust,[62] taxonomic assignment of reads via the RDP classifier,[63] and subsampling and calculating community alpha diversity and

dissimilarities.[64] Default QIIME parameters were used, save for the maximum unacceptable Phred quality score (19 instead of 3). Operational taxonomic units (OTUs) were picked using an "open-reference" scheme that combines "closed reference" and "de novo," or open, OTU picking. OTUs undergoing closed-reference picking were aligned with PyNAST[65] against the May 2013 version of the GreenGenes database[66] at 97% similarity.

After paired-end assembly and demultiplexing, the number of sequences per sample ranged from 1,984 to 34,279, with an average of 17,297 ± 6,786 per sample. Surprisingly, no sequences were mapped back to the day 90 CuS barcode. After removing low-quality and chimeric reads, an average of 15,332 ± 5,913 sequences per sample remained, not including the 90-day CuS sample. For alpha diversity (within-sample diversity) calculations, Ag and Cu-dosed communities were randomly subsampled to the lowest number of filtered reads, i.e. to 9,465 and 1,900, respectively. The Shannon index was used to investigate alpha diversity of subsampled communities.

Using QIIME, two-dimensional non-metric multidimensional scaling (NMDS) was performed on subsampled pairwise Bray-Curtis and weighted Unifrac distance matrices to visualize clusters of microbial communities. The weighted Unifrac metric deems samples with more phylogenetically distant OTUs to be more dissimilar.[67] NMDS plots were generated with the ggplot2 package[68] in R.[69]

Phylogenetic Investigation of Communities by Reconstruction of Unobserved States (PICRUSt) analysis has been shown to accurately predict metagenomes based on 16S amplicon datasets where communities consist of relatively well-characterized taxa, i.e. have a low nearest sequenced taxon index (NSTI).[70] Default PICRUSt settings were used. Within PICRUSt, predicted metagenomes were functionally annotated using Kyoto Encyclopedia of Genes and Genomes (KEGG) pathways[71] and Clusters of Orthologous Groups of proteins (COG) categories.[72] Statistical analysis

of metagenomic profiles (STAMP) version 2.0.6 was used to visualize PICRUSt-generated functionally categorized metagenomes.[73]

2.4 Results and Discussion

2.4.A Environmental transformations of Ag and Cu ENMs. We used X-ray absorption (XAS) techniques to determine the speciation of the Ag and Cu in subaquatic surficial sediment samples from the mesocosms. We observed transformation of Ag^0 NPs to Ag_2S within a month – less than ten days after the final pulse treatment (**Figure A.3A**). At 180 d, both Ag^0 and Ag_2S mesocosms featured strong Ag_2S signals, with no indication of Ag^0. This suggests that Ag^0 NPs and Ag_2S NPs would have similar bioavailability within one month after dosing and that the effects on microbial communities may be similar. This hypothesis is explored later in the manuscript.

We also observed rapid transformation of the CuO NPs. Within one month, much of the CuO had transformed to another Cu species (**Figure A.3B**). However, even after 180 d, the CuO NPs had not transformed completely to CuS. The exact speciation of Cu after 180 d could not be conclusively determined. Previous work on Cu speciation in similar systems[74] and our preliminary X-ray data point to a mix of Cu-sulfide species, both organic (Cu-S-R) and inorganic (covellite). In contrast, the CuS NPs remained as CuS over 180 days. The Cu in the Cu^{2+} mesocosm at one month was distinct from both CuO and CuS, but had transformed to CuS by six months. Thus, the Cu speciation in the mesocosms was distinct at early times for all three Cu species, but had converged by 180 d for CuS and Cu^{2+}. The speciation of Cu was different for the CuO-dosed mesocosm throughout the 300 d experiment. This suggests that there could be different bioavailability of Cu for the CuO compared to CuS NPs and Cu^{2+}, and that this could lead to differential effects on microbial communities as discussed next.

2.4.B Impacts on bacterial community cell density. Quantitative PCR (qPCR) of the 16S rRNA gene was used as an indicator of the bacterial community density. Gene copies were normalized by the mass of surficial sediment used for the extraction of DNA.

One week after the initial dosing, bacterial community cell densities largely increased (**Figure 2.1**). Only the Ag^0 mesocosm had a clear reduction, with its cell density halved (from 5 x 10^9 to 2.36 x 10^9 16S rRNA gene copies per g sediment). At 30 days, all cell densities increased. For the remainder of the experiment, NP-dosed mesocosms had relatively stable densities. In contrast, the Cu^{2+} mesocosm decreased nearly five-fold at day 90 (from 9.7 x 10^9 to 2.0 x 10^9 16S rRNA gene copies per g sediment) and decreased by 2 orders of magnitude at day 180 (to 7.7 x 10^6 16S rRNA gene copies per g sediment). No qPCR inhibition was detected for either 90 and 180 d Cu^{2+} mesocosm extracted DNA (data not shown). By 300 d, bacterial community cell densities of all of the mesocosms had recovered, converging with one another, including the undosed control mesocosm.

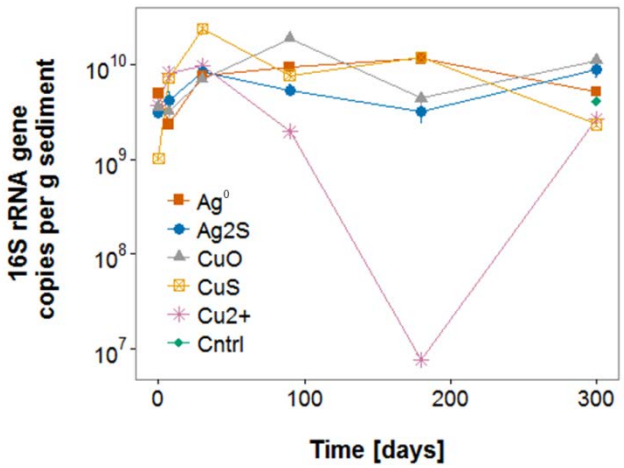

Figure 2.1. ***16S rRNA gene copies in Ag and Cu mesocosm surficial sediments.*** *Bacterial 16S rRNA gene copies were normalized by the average mass of sediment used in the duplicate DNA extractions per mesocosm sampling point. Note that day 0 Cu^{2+} is covered by CuO. Where error bars are not visible, they are obscured by the data markers. Average standard deviation of qPCR was 9.3% of gene copies per g sediment. The 300 d control mesocosm is abbreviated "Cntrl."*

Unlike NP treatments that have some kinetic limitation to the release of ions, the Cu^{2+} ions dosed into a water column are quickly dispersed and bioavailable. As such, the different effects of ENM and ion treatments on bacterial community cell density (**Figure 2.1**) were not unexpected. On the other hand, the lack of a significant impact of ENMs on bacterial community cell density was unexpected given that both Ag and Cu are known antimicrobials. This finding contrasts with that of a soil study where both pristine and transformed Ag NPs were found to reduce microbial biomass, even at lower concentrations (1 mg/kg).[32]

2.4.C Impacts on microbial community structure and composition. Microbial communities with higher alpha (within-sample) diversity can better withstand perturbation,[75,76] and lowering diversity can lead to a reduction in a community's capacity to provide important ecosystem services.[77] We used the Shannon diversity index[78] as an estimator of alpha diversity as it is a robust metric for large 16S rRNA gene datasets.[79]

We observed increases (compared to day 0) in alpha diversity for all treatments through three months (**Figure 2.2A** and **B**). The Ag^0-dosed mesocosm had a higher initial diversity than Ag_2S-dosed mesocosm, but that difference was erased by day 90 (**Figure 2.2A**). The diversities of CuO and CuS-dosed mesocosms also increased at the beginning of the experiment (**Figure 2.2B**). Only the Cu^{2+} mesocosm diversity displayed a different trend: increasing at 90 d and, otherwise, maintaining a uniquely low diversity through 300 d. At the end of the experiment, all NP-dosed (Ag^0 and Ag_2S, CuO and CuS) microbial communities had similar levels of alpha diversity.

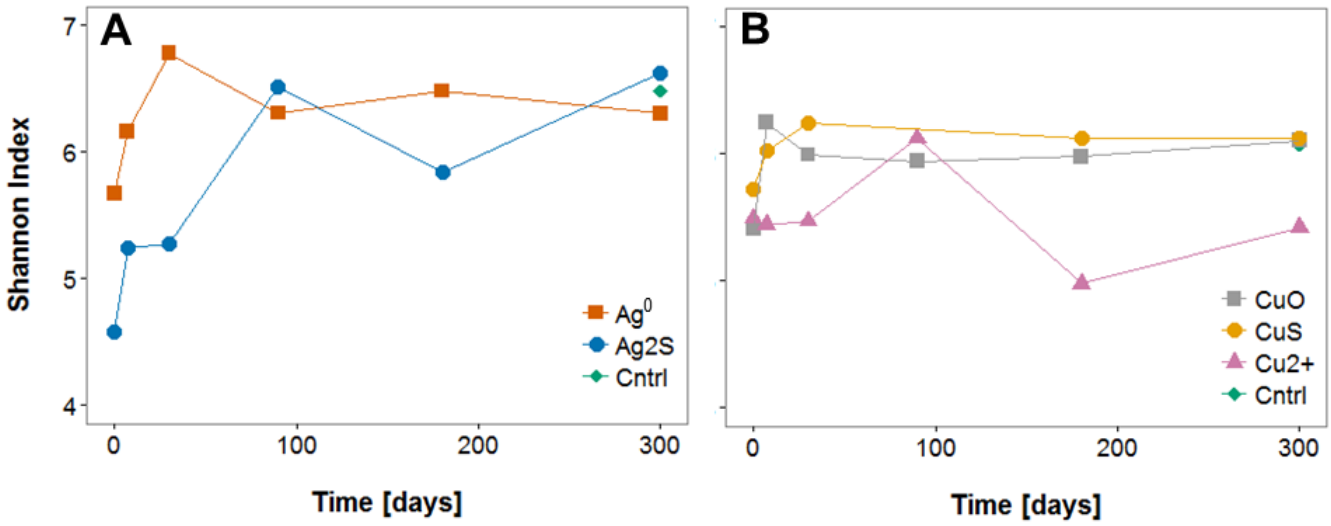

Figure 2.2. ***Shannon diversity indices for alpha (within-sample) diversity of Ag (A) and Cu (B) mesocosms.***

NMDS enables viewing of patterns within large datasets, such as those generated by next-generation sequencing (NGS) of microbial communities.[80] In these plots (**Figure 2.3**), more similar microbial communities have closer proximity than more dissimilar communities. We performed two-dimensional NMDS on a Bray-Curtis distance matrix.[81] NMDS of the phylogenetically-based weighted Unifrac distance matrices feature similar trends to that of the Bray-Curtis distance matrix and can be found in the Supporting Information (**Figure A.4** and **A.5**).

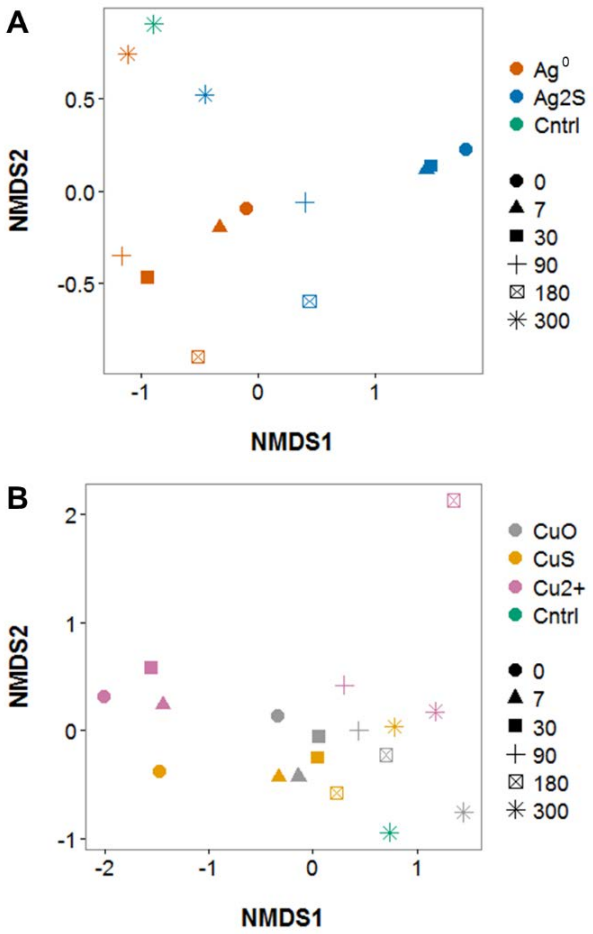

Figure 2.3. ***NMDS plots of Ag- (A) and Cu-dosed (B) mesocosm OTU tables using the Bray-Curtis distance metric.*** *Stresses were 0.074 for the Ag NMDS and 0.12 for Cu.*

NMDS showed several interesting trends. First, the Ag^0- and Ag_2S-dosed communities were dissimilar at 0, 7 and 30 and 90 d (**Figure 2.3A**). At 7 d, both Ag communities shifted slightly to the left from their 0 d communities. But at 30 d, the Ag_2S-dosed community was relatively unchanged compared to 7 d, while the Ag^0-dosed community shifted dramatically to the left. This is likely attributable to a lower overall short-term impact of Ag_2S NPs due to their lower solubility compared to Ag^0 NPs. The Ag^0- and Ag_2S-dosed communities appeared to converge at 180 d, and the communities clustered together at 300 d.

NMDS of Cu-dosed mesocosms show CuO and CuS NP-impacted microbial communities to be similar to one another, but distinct from that of the Cu^{2+} mesocosm through 180 d (**Figure 2.3B**).

Then the Cu^{2+} mesocosm diverged strongly from all other communities. This divergence was concurrent with the 2 orders of magnitude decrease in 16S rRNA gene copies measured at 180 d in the Cu^{2+}-dosed mesocosm (**Figure 2.1**). Like the Ag mesocosms, the microbial communities from all three Cu-dosed mesocosms appeared to converge at day 300.

The NMDS plots (**Figure 2.3**) suggest that surficial sediment microbial communities reacted differently to different Ag and Cu treatments. This observation led us to narrow our focus to detect differential effects of treatment on specific taxa (proportional abundances of dominant taxa for all treatments and sampling times are displayed in **Figure A.6**). We investigated PICRUSt-predicted annotated metagenomes, which suggested treatment-specific effects on important microbial processes, such as photosynthesis and methane metabolism (PICRUSt results discussed below; **Figure 5**), focusing on microbial taxa that could account for the differences in microbial processes observed within the PICRUSt results.

Within the Ag communities, there was evidence of differential impacts on *Cyanobacteria*. The Ag^0-dosed mesocosm *Cyanobacteria* population fell to half its initial proportion at day 7, then steadily dropped at 30 and 90 d, ultimately to less than 7% of the initial *Cyanobacteria* proportion (**Figure 2.4A**). The cyanobacterial population appeared to be negatively affected by Ag_2S at 7 d, as well, dropping by 28% of its initial proportion. However, it rebounded (and peaked) at day 30 and continued to be a dominant taxon on day 90. Importantly, this differential impact on *Cyanobacteria* did not appear to align with observed changes in water column turbidity (*Cyanobacteria* relative abundance in **Figure A.6** and pictures of mesocosms in **Figure A.7** and **A.8**). At 180 d, the proportion of *Cyanobacteria* in both the Ag^0- and Ag_2S-dosed mesocosms was similar (2.2% in Ag^0 and 1.2% in Ag_2S).

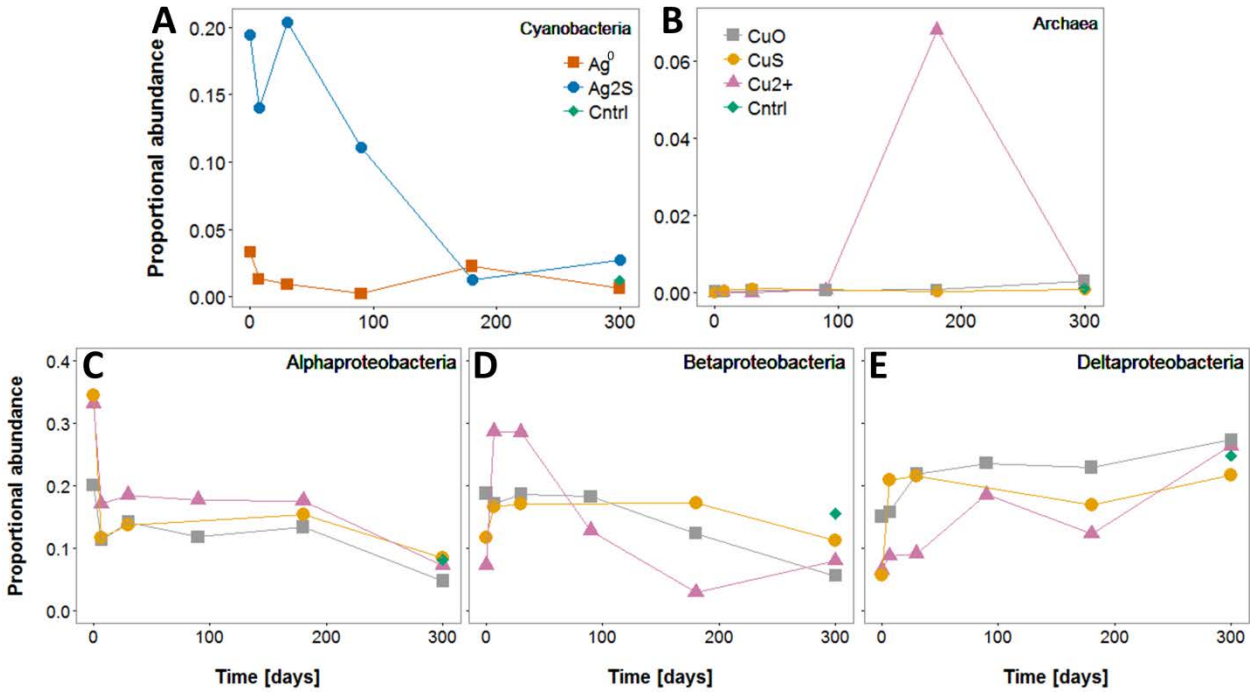

Figure 2.4. ***Proportional abundances of Ag mesocosm Cyanobacteria (A) and Cu mesocosm Archaea (B), α-proteobacteria (C), β-proteobacteria (D) and δ-proteobacteria (E).*** *Note that the legend in B applies to C, D and E.*

These data suggest that *Cyanobacteria* might be vulnerable to Ag^0 but not Ag_2S NPs. Others have similarly observed decreases in autotrophic populations[44] and inhibition of microbial photosynthesis due to Ag NPs.[45] On the longer term, these impacts appeared to be mitigated, likely due to the Ag^0 NP sulfidation that we observed (**Figure A.3A**). As it did within the Ag^0-dosed mesocosm, *Cyanobacteria* proportional abundances dropped in all of the Cu-dosed mesocosms, (**Figure A.6A** and **A.6B**), perhaps suggesting that only Ag_2S is benign towards *Cyanobacteria*.

Cu-dosed mesocosms showed signs of impacts on taxa that were common across all Cu treatments and others that had clear differences between NP and ion treatments. Among the impacts common across the CuO and CuS NPs and Cu^{2+} treatments, we observed sharp decreases (~50% or more compared to day 0) in *α-proteobacteria* for all treatments at 7 d (**Figure 2.4C**). Interestingly, *α-proteobacteria* populations remained low in the Cu mesocosms for the rest of the experiment, in contrast to the Ag mesocosms (**Figure A.6**). We saw short-term differences between the Cu NP and Cu^{2+} mesocosms in two other classes of *Proteobacteria*. For CuO and CuS

mesocosms, *δ-proteobacteria* became more abundant at days 7 and 30 compared to day 0 (jumping to more than 20% by day 30); the Cu^{2+} mesocosm *δ-proteobacteria* proportion remained less than 10% (**Figure 2.4E**). *β-proteobacteria*, meanwhile, was enriched in the Cu^{2+} mesocosm (more than a 4-fold increase from 7% on day 0 to 29% on day 7 and 30) and more or less constant in CuO and CuS NP-dosed mesocosms, where it was less than 20% (**Figure 2.4D**). More prominent than the shifts within proteobacterial classes was the archaeal bloom observed in the Cu^{2+} mesocosm at 180 d. For that sample, the archaeal abundance spiked to 6.8% (**Figure 2.4B**) – a relative abundance that is more than an order of magnitude greater than any other sample. Importantly, all of the spike in abundance consisted of *Methanobacterium*, a genus of methanogenic Archaea.[82] Proportional abundances are commonly analyzed to reveal taxonomic changes.[41,42,83,84] While we cannot be entirely sure that proportional abundances carry over to absolute abundances, the relatively constant qPCR results, save for the Cu^{2+} mesocosm at 180 d (**Figure 2.1**), support the use of proportional abundance as a valuable indicator of microbial community changes.

As discussed above, the Cu^{2+} mesocosm microbial community was unique in terms of bacterial cell density (**Figure 2.1**), alpha diversity (**Figure 2.2**) and community composition (**Figures 2.3B** and **2.4B-E**). We hypothesize that the dosed Cu^{2+} set off a series of ecological disturbances that ultimately led to an enrichment of *Methanobacterium*. At day 300, the Cu^{2+} mesocosm was unique in not having *Egeria densa*, an oxygenating aquatic plant that is considered a wetland ecosystem engineer (**Figure A.8**).[85] We posit that the disruption of the *Egeria densa* life cycle took place prior to 180 d, and most likely by 30 d. Photosynthesis in *Egeria densa* can be impeded by concentrations of Cu^{2+} above 0.5 mg/L.[86] Within the Cu^{2+}-dosed mesocosm, each dosing event contributed approximately 1.9 mg/L Cu^{2+}. Coupled with the influx of organic carbon provided to the surficial sediment by the *Egeria* die-off, the complete loss of the oxygenating *Egeria* likely

lowered the water column oxygen content and allowed for the observed spike of methanogenic *Methanobacterium*. The lower cell density observed in the Cu^{2+} mesocosm at 180 d may be partially explained by the presence of slower-growing anaerobes. [87] Other factors, e.g. water column turbidity due to the *Egeria* die-off, could have inhibited phototrophic bacteria and, thus, contributed to the lower cell density and distinguishing this microbial community, as well.

2.4.D Impacts on predicted metagenomes. Using most closely related organisms' sequenced genomes, PICRUSt translates 16S rRNA gene amplicon datasets into predicted metagenomes.[70] PICRUSt can be predictive of sequenced metagenomes in cases where samples' nearest sequenced taxon index (NSTI) is low.[70] On average, the NSTI values for our samples were 0.141 ± 0.014 (**Table A.1**), which should allow for accurate metagenome prediction.[70]

Complex microbial communities are believed to have functional redundancy, whereby a decrease in taxa performing a given function allows for other, functionally-similar taxa to increase in abundance.[88,89] Functional redundancy can thus lead to stable function, i.e. stable ecological services like geochemical cycling, in the face of perturbations ("natural" and anthropogenic) and community changes.[90] We used PICRUSt to investigate whether the changes in taxa outlined above, e.g. *Cyanobacteria*, were likely to result in functional differences – or whether other taxa were filling the functional holes (i.e. niches).

We observed differences in proportions of annotated photosynthetic genes between the Ag^0- and Ag_2S-dosed predicted metagenomes. After day 0, photosynthesis genes decreased in the Ag^0-dosed mesocosm, while they increased within the Ag_2S-dosed mesocosm through 90 d (**Figure 2.5A**). As with the proportions of *Cyanobacteria* (**Figure 2.4A**), the Ag^0- and Ag_2S-dosed mesocosms had similar levels of photosynthesis genes by 180 d. The same trends were observed in the KEGG

Level 3 Photosynthesis – antenna proteins and Photosynthesis proteins categories (data not shown).

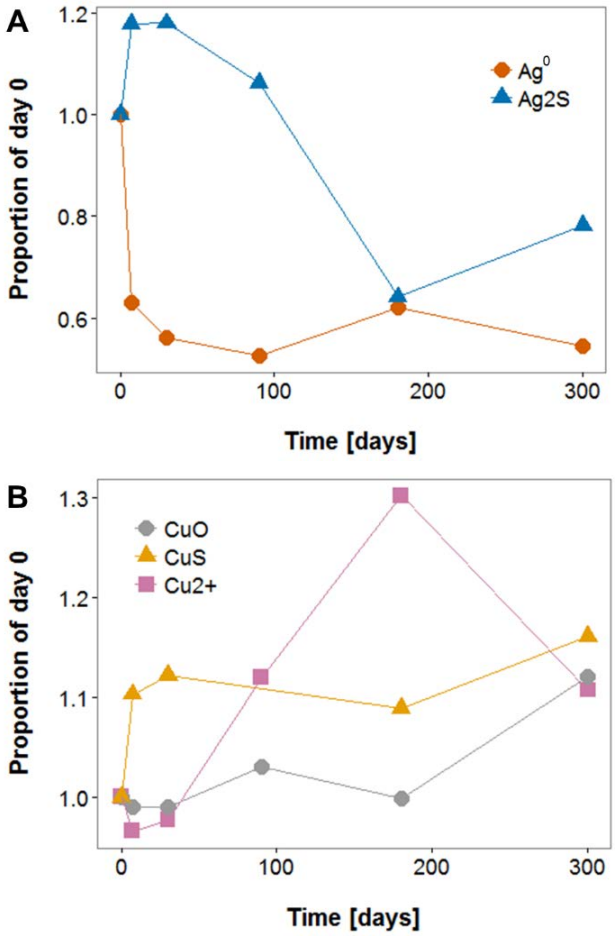

Figure 2.5. ***Proportion (compared to day 0) of Ag mesocosm PICRUSt-predicted, KEGG-categorized photosynthetic genes (A) and Cu mesocosm methane metabolism genes (B).***

Across the Cu-dosed mesocosm metagenomes, we observed differential effects on methane metabolism-annotated genes (**Figure 2.5B**) that align with the trends within the taxonomic data (Figure 4B). At 180 d, the Cu^{2+} predicted metagenome showed a marked increase in methane metabolism (**Figure 2.5B**).

The PICRUSt-predicted metagenomes support our findings that suggest that (1) pristine and transformed Ag NPs had dissimilar short-term effects on surficial sediment microbial

communities, and that (2) effects of CuO and CuS Cu NPs are similar to one another but highly dissimilar to, and less severe than, those of Cu ion.

2.4.E Convergence at 300 days. Differential effects of pristine and transformed Ag- and Cu-based NPs and Cu ion were evident according to all of our metrics. However, we noticed that at 300 days, according to most metrics, all dosed mesocosms, and especially those dosed with ENMs, were similar to the undosed control (**Figures 2.1-2.5**). In order to assess the dissimilarity across all surficial sediment microbial communities at 300 d, we performed NMDS on a Bray-Curtis distance matrix with all samples.

Looking at all samples on a single NMDS plot suggests, through 180 d, treatment-associated divergence, especially within Ag_2S- and Cu^{2+}-dosed mesocosms (**Figure 2.6**). At 300 d all samples converged with one another. This convergence at 300 d agrees with the trends observed in all other metrics (**Figures 2.1-2.5**). In sum, the effect of relatively large doses of Ag and Cu NPs, which are known to be toxic to bacteria, on the highly susceptible surficial sediment microbial community appears, by 300 d, to have been mitigated.

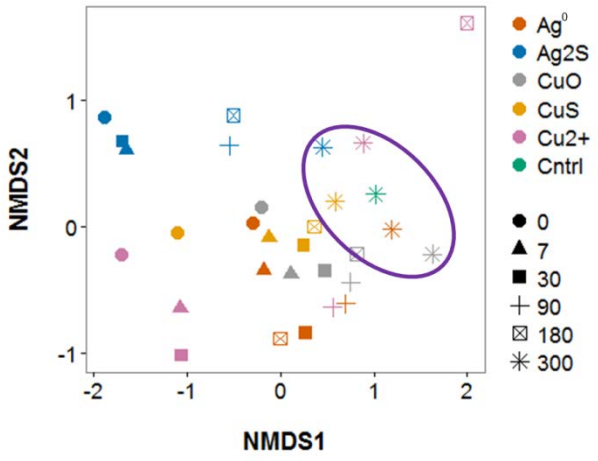

Figure 2.6. ***NMDS plot of a combined Ag- and Cu-dosed mesocosm OTU table using the Bray-Curtis distance metric.*** *NMDS stress was 0.14. Purple oval encloses 300-day samples.*

Microbial community diversity and composition are important indicators of community resilience[75,76] and functions.[77] Many microcosm and mesocosm studies have observed impacts of

ENMs on microbial communities,[42-43,45,91] while others have not.[39,40,92] In agreement with previous work,[32,93] we observed distinct impacts of Ag^0 and Ag_2S NPs on microbial communities and found Cu^{2+} to have greater impacts on microbial communities than CuO NPs. On the other hand, where we observed highly similar impacts of CuO and CuS NPs, previous work with a eukaryotic organism found CuO and CuS NPs to have differential impacts.[94] To the best of our knowledge, this is the first study to compare CuO and CuS NPs' effects on microbial communities. The early divergent behavior and convergence after 180 d support our hypothesis that sulfidation and environmental resilience can mitigate the impacts of ENMs on microbial communities and suggests that, at least in complex systems, environmental factors, such as natural ligands, seasonal turnovers, temperature and sunlight, can overcome the impacts of ENMs.

2.4.F Implications. In this study, large-scale, open air, outdoor mesocosms were used to assess the impacts of pristine and transformed Ag and Cu ENMs on surficial sediment microbial communities in a controlled, yet realistic system. Although duplicate, homogenized subaquatic surficial sediment samples were taken and pooled prior to analyses, with a single mesocosm per treatment, strong conclusions, based on specific findings, such as the differential impacts on specific taxa, are not warranted. Rather, the composite observations suggest that within chemically and biologically complex systems environmental factors, such as the presence of natural ligands, high functional redundancy within communities, and seasonal turnover, are likely to mitigate the long-term effects of these ENMs on microbial communities. The apparent environmental resilience was evident despite a worst case scenario high concentration. This is not the first study to suggest environmental resilience in complex systems exposed to ENMs.[39,40,95] However, this is the first to make this determination with environmentally relevant freshwater wetland systems and within a long-term study. Given the numerous studies suggesting environmental toxicity of ENMs,

the findings also highlight the importance of assessing the hazard of ENMs in environmentally relevant systems, where complex ecological relationships between physical, chemical and biological components are retained. Since ENM dosing regimens can affect their fate,[96] future work should determine whether a different dosing regimen, e.g. low, chronic dosing, leads to similar conclusions.

Metal speciation results did not correlate with the observed impacts on microbial communities for the ENMs, i.e. Ag species quickly converged, yet appeared to have differential short-term effects, while distinct Cu species had the same effects. This suggests that the ability of sulfidation to mitigate short-term biological effects is not universal, but is ENM (and metal) specific. One pair of pristine and transformed ENMs had distinct short-term impacts (Ag^0 v. Ag_2S), but another did not (CuO v. CuS), demonstrating the need to use environmentally relevant species of Ag ENMs, at least for short-term Ag ENM risk assessments. Distinct, and seemingly more severe, environmental effects were observed with Cu ion treatment than with either Cu NP treatment. Overall, our results point towards lower environmental health risk of ENMs than has been purported by studies with pristine ENMs under laboratory conditions.

2.5 ACKNOWLEDGMENTS

We thank Benjamin P. Colman, formerly of Duke University and the Center for Environmental Implications of NanoTechnology (CEINT) and currently of University of Montana, for conversations regarding study design and methodology. We also thank Amit Vikram and Daniel Lipus of the University of Pittsburgh for help with library preparation and DNA sequencing assistance.

2.6 REFERENCES FOR CHAPTER TWO

(1) Nanotechnologies, P. on E. Consumer Products Inventory. *Consumer Products Inventory*. 2015.

(2) Kim, B.; Park, C.-S.; Murayama, M.; Hochella, M. F. Discovery and characterization of silver sulfide nanoparticles in final sewage sludge products. *Environ. Sci. Technol.* **2010**, *44* (19), 7509–7514.

(3) Shah, V.; Jones, J.; Dickman, J.; Greenman, S. Response of soil bacterial community to metal nanoparticles in biosolids. *J. Hazard. Mater.* **2014**, *274*, 399–403.

(4) Heinlaan, M.; Ivask, A.; Blinova, I.; Dubourguier, H.-C.; Kahru, A. Toxicity of nanosized and bulk ZnO, CuO and TiO2 to bacteria Vibrio fischeri and crustaceans Daphnia magna and Thamnocephalus platyurus. *Chemosphere* **2008**, *71* (7), 1308–1316.

(5) Fabrega, J.; Fawcett, S. R.; Renshaw, J. C.; Lead, J. R. Silver nanoparticle impact on bacterial growth: effect of pH, concentration, and organic matter. *Environ. Sci. Technol.* **2009**, *43* (19), 7285–7290.

(6) Sondi, I.; Salopek-Sondi, B. Silver nanoparticles as antimicrobial agent: a case study on E. coli as a model for Gram-negative bacteria. *J. Colloid Interface Sci.* **2004**, *275* (1), 177–182.

(7) Lowry, G. V; Gregory, K. B.; Apte, S. C.; Lead, J. R. Transformations of nanomaterials in the environment. *Environ. Sci. Technol.* **2012**, *46* (13), 6893–6899.

(8) Quadros, M. E.; Marr, L. C. Silver nanoparticles and total aerosols emitted by nanotechnology-related consumer spray products. *Environ. Sci. Technol.* **2011**, *45* (24), 10713–10719.

(9) Chen, X.; Schluesener, H. J. Nanosilver: a nanoproduct in medical application. *Toxicol. Lett.* **2008**, *176* (1), 1–12.

(10) Faunce, T.; Watal, A. Nanosilver and global public health: international regulatory issues. *Nanomedicine (Lond).* **2010**, *5* (4), 617–632.

(11) Liu, R.; Lal, R. Potentials of engineered nanoparticles as fertilizers for increasing agronomic productions. *Sci. Total Environ.* **2015**, *514C*, 131–139.

(12) Blaser, S. A.; Scheringer, M.; Macleod, M.; Hungerbühler, K. Estimation of cumulative aquatic exposure and risk due to silver: contribution of nano-functionalized plastics and textiles. *Sci. Total Environ.* **2008**, *390* (2–3), 396–409.

(13) Dale, A. L.; Lowry, G. V; Casman, E. A. Modeling nanosilver transformations in freshwater sediments. *Environ. Sci. Technol.* **2013**, *47* (22), 12920–12928.

(14) Petosa, A. R.; Jaisi, D. P.; Quevedo, I. R.; Elimelech, M.; Tufenkji, N. Aggregation and deposition of engineered nanomaterials in aquatic environments: role of physicochemical interactions. *Environ. Sci. Technol.* **2010**, *44* (17), 6532–6549.

(15) Quik, J. T. K.; Stuart, M. C.; Wouterse, M.; Peijnenburg, W.; Hendriks, A. J.; van de Meent, D. Natural colloids are the dominant factor in the sedimentation of nanoparticles. *Environ. Toxicol. Chem.* **2012**, *31* (5), 1019–1022.

(16) Dale, A. L.; Lowry, G. V; Casman, E. A. Stream Dynamics and Chemical Transformations Control the Environmental Fate of Silver and Zinc Oxide Nanoparticles in a Watershed-Scale Model. *Environ. Sci. Technol.* **2015**, *49* (12), 7285–7293.

(17) Priester, J. H.; Van De Werfhorst, L. C.; Ge, Y.; Adeleye, A. S.; Tomar, S.; Tom, L. M.; Piceno, Y. M.; Andersen, G. L.; Holden, P. A. Effects of TiO2 and Ag Nanoparticles on Polyhydroxybutyrate Biosynthesis By Activated Sludge Bacteria. *Environ. Sci. Technol.*

2014, *48* (24), 14712–14720.
(18) Karlsson, H. L.; Cronholm, P.; Gustafsson, J.; Möller, L. Copper oxide nanoparticles are highly toxic: a comparison between metal oxide nanoparticles and carbon nanotubes. *Chem. Res. Toxicol.* **2008**, *21* (9), 1726–1732.
(19) Xu, C.; Peng, C.; Sun, L.; Zhang, S.; Huang, H.; Chen, Y.; Shi, J. Distinctive effects of TiO2 and CuO nanoparticles on soil microbes and their community structures in flooded paddy soil. *Soil Biol. Biochem.* **2015**, *86*, 24–33.
(20) Jonas, R. B. Acute copper and cupric ion toxicity in an estuarine microbial community. *Appl. Environ. Microbiol.* **1989**, *55* (1), 43–49.
(21) Suppi, S.; Kasemets, K.; Ivask, A.; Künnis-Beres, K.; Sihtmäe, M.; Kurvet, I.; Aruoja, V.; Kahru, A. A novel method for comparison of biocidal properties of nanomaterials to bacteria, yeasts and algae. *J. Hazard. Mater.* **2015**, *286*, 75–84.
(22) Sekine, R.; Brunetti, G.; Donner, E.; Khaksar, M.; Vasilev, K.; Jämting, Å. K.; Scheckel, K. G.; Kappen, P.; Zhang, H.; Lombi, E. Speciation and Lability of Ag-, AgCl-, and Ag2S-Nanoparticles in Soil Determined by X-ray Absorption Spectroscopy and Diffusive Gradients in Thin Films. *Environ. Sci. Technol.* **2014**, *49* (2), 897–905.
(23) Khaksar, M.; Jolley, D. F.; Sekine, R.; Vasilev, K.; Johannessen, B.; Donner, E.; Lombi, E. In Situ Chemical Transformations of Silver Nanoparticles along the Water-Sediment Continuum. *Environ. Sci. Technol.* **2014**, *49* (1), 318–325.
(24) Wang, Z.; von dem Bussche, A.; Kabadi, P. K.; Kane, A. B.; Hurt, R. H. Biological and environmental transformations of copper-based nanomaterials. *ACS Nano* **2013**, *7* (10), 8715–8727.
(25) Colman, B. P.; Arnaout, C. L.; Anciaux, S.; Gunsch, C. K.; Hochella, M. F.; Kim, B.; Lowry, G. V; McGill, B. M.; Reinsch, B. C.; Richardson, C. J.; et al. Low concentrations of silver nanoparticles in biosolids cause adverse ecosystem responses under realistic field scenario. *PLoS One* **2013**, *8* (2), e57189.
(26) Ma, R.; Stegemeier, J.; Levard, C.; Dale, J. G.; Noack, C. W.; Yang, T.; Brown, G. E.; Lowry, G. V. Sulfidation of copper oxide nanoparticles and properties of resulting copper sulfide. *Environ. Sci. Nano* **2014**, *1* (4), 347–357.
(27) Reinsch, B. C.; Levard, C.; Li, Z.; Ma, R.; Wise, a; Gregory, K. B.; Brown, G. E.; Lowry, G. V. Sulfidation of silver nanoparticles decreases Escherichia coli growth inhibition. *Environ. Sci. Technol.* **2012**, *46* (13), 6992–7000.
(28) Levard, C.; Hotze, E. M.; Colman, B. P.; Dale, A. L.; Truong, L.; Yang, X. Y.; Bone, A. J.; Brown, G. E.; Tanguay, R. L.; Di Giulio, R. T.; et al. Sulfidation of silver nanoparticles: Natural antidote to their toxicity. *Environ. Sci. Technol.* **2013**, *47* (23), 13440–13448.
(29) Liu, J.; Hurt, R. H. Ion release kinetics and particle persistence in aqueous nano-silver colloids. *Environ. Sci. Technol.* **2010**, *44* (6), 2169–2175.
(30) El Badawy, A. M.; Luxton, T. P.; Silva, R. G.; Scheckel, K. G.; Suidan, M. T.; Tolaymat, T. M. Impact of environmental conditions (pH, ionic strength, and electrolyte type) on the surface charge and aggregation of silver nanoparticles suspensions. *Environ. Sci. Technol.* **2010**, *44* (4), 1260–1266.
(31) French, R. A.; Jacobson, A. R.; Kim, B.; Isley, S. L.; Penn, R. L.; Baveye, P. C. Influence of ionic strength, pH, and cation valence on aggregation kinetics of titanium dioxide nanoparticles. *Environ. Sci. Technol.* **2009**, *43* (5), 1354–1359.
(32) Judy, J. D.; Kirby, J. K.; Creamer, C.; McLaughlin, M. J.; Fiebiger, C.; Wright, C.;

Cavagnaro, T. R.; Bertsch, P. M. Effects of silver sulfide nanomaterials on mycorrhizal colonization of tomato plants and soil microbial communities in biosolid-amended soil. *Environ. Pollut.* **2015**, *206*, 256–263.
(33) Dharsana, U. S.; Sai Varsha, M. K. N.; Khan Behlol, A. A.; Veerappan, A.; Thiagarajan, R. Sulfidation modulates the toxicity of biogenic copper nanoparticles. *RSC Adv.* **2015**, *5* (38), 30248–30259.
(34) Lin, S.; Taylor, A. A.; Ji, Z.; Chang, C. H.; Kinsinger, N. M.; Ueng, W.; Walker, S. L.; Nel, A. E. Understanding the transformation, speciation, and hazard potential of copper particles in a model septic tank system using zebrafish to monitor the effluent. *ACS Nano* **2015**, *9* (2), 2038–2048.
(35) Reyes, V. C.; Opot, S. O.; Mahendra, S. Planktonic and biofilm-grown nitrogen-cycling bacteria exhibit different susceptibilities to copper nanoparticles. *Environ. Toxicol. Chem.* **2015**, *34* (4), 887–897.
(36) Beddow, J.; Stolpe, B.; Cole, P.; Lead, J. R.; Sapp, M.; Lyons, B. P.; Colbeck, I.; Whitby, C. Effects of engineered silver nanoparticles on the growth and activity of ecologically important microbes. *Environ. Microbiol. Rep.* **2014**, *6* (5), 448–458.
(37) Yang, Y.; Wang, J.; Xiu, Z.; Alvarez, P. J. J. Impacts of silver nanoparticles on cellular and transcriptional activity of nitrogen-cycling bacteria. *Environ. Toxicol. Chem.* **2013**, *32* (7), 1488–1494.
(38) Li, Z.; Greden, K.; Alvarez, P. J. J.; Gregory, K. B.; Lowry, G. V. Adsorbed polymer and NOM limits adhesion and toxicity of nano scale zerovalent iron to E. coli. *Environ. Sci. Technol.* **2010**, *44* (9), 3462–3467.
(39) Bradford, A.; Handy, R. D.; Readman, J. W.; Atfield, A.; Mühling, M. Impact of silver nanoparticle contamination on the genetic diversity of natural bacterial assemblages in estuarine sediments. *Environ. Sci. Technol.* **2009**, *43* (12), 4530–4536.
(40) Colman, B. P.; Wang, S.-Y.; Auffan, M.; Wiesner, M. R.; Bernhardt, E. S. Antimicrobial effects of commercial silver nanoparticles are attenuated in natural streamwater and sediment. *Ecotoxicology* **2012**, *21* (7), 1867–1877.
(41) Yang, Y.; Quensen, J.; Mathieu, J.; Wang, Q.; Wang, J.; Li, M.; Tiedje, J. M.; Alvarez, P. J. J. Pyrosequencing reveals higher impact of silver nanoparticles than Ag+ on the microbial community structure of activated sludge. *Water Res.* **2014**, *48*, 317–325.
(42) Ma, Y.; Metch, J. W.; Vejerano, E. P.; Miller, I. J.; Leon, E. C.; Marr, L. C.; Vikesland, P. J.; Pruden, A. Microbial community response of nitrifying sequencing batch reactors to silver, zero-valent iron, titanium dioxide and cerium dioxide nanomaterials. *Water Res.* **2015**, *68*, 87–97.
(43) Ge, Y.; Priester, J. H.; Van De Werfhorst, L. C.; Walker, S. L.; Nisbet, R. M.; An, Y.-J.; Schimel, J. P.; Gardea-Torresdey, J. L.; Holden, P. A. Soybean Plants Modify Metal Oxide Nanoparticle Effects on Soil Bacterial Communities. *Environ. Sci. Technol.* **2014**, *48* (22), 13489–13496.
(44) Norman, B. C.; Xenopoulos, M. A.; Braun, D.; Frost, P. C. Phosphorus Availability Alters the Effects of Silver Nanoparticles on Periphyton Growth and Stoichiometry. *PLoS One* **2015**, *10* (6), e0129328.
(45) Gil-Allué, C.; Schirmer, K.; Tlili, A.; Gessner, M. O.; Behra, R. Silver Nanoparticle Effects on Stream Periphyton During Short-Term Exposures. *Environ. Sci. Technol.* **2015**, *49* (2), 1165–1172.
(46) Kayranli, B.; Scholz, M.; Mustafa, A.; Hedmark, Å. Carbon storage and fluxes within

freshwater wetlands: A critical review. *Wetlands* **2010**, *30* (1), 111–124.
(47) Verhoeven, J. T. A.; Arheimer, B.; Yin, C.; Hefting, M. M. Regional and global concerns over wetlands and water quality. *Trends Ecol. Evol.* **2006**, *21* (2), 96–103.
(48) Buesing, N.; Gessner, M. O. Benthic Bacterial and Fungal Productivity and Carbon Turnover in a Freshwater Marsh Benthic Bacterial and Fungal Productivity and Carbon Turnover in a Freshwater Marsh. *Appl. Environ. Microbiol.* **2006**, *72* (1), 596–605.
(49) Hotze, E. M.; Phenrat, T.; Lowry, G. V. Nanoparticle Aggregation: Challenges to Understanding Transport and Reactivity in the Environment. *J. Environ. Qual.* **2010**, *39* (6), 1909.
(50) Furtado, L. M.; Norman, B. C.; Xenopoulos, M. A.; Frost, P. C.; Metcalfe, C. D.; Hintelmann, H. Environmental Fate of Silver Nanoparticles in Boreal Lake Ecosystems. *Environ. Sci. Technol.* **2015**, *49* (14), 8441–8450.
(51) Reinsch, B. C. Chemical transformations of zero-valent iron and silver nanomaterials in natural and model environmental media, Carnegie Mellon University, 2012.
(52) Yin, L.; Cheng, Y.; Espinasse, B.; Colman, B. P.; Auffan, M.; Wiesner, M.; Rose, J.; Liu, J.; Bernhardt, E. S. More than the ions: the effects of silver nanoparticles on Lolium multiflorum. *Environ. Sci. Technol.* **2011**, *45* (6), 2360–2367.
(53) Djoković, V.; Krsmanović, R.; Bozanić, D. K.; McPherson, M.; Van Tendeloo, G.; Nair, P. S.; Georges, M. K.; Radhakrishnan, T. Adsorption of sulfur onto a surface of silver nanoparticles stabilized with sago starch biopolymer. *Colloids Surf. B. Biointerfaces* **2009**, *73* (1), 30–35.
(54) Marion, Giles M; Babcock, K. L. Predicting specific conductance and salt concentrations in dilute aqueous solutions. *Soil Sci.* **1976**, *122* (4), 181–187.
(55) Colman, B. P.; Espinasse, B.; Richardson, C. J.; Matson, C. W.; Lowry, G. V; Hunt, D. E.; Wiesner, M. R.; Bernhardt, E. S. Emerging contaminant or an old toxin in disguise? Silver nanoparticle impacts on ecosystems. *Environ. Sci. Technol.* **2014**, *48* (9), 5229–5236.
(56) Lowry, G. V; Espinasse, B. P.; Badireddy, A. R.; Richardson, C. J.; Reinsch, B. C.; Bryant, L. D.; Bone, A. J.; Deonarine, A.; Chae, S.; Therezien, M.; et al. Long-term transformation and fate of manufactured ag nanoparticles in a simulated large scale freshwater emergent wetland. *Environ. Sci. Technol.* **2012**, *46* (13), 7027–7036.
(57) Suzuki, M. T.; Taylor, L. T.; DeLong, E. F. Quantitative analysis of small-subunit rRNA genes in mixed microbial populations via 5'-nuclease assays. *Appl. Environ. Microbiol.* **2000**, *66* (11), 4605–4614.
(58) Murali Mohan, A.; Hartsock, A.; Bibby, K. J.; Hammack, R. W.; Vidic, R. D.; Gregory, K. B. Microbial community changes in hydraulic fracturing fluids and produced water from shale gas extraction. *Environ. Sci. Technol.* **2013**, *47* (22), 13141–13150.
(59) Caporaso, J. G.; Lauber, C. L.; Walters, W. A.; Berg-Lyons, D.; Huntley, J.; Fierer, N.; Owens, S. M.; Betley, J.; Fraser, L.; Bauer, M.; et al. Ultra-high-throughput microbial community analysis on the Illumina HiSeq and MiSeq platforms. *ISME J.* **2012**, *6* (8), 1621–1624.
(60) Masella, A. P.; Bartram, A. K.; Truszkowski, J. M.; Brown, D. G.; Neufeld, J. D. PANDAseq: paired-end assembler for illumina sequences. *BMC Bioinformatics* **2012**, *13* (1), 31.
(61) Haas, B. J.; Gevers, D.; Earl, A. M.; Feldgarden, M.; Ward, D. V; Giannoukos, G.; Ciulla, D.; Tabbaa, D.; Highlander, S. K.; Sodergren, E.; et al. Chimeric 16S rRNA sequence formation and detection in Sanger and 454-pyrosequenced PCR amplicons. *Genome Res.*

2011, *21* (3), 494–504.
(62) Edgar, R. C. Search and clustering orders of magnitude faster than BLAST. *Bioinformatics* **2010**, *26* (19), 2460–2461.
(63) Wang, Q.; Garrity, G. M.; Tiedje, J. M.; Cole, J. R. Naive Bayesian classifier for rapid assignment of rRNA sequences into the new bacterial taxonomy. *Appl. Environ. Microbiol.* **2007**, *73* (16), 5261–5267.
(64) Caporaso, J. G.; Kuczynski, J.; Stombaugh, J.; Bittinger, K.; Bushman, F. D.; Costello, E. K.; Fierer, N.; Peña, A. G.; Goodrich, J. K.; Gordon, J. I.; et al. QIIME allows analysis of high-throughput community sequencing data. *Nat. Methods* **2010**, *7* (5), 335–336.
(65) Caporaso, J. G.; Bittinger, K.; Bushman, F. D.; DeSantis, T. Z.; Andersen, G. L.; Knight, R. PyNAST: a flexible tool for aligning sequences to a template alignment. *Bioinformatics* **2010**, *26* (2), 266–267.
(66) DeSantis, T. Z.; Hugenholtz, P.; Larsen, N.; Rojas, M.; Brodie, E. L.; Keller, K.; Huber, T.; Dalevi, D.; Hu, P.; Andersen, G. L. Greengenes, a chimera-checked 16S rRNA gene database and workbench compatible with ARB. *Appl. Environ. Microbiol.* **2006**, *72* (7), 5069–5072.
(67) Lozupone, C.; Lladser, M. E.; Knights, D.; Stombaugh, J.; Knight, R. UniFrac: an effective distance metric for microbial community comparison. *ISME J.* **2011**, *5* (2), 169–172.
(68) Wickham, H. ggplot2: elegant graphics for data analysis. Springer New York 2009.
(69) R Core Team. R: A Language and Environment for Statistical Computing. Vienna, Austria 2014.
(70) Langille, M. G. I.; Zaneveld, J.; Caporaso, J. G.; McDonald, D.; Knights, D.; Reyes, J. A.; Clemente, J. C.; Burkepile, D. E.; Vega Thurber, R. L.; Knight, R.; et al. Predictive functional profiling of microbial communities using 16S rRNA marker gene sequences. *Nat. Biotechnol.* **2013**, *31* (9), 814–821.
(71) Kanehisa, M.; Goto, S. KEGG: kyoto encyclopedia of genes and genomes. *Nucleic Acids Res.* **2000**, *28* (1), 27–30.
(72) Tatusov, R. L. The COG database: a tool for genome-scale analysis of protein functions and evolution. *Nucleic Acids Res.* **2000**, *28* (1), 33–36.
(73) Parks, D. H.; Tyson, G. W.; Hugenholtz, P.; Beiko, R. G. STAMP: Statistical analysis of taxonomic and functional profiles. *Bioinformatics* **2014**, *30* (21), 3123–3124.
(74) Fulda, B.; Voegelin, A.; Ehlert, K.; Kretzschmar, R. Redox transformation, solid phase speciation and solution dynamics of copper during soil reduction and reoxidation as affected by sulfate availability. *Geochim. Cosmochim. Acta* **2013**, *123*, 385–402.
(75) Girvan, M. S.; Campbell, C. D.; Killham, K.; Prosser, J. I.; Glover, L. A. Bacterial diversity promotes community stability and functional resilience after perturbation. *Environ. Microbiol.* **2005**, *7* (3), 301–313.
(76) Awasthi, A.; Singh, M.; Soni, S. K.; Singh, R.; Kalra, A. Biodiversity acts as insurance of productivity of bacterial communities under abiotic perturbations. *ISME J.* **2014**, *8* (12), 1–8.
(77) Philippot, L.; Spor, A.; Hénault, C.; Bru, D.; Bizouard, F.; Jones, C. M.; Sarr, A.; Maron, P.-A. Loss in microbial diversity affects nitrogen cycling in soil. *ISME J.* **2013**, *7* (8), 1609–1619.
(78) Shannon, C. E. A Mathematical Theory of Communication. *Bell Syst. Tech. J.* **1948**, *27*, 623–656.

(79) Haegeman, B.; Hamelin, J.; Moriarty, J.; Neal, P.; Dushoff, J.; Weitz, J. S. Robust estimation of microbial diversity in theory and in practice. *ISME J.* **2013**, *7* (6), 1092–1101.
(80) Ramette, A. Multivariate analyses in microbial ecology. *FEMS Microbiol. Ecol.* **2007**, *62* (2), 142–160.
(81) McCoy, C. O.; Matsen, F. A. Abundance-weighted phylogenetic diversity measures distinguish microbial community states and are robust to sampling depth. *PeerJ* **2013**, *1*, e157.
(82) Bapteste, E.; Brochier, C.; Boucher, Y. Higher-level classification of the Archaea: evolution of methanogenesis and methanogens. *Archaea* **2005**, *1* (5), 353–363.
(83) Bibby, K.; Viau, E.; Peccia, J. Pyrosequencing of the 16S rRNA gene to reveal bacterial pathogen diversity in biosolids. *Water Res.* **2010**, *44* (14), 4252–4260.
(84) Caporaso, J. G.; Lauber, C. L.; Walters, W. A.; Berg-Lyons, D.; Lozupone, C. A.; Turnbaugh, P. J.; Fierer, N.; Knight, R. Global patterns of 16S rRNA diversity at a depth of millions of sequences per sample. *Proc. Natl. Acad. Sci. U. S. A.* **2011**, *108 Suppl* (Supplement_1), 4516–4522.
(85) Yarrow, M.; Marin, V. H.; Finlayson, M.; Tironi, A.; Delgado, L. E.; Fischer, F. The ecology of Egeria densa Planchón (Liliopsida: Alismatales): A wetland ecosystem engineer? *Rev. Chil. Hist. Nat.* **2009**, *82* (2), 299–313.
(86) Nekrasova, G. F.; Ushakova, O. S.; Ermakov, A. E.; Uimin, M. A.; Byzov, I. V. Effects of copper(II) ions and copper oxide nanoparticles on Elodea densa Planch. *Russ. J. Ecol.* **2011**, *42* (6), 458–463.
(87) Koike, I.; Hattori, A. Growth yield of a denitrifying bacterium, Pseudomonas denitrificans, under aerobic and denitrifying conditions. *J. Gen. Microbiol.* **1975**, *88* (1), 1–10.
(88) Yin, B.; Crowley, D.; Sparovek, G.; De Melo, W. J.; Borneman, J. Bacterial functional redundancy along a soil reclamation gradient. *Appl. Environ. Microbiol.* **2000**, *66* (10), 4361–4365.
(89) Naeem, S.; Li, S. Biodiversity enhances ecosystem reliability. **1997**, *390* (6659), 507–509.
(90) Bowen, J. L.; Ward, B. B.; Morrison, H. G.; Hobbie, J. E.; Valiela, I.; Deegan, L. A.; Sogin, M. L. Microbial community composition in sediments resists perturbation by nutrient enrichment. *ISME J.* **2011**, *5* (9), 1540–1548.
(91) Judy, J. D.; McNear, D. H.; Chen, C.; Lewis, R. W.; Tsyusko, O. V; Bertsch, P. M.; Rao, W.; Stegemeier, J.; Lowry, G. V; McGrath, S. P.; et al. Nanomaterials in Biosolids Inhibit Nodulation, Shift Microbial Community Composition, and Result in Increased Metal Uptake Relative to Bulk/Dissolved Metals. *Environ. Sci. Technol.* **2015**, *49* (14), 8751–8758.
(92) Quan, X.; Cen, Y.; Lu, F.; Gu, L.; Ma, J. Response of aerobic granular sludge to the long-term presence to nanosilver in sequencing batch reactors: Reactor performance, sludge property, microbial activity and community. *Sci. Total Environ.* **2015**, *506–507*, 226–233.
(93) Rousk, J.; Ackermann, K.; Curling, S. F.; Jones, D. L. Comparative toxicity of nanoparticulate CuO and ZnO to soil bacterial communities. *PLoS One* **2012**, *7* (3), e34197.
(94) Li, L.; Hu, L.; Zhou, Q.; Huang, C.; Wang, Y.; Sun, C.; Jiang, G. Sulfidation as a natural antidote to metallic nanoparticles is overestimated: CuO sulfidation yields CuS nanoparticles with increased toxicity in medaka (Oryzias latipes) embryos. *Environ. Sci.*

Technol. **2015**, *49* (4), 2486–2495.
(95) Tong, Z.; Bischoff, M.; Nies, L.; Applegate, B.; Turco, R. F. Impact of fullerene (C60) on a soil microbial community. *Environ. Sci. Technol.* **2007**, *41* (8), 2985–2991.
(96) Baker, L. F.; King, R. S.; Unrine, J. M.; Castellon, B. T.; Lowry, G. V.; Matson, C. W. Press or pulse exposures determine the environmental fate of cerium nanoparticles in stream mesocosms. *Environ. Toxicol. Chem.* **2016**, *35* (5), 1213–1223.

CHAPTER THREE:

Time-dependent bacterial transcriptional response to CuO nanoparticles differs from that of Cu^{2+} and provides insights into CuO nanoparticle toxicity mechanisms

This chapter is under revision for publication in *Environmental Science: Nano*.

Moore, J.D., Avellan, A., Noack, C.W., Guo, Y., Lowry, G.V., Gregory, K.B. "Time-dependent bacterial transcriptional response to CuO nanoparticles differs from that of Cu^{2+} and provides insights into CuO nanoparticle toxicity mechanisms," *In review.*

3.1 ABSTRACT

Better understanding of the time-resolved gene expression response of bacteria to CuO engineered nanomaterials (ENM) could lead to an improved mechanistic understanding of their antimicrobial effects. In this study, reverse-transcriptase quantitative polymerase chain reaction (RT-qPCR) has been used to characterize a time series of *Escherichia coli* gene expression after exposure to CuO nanoparticles (NP) (100 mg/L as Cu). Two dissolved Cu exposures in concentrations matching observed dissolution from the CuO NPs in the growth medium (1 ppm total Cu after 180 min) were included as a comparison against NP exposure. In the pulse dissolved Cu exposure, 1 ppm Cu was added at the beginning of the experiment. In the gradual dissolved Cu exposure, a total of 1 ppm dissolved Cu was divided into four doses (at 0, 10, 30, and 60 min) that matched the observed CuO NP dissolution. NP exposure led to induction of membrane damage gene expression, which aligns with hyperspectral imaging (HSI) results that identified a high NP affinity for cellular membranes shortly after exposure. Reactive oxygen species (ROS)-responsive genes were not induced for the NP-exposed *E. coli* within the 60 min time scale where Cu- (*copA*, *cueO*, and *cusC*) and protein damage gene (*cpxP*) expression were most induced – Cu^{2+} treatments led to minimal induction. Both Cu^{2+} treatments (pulse and gradual addition) led to higher levels of Cu- and protein damage-responsive gene induction than NP exposure, despite the lower total Cu exposure. For genes induced by all Cu exposures, pulse ion treatment led to temporally distinct transcriptional responses (peak inductions generally at 10 or 30 min) compared to both the gradual ion and NP treatments (peak inductions generally at 60 min). This time-resolved depiction of *E. coli*'s transcriptional response to an antimicrobial soluble ENM identifies a response unique to ENM exposure and highlights the importance of sampling time when considering soluble ENM

biological impacts. It also underscores the need, in nanotoxicity studies, to consider ionic controls that reflect the slow release of ion from soluble ENMs.

3.2 INTRODUCTION

Antimicrobial engineered nanomaterials (ENM) are incorporated into products to inhibit microbial growth. Cupric oxide (CuO) ENMs are among the most potent antimicrobial ENMs,[1] but exactly how CuO ENMs inhibit bacterial growth is not fully understood. Investigating bacterial transcriptional responses to toxicant exposure informs the mechanism of toxicity.[2,3] The dearth of CuO ENM toxicity studies considering gene expression provides an opportunity to deploy measurements of gene expression to more fully understand their interactions with bacteria. As with other soluble ENMs,[4] it is increasingly clear that the dissolved ion plays a prominent role in CuO ENM toxicity.[5] The last decade-plus of research into soluble ENMs has also found that their dissolution is often kinetically limited.[6,7] Taken together, these understandings point to gradual ion release and sampling time as important variables to consider in assessments of soluble ENMs' biological impacts.

The mechanism of CuO ENM microbial toxicity is an open area of research. Because dissolved Cu^{2+} has been described as a primary source of CuO ENM toxicity[5] and ROS generation was long held to be the primary means of Cu^{2+} antimicrobial action,[8] early research into CuO ENM microbial toxicity naturally focused on reactive oxygen species (ROS).[5,9] However, subsequent studies into dissolved Cu^{2+} bacterial toxicity have led to questions about ROS generation as the primary means of the ion's bacterial toxicity. First it was shown that Cu^{2+} does not lead to oxidative DNA damage.[10] Then Macomber & Imlay found that Cu replacement of Fe within amino acid-synthesizing Fe-S protein clusters was the primary mechanism of Cu^{2+} bacterial toxicity, not ROS

generation.[11] Studies of CuO ENM bacterial toxicity have primarily identified ROS generation as the driver of its toxicity.[5,12–15] With dissolved Cu expected to play a prominent role in CuO ENM bacterial toxicity and in light of the aforementioned revelations regarding Cu^{2+} toxicity, it is appropriate to reconsider the mechanisms of CuO ENM bacterial toxicity, which could be important to predicting environmental settings where impact is expected, e.g., oxic versus anoxic, and to efforts to incorporate CuO ENMs as antimicrobial agents.

In addition to questions about the role of ROS generation in CuO ENM microbial toxicity, there is widespread debate around ionic versus "nanoparticle-specific effects" and the relative contributions of each to soluble ENM toxicity.[4,6,16–21] One seemingly unique nanoparticle-specific effect of ENMs is their capacity to adsorb onto bacterial membranes,[22] as has been hypothesized for CuO ENMs.[12,23,24] In light of improvements to the understanding of Cu^{2+} microbial toxicity and ongoing questions of ionic versus nanoparticle-specific biological effects of soluble ENMs, the mechanisms of CuO ENM bacterial toxicity warrant further consideration.

Of the numerous efforts to advance the understanding of bacterial toxicity of ENMs,[5,8,17,23,25] few have utilized bacterial gene expression.[12,24,26–28] Studies of gene expression in response to Cu^{2+} have observed enhanced expression of genes responsive to cell envelope and oxidative stress and protein damage that impairs amino acid synthesis upon exposure to Cu^{2+}.[29–31] To the best of our knowledge, only two studies have utilized gene expression to elucidate CuO ENM bacterial toxicity, the first assaying four *E. coli* genes[12] and the second looking at *Pseudomonas aeruginosa*'s transcriptomic response.[24] In the former study Applerot *et al.* (2012) used promoter-*lux* fusions to measure approximate three-fold increases in expression of three ROS-responsive genes and one membrane biosynthesis gene in CuO ENM-exposed (100 mg/L) versus non-exposed *E. coli* one hour after exposure.[12] In the latter study Guo *et al*. (2017) identified induction of copper

resistance, membrane damage-responsive, and lysogenic bacteriophage genes in response to a range of CuO ENM exposures (1, 10, and 50 mg/L) for 2 hours.[24] Neither of these studies included an ion control for comparison against gene expression responses to CuO ENMs. McQuillan and Shaw (2014) used a microarray approach to compare Ag NP and Ag^+-exposed *E. coli* 10 min after exposure.[26] They observed induction of stress responsive genes, e.g., protein misfolding and metal ion stresses, and a differential transcriptional response to their 40 mg/L Ag NP and 0.4 mg/L $AgNO_3$ exposures that included some evidence of NPs uniquely damaging bacterial membranes.

Most studies comparing ENMs to ionic treatments employ a single pulse input of ions,[5] often at the same concentration as the dosed ENM.[26,32,33] This experimental control fails to recognize an important aspect of soluble ENMs – their kinetically-limited dissolution until the equilibrium dissolution level is reached.[7] Gradual ion addition over time, as opposed to pulse ion addition, has been shown to be important in studies of ENM fate and transport[34] and might provide for a better comparison to ENM's biological impacts. If measurements are made shortly after exposure, comparing biological impacts between a soluble ENM and a pulse exposure of its ionic counterpart would likely suggest a greater effect from the dissolved ion than the ENM because the dissolution kinetics of the ENM are ignored. However, if the measurement is taken at a later time point, when more of the ENM has dissolved, the ENM treatment might appear to have greater impact. Providing a gradual exposure of dissolved metals to match measured ENM dissolution will allow for a more temporally representative comparison of ionic and soluble ENM effects. It is important to note that there are also interesting questions one could ask about the role of space in soluble ENMs' impacts on bacteria, including the potential for enhanced dissolution at the ENM-organism interface, as some have hypothesized.[18,35]

In the present study, gene expression was assayed at four time points over three hours to compare *E. coli*'s transcriptional response to CuO nanoparticles (NP) against an undosed control and two different ionic treatments, a pulse ion exposure and a gradual ion exposure – that allowed for exposure of the bacteria to Cu^{2+} at the equivalent Cu concentration as that released by the CuO NPs, but on different time scales. Alongside the time-resolved transcriptional responses with different Cu exposure, we studied interactions between CuO NPs and *E. coli* and sought to inform the mechanism of CuO ENM bacterial toxicity, assessing (*i*) the physical association of bacteria with NPs, (*ii*) Cu-, oxidative stress-, protein damage-, and membrane damage-associated transcriptional responses, and (*iii*) ROS production and oxidative stress. Our results provide a time-resolved depiction of the effects of an antimicrobial NP on a model bacterium.

3.3 Materials and Methods

3.3.A NP characterization. Uncoated CuO NPs (Sigma Aldrich, St. Louis, MO) reported to be less than 50 nm by the manufacturer were suspended in ultra-pure water (18 megaohm; Barnstead, Ramsey, MN) and analysed by transmission electron microscopy (TEM) using a Hitachi H-9000 TEM microscope (Hitachi, Tokyo, Japan) operating at 300 kV, as has been reported before.[36,37] CuO NPs were probe sonicated (Branson Model 250, Branson Ultrasonics, Danbury, CT) in autoclaved ultrapure water for 15 min at power level 3, as has been reported for other ENMs,[38] and used immediately thereafter. The hydrodynamic diameter was measured in bacterial growth medium (discussed below) immediately after sonication, and both the hydrodynamic diameter and electrophoretic mobility (EPM) of the CuO NPs were measured in the bacterial growth medium at 10 min, 60 min, and 180 min with a Malvern Zetasizer Nano (Malvern Instruments, Malvern, United Kingdom) at 10 mg/L as Cu (**Table 3.1**). The 180 min sample was found to be too

aggregated and polydisperse to determine the ENMs' hydrodynamic diameter. EPM was converted to zeta potential (ZP) using the Smoluchowski equation. The ionic strength of the medium (**Table B.1**) was calculated to be 0.73 M.

Table 3.1 CuO ENM characterization over time. *DLS and ZP values expressed as mean ± one standard deviation (SD) based on three measurements. Hydrodynamic diameters are number means. Zeta potential was calculated from measured EPM data using the Smoluchowski equation. Ionic strength (I) of the medium was calculated to be 0.73. Hydrodynamic diameter at 0 min was 165 ± 72 nm.*

Time [min]	pH	Specific conductance [µS/cm]	Hydrodynamic diameter [nm]	Zeta Potential [mV]
10	6.52	6.23 ± 0.062	203 ± 67	-24.4 ± 1.3
60	6.36	6.38 ± 0.074	383 ± 40	-23.9 ± 0.17
180	6.38	6.45 ± 0.20	n/a	0.0137 ± 0.16

3.3.B CuO NP dissolution. CuO NPs were suspended in bacterial growth medium at 100 mg/L as Cu in triplicate 10% HNO_3 acid-washed culture tubes. Capped tubes were orbitally shaken at 160 rpm at 30ºC. Dissolved Cu was separated using 3 kDa centrifugal filters (Millipore, Billerica, MA), and total and dissolved Cu were measured by inductively coupled plasma mass spectrometry (ICP-MS; Agilent 7700x, Santa Clara, CA) of filtrates acidified to 2% HNO_3.

3.3.C Bacteria and medium. *E. coli* strain NCTC 9001 from ATCC (ATCC 11775, Manassas, Virginia) was grown in a modified bacterial growth medium, minimal Davis medium (MMDM) with glucose at 30°C and 160 rpm on an orbital shaker in capped tubes in the dark (component concentrations can be found in Supplemental Methods (**Table B.1**), unless specified otherwise. *E. coli* frozen stocks were stored at -80ºC and streaked onto Luria-Bertani (LB) agar plates prior to conducting experiments. The day before an experiment, single colonies were picked from the streaked LB plates, and overnight cultures were grown in the growth medium before being diluted 1:50 in pre-warmed medium on the day of the experiment.

3.3.D Characterization of CuO NP-bacterial interactions. *E. coli* **(**~5 x 10^7 CFU/mL according to OD-CFU calibration curves and contemporaneous plating on LB agar plates) in

MMDM was exposed to 100 mg/L (as Cu) of CuO NPs at 30ºC for 30 min, 60 min, and 180 min with shaking at 160 rpm. The exposure concentration was chosen based on preliminary inhibition experiments that suggested that at this bacterial concentration, 100 mg/L CuO NP would have a sublethal impact (as described further in the Supplemental Methods). Previous work investigating CuO ENM bacterial toxicity has also used this concentration.[12] This concentration exceeds past predictions of the environmental concentrations of the most commonly used ENMs by several orders of magnitude.[39] The high concentration is meant to elicit a bacterial response, and it could be relevant to worst-case scenario environmental releases and attempts to incorporate antimicrobial NPs. The physical association between bacteria and CuO NPs was assessed using an enhanced resolution dark–field microscope system (BX51, Olympus, Tokyo, Japan) equipped with a CytoViva Hyperspectral Imaging System (HSI, Auburn, AL). A 20 µL drop of exposed or control culture was mounted between a clean glass slide and a coverslip and observed as is. Cells were observed either at 600X or 1000X magnification. HSIs were acquired using 100% light source intensity and 0.6 s acquisition time per line.

Each pixel of the HSI contains a light reflectance spectrum, showing the light absorption of the material for 356 bands in the 400 to 1000 nm wavelength range. Each pixel thus provides a spectral signature modulated by the nature of the material it contains.[40] Each image has been corrected for the spectral contribution of the lamp used for the images acquisition. The CuO NP spectral library was constructed based on HSI of CuO in growth medium. The mean reflectance spectrum for each particle of the images has been extracted to build a preliminary library, which has been filtered to remove the light reflectance spectra of the medium alone and the undosed cells. The remaining spectra comprised the final CuO NP hyperspectral library, containing specific hyperspectral CuO NP signatures (**Figure B.1** shows specificity tests of that library).

This NP library was then used to identify CuO NPs on images of *E. coli* exposed to CuO NPs. This mapping was processed using a Spectral Angular Mapping (SAM) algorithm in the ENVI software (version 5.2). The algorithm determines a spectral similarity by calculating the angle between spectra and treating them as vectors in a space with dimensionality equal to the number of bands. Here, vectors with angles ≤0.08 rad were deemed equivalent. Pixels containing the CuO NP spectral signal were labeled red. This method has been validated in previous studies of interactions between bacteria and ENMs.[41–43]

3.3.E Transcriptional response experiments. Approximately 5 x 10^7 CFU/mL were exposed to three treatments alongside the undosed control, all in triplicate. The exposure concentration for the CuO NP treatment was 100 mg/L as Cu. There were two Cu^{2+} exposures – a pulse ion exposure and a gradual ion exposure – that allowed for exposure of the bacteria to Cu^{2+} at the equivalent Cu concentration as that released by the CuO NPs, but on different time scales (**Figure 3.1**). For the pulse ion exposure, all of the Cu^{2+} was added at the beginning of the experiment. The gradual ion exposure had the same final Cu^{2+} concentration as the pulse ion exposure, but the Cu^{2+} was added gradually to reflect the kinetically-limited dissolution of the CuO NPs. For the gradual ion exposure, the dissolved Cu concentration that had been measured at 10 min was added at the beginning of the experiment. After sampling at 10 min, enough Cu^{2+} was immediately added to reflect the dissolved Cu at 30 min. The same was done after sampling at 30 and 60 min, with brief vortexing after each addition.

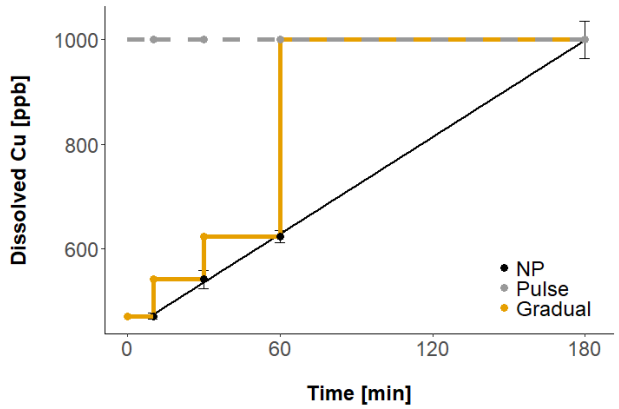

Figure 3.1. ***Dissolved Cu over time under each treatment.*** *Dissolved Cu released by the CuO NP in the exposure medium was measured over 180 min. For the pulse ion treatment, all of the equivalent Cu^{2+} was added at the start of the experiment. For the gradual ion treatment, the equivalent Cu^{2+} was added in four steps (at 0, 10, 30, and 60 min after samples were taken) to represent the slow release of dissolved Cu from the CuO NP.*

First 2.5 mL undosed growth medium, dispersed CuO NPs, and Cu^{2+} were added to acid-washed culture tubes. Next 2.5 mL of 1 x 10^8 CFU/mL bacteria (based on OD, calibration curves, and contemporaneous plating) were added, resulting in a final cell concentration of 5 x 10^7 CFU/mL. Each tube was briefly vortexed prior to being placed on the shaker. Throughout the experiment, tubes were shaken at 160 rpm at 30ºC. At each sampling time point, tubes were vortexed prior to sampling to ensure that the sample was homogeneous. The 1 mL sample was immediately added to RNAprotect Bacteria Reagent (Qiagen, Hilden, Germany), vortexed, and incubated for 10 min at room temperature. Preserved samples were then centrifuged at 5,000 x *g* for 10 min and the supernatant was discarded. RNA was isolated the same day or the following day, in which case pellets were stored at 4ºC.

3.3.F RNA extraction, cDNA synthesis, and nucleic acid quantitation and quality control. RNA was isolated using the RNeasy Mini Kit (Qiagen) following the manufacturer's procedure with slight alterations, including an on-column DNase treatment (Qiagen). One gradual ion 10 min sample became irrecoverably stuck in the centrifuge during RNA extraction, so only duplicates are available for that sample. Full details can be found in the Supporting Information (Supplemental Methods). RNA was quantitated fluorometrically using a high-sensitivity RNA kit

and a Qubit 2.0 (Life Technologies, Carlsbad, CA). RNA integrity was inspected on a 1.3% agarose gel, and RNA purity on a NanoDrop UV-Vis (Thermo Fisher Scientific, Waltham, MA). cDNA was synthesized from 400 ng RNA using iScript Reverse Transcription Supermix (Bio-Rad, Hercules, CA) and was quantitated using a ssDNA kit and the Qubit fluorometer. cDNA sample purity was also assessed on the NanoDrop. Aliquots of cDNA were diluted to 1 ng/µL in RNase/DNase-free water.

Table 3.2. RT-qPCR gene primer sequences.

Gene	Primer sequences
rrsA	F: CCTCATAAAGTGCGTCGTAGTC R: CGTATTCACCGTGGCATTCT
copA	F: GAACAGGCGGATGTGTCTATC R: TTAGCCTTTGGGTGGCTTAC
cueO	F: GGGCTGGAAAGATACCGTTAAG R: GATGGCAGTGCGCCATATAA
cusC	F: CAGCAGTCGGTGGTGAATTA R: TTGCAGCGATGCCAGATAA
ahpC	F: CTGGAGCGTCTTCTTCTTCTAC R: GTATACGTCTACGCCCAGTTTC
katG	F: CGGATCTGGTGTTTGGTTCT R: CGGTCGAGGTTCATCACTTT
soda	F: GTAGAAACCACCGCCAGTTTA R: TTCGGCTCCGTTGATAACTTC
yqhD	F: GTACACACCGTGGAACAGTAT R: TTCGGACCATCTTCGATTAGC
recA	F: GACTGCCTGGCTGAAAGATA R: CTACGCCTTCGCTATCATCTAC
otsB	F: AACCGAAAGGTACCAGTAAAGG R: GTCAGATCATCGCCCAGAAATA
sufA	F: GCTATGTGCTCGACAGTGTTA R: CGACTTCCGTGCCATCAATA
cpxP	F: CTGACGCTGATGTTCGGTTA R: GAAGTCGGTTCAGGCGATAA

3.3.G Quantitative polymerase chain reaction (qPCR) assays. Absolute quantification was performed on a 7500 Real-Time PCR System (Applied Biosystems, Foster City, CA) using

PowerUP SYBR Green master mix (Life Technologies) according to the manufacturer's protocol and primers designed with PrimerQuest (IDT, Newark, NJ). Each 20 µL reaction consisted of 1 ng cDNA, 10 µL master mix, 8 µL molecular biology grade water, and 1 µL of a 10 µM solution containing both forward and reverse primers (for a final primer concentration of 500 nM). Triplicate technical replicates were performed on each sample. (Primer sequences can be found in **Table 3.2**.) Serially diluted *E. coli* K-12 gDNA (ATCC 10798) or a customized gBlock Gene Fragment (IDT) was used for standards. Melt curve analyses showed that each assay produced a single amplicon. When *cusC*, a non-constitutively expressed gene, was not expressed at some undosed and ENM sampling time points, expression values were set equal to expression at 40 cycles to allow calculation of "Fold control" (discussed below). The 16S rRNA gene, *rrsA*, was used as a housekeeping gene against which target genes were normalized. *rrsA* has been validated for this function before.[44] Fold control, ϕ, was calculated by dividing the normalized gene expression of a target gene (x) under a given treatment (y) by the normalized gene expression of the same gene for the undosed control (*undosed*) (**Equation 3.1**).

$$Fold\ control_{xy} = \phi_{xy} = \frac{Expression_{x,y} \Big/ Expression_{\mathrm{rrsA},y}}{\overline{Expression_{x,undosed}} \Big/ \overline{Expression_{\mathrm{rrsA},undosed}}} \qquad \textit{Equation 3.1}$$

Numerous target genes associated with Cu homeostasis and stress responses to Cu^{2+} and NPs (**Figure 3.2**) were assessed. Genes assessed for Cu response were: *copA*, which encodes a Cu efflux pump spanning the inner membrane;[45] *cueO*, which encodes a periplasmic copper oxidase;[46] and *cusC*, which encodes part of a non-constitutive membrane-spanning Cu efflux pump.[47] Genes assessed for downstream stress responses dealing with ROS were: *ahpC*, which encodes for part of the alkyl hydroperoxide reductase and is the primary means by which *E. coli* responds to low

levels of H_2O_2;[48] *katG*, which encodes a catalase;[49] *sodA*, which encodes a superoxide dismutase;[50] *yqhD*, which encodes an aldehyde reductase responsive to lipid peroxidation;[51] and *recA*, which is involved in the response to oxidative DNA damage.[10] The gene assessed for membrane damage was *otsB*, which encodes a trehalose synthase that responds to various membrane stresses.[52–54] The genes assessed for Cu-induced protein damage were: *sufA*, which encodes a scaffold protein for Fe-S cluster assembly;[55] and *cpxP*, which encodes a periplasmic shuttle transporting damaged proteins to proteases.[56] Additional genes were assessed, but are not discussed here to allow for clearer depiction in Figure 3.2.

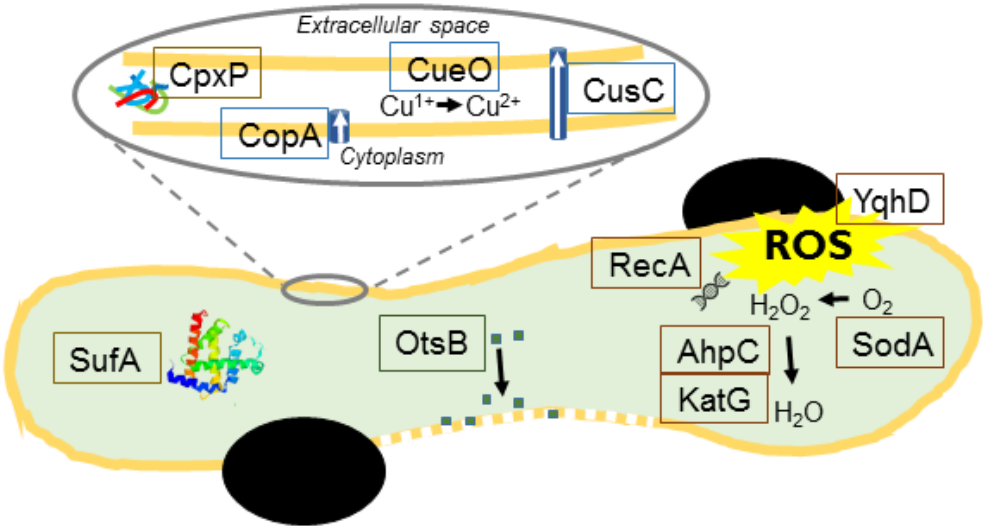

Figure 3.2. ***Schematic of target genes.*** *Proteins for genes of interest are shown in rectangles. Blue rectangles enclose Cu-responsive proteins. Brown rectangles enclose oxidative stress-responsive proteins. Yellow rectangles enclose protein damage-responsive proteins. And the green rectangle encloses the membrane damage-responsive protein. Black ovals represent CuO NPs.*

3.3.H Assessing ROS.

3.3.H.I *Intracellular oxidative stress probe.* The fluorescent H_2DCDFA probe and its derivatives (Molecular Probes, Eugene, OR) are widely used for assessing changes in levels of intracellular oxidative activity and interpreted as changes in intracellular oxidative stress,[57] including in studies assessing CuO ENM toxicity.[5,12] CM-H_2DCFDA, which is reported to have

greater intracellular retention than other forms, was used in this study. Full details are provided in the Supplemental Methods. In brief, *E. coli* that had been grown as described above were resuspended in pH 7.2 phosphate buffered saline (PBS) with 10 µM probe. After a 30 min incubation, the cells were resuspended in MMDM at ~5 x 10^7 CFU/mL. Pulse and gradual Cu^{2+} treatments and an undosed control were prepared as discussed above, again in triplicate. CuO NPs were found to quench the fluorescent signal, so could not be used with the probe. At 10, 60, and 180 min, samples were briefly vortexed and 200 µL was added to three wells within a 96-well plate. Fluorescence emitted at 517 nm after excitation at 494 nm with a 515 nm cutoff was measured on a microplate reader (SpectraMax).

3.3.H.II *Electron paramagnetic resonance (EPR).* EPR was conducted using 5,5-dimethyl-1-pyrroline-N-oxide (DMPO) (Cayman Chemical, Ann Arbor, MI) as a radical spin trap, especially for superoxide and hydroxyl radical species. Previous work has identified superoxide to be the dominant form of ROS generated by CuO NPs.[12] DMPO was dissolved in DMSO to generate a 1 M DMPO stock solution. After 60 and 180 min Cu-exposed and undosed bacteria were incubated with 20 mM DMPO for 15 min at room temperature before being frozen with liquid N_2, where they were stored until EPR measurements were taken. Positive controls in H_2O and MMDM consisted of 0.1 mM Fe^{2+}, 1 mM H_2O_2 and 20 mM DMPO. Full details can be found in the Supplemental Methods. The spin standard used in this study is 1.2 mM Cu(II)-EDTA solution. EPR spectra were processed and plotted using SpinCount software.[58] Detailed discussion of EPR spectra can be found in Supplemental Methods.

3.3.I Statistical analysis. A suite of statistical techniques was used to quantify the extent to which the Cu exposure regimens may have altered the transcriptional response of the bacterial community. All analyses were performed in R (v3.3.1),[59] and an annotated code to reproduce the

presented results is included in the SI (Supplemental statistical and computational methods). Non-parametric hypothesis tests were employed to limit false discoveries arising from possible violations of parametric assumptions (e.g., normality and homoscedasticity). Statistical comparisons of *rrsA* utilized the raw expression data and all other gene comparisons utilized the normalized expression as the independent variable to be compared among groups. To supplement *p*-values, fold change relative to the undosed control was also considered, as others have done before.[60,61] Genes were considered differentially expressed when they met both fold-change ($\geq$ 2-fold or $\leq$ 0.5-fold) and modest statistical significance ($p \leq 0.1$) criteria. Measurements of oxidative stress via probe fluorescence were considered statistically significantly different at $p < 0.05$. For gene expression comparisons, only fold change is discussed herein. Corresponding *p*-values can be found in the Supplemental statistical and computational methods.

Expression data were first visualized for quality control, examining for outliers (see Supplemental statistical and computational methods). For example, extreme values for normalized expression at 10 min within an undosed sample were observed for several genes (see Supplemental statistical and computational methods). To avoid irregular findings resulting from inclusion of outliers, this sample was excluded from calculation of fold control. This had little effect on identification of statistically significantly induced genes (discussed further in the Supplemental statistical and computational methods). After outlier removal, expression data were used as-is in non-parametric hypothesis tests. All pairwise comparisons were performed using the Mann-Whitney test, which probes a location shift, μ, between the sample distributions tested; the null hypothesis, H_0, is always $\mu = 0$. When comparing between treatments and the undosed control one-sided tests were used, while comparisons between treatment methods were made using two-sided tests. The alternative hypotheses for each of these comparisons are shown in Table B.2.

3.4 RESULTS

3.4.A NP characterization and dissolution. TEM showed the CuO NPs to be aggregates of smaller primary particles (**Figure 3.3**). We measured hydrodynamic diameter, ZP, and dissolution of the CuO NPs within the exposure medium over time. Because NPs were found to be polydisperse, number mean diameters are used here. Intensity means and polydispersity indices (PDI) can be found in the SI (**Table B.3**). Initial hydrodynamic diameters indicate that the CuO NPs aggregated quickly in the medium (165 ± 72 nm, mean ± one standard deviation unless otherwise noted). By 10 min NPs were slightly larger and negatively charged (**Table 3.1**). NPs aggregated further by 60 min and were too aggregated and polydisperse to measure at 180 min. Total and dissolved Cu were measured at 10, 30, 60, 180, and 1440 min. Dissolved Cu concentrations were 470 ± 6 μg/L (ppb) at 10 min, with slow increase out to 1,200 ± 20 ppb at 24 hr (1440 min) (**Table 3.3**).

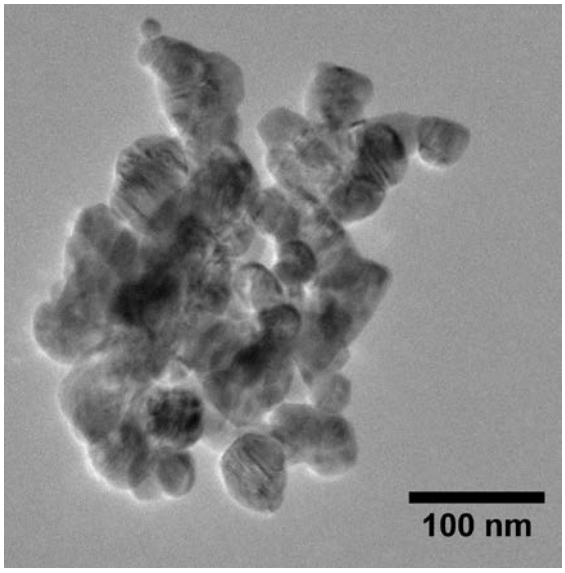

Figure 3.3. ***TEM micrograph of CuO NPs in water.***

Table 3.3. Dissolved Cu levels in the exposure medium over 24 hr. *Dissolved Cu was measured using 3 kDa centrifugal filters, acidification, and ICP-MS analysis of triplicate samples. Values are means ± one standard deviation.*

Time [min]	Dissolved Cu [ppb]
10	470 ± 6
30	540 ± 20
60	620 ± 10
180	1000 ± 40
1440	1200 ± 20

3.4.B Hyperspectral imaging identifies NP-bacterial association immediately after mixing.

HSI was used to determine whether CuO NPs were associating with bacteria. When observed within 30 min of exposure, CuO NPs had a strong tendency to associate with bacteria (**Figure 3.4** and **Figure B.2**). After 60 min, fewer bacteria were observed in association with NPs, and no NP association with cells was observed at 180 min of exposure. The CuO NP spectral signature was not identified in either ion treatment, the growth medium, or the unexposed cells (**Figure B.1** and **B.2**). At 180 min in both the NP and gradual ion treatments, circular structures that appear to be outer membrane vesicles (OMV) are evident (arrows in **Figure 3.4** and **Figure B.2**).

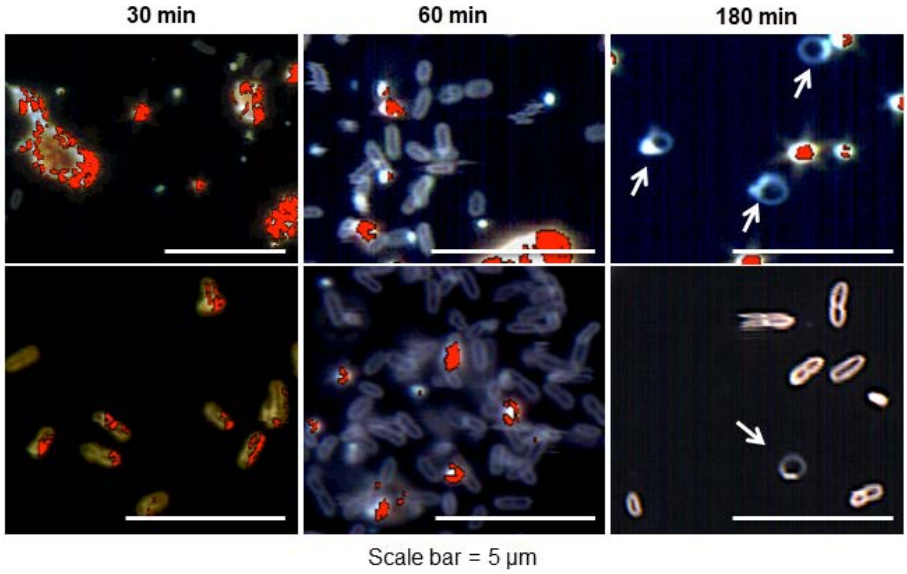

Figure 3.4. ***Time-resolved interaction between NPs and*** **E. coli.** *Hyperspectral imaging (HSI) identified strong interaction between CuO ENMs and bacteria at 30 min (left) and less interaction at 60 min (middle). Interaction could not be detected at 180 min (right). Apparent NP-coated cellular debris is only evident at 30 min. Arrows within the 180 min image point to outer membrane vesicles (OMV). The bottom images are replicates from the same time point as the top.*

3.4.C Transcriptional responses to sublethal CuO NP exposure. Having established that CuO NPs were associating with *E. coli*, we conducted an NP exposure transcriptional response experiment, using RT-qPCR to measure gene expression over time. In order to ensure that our treatment conditions would elicit a bacterial response, we dosed at 100 mg/L (as Cu) CuO NPs. Expression of *rrsA*, the 16S rRNA gene, was generally steady through the first hour of exposure for all treatments (**Figure B.3B**) and was statistically equivalent at all time points, when comparing all treatments. (Pairwise comparisons of undosed and NP-dosed *E. coli* have p-values ≤ 0.1 at the four time points, but less than two-fold differences.) At 180 min, *rrsA* expression had increased across all treatments, suggesting that *E. coli* had entered the exponential growth phase. Viability experiments measuring CFUs over time with each treatment (and the undosed control) corroborated this (**Figure B.4**). This confirms that all Cu treatments served as subinhibitory exposures, as our dose-response data suggested it would given the higher initial bacterial

concentration**.** All subsequent experiments were performed at this exposure concentration unless specified otherwise.

We then turned our attention to identifying *E. coli*'s transcriptional response to CuO NPs based on gene expression of CuO NP-exposed and unexposed cells. As expected, we observed clear increases (compared to undosed controls) in Cu-responsive gene expression in response to CuO NPs (**Figure 3.5A**). Expression of *copA*, an inner membrane-spanning Cu(I) efflux pump,[45] *cueO*, which codes for a periplasmic copper oxidase,[46] and *cusC*, part of a separate Cu(I) efflux system,[47] was induced to 2.0-, 4.5-, and 2.4-fold control, respectively, at 10 min. Induction of all Cu-responsive genes peaked at 60 min, with 13-, 6.0- and 4.8-fold control expression of *copA*, *cueO*, and *cusC*, respectively. At 180 min a decrease in the induction of these genes was observed across treatments.

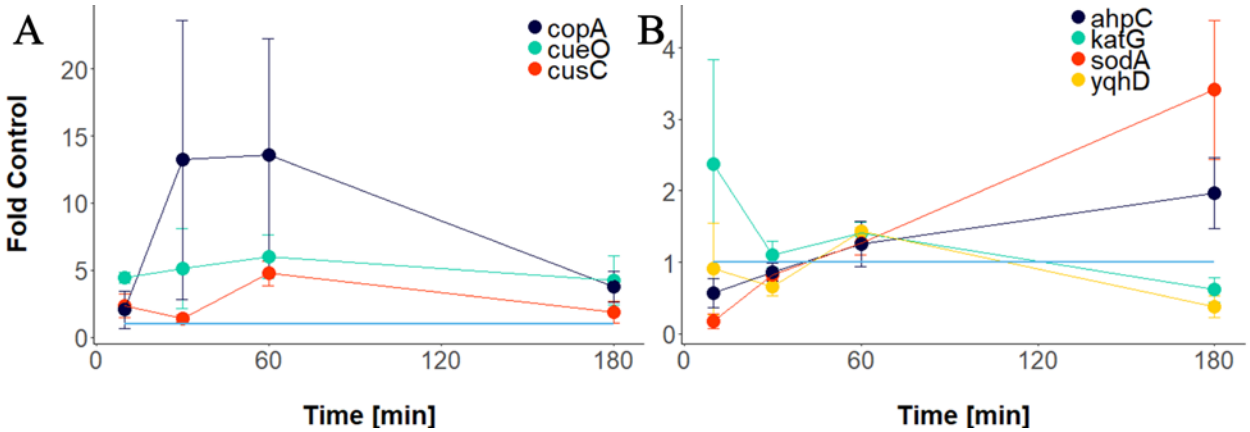

Figure 3.5. ***Gene expression of Cu- and ROS-responsive genes in response to CuO NP stress relative to the undosed control.*** *(A) Cu-responsive genes showed clear induction by 60 min, if not sooner. Statistically significant differences were observed for copA and cueO at 30, 60, and 180 min; for cusC at 10 and 60 min. (B) ROS-responsive genes were not induced by 60 min. Statistically significant differences were observed for sodA at 180 min. The blue horizontal line is fixed at one to represent the expression of the undosed control. Error bars represent one SD of triplicate samples.*

With evidence that CuO NPs were triggering Cu-specific transcriptional responses, we next investigated how the NPs' effects were propagated to other stress responses. We considered ROS-

responsive genes, genes implicated in previous reports of Cu^{2+} stress, and genes believed to be responsive to ENM membrane damage.

To determine whether Cu exposure led to induction of ROS-responsive gene expression, we assayed several separate ROS-responsive genes – *ahpC*, which encodes for part of a peroxidase, *katG*, which encodes for a catalase, *sodA*, which encodes for a superoxide dismutase, and *yqhD*, which responds to lipid peroxidation[51] (**Figure 3.2**). No induction of any of these oxidative stress-related genes was observed within the hour time scale where Cu-responsive genes were most induced (**Figure 3.5B**). *btuE*, which encodes a putative glutathione peroxidase,[62] was not induced either (**Figure B.5**). However, at 180 min one of the ROS-responsive genes was induced: *sodA* at 3.4-fold undosed control. *ahpC* expression increased to just under the 2-fold control threshold (1.96).

Others have argued that Cu-based ENMs could have the potential to induce DNA damage.[17,63] While this too has been called into question for Cu^{2+},[64] we tested expression of *recA*, which codes for a protein that responds to oxidative DNA damage.[65] No induction was evident during the first 3 sampling points, but at 180 min NP treatment appears to induce *recA* expression (**Figure B.6**). Though *recA* does not meet the criteria for differential expression (1.8-fold change), it does align with the induction of *sodA* and *ahpC* also observed at 180 min (**Figure 3.5B**). Like the ROS-responsive genes, *recA* does not appear to shed light on how the CuO NPs are perturbing the bacteria during the height of their Cu response.

We then turned to membrane-mediated and protein damage effects. At 10 min with CuO NP exposure, *otsB* expression was highly variable and not statistically significant (**Figure 3.6A**). At 30 min induction was evident (4.2-fold control) but not at other time points. Expression of *fabA*, which contributes to unsaturated fatty acid biosynthesis[66] and has been observed to be induced by

CuO NP exposure elsewhere,[12] was not induced, and was actually repressed (less than 0.5-fold control) through 60 min (**Figure B.7**). Expression of *rpoE*, which is involved in the σ^E envelope stress response[67] and has been implicated in OMV production,[68] was induced at 10 min (26-fold change) and repressed at 30 min (0.15-fold change), but was equivalent to the undosed control at later time points (**Figure B.8**).

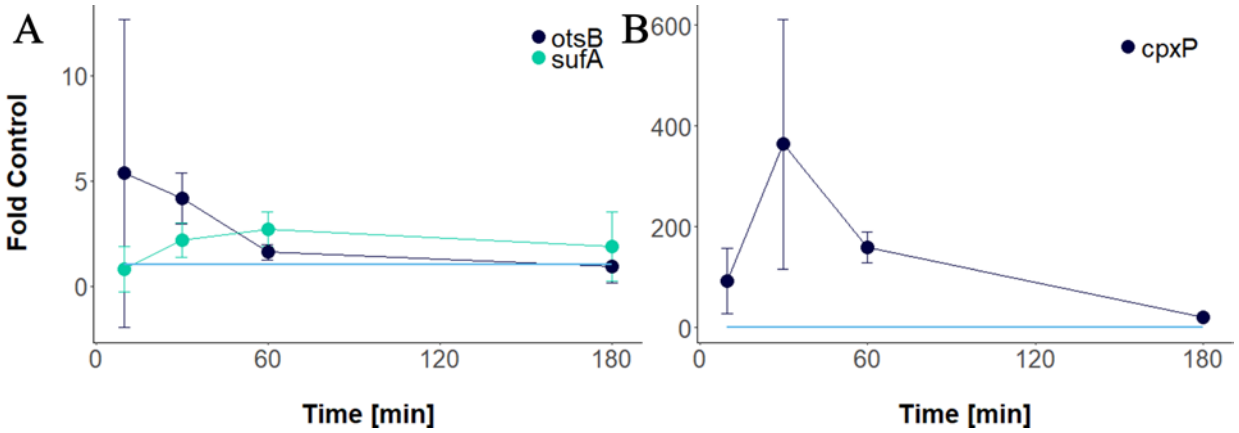

Figure 3.6. ***Gene expression of protein damage- and membrane damage-responsive genes in response to CuO NP stress relative to the undosed control.*** *(A) sufA responds to Fe-S protein damage, and otsB to membrane damage. Statistically significant differences were observed for otsB and sufA at 30 min. (B) cpxP responds to periplasmic protein damage. Statistically significant differences were observed for cpxP at 30, 60, and 180 min. Both sufA and cpxP have been identified as induced by Cu2+ in previous studies.30,31 The blue horizontal line is fixed at one to represent the expression of the undosed control. Error bars represent one SD of triplicate samples.*

Recently the antimicrobial Cu^{2+} literature has pointed to Cu damage to Fe-S protein clusters,[69] which results in the induction of an alternative Fe-S protein assembly pathway, *i.e.*, SufA.[70] We found that with NP exposure both *cpxP* and *sufA* were induced, with the former very highly induced to 92- and 360-fold control at 10 and 30 min, respectively (**Figure 3.6**). A nother gene that encodes for a protein that aids in folding new and misfolded proteins, *spy*,[71] was also highly induced by NP exposure (at 7.6-fold control at 10 min and at or above 49-fold at 30, 60, and 180 min) (**Figure B.9**).

To determine if there is a unique nanoparticle-specific effect, NP-induced responses were compared to ion-induced responses. Cu-, ROS-, and protein damage-responsive genes are all more

induced with Cu^{2+} (pulse) than CuO NP (**Figure 3.7**). Only *otsB* expression is statistically significantly induced with CuO NPs compared to ions and only at 30 min (**Figure 3.7D**), suggesting that ENMs impose a unique and, within our system at least, short-lived form of membrane damage upon *E. coli* – to be clear, a damage not imposed by their ionic counterparts.

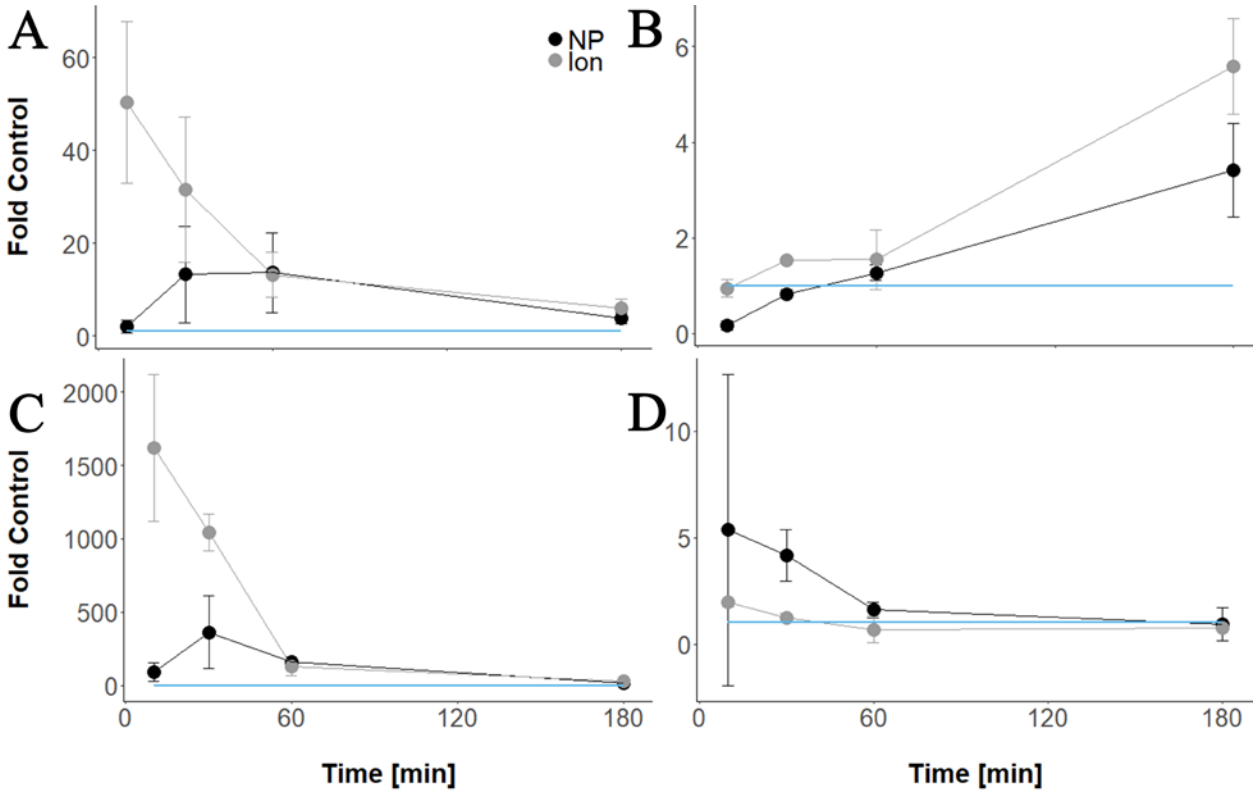

Figure 3.7. ***Gene expression of select genes in response to CuO NP and pulse Cu^{2+} stress relative to the undosed control.*** *(A) copA (Cu-responsive gene, cytoplasmic Cu efflux) shows stronger induction with Cu2+. (B) sodA responds to enhanced oxidative stress induced by superoxide. (C) cpxP responds to periplasmic protein damage. (D) otsB responds to membrane stress and is the only gene whose expression is uniquely induced by CuO NP exposure. The blue horizontal line is fixed at one to represent the expression of the undosed control. Error bars represent one SD of triplicate samples.*

Our gene expression data suggest that ROS damage plays a minimal role in explaining the bacterial toxicity of our CuO NPs. While this agrees with recent findings questioning the primacy of ROS damage in Cu^{2+} toxicity,[69] it does run counter to recent CuO ENM bacterial toxicity studies.[5,12,23] Thus, we set out to verify the ROS-responsive gene expression data with evidence of intracellular oxidative stress, with the standard fluorescent probe CM-H_2DCFDA, and ROS

abundance, with EPR with spin trapping. CuO NPs quenched the fluorescent signal from the probe, so we were not able to use them with the intracellular probe. Fortunately, Cu^{2+} did not, and ROS-responsive gene expression with either treatment was higher than that for CuO NPs in almost every case (**Figures 3.7B**, **B.5**, **B.6**, and **B.10**), suggesting that Cu^{2+}-induced oxidative stress measurements might serve as maxima for what could be expected for our CuO NP treatment. Oxidative stress of ion-exposed and undosed *E. coli* at 10 and 60 min were nearly identical (**Figure 3.8A**). At 180 min, oxidative stress was still statistically equivalent across treatments (*p*-value = 0.061), despite the clear separation between both ion treatments and the undosed control.

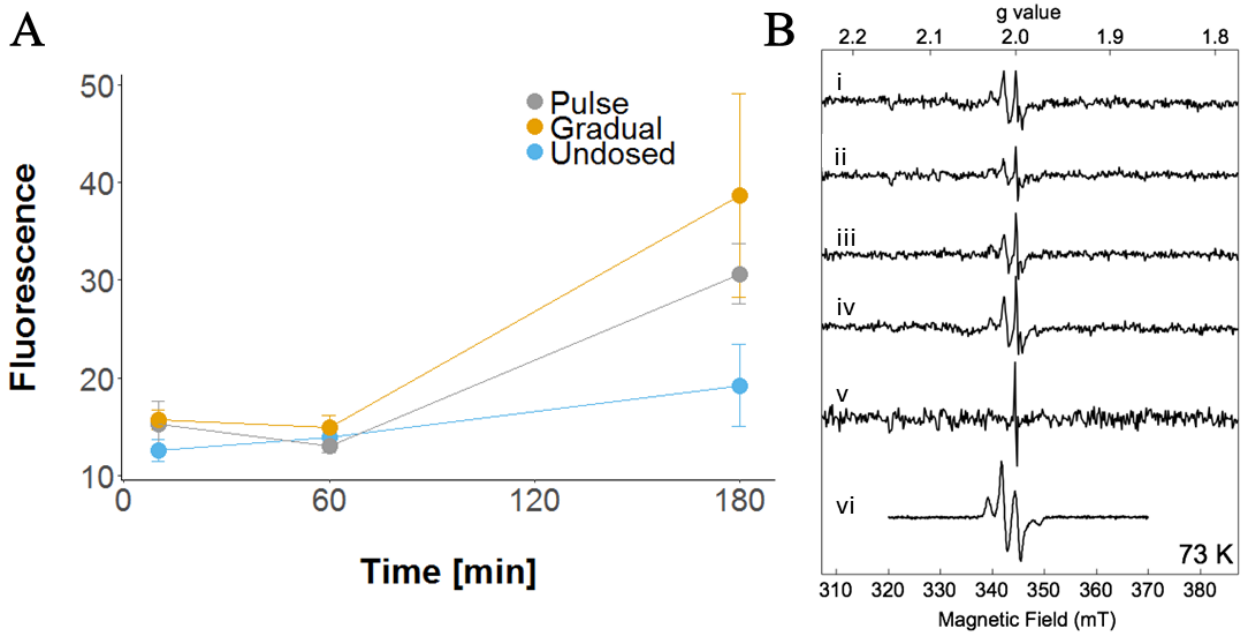

Figure 3.8. ***Oxidative stress and ROS radical measurements.*** *(A) A fluorescent probe used to measure oxidative stress found no statistical difference between Cu2+-exposed and undosed samples at 10, 60, or 180 min. The CuO ENMs were found to interfere with the fluorescent signal. Error bars represent one SD of triplicate samples. (B) Selected X-band EPR spectra of DMPO treated samples: (i) Gradual Cu2+-dosed bacteria at 180 min; (ii) Gradual Cu2+-dosed bacteria at 60 min; (iii) pulse Cu2+-dosed bacteria at 180 min; (iv) CuO NP-dosed bacteria at 180 min; (v) undosed bacteria at 180 min; (vi) positive control in H2O. The Mn2+ ion signal has been removed for each spectrum except for spectrum f, where no Mn2+ ion was present. Measurement conditions: microwave frequency, 9.64 GHz; microwave power, 20 uW; modulation amplitude, 0.3 mT; modulation frequency, 100 kHz; temperature, 73 K.*

To follow up on these inconclusive oxidative stress results and to attempt to characterize ROS generation in response to CuO NPs, we conducted EPR with a spin trapping reagent (DMPO). (Detailed discussion of EPR spectra can be found in the Supplemental Methods, along with raw

and Mn^{2+} signal-removed spectra for all samples and controls [**Figures B.11** and **B.12**].) EPR measurements of DMPO-trapped radicals at 60 min could not detect ROS (in the form of DMPO-OH radical adducts) within our CuO NP or pulse Cu^{2+}-dosed systems, but did detect low concentrations in the gradual Cu^{2+} sample (~2 µM DMPO-OH radical adduct with a four-line splitting EPR signal) (**Figures 3.8B, B.11,** and **B.12**). At 180 min low levels of DMPO radical adducts (<5 µM) were measured in all Cu-exposed samples. None was measured in the undosed bacteria. Low levels of DMPO radical adducts were also observed in abiotic controls with CuO NPs or Cu^{2+} (<5 µM).

Gradual ion addition was included as an additional treatment to replicate the slow release of dissolved Cu from our CuO NPs (**Figure 3.1**). The Kruskal-Wallis test identified differences in gene expression responses among the Cu treatments for *copA* at 10 and 180 min and for *cpxP* at 10 min (**Figure 3.9**). For *copA* the pulse treatment appeared to lead to a peak response at 10 min, while the gradual and NP treatments appeared to peak at 60 min (**Figure 3.9A**). Similarly, expression of *cpxP* for the pulse treatment appeared highest at 10 min, while the gradual ion response appeared to be highest at 30 min and exceed that of the pulse ion at 60 min (**Figure 3.9B**). This apparent temporal distinction among Cu treatments led us to investigate the response across genes induced by Cu exposure (for induced versus non-induced genes see **Figure B.14**). Expression profiles of all genes induced across Cu exposures (*copA*, *cueO*, *cusC*, *sufA*, *cpxP*, and *spy*) were significantly different at 10 min, with the pulse ion treatment inducing higher expression at early time points than either the gradual ion or NP-treated bacteria (**Figure B.9C**). To further investigate these potentially temporally distinct responses, we investigated bootstrapped change in fold control, or "lag," (from 10 to 30 min, 30 to 60 min, and 60 to 180 min) data sets (further detail provided in Supplemental statistical and computational methods). The distribution of parameters

fit to linear models of each treatment's lag show considerable overlap between gradual and NP treatments and little to no overlap among pulse and the other two treatments indicating that gradual ion addition better represents the temporal gene expression response to CuO NPs.

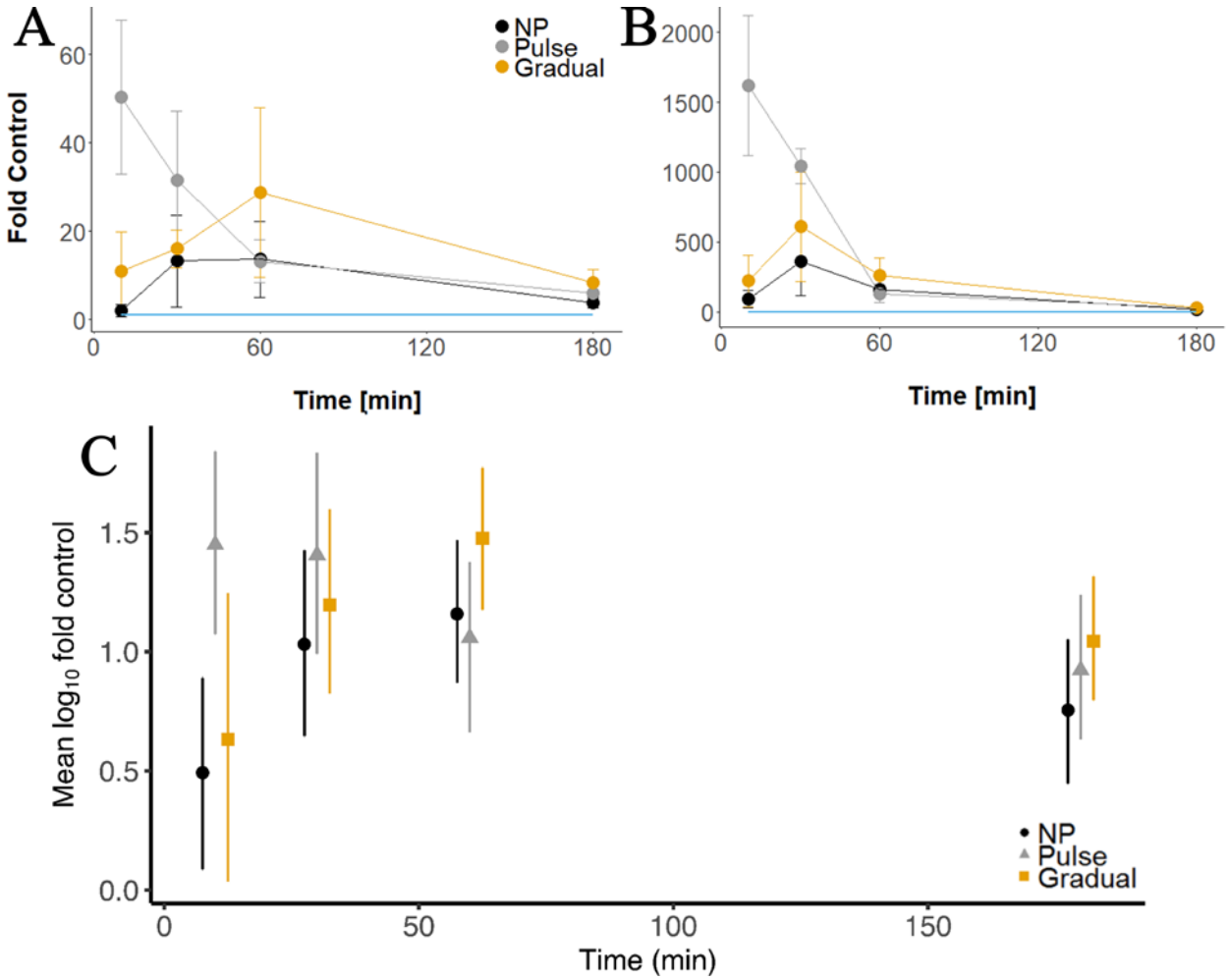

Figure 3.9. ***Gene expression of induced genes in response to CuO NPs and pulse and gradual Cu^{2+} stress relative to the undosed control.*** *Gradual ion treatment generally appeared to induce higher gene expression at later time points than the pulse ion treatment, as can be seen for (A)* copA *(Cu-responsive gene, cytoplasmic Cu efflux) and (B)* cpxP *expression. Statistically significant differences were observed for* copA *at 10 and 180 min and for* cpxP *at 10 min. The blue horizontal line is fixed at one to represent the expression of the undosed control. Error bars represent one SD of triplicate samples. (C) The mean fold control of all induced genes shows that NP treatment generally appeared to lead to the lowest expression for induced genes. The pulse ion treatment seemed to lead to a different trajectory of transcriptional responses,* e.g., *decreasing at 60 min, than either the gradual ion or NP treatment. Error bars represent the 95% credible interval on the mean from 1000 bootstraps.*

3.5 DISCUSSION

Themes cut across our time-resolved NP characterization, HSI, transcriptional assays, and oxidative stress and EPR results, namely: (*i*) CuO NPs appeared to induce a short-term membrane stress that ion exposures did not; (*ii*) Outside of apparent membrane stress, CuO NPs seemed to lead to a more moderate Cu-induced transcriptional response than two-order-of-magnitude lower equivalent dissolved Cu treatments; (*iii*) Neither ROS-responsive genes nor ROS themselves were evident on the same time scale as the peak Cu and protein damage responses, and (*iv*) Given slow ion release from our CuO NPs, time of sampling for detecting biological impacts and of ion addition for dissolved Cu controls were important experimental variables. We close this section with a discussion of the role that population dynamics likely played in this study.

3.5.A CuO NPs uniquely affect bacterial membranes. Early studies into antimicrobial ENMs pointed to membrane perturbation as a factor in their toxicity,[72,73] as have more recent studies of CuO ENMs.[5,12,23] In this study, HSI demonstrated NP association with bacterial membranes shortly after NP exposure (**Figure 3.4**). This is consistent with the induction of a membrane stress response gene, *otsB*, for the NP-dosed *E. coli* and uniquely at 30 min (**Figure 3.7D**). Previous reports of *E. coli* transcriptional responses to Ag and TiO_2 ENMs also identified increases in trehalose synthesis gene expression.[26,27] Combined, these data point to temporally distinct CuO NP adsorption onto bacterial membranes with NPs adhering onto membranes and eliciting a response shortly after exposure (within 30 min). The lack of evident NP-bacteria association and *otsB* induction at later points could be due to several factors, including: (*i*) CuO NPs killing those cells they are associated with at early time points and then being bound by cellular debris, precluding association at later time points, and/or (*ii*) aggregation and settling of NPs rendering them unavailable to the planktonic (suspended) bacteria. It is important to note that apparent cell

debris was observed at 30 min, but not at later points, which adds weight to the former argument (**Figure 3.4**). We envision a scenario where CuO NP adsorption onto a bacterium leads to considerable cell stress – exactly what form of stress, we do not yet know. Based on the reduced number of NP-bacteria associations at later time points, the associated NP might be leading to cell death, after which the NP remain attached to the cell debris, preventing further contact with new dividing cells.

3.5.B Beyond membrane stress, CuO NPs elicit similar transcriptional response to Cu^{2+}, but more moderate. Our gene expression data show inductions of *cpxP*, *sufA*, and *spy* for all Cu treatments (**Figures 3.6A**, **3.9B**, **B.9**, and **B.13**). At 30 min, *cpxP* induction ranges from 360 to 1,000-fold, and at 60 min all treatments induce over 100-fold the undosed control's expression. These data point to protein denaturation and impaired Fe-S protein cluster assembly as important contributors to the bacterial toxicity of the CuO NPs in our experimental system. Previous studies into the mechanism of bacterial toxicity of Cu^{2+} have also identified strong induction of *cpxP* and *sufA*.[30,31] It is likely, then, that both protein and membrane damage are important aspects of the mechanism of CuO ENM bacterial toxicity.

There was a clear difference between genes induced by Cu exposure (*copA*, *cueO*, *cusC*, *sufA*, *cpxP*, and *spy*) and non-induced genes (**Figure B.14**). NP-treated *E. coli* appeared to demonstrate lower maximum gene induction than pulse ion-treated *E. coli* for genes induced across all Cu exposures (**Figure 3.7A-C**). This trend is evident across the induced genes (**Figure 3.9C**), suggesting that CuO NPs generally impose a similar, but less severe perturbation than Cu^{2+}, even when Cu^{2+} is dosed at a level 1/100 of that of the CuO NP in terms of total Cu.

Some have hypothesized that by associating with bacteria, NPs could have unique effects due to their dissolution in the immediate vicinity of a bacterium.[18,35] If enhanced dissolution at the

bacterial interface were occurring, one would expect NP-exposed bacteria to face higher dissolved Cu levels than what we measured in the bulk. This should seemingly lead to higher induction of Cu-responsive genes. In this work, the ion treatments produce higher Cu-responsive gene induction (**Figure 3.9**), so this potential mechanism seems unlikely. An alternative explanation could be that NP adsorption and subsequent dissolution provides overwhelming stress that incapacitates and kills cells. In this scenario, one would not see an enhanced Cu response because the cells with NPs adsorbed onto them would be dead. In light of the NP-specific induction of *otsB* (**Figure 3.7D**), which suggests that bacteria with adsorbed NPs are able to mount some defense, this alternative scenario seems unlikely. The apparent trend of NPs inducing lower levels of expression than ion treatments observed here suggests that, at least within our experimental system, dissolution of NPs adsorbed onto bacterial outer membranes still elicits less of a Cu transcriptional response than does the bulk average dissolved ion.

Why do CuO NPs impose lower stress? Dissolved Cu has been found to induce higher bacterial toxicity than nano-based ENMs.[5,17] In this study, the NP treatment matches the dissolved Cu present in the pulse ion treatment only at 180 min, and in the gradual ion treatment at 10, 30, 60, and 180 min (**Figure 3.1**). Otherwise, the concentration of dissolved Cu is higher for both ion treatments than for the CuO NP, which most likely explains the lower observed impact of the NP treatment.

Interestingly, we also detected what appear to be OMVs at 180 min with the NP and gradual ion treatments, but not in the pulse ion treatment (arrows in **Figures 3.4** and **B.2**). A previous report investigating ZnO NPs also pointed to OMV production as a response to NP stress.[74] Envelope stress can induce bacterial OMV production, in response to damaged proteins or lipids accumulating in the periplasmic space and/or to sequester a stressor.[75] HSI (**Figure 3.4**) and *otsB*

gene expression (**Figure 3.6A**) suggest that NP treatment perturbs bacterial membranes, while *cpxP* expression (**Figure 3.6B**) provides support for degraded periplasmic proteins across all treatments. OMVs were only produced with NP and gradual ion treatments, suggesting that this might be in response to the sustained stress posed by NPs and gradual ion addition. Future efforts to elucidate NP impacts on bacteria should investigate their effect on OMV production.

3.5.C No evidence of oxidative stress during peak Cu response. ROS damage was long the paradigm under which Cu^{2+} toxicity was viewed.[64,76] This paradigm has continued to dominate explanations of CuO ENMs' antimicrobial effects,[5,12,15] whereas the Cu^{2+} literature has identified alternatives as the primary means of toxicity, namely, damage of Fe-S protein clusters.[11,77] The oxidative stress probe and EPR data corroborate the findings of our gene expression time series and further suggest that ROS played little to no role in the hour time frame where the strongest signs of toxic response to CuO NPs and Cu^{2+} were observed. Two possible explanations for the higher oxidative stress (if not statistically significantly higher) (**Figure 3.8A**), spin-trapped ROS radicals (**Figure 3.8B**), and the *sodA* induction (**Figure 3.5B**), and apparent *ahpC* and *recA* induction (**Figure B.6**), at three hours are: (*i*) displacement of Fe in Fe-S proteins by Cu, allowing for Fe-induced Fenton chemistry and (*ii*) enhanced ROS production due to accelerated metabolism during the exponential growth phase (**Figure B.4**). Both explanations warrant further study in future reports of the role of ROS in CuO ENM bacterial toxicity. To fully explain this unique induction of ROS-responsive genes at 180 min might also require an improved understanding of the role growth phase plays in stress-responsive gene expression, given that all samples were growing exponentially at this time point.

Gunawan *et al.* and Applerot *et al.* report on the ROS-mediated bacterial toxicity of CuO ENMs.[5,12] Our data contrast with their findings. We believe CuO NP dissolution and related

factors, e.g., dose, particle size, and exposure medium, are likely contributors to our contrasting findings. In Applerot *et al.* CuO NPs with a 5 nm diameter (per DLS) were dosed at 100 mg/L into an aqueous buffer.[12] Importantly, Applerot *et al.* found that these small CuO NPs generated more ROS than larger CuO NPs with a 45 nm hydrodynamic diameter (per DLS), which both generated more ROS than a micron-scale CuO (~900 nm per DLS).[12] According to initial DLS measurements in the bacterial medium, our CuO NPs were large, polydisperse aggregates with a hydrodynamic diameter of 165 ± 72 nm. Applying the same logic as that in Applerot *et al.*, we would expect less ROS than is generated by either of Applerot *et al.*'s NPs. Our results suggest that this might be the result of lower dissolution. The ROS-generating Fenton chemistry that is typical of Fe and Cu is based upon the presence of dissolved metal species.[78] We measured 1% dissolution at 180 min, generating only 1 ppm Cu^{2+}. With smaller CuO NPs, Applerot *et al.*'s system might have been expected to produce more dissolved Cu than ours.[79] Dissolution data is not provided in their study.

In Gunawan *et al.* CuO NPs with a diameter of 14 nm (d_{ssa}) were dosed at 480 mg/L into LB medium, a rich growth medium.[5] The rich growth medium facilitated the dissolution of the CuO NPs, and 365 ppm dissolved Cu were measured at 180 min, over 300 times the dissolved Cu released by our CuO ENMs. Here again, the concentration of dissolved Cu is likely the predominant factor that explains the differences between our findings and those of Gunawan *et al*.

3.5.D Time-dependency of transcriptional response to ENM and ion treatments and its implications. We measured increasing levels of dissolved Cu released by CuO NPs over time (**Table 3.4**), and we assayed *E. coli*'s transcriptional responses to CuO NP exposure at four different time points over three hours. Given the importance of dissolved Cu to CuO ENM toxicity, and the slow dissolution of the CuO NPs, we expected the biological impacts of CuO ENM treatment to be time-dependent. As we had hypothesized, the time-dependency of CuO NP gene

induction was different than that of the pulse ion, with maximum NP induction levels appearing lower than and delayed compared to the pulse ion treatment (**Figures 3.7** and **3.9**).

Alongside the typical NP and pulse ion treatments, we included a gradual ion treatment where Cu^{2+} was added at the same total level as in the pulse treatment but in four steps (**Figure 3.1**). This treatment was intended to better reflect, compared to the pulse treatment, the gradual release of ion from the CuO NPs. Expression of *copA* and *cpxP* exemplify the differences between the two ion treatments over time (**Figures 3.9A-B**). In the case of *copA* and *cpxP*, statistically significantly different expression among Cu treatments was measured at 10 min. Linear modeling of the lag response over time show that the gradual ion better represents the gene expression response to CuO NPs than does the pulse ion treatment. The differences between pulse and gradual ion addition demonstrate that differential impacts can result from different ion input regimens and highlight the importance of selecting appropriate controls and experimental designs for relevant comparisons between soluble ENMs and their ionic phases.

3.5.E The role of population growth in observed responses to Cu exposure. Through 90 min bacteria under all conditions (treated and undosed) were in lag phase (**Figures B.3B** and **B.4**). At 180 min all bacteria have increased in number and entered exponential growth (**Figure B.4**), reducing the ratio of Cu to bacteria, which is known to affect bacterial impacts of antimicrobial ENMs.[80] In our experiment, the reduced ratio of Cu to bacteria at 180 min, coupled with the apparent sequestration of NPs and presumed complexation of Cu^{2+}, appears to result in the overall reduction of Cu-responsive gene induction (**Figures 3.5A**, **3.6**, **3.7A**, **3.7C**, **3.7D**, **3.9**).

3.6 CONCLUSIONS

We investigated bacterial responses to CuO NPs over three hours to improve the understanding of the bacterial effects of CuO ENMs. Our data suggest that CuO ENMs exert NP-specific membrane damage that equivalent ionic treatments do not. Beyond the membrane damage, CuO NPs appear to induce a similar, but more moderate stress response than Cu^{2+}. Importantly, the response to the ENM is temporally distinct from that of the pulse ion. Our data, which demonstrate little to no ROS response to NP exposure concurrent with peak Cu stress transcriptional response, also call for future studies to examine factors beyond oxidative stress when explaining CuO ENM bacterial toxicity. Along with these insights into the likely mechanisms of CuO ENM bacterial toxicity, our study appears to reveal important takeaways regarding time and ion controls for future nanotoxicity research. Soluble ENM dissolution is typically kinetically limited. Given that the biological impacts are often linked to released ionic species, a full picture of soluble ENM toxicity requires consideration of time. Despite an improved understanding of the role of slow ion release from soluble ENMs, many studies of dissolving ENMs compare ENM impacts to those of an ion by adding the ENM and ion at the beginning of the experiment (including previous work from this team). When adding Cu^{2+} in a single pulse versus gradually, temporally distinct bacterial transcriptional responses were evident, with the latter tracking better with responses to the NPs. We expect that, if others incorporate gradual ion controls, they will see the same.

Many of the antimicrobial ENMs whose nanotoxicology is the focus of vast research efforts, *e.g.*, Ag, ZnO, and, of course, Cu-based ENMs, are soluble and the dissolved ion is expected to play a large role in the ENMs' toxicity, if not the primary role.[4,6,16–21] It is likely that the biological impacts of these ENMs and others demonstrate similar time and dependence. That fact, coupled

with the apparent time-dependency of CuO NP biological impacts assessed herein, highlight two points relevant to future studies investigating nanotoxicology: (*i*) sampling time for soluble ENM impacts can be an important variable and (*ii*) comparing soluble ENM and ion impacts at a single time point may be inadequate. If multiple time points are not considered, it is possible that potential impacts might be underestimated, or missed altogether. This could be especially important in consideration of appropriate sampling time points for ENM toxicity assessments. And for those studies comparing ENM and ionic impacts, if ENM and ion impacts are analyzed at a single time point, it is possible, if not likely, that parameters important to the respective potential impacts, including peak impact and duration of impact, will remain unknown.

3.7 Acknowledgments

The authors wish to acknowledge Alex Bertuccio of Carnegie Mellon University for helpful conversations that initiated this research endeavor and Eleanor Spielman-Sun of Carnegie Mellon University and Dr. Sónia Morais Rodrigues of the University of Aveiro (Portgual) for help with TEM micrographs.

3.8 References for Chapter Three

(1) Aruoja, V.; Pokhrel, S.; Sihtmäe, M.; Mortimer, M.; Mädler, L.; Kahru, A. Toxicity of 12 metal-based nanoparticles to algae, bacteria and protozoa. *Environ. Sci. Nano* **2015**, *2* (6), 630–644.

(2) Krivoshiev, B. V.; Dardenne, F.; Blust, R.; Covaci, A.; Husson, S. J. Elucidating toxicological mechanisms of current flame retardants using a bacterial gene profiling assay. *Toxicol. Vitr.* **2015**, *29* (8), 2124–2132.

(3) Vikram, A.; Bomberger, J. M.; Bibby, K. J. Efflux as a glutaraldehyde resistance mechanism in Pseudomonas fluorescens and Pseudomonas aeruginosa biofilms. *Antimicrob. Agents Chemother.* **2015**, *59* (6), 3433–3440.

(4) Xiu, Z.; Zhang, Q.; Puppala, H.; Colvin, V.; Alvarez, P. Negligible particle-specific antibacterial activity of silver nanoparticles. *Nano Lett.* **2012**, 10–14.

(5) Gunawan, C.; Teoh, W. Y.; Marquis, C. P.; Amal, R. Cytotoxic Origin of Copper (II)

Oxide Nanoparticles : Comparative Studies and Metal Salts. *ACS Nano* **2011**, No. 9, 7214–7225.

(6) Liu, J.; Hurt, R. H. Ion release kinetics and particle persistence in aqueous nano-silver colloids. *Environ. Sci. Technol.* **2010**, *44* (6), 2169–2175.

(7) Vencalek, B. E.; Laughton, S. N.; Spielman-Sun, E.; Rodrigues, S. M.; Unrine, J. M.; Lowry, G. V.; Gregory, K. B. In Situ Measurement of CuO and Cu(OH)2 Nanoparticle Dissolution Rates in Quiescent Freshwater Mesocosms. *Environ. Sci. Technol. Lett.* **2016**, *3* (10), 375–380.

(8) Bondarenko, O.; Ivask, A.; Kakinen, A.; Kahru, A. Sub-toxic effects of CuO nanoparticles on bacteria : Kinetics , role of Cu ions and possible mechanisms of action. *Environ. Pollut.* **2012**, *169*, 81–89.

(9) Heinlaan, M.; Ivask, A.; Blinova, I.; Dubourguier, H.-C.; Kahru, A. Toxicity of nanosized and bulk ZnO, CuO and TiO2 to bacteria Vibrio fischeri and crustaceans Daphnia magna and Thamnocephalus platyurus. *Chemosphere* **2008**, *71* (7), 1308–1316.

(10) Macomber, L.; Rensing, C.; Imlay, J. A. Intracellular copper does not catalyze the formation of oxidative DNA damage in Escherichia coli. *J. Bacteriol.* **2007**, *189* (5), 1616–1626.

(11) Macomber, L.; Imlay, J. A. The iron-sulfur clusters of dehydratases are primary intracellular targets of copper toxicity. *Proc. Natl. Acad. Sci. U. S. A.* **2009**, *106* (20), 8344–8349.

(12) Applerot, G.; Lellouche, J.; Lipovsky, A.; Nitzan, Y.; Lubart, R.; Gedanken, A.; Banin, E. Understanding the antibacterial mechanism of CuO nanoparticles: revealing the route of induced oxidative stress. *Small* **2012**, *8* (21), 3326–3337.

(13) Bao, S.; Lu, Q.; Fang, T.; Dai, H.; Zhang, C. Assessment of the toxicity of CuO nanoparticles by using Saccharomyces cerevisiae mutants with multiple genes deleted. *Appl. Environ. Microbiol.* **2015**, *81* (23), 8098–8107.

(14) Kaweeteerawat, C.; Ivask, A.; Liu, R.; Zhang, H.; Chang, C. H.; Low-Kam, C.; Fischer, H.; Ji, Z.; Pokhrel, S.; Cohen, Y.; et al. Toxicity of metal oxide nanoparticles in Escherichia coli correlates with conduction band and hydration energies. *Environ. Sci. Technol.* **2015**, *49* (2), 1105–1112.

(15) Angelé-Martínez, C.; Nguyen, K. V. T.; Ameer, F. S.; Anker, J. N.; Brumaghim, J. L. Reactive oxygen species generation by copper(II) oxide nanoparticles determined by DNA damage assays and EPR spectroscopy. *Nanotoxicology* **2017**, *11* (2), 278–288.

(16) Tsai, Y. Y.; Huang, Y. H.; Chao, Y. L.; Hu, K. Y.; Chin, L. Te; Chou, S. H.; Hour, A. L.; Yao, Y. Der; Tu, C. S.; Liang, Y. J.; et al. Identification of the nanogold particle-induced endoplasmic reticulum stress by omic techniques and systems biology analysis. *ACS Nano* **2011**, *5* (12), 9354–9369.

(17) Kaweeteerawat, C.; Chang, C. H.; Roy, K. R.; Liu, R.; Li, R.; Toso, D.; Fischer, H.; Ivask, A.; Ji, Z.; Zink, J. I.; et al. Cu Nanoparticles Have Different Impacts in *Escherichia coli* and *Lactobacillus brevis* than Their Microsized and Ionic Analogues. *ACS Nano* **2015**, *9* (7), 7215–7225.

(18) Lubick, N. Nanosilver toxicity: ions, nanoparticles--or both? *Environ. Sci. Technol.* **2008**, *42* (23), 8617–8617.

(19) Studer, A. M.; Limbach, L. K.; Van Duc, L.; Krumeich, F.; Athanassiou, E. K.; Gerber, L. C.; Moch, H.; Stark, W. J. Nanoparticle cytotoxicity depends on intracellular solubility: comparison of stabilized copper metal and degradable copper oxide nanoparticles. *Toxicol. Lett.* **2010**, *197* (3), 169–174.

(20) Xiu, Z.-M.; Ma, J.; Alvarez, P. J. J. Differential effect of common ligands and molecular

oxygen on antimicrobial activity of silver nanoparticles versus silver ions. *Environ. Sci. Technol.* **2011**, *45* (20), 9003–9008.
(21) Yang, Y.; Quensen, J.; Mathieu, J.; Wang, Q.; Wang, J.; Li, M.; Tiedje, J. M.; Alvarez, P. J. J. Pyrosequencing reveals higher impact of silver nanoparticles than Ag+ on the microbial community structure of activated sludge. *Water Res.* **2014**, *48*, 317–325.
(22) Lesniak, A.; Salvati, A.; Santos-Martinez, M. J.; Radomski, M. W.; Dawson, K. A.; Åberg, C. Nanoparticle Adhesion to the Cell Membrane and Its Effect on Nanoparticle Uptake Efficiency. *J. Am. Chem. Soc.* **2013**, *135* (4), 1438–1444.
(23) Meghana, S.; Kabra, P.; Chakraborty, S.; Padmavathy, N. Understanding the pathway of antibacterial activity of copper oxide nanoparticles. *RSC Adv.* **2015**, *5* (16), 12293–12299.
(24) Guo, J.; Gao, S.-H.; Lu, J.; Bond, P. L.; Verstraete, W.; Yuan, Z. Copper Oxide Nanoparticles Induce Lysogenic Bacteriophage and Metal-Resistance Genes in Pseudomonas aeruginosa PAO1. *ACS Appl. Mater. Interfaces* **2017**, in press.
(25) Li, M.; Zhu, L.; Lin, D. Toxicity of ZnO nanoparticles to Escherichia coli: mechanism and the influence of medium components. *Environ. Sci. Technol.* **2011**, *45* (5), 1977–1983.
(26) McQuillan, J. S.; Shaw, A. M. Differential gene regulation in the Ag nanoparticle and Ag(+)-induced silver stress response in Escherichia coli: A full transcriptomic profile. *Nanotoxicology* **2014**, *5390* (I), 1–8.
(27) Sohm, B.; Immel, F.; Bauda, P.; Pagnout, C. Insight into the primary mode of action of TiO2 nanoparticles on Escherichia coli in the dark. *Proteomics* **2015**, *15* (1), 98–113.
(28) Gomes, S. I. L.; Roca, C. P.; Scott-Fordsmand, J. J.; Amorim, M. J. B. High-throughput transcriptomics reveals uniquely affected pathways: AgNPs, PVP-coated AgNPs and Ag NM300K case studies. *Environ. Sci. Nano* **2017**, *4* (4), 929–937.
(29) Baker, J.; Sitthisak, S.; Sengupta, M.; Johnson, M.; Jayaswal, R. K.; Morrissey, J. A. Copper stress induces a global stress response in Staphylococcus aureus and represses sae and agr expression and biofilm formation. *Appl. Environ. Microbiol.* **2010**, *76* (1), 150–160.
(30) Kershaw, C. J.; Brown, N. L.; Constantinidou, C.; Patel, M. D.; Hobman, J. L. The expression profile of Escherichia coli K-12 in response to minimal, optimal and excess copper concentrations. *Microbiology* **2005**, *151* (4), 1187–1198.
(31) Yamamoto, K.; Ishihama, A. Transcriptional response of Escherichia coli to external copper. *Mol. Microbiol.* **2005**, *56* (1), 215–227.
(32) Yang, Y.; Wang, J.; Xiu, Z.; Alvarez, P. J. J. Impacts of silver nanoparticles on cellular and transcriptional activity of nitrogen-cycling bacteria. *Environ. Toxicol. Chem.* **2013**, *32* (7), 1488–1494.
(33) Moore, J. D.; Stegemeier, J. P.; Bibby, K.; Marinakos, S. M.; Lowry, G. V; Gregory, K. B. Impacts of Pristine and Transformed Ag and Cu Engineered Nanomaterials on Surficial Sediment Microbial Communities Appear Short-Lived. *Environ. Sci. Technol.* **2016**, *50* (5), 2641–2651.
(34) Baker, L. F.; King, R. S.; Unrine, J. M.; Castellon, B. T.; Lowry, G. V.; Matson, C. W. Press or pulse exposures determine the environmental fate of cerium nanoparticles in stream mesocosms. *Environ. Toxicol. Chem.* **2016**, *35* (5), 1213–1223.
(35) Navarro, E.; Piccapietra, F.; Wagner, B.; Marconi, F.; Kaegi, R.; Odzak, N.; Sigg, L.; Behra, R. Toxicity of Silver Nanoparticles to *Chlamydomonas reinhardtii*. *Environ. Sci. Technol.* **2008**, *42* (23), 8959–8964.
(36) Gao, X.; Spielman-Sun, E.; Rodrigues, S. M.; Casman, E. A.; Lowry, G. V. Time and Nanoparticle Concentration Affect the Extractability of Cu from CuO NP-Amended Soil.

Environ. Sci. Technol. **2017**, *51* (4), 2226–2234.
(37) Tavares, D. S.; Rodrigues, S. M.; Cruz, N.; Carvalho, C.; Teixeira, T.; Carvalho, L.; Duarte, A. C.; Trindade, T.; Pereira, E.; R?mkens, P. F. A. M. Soil?pore water distribution of silver and gold engineered nanoparticles in undisturbed soils under unsaturated conditions. *Chemosphere* **2015**, *136*, 86–94.
(38) Taurozzi, J. S.; Hackley, V. A.; Wiesner, M. R. Ultrasonic dispersion of nanoparticles for environmental, health and safety assessment – issues and recommendations. *Nanotoxicology* **2011**, *5* (4), 711–729.
(39) Maurer-Jones, M. A.; Gunsolus, I. L.; Murphy, C. J.; Haynes, C. L. Toxicity of engineered nanoparticles in the environment. *Anal. Chem.* **2013**, *85* (6), 3036–3049.
(40) Badireddy, A. R.; Wiesner, M. R.; Liu, J. Detection, characterization, and abundance of engineered nanoparticles in complex waters by hyperspectral imagery with enhanced darkfield microscopy. *Environ. Sci. Technol.* **2012**, *46* (18), 10081–10088.
(41) Avellan, A.; Auffan, M.; Masion, A.; Levard, C.; Bertrand, M.; Rose, J.; Santaella, C.; Achouak, W. Remote Biodegradation of Ge–Imogolite Nanotubes Controlled by the Iron Homeostasis of *Pseudomonas brassicacearum*. *Environ. Sci. Technol.* **2016**, *50* (14), 7791–7798.
(42) McGivney, E.; Han, L.; Avellan, A.; VanBriesen, J.; Gregory, K. B. Disruption of Autolysis in Bacillus subtilis using TiO2 Nanoparticles. *Sci. Rep.* **2017**, *7*, 44308.
(43) Avellan, A.; Levard, C.; Rose, J.; Auffan, M.; Bertrand, M.; Olivi, L.; Santaella, C.; Achouak, W.; Masion, A.; Gallice, P.; et al. Influence of structural defects of Ge-imogolite nanotubes on their toxicity towards Pseudomonas brassicacearum. *Environ. Sci. Nano* **2016**, *3* (4), 839–846.
(44) Peng, S.; Stephan, R.; Hummerjohann, J.; Tasara, T. Evaluation of three reference genes of Escherichia coli for mRNA expression level normalization in view of salt and organic acid stress exposure in food. *FEMS Microbiol. Lett.* **2014**, *355* (1), 78–82.
(45) Rensing, C.; Fan, B.; Sharma, R.; Mitra, B.; Rosen, B. P. CopA: An Escherichia coli Cu(I)-translocating P-type ATPase. *Proc. Natl. Acad. Sci. U. S. A.* **2000**, *97* (2), 652–656.
(46) Grass, G.; Rensing, C. CueO is a multi-copper oxidase that confers copper tolerance in Escherichia coli. *Biochem. Biophys. Res. Commun.* **2001**, *286* (5), 902–908.
(47) Franke, S.; Grass, G.; Rensing, C.; Nies, D. H. Molecular Analysis of the Copper-Transporting Efflux System CusCFBA of Escherichia coli. *J. Bacteriol.* **2003**, *185* (13), 3804–3812.
(48) Imlay, J. A. The molecular mechanisms and physiological consequences of oxidative stress: lessons from a model bacterium. *Nat. Rev. Microbiol.* **2013**, *11* (7), 443–454.
(49) Triggs-Raine, B. L.; Doble, B. W.; Mulvey, M. R.; Sorby, P. A.; Loewen, P. C. Nucleotide sequence of katG, encoding catalase HPI of Escherichia coli. *J. Bacteriol.* **1988**, *170* (9), 4415–4419.
(50) Fee, J. A. Regulation of sod genes in Escherichia coli: relevance to superoxide dismutase function. *Mol. Microbiol.* **1991**, *5* (11), 2599–2610.
(51) Pérez, J. M.; Arenas, F. A.; Pradenas, G. A.; Sandoval, J. M.; Vásquez, C. C. Escherichia coli YqhD exhibits aldehyde reductase activity and protects from the harmful effect of lipid peroxidation-derived aldehydes. *J. Biol. Chem.* **2008**, *283* (12), 7346–7353.
(52) Strøm, A. R.; Kaasen, I. Trehalose metabolism in Escherichia coli: stress protection and stress regulation of gene expression. *Mol. Microbiol.* **1993**, *8* (2), 205–210.
(53) Kandror, O.; DeLeon, A.; Goldberg, A. L. Trehalose synthesis is induced upon exposure of

Escherichia coli to cold and is essential for viability at low temperatures. *Proc. Natl. Acad. Sci. U. S. A.* **2002**, *99* (15), 9727–9732.
(54) Balaji, B.; O'Connor, K.; Lucas, J. R.; Anderson, J. M.; Csonka, L. N. Timing of induction of osmotically controlled genes in Salmonella enterica Serovar Typhimurium, determined with quantitative real-time reverse transcription-PCR. *Appl. Environ. Microbiol.* **2005**, *71* (12), 8273–8283.
(55) Ayala-Castro, C.; Saini, A.; Outten, F. W. Fe-S cluster assembly pathways in bacteria. *Microbiol. Mol. Biol. Rev.* **2008**, *72* (1), 110–25, table of contents.
(56) Price, N. L.; Raivio, T. L. Characterization of the Cpx regulon in Escherichia coli strain MC4100. *J. Bacteriol.* **2009**, *191* (6), 1798–1815.
(57) Kalyanaraman, B.; Darley-Usmar, V.; Davies, K. J. A.; Dennery, P. A.; Forman, H. J.; Grisham, M. B.; Mann, G. E.; Moore, K.; Roberts, L. J.; Ischiropoulos, H. Measuring reactive oxygen and nitrogen species with fluorescent probes: challenges and limitations. *Free Radic. Biol. Med.* **2012**, *52* (1), 1–6.
(58) Petasis, D. T.; Hendrich, M. P. Quantitative interpretation of multifrequency multimode EPR spectra of metal containing proteins, enzymes, and biomimetic complexes. In *Methods in Enzymology*; 2015; Vol. 563, pp 171–208.
(59) R Core Team. R: A Language and Environment for Statistical Computing. Vienna, Austria 2014.
(60) McCarthy, D. J.; Smyth, G. K. Testing significance relative to a fold-change threshold is a TREAT. *Bioinformatics* **2009**, *25* (6), 765–771.
(61) Huggins, C. E.; Domenighetti, A. A.; Ritchie, M. E.; Khalil, N.; Favaloro, J. M.; Proietto, J.; Smyth, G. K.; Pepe, S.; Delbridge, L. M. D. Functional and metabolic remodelling in GLUT4-deficient hearts confers hyper-responsiveness to substrate intervention. *J. Mol. Cell. Cardiol.* **2008**, *44* (2), 270–280.
(62) Arenas, F. A.; Díaz, W. A.; Leal, C. A.; Pérez-Donoso, J. M.; Imlay, J. A.; Vásquez, C. C. The Escherichia coli btuE gene, encodes a glutathione peroxidase that is induced under oxidative stress conditions. *Biochem. Biophys. Res. Commun.* **2010**, *398* (4), 690–694.
(63) Karlsson, H. L.; Cronholm, P.; Gustafsson, J.; Möller, L. Copper oxide nanoparticles are highly toxic: a comparison between metal oxide nanoparticles and carbon nanotubes. *Chem. Res. Toxicol.* **2008**, *21* (9), 1726–1732.
(64) Macomber, L.; Rensing, C.; Imlay, J. A. Intracellular copper does not catalyze the formation of oxidative DNA damage in Escherichia coli. *J. Bacteriol.* **2007**, *189* (5), 1616–1626.
(65) Roca, A. I.; Cox, M. M. RecA protein: structure, function, and role in recombinational DNA repair. *Prog. Nucleic Acid Res. Mol. Biol.* **1997**, *56*, 129–223.
(66) Feng, Y.; Cronan, J. E. Escherichia coli unsaturated fatty acid synthesis: complex transcription of the fabA gene and in vivo identification of the essential reaction catalyzed by FabB. *J. Biol. Chem.* **2009**, *284* (43), 29526–29535.
(67) Raivio, T. L. MicroReview: Envelope stress responses and Gram-negative bacterial pathogenesis. *Mol. Microbiol.* **2005**, *56* (5), 1119–1128.
(68) McBroom, A. J.; Kuehn, M. J. Release of outer membrane vesicles by Gram-negative bacteria is a novel envelope stress response. *Mol. Microbiol.* **2007**, *63* (2), 545–558.
(69) Macomber, L.; Imlay, J. A. The iron-sulfur clusters of dehydratases are primary intracellular targets of copper toxicity. *Proc. Natl. Acad. Sci. U. S. A.* **2009**, *106* (20), 8344–8349.
(70) Fung, D. K. C.; Lau, W. Y.; Chan, W. T.; Yan, A. Copper efflux is induced during anaerobic amino acid limitation in escherichia coli to protect iron-sulfur cluster enzymes and

biogenesis. *J. Bacteriol.* **2013**, *195* (20), 4556–4568.
(71) Srivastava, S. K.; Lambadi, P. R.; Ghosh, T.; Pathania, R.; Navani, N. K. Genetic regulation of spy gene expression in Escherichia coli in the presence of protein unfolding agent ethanol. *Gene* **2014**, *548* (1), 142–148.
(72) Sondi, I.; Salopek-Sondi, B. Silver nanoparticles as antimicrobial agent: a case study on E. coli as a model for Gram-negative bacteria. *J. Colloid Interface Sci.* **2004**, *275* (1), 177–182.
(73) Morones, J. R.; Elechiguerra, J. L.; Camacho, A.; Holt, K.; Kouri, J. B.; Ramírez, J. T.; Yacaman, M. J. The bactericidal effect of silver nanoparticles. *Nanotechnology* **2005**, *16* (10), 2346–2353.
(74) Zhang, B.; Cui, L.; Zhang, K. Dosage- and time-dependent antibacterial effect of zinc oxide nanoparticles determined by a highly uniform SERS negating undesired spectral variation. *Anal. Bioanal. Chem.* **2016**, *408* (14), 3853–3865.
(75) Schwechheimer, C.; Kuehn, M. J. Outer-membrane vesicles from Gram-negative bacteria: biogenesis and functions. *Nat. Rev. Microbiol.* **2015**, *13* (10), 605–619.
(76) Stohs, S.; Bagchi, D. Oxidative mechanisms in the toxicity of metal ions. *Free Radic. Biol. Med.* **1995**, *18* (2), 321–336.
(77) Park, H. J.; Nguyen, T. T. M.; Yoon, J.; Lee, C. Role of reactive oxygen species in Escherichia coli inactivation by cupric ion. *Environ. Sci. Technol.* **2012**, *46* (20), 11299–11304.
(78) Jung, Y. S.; Lim, W. T.; Park, J.; Kim, Y. Effect of pH on Fenton and Fenton-like oxidation. *Environ. Technol.* **2009**, *30* (2), 183–190.
(79) Mudunkotuwa, I. A.; Rupasinghe, T.; Wu, C.-M.; Grassian, V. H. Dissolution of ZnO Nanoparticles at Circumneutral pH : A Study of Size Effects in the Presence and Absence of Citric Acid. *Langmuir* **2012**, *28*, 396–403.
(80) Bertuccio, A. J.; Tilton, R. D. Silver Sink Effect of Humic Acid on Bacterial Surface Colonization in the Presence of Silver Ions and Nanoparticles. *Environemntal Sci. Technol.* **2017**, *51* (3), 1754–1763.

CHAPTER FOUR:

In laboratory and clinical methicillin-resistant *Staphylococcus aureus*, CuO nanoparticles reduce virulence factor gene expression and induce transcriptional response distinct from ion

4.1 ABSTRACT

Methicillin-resistant *Staphylococcus aureus* (MRSA) has reached epidemic levels, infecting skin and soft tissues, the lungs, heart, and bloodstream. It continues to cause severe morbidity, which can lead to patient death, and higher healthcare costs in the United States and elsewhere. Antibiotics are becoming less effective, and alternative antimicrobial agents are being explored for control of bacterial growth in sensitive, i.e., medical, settings. Soluble engineered nanomaterials (ENM) are an attractive alternative due to their slow release of toxic ion. Cu has long been used as an antimicrobial and is relatively non-toxic to humans, making copper oxide (CuO) nanoparticles (NP) particularly attractive. The effects of CuO NPs on *S. aureus* laboratory strains are very poorly characterized, and no studies have investigated the effect of CuO NPs on *S. aureus* clinical isolates. We investigated the interactions, inhibition, and transcriptional responses to CuO NPs of four *S. aureus* isolates – one methicillin-susceptible *S. aureus* (MSSA) laboratory strain (SH1000), one MRSA laboratory strain (BAA-1556), and two MRSA clinical isolates. Cu homeostasis genes (*copA* and *copB*) and at least one ROS-responsive gene (*ahpF* and/or *sodA*) were induced for all Cu treatments (100 mg/L CuO NP as Cu and a Cu^{2+} control) and isolates. Only SH1000 had induced expression of protein damage-responsive (*clpC*), heat shock and general stress-responsive (*ctsR*), and metal binding (*mcsA*) genes that have been observed to be induced in previous reports of transcriptional responses to Cu exposure in *S. aureus*. All strains displayed reduction in virulence factor gene expression (*agrA*, *RNAIII*, and/or *saeS*) in response to Cu exposures, especially with CuO NP exposure and especially for the clinical isolates. Comparison across genes showed high strain-specific transcriptional responses and conspicuous treatment-specific responses within each strain. Our results demonstrate potential for CuO NP

application to reduce *S. aureus* virulence and stress the importance of considering relevant clinical isolates when characterizing antimicrobial effects on *S. aureus*.

4.2 INTRODUCTION

The healthcare industry is in need of new antimicrobial agents. Healthcare-associated infections (HAI) afflict two million Americans and costs hospitals alone between $28 and 45 billion annually,[1] and antibiotic-resistant infections kill at least 23,000 Americans a year.[2] Few new antibiotics are being developed,[1] leaving a gap that could be filled by alternative antimicrobial agents. Engineered nanomaterials (ENM) have been proposed as a stopgap.[3,4]

Antimicrobial ENMs are known to inhibit microbial growth and are increasingly incorporated into products as antimicrobial agents.[5–8] Interest spans from application in water disinfection[9] and antimicrobial textiles,[10] to wound healing.[11] Cupric oxide (CuO) ENMs are among the most antimicrobial.[12] Efforts to exploit this property by incorporating CuO ENMs, and other Cu-based ENMs, into antimicrobial products are underway.[7,8,13]

Cu is relatively non-toxic to humans and other mammals,[14] yet has strong bacterial toxicity.[15,16] In the gram-negative *Escherichia coli* and gram-positive *Bacillus subtilis*, Cu^{2+} inhibits growth by impeding formation of iron-sulfur protein clusters.[17,18] Cu^{2+} also inhibits *Staphylococcus aureus* growth, though the mechanism is not as well elucidated as for *E. coli* and *B. subtilis*. Transcriptomic analysis found that Cu^{2+} exposure led to activation of Cu homeostasis, oxidative stress, and misfolded protein genes,[19] responses that have also been observed in *E. coli*.[20] Alongside induction of these stress response genes, Cu^{2+} led to reduction in *S. aureus* virulence factor gene expression.[19] Subinhibitory Cu^{2+} doses resulted in significant reductions in biofilm

growth, as well. CuO ENMs are soluble[21,22] and are known to inhibit *S. aureus* growth,[12,23] as well, though *S. aureus*' transcriptional response to CuO ENMs has not yet been explored.

There is no consensus around the source of soluble ENM toxicity, whether the ENM itself is the causative agent or its released ion.[24–27] Comparing responses to nanoparticulate and ionic species could highlight differences that inform efforts to incorporate antimicrobial ENMs for effective control of bacterial growth. For example, if toxicity is entirely ion-mediated, the soluble ENM application must allow for sustained dissolution, which is dependent upon numerous factors, e.g., pH, ligands, and ENM chemical species, aggregation, and coating.[28–32] Whereas nano-specific toxicity, which could take the form of unique cell wall damage,[23,33,34] might require that ENM application allow for preservation of its nanoscale dimensions and/or ensure association of an ENM onto bacterial surfaces. Differentiating antimicrobial interactions of CuO ENMs and Cu^{2+} with target pathogens, such as *S. aureus*, is likely an important step towards effective antimicrobial application of these ENMs.

S. aureus is the leading cause of surgical site infections (SSI) in the U.S., accounting for over 60,000 SSIs a year.[35] Methicillin-resistant *S. aureus* (MRSA) is particularly pernicious, leading to increases in treatment costs and patient morbidity.[36] An increasing number of SSIs are due to MRSA,[35] leading to questions about improving screening for and inhibition of staphylococci in medical settings.[37] Researchers have taken an interest in testing anti-staphylococci medical devices, including use of Cu.[38,39]

One obstacle that could complicate research into antimicrobial effects on *S. aureus* is intra-species genomic variability, both natural and engineered. For example, the accessory gene regulator (agr) system, which plays a prominent role in staphylococcal quorum sensing and virulence gene expression, has diverged across strains.[40,41] Beyond natural variation, engineering

of a commonly studied laboratory lineage, NCTC 8325, has removed prophage genetic elements.[42] Later, it was discovered that the engineered strain and its many derivatives demonstrate reduced activity of a stress factor (sigma B) due to a mutation in the *rsbU* gene[43] and were more susceptible to antimicrobial treatment as a result.[44] A daughter strain was engineered to be *rsbU+*, but other mutations have surfaced in this strain.[42] Previous work with *Streptococcus* has shown that laboratory and clinical isolates can display distinct responses to antimicrobial treatment.[45] Studies of antimicrobial agents that are hoping to inform efforts to control *S. aureus* in medical settings should consider the effects on clinically-relevant strains alongside laboratory strains.

Here we report a series of experiments investigating the effects, interactions, and transcriptional responses of four *S. aureus* isolates to CuO nanoparticle (NP) and Cu^{2+} exposure. We study two laboratory strains: *rsbU+* NCTC lineage SH1000, a methicillin-susceptible *S. aureus* (MSSA), and BAA-1556, a USA300 MRSA strain that contains an additional Cu-responsive gene, *copB*. We also study two clinically-isolated strains, herein referred to as SA1 and SA2. Both are believed to be USA300, and so should also contain the *copB* gene.[46] We hypothesized that Cu exposures would induce transcription of Cu homeostasis and previously reported downstream stress-responsive genes and that NP exposure would induce differential transcriptional responses than would the ion. We further hypothesized that strain-specific effects and responses would be evident, especially for SH1000. And we hypothesized that Cu treatments would lead to reduction in virulence factor gene expression. Our results demonstrate the potential usefulness of CuO ENMs in reducing *S. aureus* virulence gene expression and highlight the need to study clinically-relevant *S. aureus* strains when asking research questions that pertain to them.

4.3 MATERIALS AND METHODS

4.3.A NP characterization. Uncoated CuO NPs (Sigma Aldrich, St. Louis, MO) reported to be less than 50 nm by the manufacturer were suspended in ultra-pure water and analyzed by transmission electron microscopy (TEM) using a Hitachi H-9000 TEM microscope (Hitachi, Tokyo, Japan) operated at 300 kV, as has been reported before.[47,48] CuO NPs were probe sonicated (Branson Model 250, Branson Ultrasonics, Danbury, CT) in autoclaved ultrapure water (Barnstead, Ramsey, MN) for 15 min at power level 3, as has been reported for other ENMs.[49] The hydrodynamic diameter and electrophoretic mobility (EPM) were measured in the growth medium (discussed below) immediately after sonication with a Malvern Zetasizer Nano (Malvern Instruments, Malvern, United Kingdom) at 10 mg/L as Cu.

4.3.B CuO NP dissolution. CuO NPs were suspended in bacterial growth medium at 100 mg/L as Cu in triplicate acid-washed culture tubes. Tubes were shaken at 160 rpm at 37ºC in the dark. Dissolved Cu was separated using 3 kDa centrifugal filters (Millipore, Billerica, MA), and total and dissolved Cu were measured by inductively coupled plasma mass spectrometry (ICP-MS; Agilent 7700x, Santa Clara, CA) of acidified filtrates.

4.3.C Bacteria and medium. All *S. aureus* strains – *S. aureus* SH1000, *S. aureus* subsp. *aureus* Rosenbach (ATCC BAA-1556), and two clinically isolated MRSA strains (herein referred to as SA1 and SA2) – were generously provided by Dr. Ken Urish of the University of Pittsburgh Medical Center. All strains were grown planktonically in a glucose-supplemented chemically defined medium (CDM) that has been used in previous staphylococcal studies.[50,51] Essential and non-essential amino acid supplements (Gibco Laboratories, Gaithersburg, MD) were added to enable robust growth (component concentrations can be found in **Table 4.1**). *S. aureus* strain frozen stocks were stored at -80ºC and streaked onto Tryptic Soy Broth (TSB) agar plates prior to

conducting experiments. The day before an experiment, single colonies were picked from the streaked TSB plates. Overnight cultures were grown in CDM before being diluted 1:50 in pre-warmed CDM on the day of the experiment.

Table 4.1 ***CDM component concentrations.*** *pH was adjusted to 6.3 using H_2SO_4 and NaOH. Gibco MEM Amino Acids Solution contains: L-arginine hydrochloride, L-cystine, L-histidine hydrochloride-H_2O, L-isoleucine, L-lysine hydrochloride, L-methionine, L-phenylalanine, L-threonine, L-tryptophan, L-tyrosine, and L-valine.. Gibco MEM Non-Essential Amino Acids Solution contains: glycine, L-alanine, L-asparagine, L-aspartic acid, L-glutamic acid, L-proline, and L-serine. Concentrations are as final concentrations in mixed CDM.*

Component	Concentration [mM]
K_2HPO_4	20
KH_2PO4	40
$(NH_4)_2SO_4$	7.6
$MgSO_4 \cdot 7H2O$	2.0×10^{-1}
$FeCl_3$	4.9×10^{-2}
ZnCl	5.1×10^{-4}
$MnCl \cdot 4H_2O$	5.0×10^{-4}
H_3BO_3	9.7×10^{-5}
$CoCl_2 \cdot 6H2O$	1.7×10^{-3}
$CuCl_2 \cdot 2H2O$	1.5×10^{-5}
$NiCl_2 \cdot 6H2O$	1.0×10^{-4}
Na_2MoO_4	1.5×10^{-4}
Thiamine	3.8×10^{-3}
Niacin	9.8×10^{-3}
Biotin	2.0×10^{-5}
Ca pantothenate	5.4×10^{-4}
Adenine	3.7×10^{-2}
Cytosine	4.5×10^{-2}
Guanine	3.3×10^{-2}
Thymine	1.6×10^{-1}
Uracil	4.5×10^{-2}
Essential amino acids[1]	2.5 to 30
Non-essential amino acids[2]	10
Glucose	28

[1] Components of MEM Amino Acids Solution can be found here: http://www.thermofisher.com/us/en/home/technical-resources/media-formulation.164.html

[2] Components of Non-Essential Amino Acids Solution can be found here: http://www.thermofisher.com/us/en/home/technical-resources/media-formulation.165.html

4.3.D Characterization of CuO NP-bacterial interactions. *S. aureus* strains **(**~5 x 10^7 CFU/mL) in CDM were exposed to 100 mg/L (as Cu) of CuO NPs at 37ºC with shaking at 160 rpm in the dark. These conditions were used for all experiments unless specified otherwise. The interaction between bacteria and CuO NPs 60 min after exposure was assessed using an enhanced resolution dark–field microscope system (BX51, Olympus, Tokyo, Japan) equipped with a CytoViva Hyperspectral Imaging (HSI) System (Auburn, AL). A 20 µL drop of sample was mounted between a clean glass slide and a coverslip and observed as is. Cells were observed either at 60x or 100x magnification. HSIs were acquired using 100% light source intensity and 0.6 s acquisition time per line.

Each pixel of the HSI contains a light reflectance spectrum, showing the light absorption of the material for 356 bands in the 400 to 1000 nm wavelength range. Each pixel thus provides a spectral signature modulated by the nature of the material it contains.[52] Each image has been corrected for the spectral contribution of the lamp used for the image acquisition. The CuO NP spectral library was constructed based on HSI of CuO in CDM. The mean reflectance spectrum for each particle of the images was extracted to build a preliminary library, which has been filtered to remove the light reflectance spectra of the medium alone and the undosed cells. The remaining spectra comprised the final CuO NP hyperspectral library, containing specific hyperspectral CuO NP signatures.

This NP library was then used to identify CuO NPs on images of *S. aureus* exposed to CuO NPs. This mapping was processed using a Spectral Angular Mapping (SAM) algorithm in the ENVI software (version 5.2). The algorithm determines a spectral similarity by calculating the angle between spectra and treating them as vectors in space with dimensionality equal to the number of bands. Here, vectors with angles ≤ 0.08 rad were deemed equivalent. Pixels containing the CuO

NP spectral signal were labeled red. This method has been validated in previous studies of interactions between bacteria and ENMs.[53–55]

4.3.E Growth inhibition experiments. Inhibition of *S. aureus* isolates' growth by varying concentrations of CuO ENMs and Cu^{2+} was measured using 96-well plates and a microplate reader (SpectraMax, Molecular Devices, Sunnyvale, CA). Approximately 10^6 colony forming units (CFU) per mL were added to a 96-well plate containing serially diluted CuO NPs or Cu^{2+} in the growth medium. The plate was shaken at 160 rpm at 37ºC in the dark, and OD600 was measured at 0 hr and 24 hr. Growth was determined by subtracting the 0 hr reading from the 24 hr reading. Abiotic and undosed biotic controls were included alongside CuO NP and Cu^{2+} treatments, and eight wells were used per treatment or control condition. Stocks of Cu^{2+} were made from $Cu(NO_3)_2$ in ultrapure water. ICP-MS analysis (as described above) was used to ensure that nominal Cu concentrations agreed with analytical concentrations.

4.3.F Transcriptional response experiments. Approximately 5 x 10^7 CFU/mL were exposed to CuO NP and Cu^{2+} treatments alongside the undosed control, all in triplicate. The exposure concentration for the CuO NP treatment was 100 mg/L as Cu, and the Cu^{2+} exposure concentration was 16 ppm, the amount of dissolved Cu released in abiotic CDM at 60 min.

Undosed CDM, dispersed CuO NPs, and Cu^{2+} were first added to acid-washed culture tubes. Bacteria were added next, after which each tube was briefly vortexed. Throughout the experiment, tubes were shaken at 160 rpm at 37ºC. After the one hour exposure, samples were preserved as has been reported previously.[50] In brief, 10 mL sample was immediately added to 10 mL of -20 ºC 1:1 acetone:ethanol, briefly vortexed, then frozen at -80 ºC until RNA was isolated.

4.3.G RNA extraction, cDNA synthesis, and nucleic acid quantitation and quality control. RNA was isolated according to a previously reported protocol.[50] Briefly, cell suspensions were

thawed at room temperature, then centrifuged at 10,000x *g* and resuspended in 500 µL TE buffer (pH 7.6). Cells were mechanically disrupted by bead beating in Lysing Matrix B tubes (MP Biomedicals, Solon, OH) 2x for 10 min intervals on high with a 5 min incubation on ice in between. Tubes were then centrifuged at 16,100x *g* for 5 min at 4ºC. RNA isolation was performed on the supernatant using the RNeasy Mini Kit (Qiagen, Hilden, Germany) following the manufacturer's procedure with slight alterations, including an on-column DNase treatment (Qiagen) as we have described previously.[33] RNA was quantitated fluorometrically using a high-sensitivity RNA kit and a Qubit 2.0 (Life Technologies, Carlsbad, CA). Quality information was derived from a 1.3% agarose gel. cDNA was synthesized from 400 ng RNA using iScript Reverse Transcription Supermix (Bio-Rad, Hercules, CA) and was quantitated using a ssDNA kit and the Qubit fluorometer. Negative RNA template and negative reverse-transcriptase controls were included alongside experimental samples. cDNA was diluted to 1 ng/µL aliquots in RNase/DNase-free water and stored at 4ºC until transcriptional assays were completed.

Table 4.2. ***RT-qPCR gene primer sequences.***

Gene	Primer sequences
rrsA	F: GTGGAGGGTCATTGGAAACT R: CACTGGTGTTCCTCCATATCTC
copA	F: TGGTTGGTGACGGTGTAAAT R: TCAAGTCGCCACCAAGAATAG
copB	F: TCATAGTGGCCATGCACATC R: CACCCATCAGTGGCGATAAA
ahpF	F: CCAGGACGATTGACTGAGAAA R: CCAGCCTTGGTTCAGATGATA
sodA	F: GCGTGTTCCCATACGTCTAAA R: TTCAGGTTGGGCTTGGTTAG
sodM	F: GGATCAGGTTGGACTTGGTTAG R: GCATGCTCCCAAACATCAAATAG
clpC	F: AGGTTTAGCGCAAGCCATAG R: CCTGCAACTACTGTTCCCATATC
ctsR	F: CAGAGAGCGAATATCGCACAG R: CACCACCACCACGTTTACTT
mcsA	F: ACGTTGCCCATCATGTCATA R: GAACTCTGCGGACGATATCAA
agrA	F: CAAAGTTGCAGCGATGGATTT R: AGCGTGTATGTGCAGTTTCT
RNAIII	F: CTGAGTCCAAGGAAACTAACTCTAC R: TGAGTTATTAAGCCATCCCAACT
saeS	F: GCTCAAGTGGCGTTCGATATT R: GCAACCATATGAGCAACGTATCA

4.3.H Quantitative polymerase chain reaction (qPCR) assays. Relative quantification was performed on a 7500 Real-Time PCR System (Applied Biosystems, Foster City, CA) using PowerUP SYBR Green master mix (Life Technologies) according to the manufacturer's protocol and primers designed with PrimerQuest (IDT, Newark, NJ). Each well consisted of 500 µM cDNA, 1x master mix, and 500 nM forward and reverse primers. Triplicate technical replicates were performed on each sample. (Primer sequences can be found in **Table 4.2**) The 16S rRNA gene, *rrsA*, was used as a housekeeping gene against which target genes were normalized. *rrsA* has been validated for this function before.[56] Fold control is generally calculated by dividing the normalized

expression of a target gene (x) under a given treatment (y) by the normalized gene expression of the same target gene (x) for the undosed control (undosed) (**Equation 4.1**). We calculated fold control using relative quantification and the ΔΔCt method (**Equation 4.2**),[57] where $\overline{\Delta C}$ is equal to the average difference between the target (x) and housekeeping gene (*rrsA*) Ct values for the same treatment (**Equation 4.3**). Ct values are a proxy for relative gene expression, and throughout the text the terms "gene expression" and "Ct value" are used interchangeably0.

$$Fold\ control_{xy} = \frac{Expression_{x,y} \Big/ Expression_{\mathrm{rrsA},y}}{\overline{Expression_{x,undosed}} \Big/ \overline{Expression_{\mathrm{rrsA},undosed}}} \qquad \textit{Equation 4.1}$$

$$Fold\ control_{xy} = \Delta\Delta Ct = \ 2^{-(\overline{\Delta C_y} - \overline{\Delta C_{control}})} \qquad \textit{Equation 4.2}$$

$$\Delta C_y = \ C_x - C_{\mathrm{rrsA}} \qquad \textit{Equation 4.3}$$

Numerous target genes associated with Cu homeostasis and stress responses to Cu^{2+} (**Figure 4.1**) were assayed. For Cu response: *copA*, which encodes a Cu-transporting ATPase and is present across *S. aureus* strains,[58] and *copB*, which encodes an additional Cu-transporting ATPase, but is not present in all *S. aureus*.[59] For downstream stress responses dealing with ROS: *ahpF*, which joins the alkyl hydroperoxide reducatase (*ahpC*) gene on an operon, and encodes a flavoprotein that regenerates AhpC in the presence of oxidative stress,[60,61] and *sodA* and *sodM*, which encode superoxide dismutases.[62,63] For Cu-induced protein damage: *clpC*, which encodes a protease that controls protein quality,[62] and *ctsR*, which is involved in general stress response regulation, including to protein misfolding and heat shock.[64,65] For detection of intracellular metals, *mcsA*, which encodes for an intracellular metal ion-binding protein.[66] And for virulence-related gene expression, *agrA*, a transcriptional activator of the *agr* system,[66,67] *RNAIII*, an RNA molecule that

affects virulence gene expression and translation,[68] and *saeS*, which encodes a sensor kinase for the *saeRS* two-component regulatory system that leads to exotoxin production.[69,70]

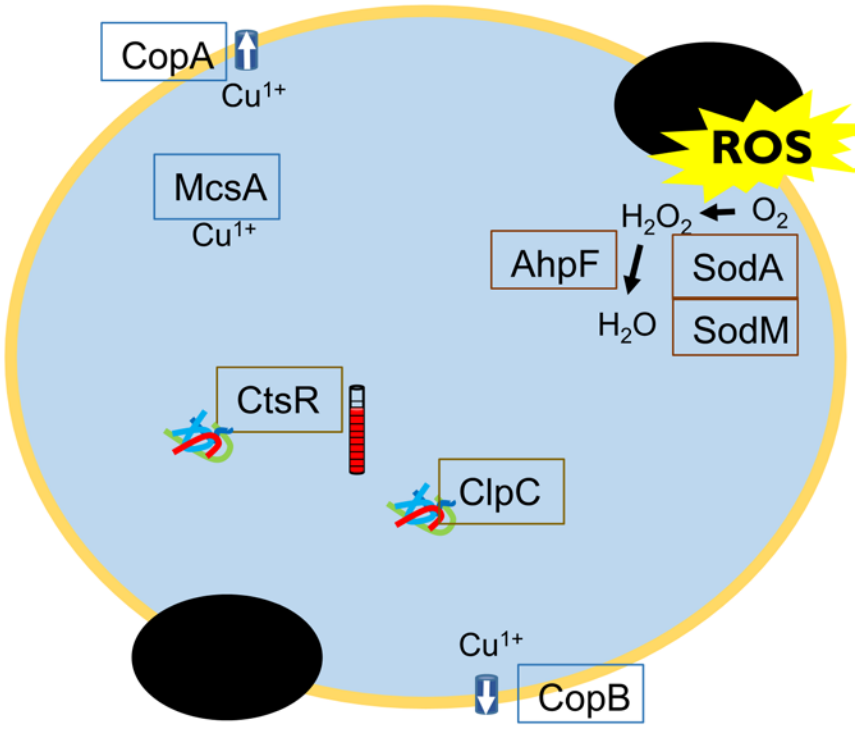

Figure 4.1. ***Schematic of target genes.*** *Proteins for genes of interest are shown in rectangles. Blue rectangles enclose Cu-responsive proteins. Brown rectangles enclose oxidative stress-responsive proteins. Yellow rectangles enclose protein damage-responsive proteins. Virulence-related proteins are not depicted. Black ovals represent CuO NPs.*

4.3.I Statistical analysis. Genes demonstrating at least two-fold increase or decrease compared to the undosed control were considered statistically significant (so $\geq$ 2.0-fold control or $\leq$ 0.5-fold control). Non-metric multidimensional scaling (NMDS) can effectively identify patterns within gene expression datasets[71] and was implemented here to visualize relationships among treatment and isolate relative gene expression (ΔC_y values from **Equation 4.3**) across all genes assayed. NMDS was performed within R version (3.4.0)[72] using the vegan package (version 2.4-3).[71] The dissimilarity matrix was generated based on Euclidean distance between samples. Otherwise default settings were used. No sample or gene with missing data could be considered, so one of

the SH1000 NP-dosed samples (because of numerous outlier values) and the *copB* gene (because of no signal from SH1000) were removed prior to NMDS analysis.

4.4 Results and Discussion

4.4.A NP characterization and dissolution. TEM showed the CuO NPs to be aggregates of smaller primary particles (**Figure 4.2**). We measured hydrodynamic diameter, electrophoretic mobility (EPM), and dissolution of the CuO NPs within the exposure medium. EPM was converted into zeta potential (ZP) using the Smoluchowski equation. CuO NPs were found to be 135 ± 22 nm in diameter with a surface charge of -31.2 ± 1.4 mV in the CDM (**Table 4.3**). When suspended in water, they were less aggregated, at 86.7 ± 20 nm in diameter, but they were still polydisperse. At a 100 mg/L as Cu CuO NP dose, we measured dissolved Cu at 60 min to be 16 ± 1 mg/L (ppm) and 35.9 ± 0.92 ppm at 24 hr.

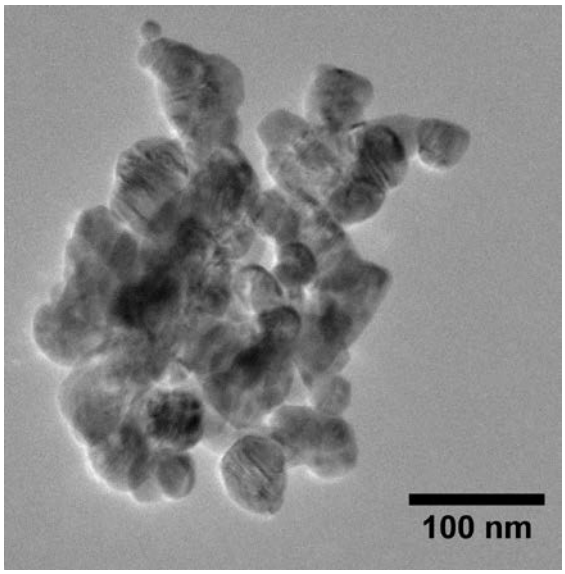

Figure 4.2. ***TEM micrograph of CuO NPs in water.***

Table 4.3 ***CuO NP characterization.*** *DLS and ZP values expressed as mean ± one standard deviation (SD) based on three measurements. Hydrodynamic diameters (HD) are number means, and polydispersity indices (PdI) indicate how polydisperse NPs are. ZP was calculated from measured EPM data using the Smoluchowski equation.*

Solvent	pH	Specific conductance [μS/cm]	HD [nm]	Intensity mean diameter [nm]	PdI	Zeta Potential [mV]
CDM	6.38	11.8 ± 0.16	135 ± 22	651 ± 120	0.414 ± 0.013	-31.2 ± 1.4
H_2O	5.89	0.0325 ± 0.0035	86.7 ± 20	582 ± 48	0.376 ± 0.048	-29.7 ± 1.1

4.4.B NP-bacteria interactions via hyperspectral imaging (HSI). We used HSI to visualize association of bacterial cells and NPs. HSI demonstrated that CuO NPs adsorb onto the cell walls of all isolates, typically with multiple bacteria seeming to associate with one or more NP aggregates (**Figure 4.3**). SH1000 seemed to form larger cellular aggregates in the presence of CuO NPs than the other isolates. The other isolates showed a range of a few to many aggregated cells associating with NP aggregates.

HSI has been used to observe the association of NPs with large aggregates of *Bacillus subtilis*, another gram-positive bacterium.[54] Part of what makes antibiotic-resistant *S. aureus* strains, including MRSA, distinct from antibiotic-susceptible isolates is their cell wall synthesis,[73,74] which could be leading to the observed differences in affinity between NPs and bacteria.

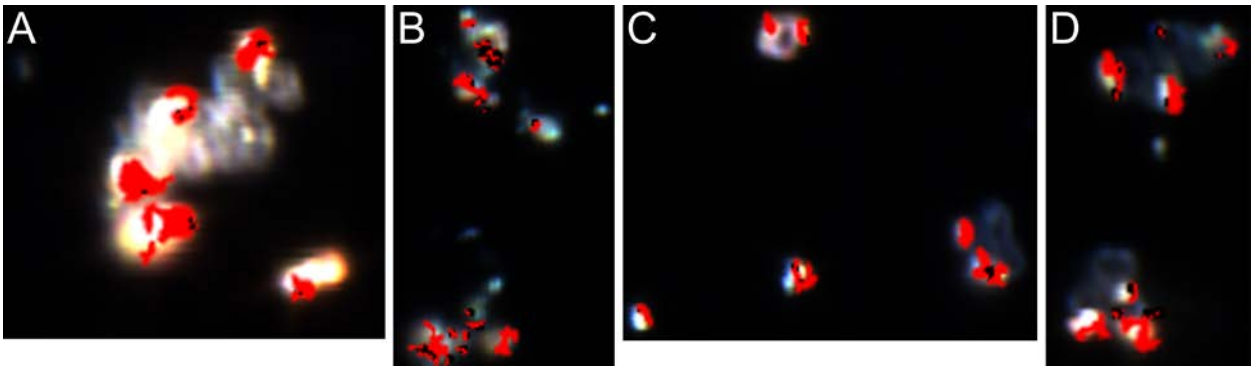

Figure 4.3. ***HSI of CuO NP-exposed*** **S. aureus** ***isolates.*** *Representative images of SH1000 (A), BAA-1556 (B), SA1 (C), and SA2 (D) with CuO NPs. Note the aggregated state of the SH1000 associating with the NPs. Pixels that fit the CuO NP signature are highlighted in red.*

4.4.C CuO NPs and Cu^{2+} inhibit *S. aureus* growth. Growth inhibition experiments allowed for comparison of *S. aureus* isolate growth across Cu concentrations and comparison of susceptibility to equal as Cu concentrations of nanoparticulate and ionic species. At higher concentrations, increasing Cu led to inhibition of isolate growth (**Figure 4.4**). MRSA isolates appeared to be inhibited by lower Cu concentrations of CuO NP, especially the clinical isolates, whose growth appeared inhibited when CuO NP concentration was increased from 0.781 (first CuO NP data point) to 1.56 mg/L (second CuO NP data point) as Cu (**Figure 4.4C** and **D**). The laboratory isolates did not appear to be inhibited until CuO NP concentrations were higher, i.e., between 6.25 and 12.5 mg/L as Cu (**Figure 4.4A** and **B**), though BAA-1556 was more inhibited by the increase to 12.5 mg/L than was SH1000. All isolates' growth appeared less sensitive to Cu^{2+}, with >10 ppm Cu^{2+} required for inhibition, with the possible exception of SH1000, which appears to be inhibited by doses higher than 1.56 ppm (**Figure 4.4A**). BAA-1556's growth was not inhibited until Cu^{2+} levels reached 25 ppm (**Figure 4.4B**).

High concentrations of metal cation-binding ligands in the CDM likely explain the enhanced inhibition of the NPs compared to the ions. Most studies comparing NP and ionic bacterial effects have found the opposite – that growth or viability is more sensitive to ion than NP.[75–77] Previous

unpublished work from our lab showed that the presence of strong metal cation-binding ligands, i.e., EDTA and citrate, resulted in similar CuO NP and Cu^{2+} growth inhibition of *E. coli*. Upon removal of these ligands, inhibition of both dropped significantly, though that of Cu^{2+} dropped significantly more. The CDM used here does not contain EDTA or citrate, but does include high concentrations of amino acids featuring thiol groups, i.e., methionine and the oxidized form of cysteine, cystine. *S. aureus* growth was impaired without or with less of the amino acids. These amino acids are known to have high binding affinities for Cu^{2+}.[78]

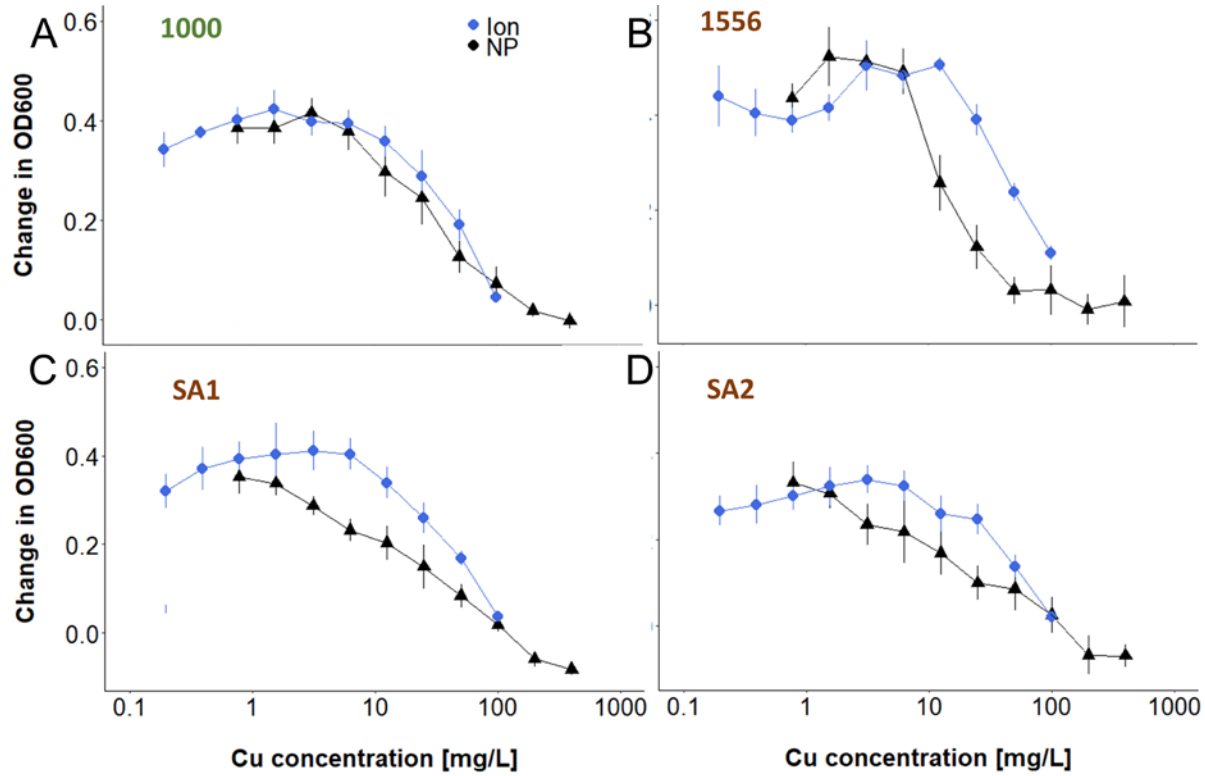

Figure 4.4. ***High-throughput inhibition of* S. aureus *isolates with various CuO NP and Cu^{2+} doses.*** *Laboratory strains are on top (A and B), and clinical strains on bottom (C and D), with MSSA labeled in green (A) and MRSA labeled in red (B-D). ~10^6 CFU/mL were exposed in 96-well plates. Means and standard deviations of eight wells per treatment dose are depicted.*

4.4.D Transcriptional response experiments. RNA was preserved after one hour CuO NP and Cu^{2+} exposures to enable gene expression assays via RT-qPCR. *rrsA* expression was found to be similar across treatments (**Figure 4.5**) allowing for its use as a housekeeping gene for normalization of target genes. Some within-sample variability is observed, specifically among the

1556 ion samples and the SA2 NP samples. In both cases, the range of Ct values within the sample set is less than Ct, suggesting that the gene expression differences are less than 2-fold. The 1556 ion samples have Ct values of 14.1 ± 0.0023 (mean ± standard deviation of the triplicate technical replicates), 14.4 ± 0.050, and 16.0 ± 0.11. The SA2 NP samples have Ct values of 14.6 ± 0.044, 14.7 ± 0.051, and 15.6 ± 0.053.

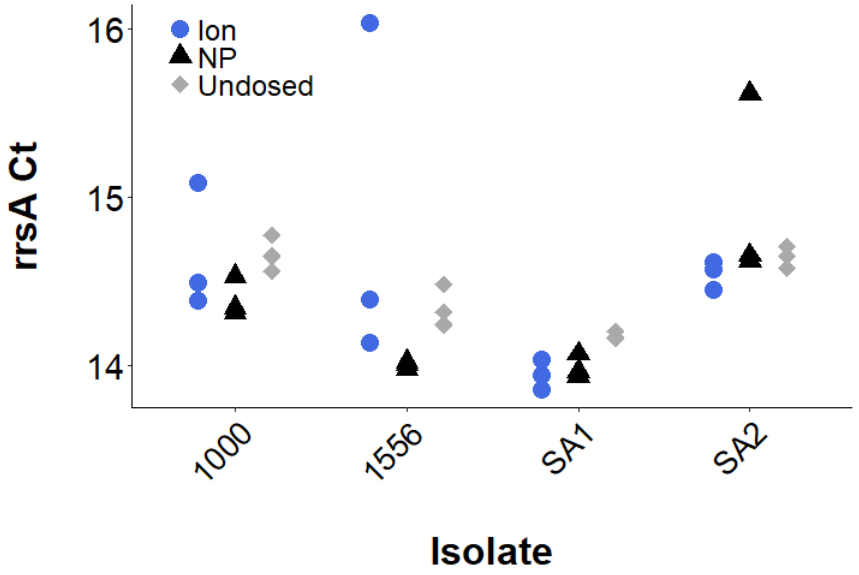

Figure 4.5. rrsA *Ct values.* rrsA *Ct values are a proxy for* rrsA *expression. Across treatments, expression was statistically similar for each isolate, validating its use as a housekeeping gene for the normalization of target gene expression. Mean* rrsA *Ct values for each of the triplicate samples are depicted.*

4.4.D.I Cu homeostasis gene expression. We were first interested in looking at expression of *rrsA*-normalized Cu homeostasis gene expression relative to the undosed controls to see what effect the different Cu treatments had on the isolates. SH1000 has only *copA*, while USA300 strains typically have an additional gene, *copB*, that encodes for another Cu efflux pump.[46]

Cu treatment induced *copA* and, where applicable, *copB* expression for all isolates (**Figure 4.6**). For laboratory isolates SH1000 and BAA-1556, NP-exposure induced higher *copA*, while the opposite is true for the SA1 and SA2 clinical isolates. Most strikingly, clinical isolates experienced heavily induced *copB* expression in response to Cu^{2+}, 580-fold control for SA1 and 170-fold

control for SA2. NP exposure also induced *copB* expression for these strains, though much more moderately, at 14- and 6.2-fold control, respectively. BAA-1556 had higher *copB* expression with ion exposure (7.3-fold control) than with the NP (4.4-fold control), and, as expected, *copB* expression could not be detected for SH1000. These data suggest the potential for both treatment- and strain-specific transcriptional responses, especially for the clinical isolates.

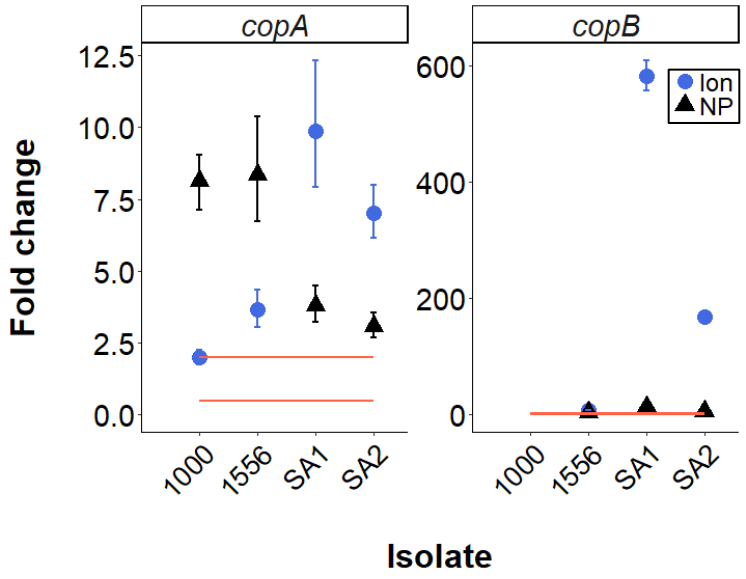

Figure 4.6. ***Cu-homeostasis relative gene expression.*** *Note the different y-axes for each gene and that SH1000 does not have the* copB *gene. Means and standard deviations of triplicate experiments are depicted, though error bars are obscured by several data points. Red lines are located at 0.5- and 2.0-fold change, where differences were considered statistically significant.*

4.4.D.II Downstream Cu stress transcriptional response. We assayed genes that have been shown to be induced by Cu exposure.[19,66] *clpC* and *ctsR* are induced by protein damage.[62,64,65] *ctsR* is also induced by general stress, including heat shock.[64,65] *mcsA* is involved in metal sensing.[66] Across the four isolates, Cu^{2+} did not induce any of these genes (**Figure 4.7**). The same is true of CuO NP exposure with the exception of SH1000, which experienced 2.9-, 4.1-, and 4.0-fold control induction of *clpC*, *ctsR*, and *mcsA*, respectively. This finding suggests that SH1000 could be uniquely susceptible to CuO NP treatment compared to the other isolates. This would align with HSI observations, where aggregated SH1000 cells appeared to be associating with aggregates of

NPs (**Figure 4.3**). Surprisingly, while Cu-responsive genes were induced in all MRSA isolates and clinical isolates experienced very high induction of *copB* under Cu^{2+} exposure (**Figure 4.6**), these genes that have been shown to play a part in *S. aureus*' transcriptional response to Cu^{2+} before,[19,66] were not activated here. This could be an indication that with the activation of the two Cu efflux systems, the MRSA isolates were able to stave off downstream stress from Cu exposure.

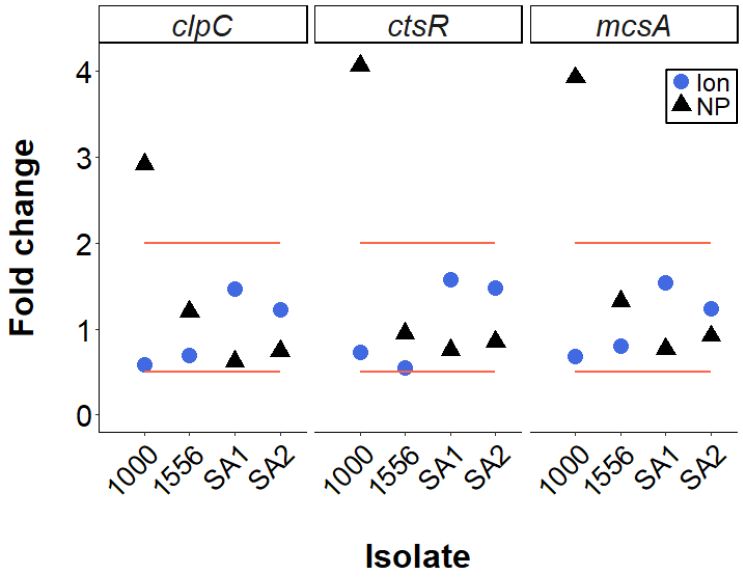

Figure 4.7. ***Downstream Cu stress relative gene expression****. Means and standard deviations of triplicate experiments are depicted, though error bars are obscured by several data points. Red lines are located at 0.5- and 2.0-fold change, where differences were considered statistically significant.*

ROS is believed to play a role in Cu bacterial toxicity,[16] and induction of ROS-responsive genes has been observed in Cu^{2+}-exposed *S. aureus*.[19] We next looked at ROS-responsive genes *ahpF*, *sodA*, and *sodM*. We measured induced expression of *ahpF* only for Cu^{2+}-exposed SA1 and SA2 at 3.2- and 2.4-fold control, respectively (**Figure 4.8**). *sodA* was induced more broadly, including by NP exposure for SH1000 (3.4-fold control), BAA-1556 (3.4-fold control), and SA1 (2.6-fold control) and by Cu^{2+} exposure for BAA-1556 (6.4-fold control) and SA1 (2.9-fold control). *sodM* displayed similar expression levels to that of the undosed control regardless of isolate or treatment.

SodA serves as *S. aureus*' primary superoxide dismutase[63] and SodM activity is limited to the stationary phase or extreme oxidative stress.[62] It is not surprising, then, that *sodA* would be induced

and *sodM* would not be. This likely suggests that at least for some of the isolates our Cu exposures result in a slight, but manageable induction of superoxide stress that can be effectively managed by enhanced expression of *sodA*. The induction of *ahpF* in Cu^{2+}-exposed clinical isolates suggests that for those isolates Cu^{2+} treatment results in H_2O_2 stress that requires induction of *ahpF* to enable regeneration of AhpC. This provides further evidence that Cu stress is leading to isolate-specific effects. Importantly, recent studies have begun to question the primacy of ROS generation in Cu bacterial toxicity,[17,33,79,80] so the lack of consistent ROS-responsive gene induction might suggest that alternative stress pathways are also more important to *S. aureus* Cu toxicity.

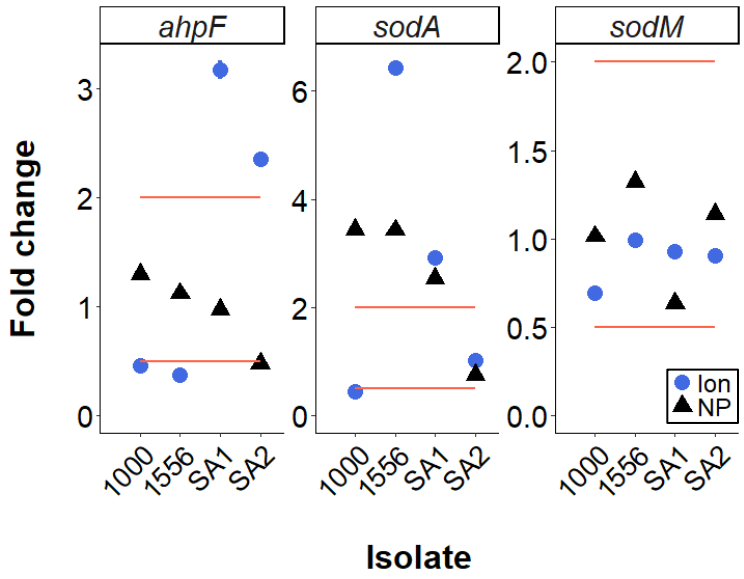

Figure 4.8. ***ROS stress relative gene expression.*** *Note that each gene has a different y-axis. Means and standard deviations of triplicate experiments are depicted, though error bars are obscured by several data points. Red lines are located at 0.5- and 2.0-fold change, where differences were considered statistically significant.*

4.4.D.III Virulence factor transcriptional response. Previous work with Cu^{2+}-exposed SH1000 found reduced expression of genes within the agr and sae operons.[19] We quantified relative expression of genes involved in the primary *agr* and *sae* virulence regulatory systems, namely *agrA*, *RNAIII*, and *saeS*. For many isolates and Cu treatments, especially CuO NP treatments, we measured reductions in *agrA*, *RNAIII*, and *saeS* (**Figure 4.9**). *agrA* expression was

below ½ of the undosed control in the case of the NP-exposed SH1000 (0.25-fold control), SA1 (0.18-fold control), and SA2 (0.31-fold control) and Cu^{2+}-exposed BAA-1556 (0.29-fold control). For SH1000, expression of *agrA* was induced in the presence of Cu^{2+} to 2.6-fold control and *RNAIII* was induced for both Cu^{2+} and CuO NP exposures (2.1- and 3.3-fold control, respectively). All other isolates had reductions in *RNAIII* expression with Cu exposure: CuO NP exposure led to reduction for BAA-1556 (0.45-fold control), SA1 (0.092-fold control), and SA2 (0.12-fold control), and Cu^{2+} led to reduction for SA1 (0.30-fold control) and SA2 (0.32-fold control). *saeS* expression was lower with Cu exposure in all cases, and less than ½ the control with CuO NP exposure for BAA-1556 (0.44-fold control) and SA1 (0.27-fold control) and with Cu^{2+} exposure for SH1000 (0.38-fold control) and BAA-1556 (0.45-fold control).

agrA and *RNAIII* expression of SH1000 again demonstrated a unique transcriptional response to Cu exposure (**Figure 4.9**). Several points could explain why this is, namely the lack of a *copB* gene for additional Cu efflux and, thus, a potentially enhanced stress response to Cu exposure and/or distinct cell wall architecture.

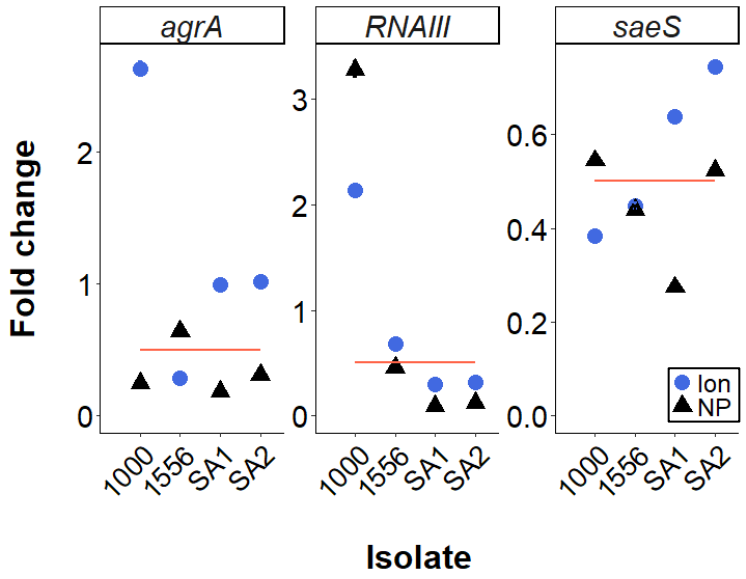

Figure 4.9. ***Virulence-related relative gene expression.*** *Note that each gene has a different y-axis. Means and standard deviations of triplicate experiments are depicted, though error bars are obscured by several data points. Red lines are located at 0.5- and 2.0-fold change, where differences were considered statistically significant.*

4.4.D.IV NMDS across genes for all treatments and isolates. The previous sections discuss specific differences within a class of related genes. But we were interested in looking at trends across all of the genes assayed. NMDS can be used to identify patterns within gene expression datasets,[81] and we implemented it to investigate treatment- and isolate-specific responses to Cu exposure for all of the assayed genes.

Two-dimensional NMDS analysis demonstrates both treatment- and isolate-specific responses to the two Cu exposures (**Figure 4.10**). Most striking is the separation of SH1000 (circles) from other isolates, regardless of treatment. This suggests that SH1000 not only has a unique response to the Cu treatments (**Figures 4.7** and **4.9**), but that its baseline undosed expression is also distinct from that of the other isolates. This aligns with SH1000's differences in CuO NP association (**Figure 4.3**) and, potentially, susceptibility to Cu^{2+} (**Figure 4.4**). It is important to note that *copB* was not considered in the NMDS analysis, so this strain-specific response separation of SH1000 is not simply due to inclusion of a gene that it does not have and cannot

express. While potentially overshadowed by its degree of separation from the MRSA isolates, there is also clear separation among the undosed and Cu-exposed samples, with ion- and NP-dosed samples forming distinct clusters removed from that of the undosed samples.

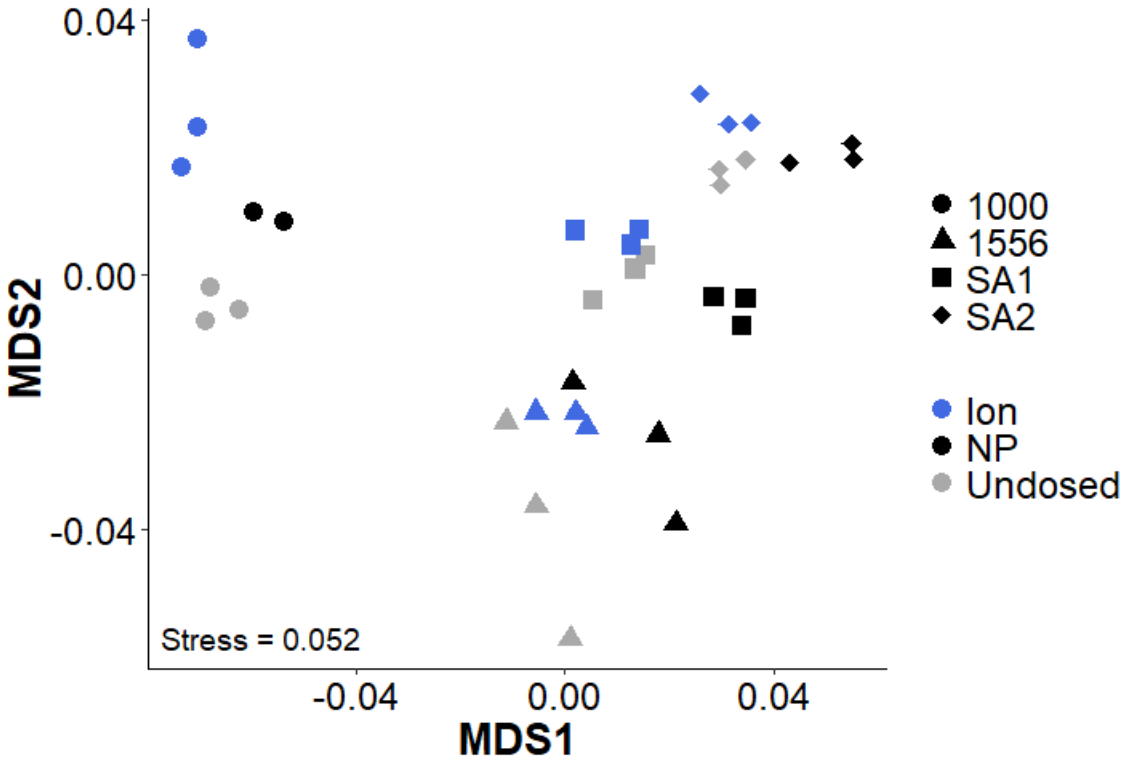

Figure 4.10. ***Non-metric multidimensional scaling (NMDS) across all genes.*** copB *could not be included because of missing data for SH1000, which lacks that gene. And only two NP-dosed SH1000 samples are included because of removed outliers from one of the triplicate samples.*

Among the MRSA isolates, the most conspicuous trend is the separation of the three isolates from one another. The two clinical isolates (squares) form particularly tight clusters that are adjacent to one another. And BAA-1556 samples (triangles) form a looser cluster towards the bottom of the plot. In addition to the isolate-specific responses, there are again clear differences among treatments for each isolate. Interestingly, for all MRSA isolates, Cu^{2+} responses appear more similar to the undosed samples than do the NP responses. For SA1 and SA2, this most likely stems from the reduced expression of virulence factor genes with NP treatment compared

to the undosed control and ion-treated samples (**Figure 4.9**) and is despite particularly strong induction of *copA* and especially *copB* with Cu^{2+} exposure (**Figure 4.6**).

4.5 CONCLUSIONS

Our results provide strong support for further research into the use of CuO NPs for *S. aureus* virulence reduction. They also demonstrate that the four isolates have distinct transcriptional responses to the NP and ion. Lastly, this work provides strong evidence of isolate-specific interactions with and responses to CuO NP and Cu^{2+} exposures.

4.5.A CuO NP exposure inhibits *S. aureus* growth and reduces virulence factor gene expression. There is increasing interest in alternative antimicrobial agents due to high levels of antibiotic resistance and decreases in development of new antibiotics.[2,39,82,83] Cu has a well-established antimicrobial property[15,16] and is relatively non-toxic to humans.[14] With their ability to slowly dissolve,[21,22] CuO NPs are an attractive alternative antimicrobial agent for long-lasting release of the toxic Cu ion. Others have already taken an interest in applying CuO NPs for control of bacterial growth, especially pathogenic organisms.[6–8,10,11] Our results establish the ability of CuO NP exposure to reduce virulence factor gene expression (**Figure 4.9**), in several cases significantly lower than that of ion exposure. This has been shown previously for Cu^{2+} with a MSSA laboratory strain (SH1000).[19] The genes tested here have been directly linked to production of extracellular toxins and virulence within model organisms.[84–87] We additionally demonstrate that CuO NPs can inhibit growth of four *S. aureus* isolates (**Figure 4.4**), including clinically-relevant ones. To the best of our knowledge, ours is the first study to consider effects of Cu exposures on clinically-relevant *S. aureus* isolates and to investigate transcriptional responses of

MRSA strains, including clinically-relevant isolates, to Cu exposures. We are also the first to consider Cu-based NP exposures.

4.5.B *S. aureus* isolates respond to CuO NPs distinctly from Cu^{2+}. A longstanding debate within the ENM toxicity literature is whether soluble NPs impose a unique form of stress than their ionic forms.[24,88–90] We recently showed that the same CuO NPs used in this study induced a membrane damage response in *E. coli* that Cu^{2+} exposure does not.[33] As in our previous work, here we identified association of CuO NPs with bacteria (**Figure 4.3**). NP and ionic exposures led to differential induction of Cu homeostasis genes (*copA* and *copB*; **Figure 4.6**), downstream stress responses in SH1000 (**Figure 4.7**), ROS-responsive genes (*ahpF* and sodA; **Figure 4.8**), and virulence factor genes (*agrA* and *saeS*; **Figure 4.9**). All of these treatment-specific responses for individual genes led us to wonder about treatment-specific transcriptional responses across all of the genes. NMDS showed that, within each isolate, NP- and ion-induced transcriptional responses clustered separately away from that of the undosed samples (**Figure 4.10**). Interestingly, for the MRSA strains, and the clinical isolates in particular, ion-induced responses clustered closer to undosed samples than did CuO NP-treated samples. This suggests that CuO NPs impose a unique stress upon *S. aureus*, including clinically-relevant MRSA, which calls for further improving our understanding of interactions and effects of these antimicrobial NPs on this pathogen and others.

4.5.C Strain-specific responses of *S. aureus* to CuO NP and Cu^{2+} exposures. The genomic diversity of *S. aureus* strains is well documented,[42,46] and it extends beyond integration of antibiotic resistance genes.[91] As might be expected, comparisons of laboratory and clinical isolates of pathogenic bacteria have identified differences in response to antimicrobial agents.[45] Here we compared transcriptional responses of four *S. aureus* isolates – two laboratory isolates and two clinical isolates – and found clear divergence among them (**Figure 4.10**). We expected SH1000,

the MSSA laboratory isolate, to be most distinct based on its lack of an additional Cu homeostasis gene (*copB*) and on the genetic similarity expected of the MRSA strains. The large aggregates it formed in association with CuO NPs was distinct from other isolates (**Figure 4.3**) and unexpected. This could be attributed to disproportionately higher stress arising from the CuO NP exposure, as the induction of the protein damage-responsive, heat and general stress shock, and metal binding genes is also unique to SH1000 (**Figure 4.7**). However, this is not borne out by the growth inhibition data that do not show enhanced susceptibility of SH1000 to CuO NP exposure (**Figure 4.4**), though they do suggest enhanced susceptibility to Cu^{2+}. The MRSA strains' transcriptional responses cluster more closely, but still conspicuously group according to isolate rather than treatment (**Figure 4.10**). These lines of data collectively highlight the need to characterize clinically-relevant organisms alongside the standard laboratory isolates. The hope is that the latter will serve as adequate proxies for the former, but here and elsewhere[45] this has been shown to not be the case.

Our data demonstrate the potential for CuO NP inhibition of *S. aureus* growth and virulence for both laboratory and clinical isolates, including MRSA. Future work should consider transcriptomic responses to CuO NP exposure to ensure that the compelling trends we have identified hold across all expressed genes. Proteomic responses could also be investigated, which could be especially important given the reductions in virulence related gene expression observed here and the use of exotoxins for *S. aureus* pathogenesis.

4.6 ACKNOWLEDGMENTS

The authors wish to acknowledge Dr. Ken Urish of the University of Pittsburgh Medical Center for providing *S. aureus* isolates. Dr. Sónia Morais Rodrigues of the University of Aveiro (Portgual) for help with TEM micrographs.

4.7 REFERENCES FOR CHAPTER FOUR

(1) Stone, P. W. Economic burden of healthcare-associated infections: an American perspective. *Expert Rev. Pharmacoecon. Outcomes Res.* **2009**, *9* (5), 417–422.
(2) Prevention, C. for D. C. and. *Antibiotic resistance threats in the United States, 2013*; Atlanta, 2013.
(3) Beyth, N.; Houri-Haddad, Y.; Domb, A.; Khan, W.; Hazan, R. Alternative Antimicrobial Approach: Nano-Antimicrobial Materials. *Evidence-Based Complement. Altern. Med.* **2015**, *2015*, 1–16.
(4) Wang, L.; Hu, C.; Shao, L. The antimicrobial activity of nanoparticles: present situation and prospects for the future. *Int. J. Nanomedicine* **2017**, *12*, 1227–1249.
(5) Parnia, F.; Yazdani, J.; Javaherzadeh, V.; Maleki Dizaj, S. Overview of Nanoparticle Coating of Dental Implants for Enhanced Osseointegration and Antimicrobial Purposes. *J. Pharm. Pharm. Sci.* **2017**, *20* (0), 148–160.
(6) Mackevica, A.; Revilla, P.; Brinch, A.; Hansen, S. F.; Køber, C.; Mølhave, K.; Larsen, E. H.; Hungerbühler, K.; Ulrich, A.; Thomas, K. V.; et al. Current uses of nanomaterials in biocidal products and treated articles in the EU. *Environ. Sci. Nano* **2016**, *3* (5), 1195–1205.
(7) Tamayo, L.; Azócar, M.; Kogan, M.; Riveros, A.; Páez, M. Copper-polymer nanocomposites: An excellent and cost-effective biocide for use on antibacterial surfaces. *Mater. Sci. Eng. C* **2016**, *69*, 1391–1409.
(8) Ong, H. R.; Ramli, R.; Khan, M. M. R.; Yunus, R. M. The influence of CuO nanoparticle on non-edible rubber seed oil based alkyd resin preparation and its antimicrobial activity. *Prog. Org. Coatings* **2016**, *101*, 245–252.
(9) Musee, N.; Thwala, M.; Nota, N. The antibacterial effects of engineered nanomaterials: implications for wastewater treatment plants. *J. Environ. Monit.* **2011**, *13* (5), 1164.
(10) Dastjerdi, R.; Montazer, M. A review on the application of inorganic nano-structured materials in the modification of textiles: Focus on anti-microbial properties. *Colloids Surfaces B Biointerfaces* **2010**, *79* (1), 5–18.
(11) Parani, M.; Lokhande, G.; Singh, A.; Gaharwar, A. K. Engineered Nanomaterials for Infection Control and Healing Acute and Chronic Wounds. *ACS Appl. Mater. Interfaces* **2016**, *8* (16), 10049–10069.
(12) Aruoja, V.; Pokhrel, S.; Sihtmäe, M.; Mortimer, M.; Mädler, L.; Kahru, A. Toxicity of 12 metal-based nanoparticles to algae, bacteria and protozoa. *Environ. Sci. Nano* **2015**.
(13) Gabbay, J.; Borkow, G.; Mishal, J.; Zatcoff, R.; Shemer-Avni, Y. Copper Oxide Impregnated Textiles with Potent Biocidal Activities. *J. Ind. Text.* **2006**, *35* (4), 323–335.
(14) Flemming, C. A.; Trevors, J. T. Copper toxicity and chemistry in the environment: a review.

Water. Air. Soil Pollut. **1989**, *44* (1–2), 143–158.
(15) Grass, G.; Rensing, C.; Solioz, M. Metallic copper as an antimicrobial surface. *Appl. Environ. Microbiol.* **2011**, *77* (5), 1541–1547.
(16) Dupont, C. L.; Grass, G.; Rensing, C. Copper toxicity and the origin of bacterial resistance--new insights and applications. *Metallomics* **2011**, *3* (11), 1109–1118.
(17) Macomber, L.; Imlay, J. A. The iron-sulfur clusters of dehydratases are primary intracellular targets of copper toxicity. *Proc. Natl. Acad. Sci. U. S. A.* **2009**, *106* (20), 8344–8349.
(18) Chillappagari, S.; Seubert, A.; Trip, H.; Kuipers, O. P.; Marahiel, M. A.; Miethke, M. Copper stress affects iron homeostasis by destabilizing iron-sulfur cluster formation in Bacillus subtilis. *J. Bacteriol.* **2010**, *192* (10), 2512–2524.
(19) Baker, J.; Sitthisak, S.; Sengupta, M.; Johnson, M.; Jayaswal, R. K.; Morrissey, J. A. Copper stress induces a global stress response in Staphylococcus aureus and represses sae and agr expression and biofilm formation. *Appl. Environ. Microbiol.* **2010**, *76* (1), 150–160.
(20) Yamamoto, K.; Ishihama, A. Transcriptional response of Escherichia coli to external copper. *Mol. Microbiol.* **2005**, *56* (1), 215–227.
(21) Vencalek, B. E.; Laughton, S. N.; Spielman-Sun, E.; Rodrigues, S. M.; Unrine, J. M.; Lowry, G. V.; Gregory, K. B. In Situ Measurement of CuO and Cu(OH)2 Nanoparticle Dissolution Rates in Quiescent Freshwater Mesocosms. *Environ. Sci. Technol. Lett.* **2016**, *3* (10), 375–380.
(22) Kent, R. D.; Vikesland, P. J. Dissolution and Persistence of Copper-Based Nanomaterials in Undersaturated Solutions with Respect to Cupric Solid Phases. *Environ. Sci. Technol.* **2016**, *50* (13), 6772–6781.
(23) Applerot, G.; Lellouche, J.; Lipovsky, A.; Nitzan, Y.; Lubart, R.; Gedanken, A.; Banin, E. Understanding the antibacterial mechanism of CuO nanoparticles: revealing the route of induced oxidative stress. *Small* **2012**, *8* (21), 3326–3337.
(24) Navarro, E.; Piccapietra, F.; Wagner, B.; Marconi, F.; Kaegi, R.; Odzak, N.; Sigg, L.; Behra, R. Toxicity of Silver Nanoparticles to Chlamydomonas reinhardtii. *Environ. Sci. Technol.* **2008**, *42* (23), 8959–8964.
(25) Xiu, Z.; Zhang, Q.; Puppala, H.; Colvin, V.; Alvarez, P. Negligible particle-specific antibacterial activity of silver nanoparticles. *Nano Lett.* **2012**, 10–14.
(26) Yin, L.; Cheng, Y.; Espinasse, B.; Colman, B. P.; Auffan, M.; Wiesner, M.; Rose, J.; Liu, J.; Bernhardt, E. S. More than the ions: the effects of silver nanoparticles on Lolium multiflorum. *Environ. Sci. Technol.* **2011**, *45* (6), 2360–2367.
(27) Kaweeteerawat, C.; Chang, C. H.; Roy, K. R.; Liu, R.; Li, R.; Toso, D.; Fischer, H.; Ivask, A.; Ji, Z.; Zink, J. I.; et al. Cu Nanoparticles Have Different Impacts in *Escherichia coli* and *Lactobacillus brevis* than Their Microsized and Ionic Analogues. *ACS Nano* **2015**, *9* (7), 7215–7225.
(28) Yang, X.; Gondikas, A. P.; Marinakos, S. M.; Auffan, M.; Liu, J.; Hsu-Kim, H.; Meyer, J. N. Mechanism of Silver Nanoparticle Toxicity Is Dependent on Dissolved Silver and Surface Coating in *Caenorhabditis elegans*. *Environ. Sci. Technol.* **2012**, *46* (2), 1119–1127.
(29) Li, X.; Lenhart, J. J. Aggregation and Dissolution of Silver Nanoparticles in Natural Surface Water. *Environ. Sci. Technol.* **2012**, *46* (10), 5378–5386.
(30) Peretyazhko, T. S.; Zhang, Q.; Colvin, V. L. Size-Controlled Dissolution of Silver Nanoparticles at Neutral and Acidic pH Conditions: Kinetics and Size Changes. *Environ. Sci. Technol.* **2014**, *48* (20), 11954–11961.

(31) Wang, Z.; von dem Bussche, A.; Kabadi, P. K.; Kane, A. B.; Hurt, R. H. Biological and environmental transformations of copper-based nanomaterials. *ACS Nano* **2013**, *7* (10), 8715–8727.
(32) Ma, R.; Stegemeier, J.; Levard, C.; Dale, J. G.; Noack, C. W.; Yang, T.; Brown, G. E.; Lowry, G. V. Sulfidation of copper oxide nanoparticles and properties of resulting copper sulfide. *Environ. Sci. Nano* **2014**, *1* (4), 347–357.
(33) Moore, J. D.; Avellan, A.; Noack, C. W.; Guo, Y.; Lowry, G. V.; Gregory, K. B. Time-dependent bacterial transcriptional response to CuO nanoparticles differs from that of Cu2+ and provides insights into CuO nanoparticle toxicity mechanisms. **2017**, In review.
(34) Sondi, I.; Salopek-Sondi, B. Silver nanoparticles as antimicrobial agent: a case study on E. coli as a model for Gram-negative bacteria. *J. Colloid Interface Sci.* **2004**, *275* (1), 177–182.
(35) Anderson, D. J.; Kaye, K. S. Staphylococcal Surgical Site Infections. *Infect. Dis. Clin. North Am.* **2009**, *23* (1), 53–72.
(36) Harbarth, S. Control of endemic methicillin-resistant Staphylococcus aureus–-recent advances and future challenges. *Clin. Microbiol. Infect.* **2006**, *12* (12), 1154–1162.
(37) Murthy, A.; De Angelis, G.; Pittet, D.; Schrenzel, J.; Uckay, I.; Harbarth, S. Cost-effectiveness of universal MRSA screening on admission to surgery. *Clin. Microbiol. Infect.* **2010**, *16* (12), 1747–1753.
(38) Patenge, N.; Arndt, K.; Eggert, T.; Zietz, C.; Kreikemeyer, B.; Bader, R.; Nebe, B.; Stranak, V.; Hippler, R.; Podbielski, A. Evaluation of antimicrobial effects of novel implant materials by testing the prevention of biofilm formation using a simple small scale medium-throughput growth inhibition assay. *Biofouling* **2012**, *28* (3), 267–277.
(39) Hogan, S.; Stevens, N. T.; Humphreys, H.; O'Gara, J. P.; O'Neill, E. Current and future approaches to the prevention and treatment of staphylococcal medical device-related infections. *Curr. Pharm. Des.* **2015**, *21* (1), 100–113.
(40) Dufour, P.; Jarraud, S.; Vandenesch, F.; Greenland, T.; Novick, R. P.; Bes, M.; Etienne, J.; Lina, G. High genetic variability of the agr locus in Staphylococcus species. *J. Bacteriol.* **2002**, *184* (4), 1180–1186.
(41) Feng, Y.; Chen, C.-J.; Su, L.-H.; Hu, S.; Yu, J.; Chiu, C.-H.; HS, G. Evolution and pathogenesis of *Staphylococcus aureus* : lessons learned from genotyping and comparative genomics. *FEMS Microbiol. Rev.* **2008**, *32* (1), 23–37.
(42) Herbert, S.; Ziebandt, A. K.; Ohlsen, K.; Schafer, T.; Hecker, M.; Albrecht, D.; Novick, R.; Gotz, F. Repair of Global Regulators in Staphylococcus aureus 8325 and Comparative Analysis with Other Clinical Isolates. *Infect. Immun.* **2010**, *78* (6), 2877–2889.
(43) Gertz, S.; Engelmann, S.; Schmid, R.; Ohlsen, K.; Hacker, J.; Hecker, M. Regulation of σ B -dependent transcription of sigB and asp23 in two different Staphylococcus aureus strains. *Mol. Gen. Genet. MGG* **1999**, *261* (3), 558–566.
(44) Giachino, P.; Engelmann, S.; Bischoff, M. B Activity Depends on RsbU in Staphylococcus aureus. *J. Bacteriol.* **2001**, *183* (6), 1843–1852.
(45) Dridi, B.; Lupien, A.; Bergeron, M. G.; Leprohon, P.; Ouellette, M. Differences in antibiotic-induced oxidative stress responses between laboratory and clinical isolates of streptococcus pneumoniae. *Antimicrob. Agents Chemother.* **2015**, *59* (9), 5420–5426.
(46) Planet, P. J.; Diaz, L.; Kolokotronis, S.-O.; Narechania, A.; Reyes, J.; Xing, G.; Rincon, S.; Smith, H.; Panesso, D.; Ryan, C.; et al. Parallel Epidemics of Community-Associated Methicillin-Resistant Staphylococcus aureus USA300 Infection in North and South

America. *J. Infect. Dis.* **2015**, *212* (12), 1874–1882.
(47) Gao, X.; Spielman-Sun, E.; Rodrigues, S. M.; Casman, E. A.; Lowry, G. V. Time and Nanoparticle Concentration Affect the Extractability of Cu from CuO NP-Amended Soil. *Environ. Sci. Technol.* **2017**, *51* (4), 2226–2234.
(48) Tavares, D. S.; Rodrigues, S. M.; Cruz, N.; Carvalho, C.; Teixeira, T.; Carvalho, L.; Duarte, A. C.; Trindade, T.; Pereira, E.; R?mkens, P. F. A. M. Soil?pore water distribution of silver and gold engineered nanoparticles in undisturbed soils under unsaturated conditions. *Chemosphere* **2015**, *136*, 86–94.
(49) Taurozzi, J. S.; Hackley, V. A.; Wiesner, M. R. Ultrasonic dispersion of nanoparticles for environmental, health and safety assessment – issues and recommendations. *Nanotoxicology* **2011**, *5* (4), 711–729.
(50) Pattee, P. A.; Neveln, D. S. Transformation analysis of three linkage groups in Staphylococcus aureus. *J. Bacteriol.* **1975**, *124* (1), 201–211.
(51) Vitko, N. P.; Richardson, A. R. Laboratory Maintenance of Methicillin-Resistant *Staphylococcus aureus* (MRSA). In *Current Protocols in Microbiology*; John Wiley & Sons, Inc.: Hoboken, NJ, USA, 2013; p 9C.2.1-9C.2.14.
(52) Badireddy, A. R.; Wiesner, M. R.; Liu, J. Detection, characterization, and abundance of engineered nanoparticles in complex waters by hyperspectral imagery with enhanced darkfield microscopy. *Environ. Sci. Technol.* **2012**, *46* (18), 10081–10088.
(53) Avellan, A.; Auffan, M.; Masion, A.; Levard, C.; Bertrand, M.; Rose, J.; Santaella, C.; Achouak, W. Remote Biodegradation of Ge–Imogolite Nanotubes Controlled by the Iron Homeostasis of *Pseudomonas brassicacearum*. *Environ. Sci. Technol.* **2016**, *50* (14), 7791–7798.
(54) McGivney, E.; Han, L.; Avellan, A.; VanBriesen, J.; Gregory, K. B. Disruption of Autolysis in Bacillus subtilis using TiO2 Nanoparticles. *Sci. Rep.* **2017**, *7*, 44308.
(55) Avellan, A.; Levard, C.; Rose, J.; Auffan, M.; Bertrand, M.; Olivi, L.; Santaella, C.; Achouak, W.; Masion, A.; Gallice, P.; et al. Influence of structural defects of Ge-imogolite nanotubes on their toxicity towards Pseudomonas brassicacearum. *Environ. Sci. Nano* **2016**, *3* (4), 839–846.
(56) Peng, S.; Stephan, R.; Hummerjohann, J.; Tasara, T. Evaluation of three reference genes of Escherichia coli for mRNA expression level normalization in view of salt and organic acid stress exposure in food. *FEMS Microbiol. Lett.* **2014**, *355* (1), 78–82.
(57) Livak, K. J.; Schmittgen, T. D. Analysis of Relative Gene Expression Data Using Real-Time Quantitative PCR and the 2−ΔΔCT Method. *Methods* **2001**, *25* (4), 402–408.
(58) Sitthisak, S.; Knutsson, L.; Webb, J. W.; Jayaswal, R. K. Molecular characterization of the copper transport system in Staphylococcus aureus. *Microbiology* **2007**, *153* (12), 4274–4283.
(59) Baker, J.; Sengupta, M.; Jayaswal, R. K.; Morrissey, J. A. The Staphylococcus aureus CsoR regulates both chromosomal and plasmid-encoded copper resistance mechanisms. *Environ. Microbiol.* **2011**, *13* (9), 2495–2507.
(60) Poole, L. B. Bacterial defenses against oxidants: mechanistic features of cysteine-based peroxidases and their flavoprotein reductases. *Arch. Biochem. Biophys.* **2005**, *433* (1), 240–254.
(61) Gaupp, R.; Ledala, N.; Somerville, G. A. Staphylococcal response to oxidative stress. *Front. Cell. Infect. Microbiol.* **2012**, *2*, 33.
(62) Valderas, M. W.; Hart, M. E. Identification and characterization of a second superoxide

dismutase gene (sodM) from Staphylococcus aureus. *J. Bacteriol.* **2001**, *183* (11), 3399–3407.
(63) Clements, M. O.; Watson, S. P.; Foster, S. J. Characterization of the major superoxide dismutase of Staphylococcus aureus and its role in starvation survival, stress resistance, and pathogenicity. *J. Bacteriol.* **1999**, *181* (13), 3898–3903.
(64) Elsholz, A. K. W.; Michalik, S.; Zühlke, D.; Hecker, M.; Gerth, U. CtsR, the Gram-positive master regulator of protein quality control, feels the heat. *EMBO J.* **2010**, *29* (21), 3621–3629.
(65) Derre, I.; Rapoport, G.; Msadek, T. CtsR, a novel regulator of stress and heat shock response, controls clp and molecular chaperone gene expression in Gram-positive bacteria. *Mol. Microbiol.* **1999**, *31* (1), 117–131.
(66) Sitthisak, S.; Kitti, T.; Boonyonying, K.; Wozniak, D.; Mongkolsuk, S.; Jayaswal, R. K.; C, K. McsA and the roles of metal-binding motif in Staphylococcus aureus. *FEMS Microbiol. Lett.* **2012**, *327* (2), 126–133.
(67) Peng, H. L.; Novick, R. P.; Kreiswirth, B.; Kornblum, J.; Schlievert, P. Cloning, characterization, and sequencing of an accessory gene regulator (agr) in Staphylococcus aureus. *J. Bacteriol.* **1988**, *170* (9), 4365–4372.
(68) Novick, R. P.; Ross, H. F.; Projan, S. J.; Kornblum, J.; Kreiswirth, B.; Moghazeh, S. Synthesis of staphylococcal virulence factors is controlled by a regulatory RNA molecule. *EMBO J.* **1993**, *12* (10), 3967–3975.
(69) Giraudo, A. T.; Raspanti, C. G.; Calzolari, A.; Nagel, R. Characterization of a Tn551-mutant of Staphylococcus aureus defective in the production of several exoproteins. *Can. J. Microbiol.* **1994**, *40* (8), 677–681.
(70) Giraudo, A. T.; Calzolari, A.; Cataldi, A. A.; Bogni, C.; Nagel, R. The sae locus of Staphylococcus aureus encodes a two-component regulatory system. *FEMS Microbiol. Lett.* **1999**, *177* (1), 15–22.
(71) Dixon, P. VEGAN, a package of R functions for community ecology. *J. Veg. Sci.* **2003**, *14* (6), 927–930.
(72) R Core Team. R: A Language and Environment for Statistical Computing. Vienna, Austria 2014.
(73) Llarrull, L. I.; Fisher, J. F.; Mobashery, S. Molecular basis and phenotype of methicillin resistance in Staphylococcus aureus and insights into new beta-lactams that meet the challenge. *Antimicrob. Agents Chemother.* **2009**, *53* (10), 4051–4063.
(74) Mongodin, E.; Finan, J.; Climo, M. W.; Rosato, A.; Gill, S.; Archer, G. L. Microarray transcription analysis of clinical Staphylococcus aureus isolates resistant to vancomycin. *J. Bacteriol.* **2003**, *185* (15), 4638–4643.
(75) Gunawan, C.; Teoh, W. Y.; Marquis, C. P.; Amal, R. Cytotoxic Origin of Copper (II) Oxide Nanoparticles : Comparative Studies and Metal Salts. *ACS Nano* **2011**, No. 9, 7214–7225.
(76) Fabrega, J.; Fawcett, S. R.; Renshaw, J. C.; Lead, J. R. Silver Nanoparticle Impact on Bacterial Growth: Effect of pH, Concentration, and Organic Matter. *Environ. Sci. Technol.* **2009**, *43* (19), 7285–7290.
(77) Jin, X.; Li, M.; Wang, J.; Marambio-Jones, C.; Peng, F.; Huang, X.; Damoiseaux, R.; Hoek, E. M. V. High-throughput screening of silver nanoparticle stability and bacterial inactivation in aquatic media: influence of specific ions. *Environ. Sci. Technol.* **2010**, *44* (19), 7321–7328.

(78) Lenz, G. R.; Martell, A. E. Metal Chelates of Some Sulfur-containing Amino Acids *. *Biochemistry* **1964**, *3* (6), 745–750.
(79) Chillappagari, S.; Seubert, A.; Trip, H.; Kuipers, O. P.; Marahiel, M. A.; Miethke, M. Copper stress affects iron homeostasis by destabilizing iron-sulfur cluster formation in Bacillus subtilis. *J. Bacteriol.* **2010**, *192* (10), 2512–2524.
(80) Macomber, L.; Rensing, C.; Imlay, J. A. Intracellular copper does not catalyze the formation of oxidative DNA damage in Escherichia coli. *J. Bacteriol.* **2007**, *189* (5), 1616–1626.
(81) Taguchi, Y. -h.; Oono, Y. Relational patterns of gene expression via non-metric multidimensional scaling analysis. *Bioinformatics* **2005**, *21* (6), 730–740.
(82) Shlaes, D. M.; Sahm, D.; Opiela, C.; Spellberg, B. The FDA reboot of antibiotic development. *Antimicrob. Agents Chemother.* **2013**, *57* (10), 4605–4607.
(83) Agnihotri, S.; Dhiman, N. K. *Development of Nano-antimicrobial Biomaterials for Biomedical Applications*; 2016.
(84) Rogasch, K.; Ruhmling, V.; Pane-Farre, J.; Hoper, D.; Weinberg, C.; Fuchs, S.; Schmudde, M.; Broker, B. M.; Wolz, C.; Hecker, M.; et al. Influence of the Two-Component System SaeRS on Global Gene Expression in Two Different Staphylococcus aureus Strains. *J. Bacteriol.* **2006**, *188* (22), 7742–7758.
(85) Abdelnour, A.; Arvidson, S.; Bremell, T.; Rydén, C.; Tarkowski, A. The accessory gene regulator (agr) controls Staphylococcus aureus virulence in a murine arthritis model. *Infect. Immun.* **1993**, *61* (9), 3879–3885.
(86) Wright, J. S.; Jin, R.; Novick, R. P. Transient interference with staphylococcal quorum sensing blocks abscess formation. *Proc. Natl. Acad. Sci.* **2005**, *102* (5), 1691–1696.
(87) Morfeldt, E.; Taylor, D.; von Gabain, A.; Arvidson, S. Activation of alpha-toxin translation in Staphylococcus aureus by the trans-encoded antisense RNA, RNAIII. *EMBO J.* **1995**, *14* (18), 4569–4577.
(88) Arai, Y.; Miyayama, T.; Hirano, S. Difference in the toxicity mechanism between ion and nanoparticle forms of silver in the mouse lung and in macrophages. *Toxicology* **2015**, *328*, 84–92.
(89) Kaweeteerawat, C.; Chang, C. H.; Roy, K. R.; Liu, R.; Li, R.; Toso, D.; Fischer, H.; Ivask, A.; Ji, Z.; Zink, J. I.; et al. Cu Nanoparticles Have Different Impacts in Escherichia coli and Lactobacillus brevis than Their Microsized and Ionic Analogues. *ACS Nano* **2015**, *9* (7), 7215–7225.
(90) Yin, L.; Cheng, Y.; Espinasse, B.; Colman, B. P.; Auffan, M.; Wiesner, M.; Rose, J.; Liu, J.; Bernhardt, E. S. More than the ions: the effects of silver nanoparticles on Lolium multiflorum. *Environ. Sci. Technol.* **2011**, *45* (6), 2360–2367.
(91) Feng, Y.; Chen, C.-J.; Su, L.-H.; Hu, S.; Yu, J.; Chiu, C.-H. Evolution and pathogenesis of *Staphylococcus aureus* : lessons learned from genotyping and comparative genomics. *FEMS Microbiol. Rev.* **2008**, *32* (1), 23–37.

CHAPTER FIVE:

SUMMARY, MAJOR CONTRIBUTIONS, LIMITATIONS, BROADER IMPACTS, AND FUTURE WORK

5.1 SUMMARY OF THIS THESIS

Antimicrobial ENMs are being incorporated into products despite poor understanding of the interactions between ENMs and bacteria that will ensure those ENMs serve their intended purpose. It is also unclear what potential hazard is posed by increasing release of ENMs into the environment.

The overall objective of this thesis was to inform questions about the types of interactions that lead to an ENM inducing bacterial toxicity. The overall goals were to: (1) improve our understanding of antimicrobial ENMs' impacts on microbial communities within complex environmental systems; (2) inform the mechanism of bacterial toxicity of CuO ENMs, including identification of nanoparticle (NP)-specific impacts; and (3) gauge the potential of an antimicrobial ENM to reduce virulence and growth of bacterial pathogens. Experimental settings ranged from highly complex environmentally-relevant wetland mesocosms to pure bacterial cultures in chemically-defined bacterial growth medium in the laboratory.

Our work in the mesocosms suggests that complex environments have the capacity to mitigate long-term impacts of antimicrobial ENMs on microbial community structure and composition. A metal ion treatment (Cu^{2+}) appeared to have more profound short-term impacts than the two Cu ENM, putting the antimicrobial ENM treatments' effects in context. This work also showed that environmental transformation of antimicrobial ENMs does not universally lead to distinct impacts, as Ag^0 and Ag_2S NPs had dissimilar short-term effects, while those of CuO and CuS NPs were similar.

With some confidence that antimicrobial ENMs are not likely to have devastating effects on environmental microbial communities, we next turned our questions about ENM and bacterial

interactions towards improving our understanding of the source and consequences of antimicrobial ENMs' bacterial effects. Time-resolved transcriptional assays with *E. coli* and CuO NP and Cu^{2+} exposures demonstrated temporally distinct responses to NP treatment compared to that of pulse ion. Response to a gradual ion treatment better tracked with the NP response, but both ion treatments induced significantly higher gene expression than the NP. This work also informed the mechanism of CuO ENM bacterial toxicity and captured a NP-specific transcriptional response. At the same time as Cu-responsive genes were heavily induced, CuO ENM treatment activated a transcriptional response to protein damage and protein cluster assembly, but not ROS, which calls into question the primacy of ROS generation in explaining CuO ENM bacterial toxicity. Additionally, CuO ENMs were found to associate with bacteria and to induce a NP-specific transcriptional response to membrane stress, a stress response not evident with either ion exposure.

We applied lessons learned from our work with a model bacterium to an investigation of CuO NPs' interactions with an important pathogen, *S. aureus*. *S. aureus,* including its methicillin-resistant strains, is a leading cause of infection within healthcare facilities, where there is particular interest in application of antimicrobial agents. Transcriptional assays showed reduction in virulence factor gene expression with CuO NP (and Cu^{2+}) exposure, especially in MRSA clinical isolates. In this work we again found that CuO NP treatment elicited distinct transcriptional responses from Cu^{2+}. Even more distinct than the treatment-specific responses were the isolate-specific responses, with each strain clustering distinctly from the others in an across-gene analysis.

In total, the work compiled in thesis suggests that antimicrobial ENMs' long-term impacts on microbial community structure and composition within complex environments are likely to be

attenuated. More mechanistically, our transcriptional work shows that soluble ENMs have the capacity to affect bacteria beyond their ion release. As others have hypothesized before, our work suggests that ENMs can exert a membrane stress that equivalent ion treatments do not. With *S. aureus* laboratory and clinical isolates we again saw distinct responses to NP and ion exposure. Lastly, we demonstrated that CuO ENM application could have the potential to reduce virulence of a leading cause of healthcare-acquired infection (HAI).

5.2 Major Contribution of this Thesis

5.2.A Major contribution of Objective 1. This work sought to characterize the potential hazard of antimicrobial pristine and transformed Ag and Cu ENMs and Cu^{2+} on microbial communities within an environmentally relevant complex matrix. It further sought to correlate ENM microbial community impacts with metal speciation over time.

5.2.A.I Characterizing microbial community impacts of antimicrobial ENMs within a complex environmental matrix. Considerable research has investigated the short-term effects of antimicrobial ENMs on bacteria in laboratory settings.[1–3] More recent work has observed the ability of naturally occurring ligands, such as natural organic matter (NOM), to mitigate ENMs' biological impacts.[4] Among the studies that have sought to characterize impacts of ENMs within more complex environments,[5–10] the longest we were aware of lasted two months. We compared time-resolved impacts of four different Ag- and Cu-based ENMs and Cu^{2+} on surficial sediment microbial communities within environmentally relevant wetland mesocosms over the course of nearly a year.

We found that short-term effects of high doses of antimicrobial ENMs on microbial communities within a complex environment were dissipated by 300 days. Our experiments did not determine what the source of the dissipation was; however, we can offer a few hypotheses. One possibility is that ENM transformation effectively obviated ion release. Alternatively, seasonal turnover, with its addition of detritus to the surficial sediment, might have led to removal of the ENMs from the surficial sediment layer and deposition into the actual sediment. We also found that Cu^{2+} dosing led to more profound impacts than either of the Cu-based ENMs, or, seemingly, than any of the ENM treatments. Combined, these findings suggest that antimicrobial ENM impacts on microbial communities within complex environments might be less than initially feared.

5.2.A.II Assessing the role of sulfidation on ENM microbial community impacts. Previous work has shown that ENMs can transform in environmental matrices, e.g., Ag^0 can sulfidize to Ag_2S.[11,12] Sulfidation of Ag produces a much less soluble chemical species that releases very little dissolved Ag and, thus, has lower biological impacts.[13–15] While this observation had been made in laboratory settings, no work that we were aware of had investigated biological impacts of pristine and transformed ENMs within environmentally relevant settings. We sought to compare effects of pristine (Ag^0 and CuO) and sulfidized (Ag_2S and CuS) Ag and Cu ENMs on microbial communities within an environmentally relevant system.

We found that metal speciation did not necessarily correlate with observed ENM impacts on microbial communities. Speciation results showed that the chemical species of the Ag ENMs quickly converged, yet their short-term impacts on the surficial sediment microbial communities were highly divergent. Meanwhile, Cu species remained distinct through the course of the 300-day experiment, but their effects on the microbial communities were similar. These results

suggest that sulfidation might not fully mitigate short-term biological impacts. Instead, its capacity to mitigate effects appears to be ENM (and metal) specific.

5.2.B Major contributions of Objective 2. This work sought to improve our understanding of bacterial interactions with an antimicrobial ENM, CuO NPs, and to identify NP-specific effects of that ENM on a model bacterium. Specifically, it attempted to inform the mechanism of toxicity of CuO NPs against *E. coli*, especially the role of ROS generation in CuO NP bacterial toxicity. It further sought to characterize the transcriptional response profiles of pulse versus gradual inputs of Cu^{2+}.

5.2.B.I Identifying a NP-specific transcriptional effect of CuO NPs on *E. coli*. Much debate within the nanotoxicity literature has dealt with the existence of unique NP-specific effects versus wholly ion-mediated effects.[7,16–20] The most common proposed NP-specific impact is membrane damage due to preferential adsorption of NPs onto bacterial membranes.[21–24] We sought to consider both NP association with bacteria and expression of genes involved in membrane stress response to determine if NP exposure within our system yielded a unique NP-specific effect on *E. coli* membranes.

We observed induction of a membrane stress-responsive gene only with NP exposure, whose induction aligned with imaging of NP-*E. coli* associations. *otsB*, which encodes for a protein that produces trehalose bound for the membrane, is responsive to various membrane stressors, including other NPs.[25–29] *otsB* was induced only under NP treatment and only at 30 min. The time-sensitivity of the effect agrees with hyperspectral imaging (HSI) that show strong association of NPs and *E. coli* at 30 min, and diminishing association thereafter. We suspect that adsorption of a NP onto a bacterium effectively sequestered the NP for the duration of the three hour experiment. This would explain the ephemeral nature of the NP-bacteria association. We

posit that the ephemeral nature of the *otsB* induction is due to NP association leading to cell death due to a combination of membrane stress and potentially high ion release n the immediate vicinity of the bacteria. If NPs are sequestered by this cellular debris, one would not expect to see later induction of *otsB*.

5.2.B.II Updating the mechanistic understanding of CuO ENM bacterial toxicity. Since 2007, research into the bacterial toxicity of Cu^{2+} has questioned the primacy of ROS generation for explaining the toxicity of the Cu ion.[30,31] CuO ENM bacterial toxicity research has continued to identify ROS as the most important factor conferring its toxicity.[22,32] Using time-resolved transcriptional assays, we detected when Cu exposures led to induction of *E. coli* gene expression and what downstream stress responses followed. We used two methods to look at oxidative stress and ROS abundance.

We found induction of Cu-responsive genes to occur concurrently with protein damage responses, with little evidence of ROS-generated stress occurring on the same time scale. Interestingly, while low at the time of peak Cu and protein damage transcriptional responses, oxidative stress and ROS abundance were heightened at a later time point when Cu-responsive gene induction was diminished. Why might this be? One explanation could be the displacement of Fe by Cu within Fe-S cluster proteins. With higher concentrations of free intracellular Fe, classic Fe-based Fenton chemistry could ensue, generating ROS and triggering ROS-responsive gene expression.

5.2.B.III Comparing transcriptional responses to pulse and gradual ionic and NP inputs. Many nanotoxicity studies compare biological impacts of soluble ENMs to ionic species.[29,32,33] The vast majority of these studies add the ion at the start of the experiment, despite the kinetically-limited dissolution of most biological systems containing soluble ENMs.[34] The

amount of ion deemed equivalent to the ENM treatment also varies, with some studies using the same mass concentration of ENM and ionic metal.[7,29] We measured the dissolution of CuO NPs in our biological growth medium and employed a pulse ion treatment where all equivalent ion was added at the beginning of the experiment and a gradual ion treatment where the same total equivalent ion was added in four inputs to better reflect the slow dissolution of the NPs. By using time-resolved transcriptional assays, we measured gene expression responses to these two ionic treatments and that of the ion.

We found that gradual ion input led to temporally distinct transcriptional responses than the pulse ion treatment and, importantly, gradual ion was more similar to that of the NP. Pulse ion treatment led to peak induction by 30 min and then lower induction, while gradual ion and NP treatments led to increasing induction through 60 min. Both ionic treatments led to higher maximum induction levels than did the NP, despite comprising just 1% of the ENM's total Cu input. This demonstrates the importance of the ion in eliciting bacterial transcriptional responses to soluble CuO NP exposures.

5.2.C Major contribution of Objective 3. In this work we sought to characterize the potential for CuO NP application to limit different *S. aureus* isolates' virulence. We used RT-qPCR transcriptional assays to measure relative gene expression of methicillin-susceptible *S. aureus* (MSSA) and methicillin-resistant *S. aureus* (MRSA) isolates in response to CuO NP and Cu^{2+} exposures. *S. aureus* strains display genomic variability, including within virulence factor operons, e.g., *agr*,[35] so we included both laboratory and clinical strains for this work. Three out of the four strains were MRSA.

5.2.C.I Characterizing transcriptional responses to CuO nanoparticle and Cu^{2+} exposures. As discussed above, nanotoxicity researchers continue to debate the source of

bacterial toxicity: Is it released ion or a NP-specific effect?[20,36–38] We previously showed that equivalent NP and ion doses lead to differential transcriptional responses in *E. coli*,[39] and here we wondered if the same would be true for *S. aureus* isolates. As in that prior study, we exposed the bacteria to CuO NPs and the equivalent dissolved fraction of the NPs in the growth medium – 100 mg/L CuO NPs as Cu and 16 ppm Cu^{2+}, in this case. We investigated transcriptional responses after a one hour exposure.

We observed clear differences between NP- and ion-induced transcriptional responses with individual genes and across all genes considered. Genes involved in Cu homeostasis, stress response, ROS-response, and virulence all displayed differential relative expression for at least one of the isolates. Across all genes, except for *copB*, within-strain differential transcription was evident for all isolates. Interestingly, non-metric multidimensional scaling (NMDS) results suggest that transcriptional responses to NP exposures were more different from the undosed samples than were the ion-exposed samples, especially for the clinical isolates.

5.2.C.II Impacts of CuO NP and Cu^{2+} exposures on *S. aureus* isolates' virulence gene expression. Previous work showed the potential for Cu^{2+} exposure to lead to reductions in virulence factor gene expression of the *S. aureus* laboratory strain SH1000.[40] Given their slow release of dissolved Cu, CuO NP application could be an attractive means by which to achieve Cu^{2+} release where potential for *S. aureus* and other pathogen infection is high, e.g., medical settings. We sought to understand the potential of CuO NPs for reducing virulence factor gene expression in both laboratory and clinical isolates.

We found that Cu exposure, and CuO NPs in particular, led to reductions in expression of the three virulence factor genes assessed, especially for MRSA strains. For MRSA strains, NP exposure universally resulted in reduction of expression of all three genes. In six of the nine

cases, expression was reduced below half of that of the undosed control. Expression of *agrA* for NP-exposed clinical isolates was less than half of that of their Cu^{2+}-exposed counterparts, too.

5.2.C.III Analysis of isolate-specific relative gene expression. Laboratory and clinical isolates of pathogenic bacteria have previously been reported to respond differently to antimicrobial treatments.[41] *S. aureus* is known to be genomically diverse,[42,43] providing further reason to suspect that different *S. aureus* isolates might have unique responses to stress.

We identified isolate-specific transcriptional responses to CuO NP and Cu^{2+} treatments. Plotting of NMDS results demonstrated clear preference for clustering by isolate compared to by treatment. Both were conspicuous, but isolate was dominant. This calls for, at the least, consideration of relevant *S. aureus* isolates when studying responses to Cu treatments. The differences among isolates could be attributed to their genomic diversity. SH1000 lacks *copB*, and the MRSA isolates have *mec* genes conferring methicillin resistance. But we have not amassed an exhaustive list of their genomic differences.

5.3 Limitations of this Thesis

Every attempt was made to perceive and address potential limitations at the start of these studies. The first two studies were widely presented to seek outsider feedback, too. Despite these efforts, there are limitations to each area of research.

5.3.A Limitations of Objective 1. The ability to extrapolate from this work is limited by the lack of replicates involved in this study. We cannot predict how different of a response a similar system exposed to the same metal exposure might have had. Fortunately the time-resolved data present a consistent story across measurements that converges with an undosed control.

Additionally, it is known that the regimen by which ENMs are added to a system influences their ultimate fate.[44] In this experiment, we employed pulse inputs (divided into four equal doses over the course of the first month of the experiment to ensure aquatic concentrations did not lead to a plant die-off) that ultimately achieved a high dose of Ag or Cu to the surficial sediment layer. A pulse input might represent a worst case scenario input of ENMs into an environment, perhaps via an accidental release at a ENM manufacturing center or a spill during transportation of ENMs. It is probably less likely than a chronic input, or continuous low level addition of ENM.

5.3.B Limitations of Objective 2. For this work we attempted to identify the most relevant genes for both Cu and ENM exposures. We relied heavily upon past work investigating *E. coli*'s response to various Cu^{2+} treatments. We also perused the oxidative stress literature to determine which of the numerous oxidative stress-responsive genes are believed to be the most important to *E. coli*. Fortunately *E. coli* is a model organism, and the literature was ample. We considered other studies of transcriptional responses to NP exposures, as well. Nevertheless, the primary limitation of this work is the number of genes that were investigated via reverse transcriptase quantitative polymerase chain reaction (RT-qPCR). Such targeted approaches are inevitably susceptible to the "you don't know what you don't know" criticism. Future Research presents options for addressing this limitation.

The lack of protein quality data is an additional limitation. Our gene expression data provide a strong basis for suspecting that protein damage is a primary mechanism of CuO NP bacterial toxicity, but we did not corroborate those data with measurements of protein quality. This, too, will be addressed in Future Research below.

5.3.C Limitations of Objective 3. As was the case for Objective 3, one of the primary limitations of this work is the targeted RT-qPCR approach. In comparison to the model

bacterium *E. coli*, *S. aureus* transcriptional responses are poorly characterized, which further confounded the identification of relevant genes, including those that are responsive to membrane damage and might be uniquely induced by NP exposure. Other limitations include the use of poorly characterized clinical *S. aureus* isolates. It is believed that these are USA300 strains, like BAA-1556, but that has not been proved. The lack of exoprotein quantification with CuO NP exposure is also a limitation. These will be discussed in Future Research below.

5.4 Significance and Broader Impacts

5.4.A Significance and broader impacts of objective 1. This work established that impacts of high doses of antimicrobial ENMs on microbial communities were mitigated by 300 days, potentially lessening the impetus to regulate antimicrobial ENMs in order to limit environmental release. The observation that sulfidation mitigated impacts of one ENM (Ag^0) and not another (CuO) could ensure that future researchers do not attempt to characterize ENM transformation as a universal attenuator of ENMs' impacts on microbial communities.

5.4.B Significance and broader impacts of objective 2. By updating the mechanism of CuO NP bacterial toxicity, this work could enable future efforts to apply CuO NPs to commercial products with the goal of inhibiting bacterial growth. This is also one of the first attempts to question the role of ROS within CuO NP bacterial toxicity, which could open new areas of research within CuO NP bacterial toxicity. This work identified a unique membrane damage response to NP exposure, which should inform the ongoing debate within the nanotoxicity field about the origin of soluble antimicrobial ENMs. And by measuring temporally distinct transcriptional responses with pulse and gradual ion treatments, this work should compel the

field to employ more representative ionic controls for comparison against soluble ENMs' biological impacts.

5.4.C Significance and broader impacts of objective 3. By showing reductions in virulence gene expression in response to CuO NP exposure this work should motivate greater research and commercial interest in applying CuO NPs and other Cu-based NPs for inhibition of *S. aureus* growth and virulence in sensitive settings. Considerable research efforts are already being made to understand the potential of antimicrobial ENMs to inhibit bacteria growth, e.g., Ref 45-48. But as far as we know, this is the first to demonstrate an ENM's capacity to lower virulence gene expression. This work should also propel the nanotoxicity community to consider more clinically-relevant experimental systems and non-model strains that we showed can have distinct transcriptional responses to Cu exposures and interactions with CuO NPs than the commonly studied laboratory strain (SH1000 in our case).

5.5 FUTURE RESEARCH

5.5.A Future research for objective 1. Future research efforts could focus on replication of this work within similarly complex systems, use of alternative dosing regimens, or metagenomic analysis of samples. Within our complex wetland system, we determined that impacts of high doses of Ag- and Cu-based ENMs were mitigated by 300 d, but we did not have access to enough mesocosms to run this experiment in triplicate or even duplicate. Future work could investigate whether the same long-term trend is observed in a similar wetland system or other complex environmental system.

Our study employed worst case scenario pulse inputs, but a more environmentally relevant input scenario is likely continuous, low-level ENM addition, e.g., from a wastewater treatment plant or agricultural run-off. It is known that pulse ENM additions lead to different ENM fate and transport than gradual additions of the same ENM.[44] Future work could compare the long-term effects of the alternative dosing regimens on microbial communities within complex environmental systems.

Our work used 16S amplicon sequencing to investigate short- and long-term microbial community impacts and ultimately showed that microbial community structure and composition re-converged by 300 days. Efforts were made to extrapolate out from microbial community trends and identify potentially enriched or depleted functional processes, e.g., heightened methanogenesis potential at 180 days based on a blooming of *Methanobacterium*. Metagenomic and metatranscriptomic tools exist that could obviate the need to make such leaps in future studies. A metagenomic approach would sequence all DNA within a sample and allow for quantification of genetic potential. Metatranscriptomics would instead sequence mRNA and thus provide a view of active processes.

Either of these "meta-" approaches could also provide a means to test additional hypotheses about the impacts of metal addition on microbial communities. One area of particular interest is the potential for co-selection of metal and antibiotic resistance genes (ARG). Many studies have identified a correlation between metal concentrations and ARGs.[49–56] A few have even shown that ENM exposure can lead to enhanced horizontal gene transfer (HGT).[57,58] Other stressors have also been found to induce bacterial conjugation.[59–61] One might theorize that the low level of dissolved ion a soluble antimicrobial ENM might release could provide a sublethal stress that

could induce conjugation and result in higher frequencies of mobile genetic elements (MGE), like the ones that ARGs are known to reside on.[62]

5.5.B Future research for objective 2. Future research efforts could fully explore the transcriptomic response and attempt to measure protein quality after CuO NP treatment. The former could be achieved by RNA-seq, which can sequence all mRNA within a sample,[63] and is thus not limited to expression of selected target genes, as is the RT-qPCR approach employed. RNA-seq would allow for both hypothesis-driven analyses that focus on genes of known interest and data mining that could reveal discovery of novel genes and pathways affected by CuO NP exposure over time. While sequencing costs have decreased considerably,[64] cost can still be a limiting factor that requires prioritization of samples. CuO NP-exposed and undosed *E. coli* could be prioritized for RNA-seq, and follow up experiments using RT-qPCR could be conducted to investigate differential gene expression in Cu^{2+}-exposed *E. coli*.

Another area of future research could be investigating protein quality impacts of CuO NP exposure. One study investigating the bacterial impacts of Cu-based NPs reported reduced activity of a single protein in the presence of Cu_2O NPs, but not in the presence of CuO NPs.[23] Our study identified significant induction of genes involved in periplasmic protein damage and folding responses, *cpxP* and *spy*, respectively, with CuO NP exposure. Alkaline phosphatase is an abundant periplasmic protein whose activity within bacteria has been the subject of considerable research efforts.[65,66] Alkaline phosphatase protein standards and activity assays exist, making this an attractive option for corroborating our gene expression results and identifying periplasmic protein damage as another mechanism of CuO NP bacterial toxicity.

5.5.C Future research for objective 3. As with Objective 2, future research efforts should consider using RNA-seq to look at the entire transcriptomic response of the clinical isolates to

CuO NP exposure. This would allow for more holistic analysis of the gene expression similarities and differences across treatments and isolates. It could also help to explain the link between Cu stress and virulence factor gene expression and to identify additional genes of interest, especially other virulence-related genes and membrane stress-responsive genes induced by NP exposure.

Other follow up experiments could attempt to more directly assess the treatments' effects on virulence. One path forward would be to investigate virulence-related exoprotein production. *S. aureus* infection is due in large part to its production of toxins.[67] Phenol soluble modulins (PSM) are important to *S. aureus* pathogenicity, and are widely conserved across the various *S. aureus* strains.[67] Importantly given our findings, at least one class of the few classes of *S. aureus* PSMs, δ-toxin, have been linked to the *agr* system, and *RNAIII* in particular.[68] Quantification of PSMs with and without CuO NP exposure would have a strong link to our gene expression results and could provide a more direct connection between CuO NP exposure and reductions in *S. aureus* virulence.

Another follow up of the gene expression work would involve assessing biofilm formation in response to the Cu exposures. In addition to playing a role in virulence, the agr regulatory system affects *S. aureus* biofilm formation.[69–71] Regulation of biofilm formation is multifactorial,[70,71] but agr appears to enable dispersal from a biofilm.[69] Investigating *S. aureus* isolate biofilm dispersal as a function of CuO NP exposure could show that function and not just gene expression are affected by Cu exposure.

Efforts should also be made to confirm the identities of the SA1 and SA2 clinical isolates as USA300 and determine their genomes. This would be especially important were RNA-seq pursued.

5.6 REFERENCES FOR CHAPTER FIVE

(1) Fabrega, J.; Fawcett, S. R.; Renshaw, J. C.; Lead, J. R. Silver Nanoparticle Impact on Bacterial Growth: Effect of pH, Concentration, and Organic Matter. *Environ. Sci. Technol.* **2009**, *43* (19), 7285–7290.

(2) Sondi, I.; Salopek-Sondi, B. Silver nanoparticles as antimicrobial agent: a case study on E. coli as a model for Gram-negative bacteria. *J. Colloid Interface Sci.* **2004**, *275* (1), 177–182.

(3) Heinlaan, M.; Ivask, A.; Blinova, I.; Dubourguier, H.-C.; Kahru, A. Toxicity of nanosized and bulk ZnO, CuO and TiO2 to bacteria Vibrio fischeri and crustaceans Daphnia magna and Thamnocephalus platyurus. *Chemosphere* **2008**, *71* (7), 1308–1316.

(4) Bertuccio, A. J.; Tilton, R. D. Silver Sink Effect of Humic Acid on Bacterial Surface Colonization in the Presence of Silver Ions and Nanoparticles. *Environemntal Sci. Technol.* **2017**, *51* (3), 1754–1763.

(5) Bradford, A.; Handy, R. D.; Readman, J. W.; Atfield, A.; Mühling, M. Impact of silver nanoparticle contamination on the genetic diversity of natural bacterial assemblages in estuarine sediments. *Environ. Sci. Technol.* **2009**, *43* (12), 4530–4536.

(6) Colman, B. P.; Wang, S.-Y.; Auffan, M.; Wiesner, M. R.; Bernhardt, E. S. Antimicrobial effects of commercial silver nanoparticles are attenuated in natural streamwater and sediment. *Ecotoxicology* **2012**, *21* (7), 1867–1877.

(7) Yang, Y.; Quensen, J.; Mathieu, J.; Wang, Q.; Wang, J.; Li, M.; Tiedje, J. M.; Alvarez, P. J. J. Pyrosequencing reveals higher impact of silver nanoparticles than Ag+ on the microbial community structure of activated sludge. *Water Res.* **2014**, *48*, 317–325.

(8) Ma, Y.; Metch, J. W.; Vejerano, E. P.; Miller, I. J.; Leon, E. C.; Marr, L. C.; Vikesland, P. J.; Pruden, A. Microbial community response of nitrifying sequencing batch reactors to silver, zero-valent iron, titanium dioxide and cerium dioxide nanomaterials. *Water Res.* **2015**, *68*, 87–97.

(9) Norman, B. C.; Xenopoulos, M. A.; Braun, D.; Frost, P. C. Phosphorus Availability Alters the Effects of Silver Nanoparticles on Periphyton Growth and Stoichiometry. *PLoS One* **2015**, *10* (6), e0129328.

(10) Gil-Allué, C.; Schirmer, K.; Tlili, A.; Gessner, M. O.; Behra, R. Silver Nanoparticle Effects on Stream Periphyton During Short-Term Exposures. *Environ. Sci. Technol.* **2015**, *49* (2), 1165–1172.

(11) Levard, C.; Reinsch, B. C.; Michel, F. M.; Oumahi, C.; Lowry, G. V; Brown, G. E. Sulfidation processes of PVP-coated silver nanoparticles in aqueous solution: impact on dissolution rate. *Environ. Sci. Technol.* **2011**, *45* (12), 5260–5266.

(12) Wang, Z.; von dem Bussche, A.; Kabadi, P. K.; Kane, A. B.; Hurt, R. H. Biological and environmental transformations of copper-based nanomaterials. *ACS Nano* **2013**, *7* (10), 8715–8727.

(13) Reinsch, B. C.; Levard, C.; Li, Z.; Ma, R.; Wise, a; Gregory, K. B.; Brown, G. E.; Lowry, G. V. Sulfidation of silver nanoparticles decreases Escherichia coli growth inhibition. *Environ. Sci. Technol.* **2012**, *46* (13), 6992–7000.

(14) Dharsana, U. S.; Sai Varsha, M. K. N.; Khan Behlol, A. A.; Veerappan, A.; Thiagarajan, R. Sulfidation modulates the toxicity of biogenic copper nanoparticles. *RSC Adv.* **2015**, *5* (38), 30248–30259.

(15) Levard, C.; Hotze, E. M.; Colman, B. P.; Dale, A. L.; Truong, L.; Yang, X. Y.; Bone, A.

J.; Brown, G. E.; Tanguay, R. L.; Di Giulio, R. T.; et al. Sulfidation of silver nanoparticles: Natural antidote to their toxicity. *Environ. Sci. Technol.* **2013**, *47* (23), 13440–13448.
(16) Lubick, N. Nanosilver toxicity: ions, nanoparticles□or both? *Environ. Sci. Technol.* **2008**, *42* (23), 8617–8617.
(17) Studer, A. M.; Limbach, L. K.; Van Duc, L.; Krumeich, F.; Athanassiou, E. K.; Gerber, L. C.; Moch, H.; Stark, W. J. Nanoparticle cytotoxicity depends on intracellular solubility: comparison of stabilized copper metal and degradable copper oxide nanoparticles. *Toxicol. Lett.* **2010**, *197* (3), 169–174.
(18) Tsai, Y. Y.; Huang, Y. H.; Chao, Y. L.; Hu, K. Y.; Chin, L. Te; Chou, S. H.; Hour, A. L.; Yao, Y. Der; Tu, C. S.; Liang, Y. J.; et al. Identification of the nanogold particle-induced endoplasmic reticulum stress by omic techniques and systems biology analysis. *ACS Nano* **2011**, *5* (12), 9354–9369.
(19) Kaweeteerawat, C.; Chang, C. H.; Roy, K. R.; Liu, R.; Li, R.; Toso, D.; Fischer, H.; Ivask, A.; Ji, Z.; Zink, J. I.; et al. Cu Nanoparticles Have Different Impacts in *Escherichia coli* and *Lactobacillus brevis* than Their Microsized and Ionic Analogues. *ACS Nano* **2015**, *9* (7), 7215–7225.
(20) Xiu, Z.; Zhang, Q.; Puppala, H.; Colvin, V.; Alvarez, P. Negligible particle-specific antibacterial activity of silver nanoparticles. *Nano Lett.* **2012**, 10–14.
(21) Lesniak, A.; Salvati, A.; Santos-Martinez, M. J.; Radomski, M. W.; Dawson, K. A.; Åberg, C. Nanoparticle Adhesion to the Cell Membrane and Its Effect on Nanoparticle Uptake Efficiency. *J. Am. Chem. Soc.* **2013**, *135* (4), 1438–1444.
(22) Applerot, G.; Lellouche, J.; Lipovsky, A.; Nitzan, Y.; Lubart, R.; Gedanken, A.; Banin, E. Understanding the antibacterial mechanism of CuO nanoparticles: revealing the route of induced oxidative stress. *Small* **2012**, *8* (21), 3326–3337.
(23) Meghana, S.; Kabra, P.; Chakraborty, S.; Padmavathy, N. Understanding the pathway of antibacterial activity of copper oxide nanoparticles. *RSC Adv.* **2015**, *5* (16), 12293–12299.
(24) Guo, J.; Gao, S.-H.; Lu, J.; Bond, P. L.; Verstraete, W.; Yuan, Z. Copper Oxide Nanoparticles Induce Lysogenic Bacteriophage and Metal-Resistance Genes in Pseudomonas aeruginosa PAO1. *ACS Appl. Mater. Interfaces* **2017**, in press.
(25) Balaji, B.; O'Connor, K.; Lucas, J. R.; Anderson, J. M.; Csonka, L. N. Timing of induction of osmotically controlled genes in Salmonella enterica Serovar Typhimurium, determined with quantitative real-time reverse transcription-PCR. *Appl. Environ. Microbiol.* **2005**, *71* (12), 8273–8283.
(26) Strøm, A. R.; Kaasen, I. Trehalose metabolism in Escherichia coli: stress protection and stress regulation of gene expression. *Mol. Microbiol.* **1993**, *8* (2), 205–210.
(27) Kandror, O.; DeLeon, A.; Goldberg, A. L. Trehalose synthesis is induced upon exposure of Escherichia coli to cold and is essential for viability at low temperatures. *Proc. Natl. Acad. Sci. U. S. A.* **2002**, *99* (15), 9727–9732.
(28) Sohm, B.; Immel, F.; Bauda, P.; Pagnout, C. Insight into the primary mode of action of TiO2 nanoparticles on Escherichia coli in the dark. *Proteomics* **2015**, *15* (1), 98–113.
(29) McQuillan, J. S.; Shaw, A. M. Differential gene regulation in the Ag nanoparticle and Ag(+)-induced silver stress response in Escherichia coli: A full transcriptomic profile. *Nanotoxicology* **2014**, *5390* (I), 1–8.
(30) Macomber, L.; Imlay, J. A. The iron-sulfur clusters of dehydratases are primary intracellular targets of copper toxicity. *Proc. Natl. Acad. Sci. U. S. A.* **2009**, *106* (20),

8344–8349.
(31) Macomber, L.; Rensing, C.; Imlay, J. A. Intracellular copper does not catalyze the formation of oxidative DNA damage in Escherichia coli. *J. Bacteriol.* **2007**, *189* (5), 1616–1626.
(32) Gunawan, C.; Teoh, W. Y.; Marquis, C. P.; Amal, R. Cytotoxic Origin of Copper (II) Oxide Nanoparticles : Comparative Studies and Metal Salts. *ACS Nano* **2011**, No. 9, 7214–7225.
(33) Yang, Y.; Wang, J.; Xiu, Z.; Alvarez, P. J. J. Impacts of silver nanoparticles on cellular and transcriptional activity of nitrogen-cycling bacteria. *Environ. Toxicol. Chem.* **2013**, *32* (7), 1488–1494.
(34) Vencalek, B. E.; Laughton, S. N.; Spielman-Sun, E.; Rodrigues, S. M.; Unrine, J. M.; Lowry, G. V.; Gregory, K. B. In Situ Measurement of CuO and Cu(OH)2 Nanoparticle Dissolution Rates in Quiescent Freshwater Mesocosms. *Environ. Sci. Technol. Lett.* **2016**, *3* (10), 375–380.
(35) Feng, Y.; Chen, C.-J.; Su, L.-H.; Hu, S.; Yu, J.; Chiu, C.-H. Evolution and pathogenesis of *Staphylococcus aureus* : lessons learned from genotyping and comparative genomics. *FEMS Microbiol. Rev.* **2008**, *32* (1), 23–37.
(36) Navarro, E.; Piccapietra, F.; Wagner, B.; Marconi, F.; Kaegi, R.; Odzak, N.; Sigg, L.; Behra, R. Toxicity of Silver Nanoparticles to Chlamydomonas reinhardtii. *Environ. Sci. Technol.* **2008**, *42* (23), 8959–8964.
(37) Arai, Y.; Miyayama, T.; Hirano, S. Difference in the toxicity mechanism between ion and nanoparticle forms of silver in the mouse lung and in macrophages. *Toxicology* **2015**, *328*, 84–92.
(38) Kaweeteerawat, C.; Chang, C. H.; Roy, K. R.; Liu, R.; Li, R.; Toso, D.; Fischer, H.; Ivask, A.; Ji, Z.; Zink, J. I.; et al. Cu Nanoparticles Have Different Impacts in Escherichia coli and Lactobacillus brevis than Their Microsized and Ionic Analogues. *ACS Nano* **2015**, *9* (7), 7215–7225.
(39) Moore, J. D.; Avellan, A.; Noack, C. W.; Guo, Y.; Lowry, G. V.; Gregory, K. B. Time-dependent bacterial transcriptional response to CuO nanoparticles differs from that of Cu2+ and provides insights into CuO nanoparticle toxicity mechanisms. **2017**, In review.
(40) Baker, J.; Sitthisak, S.; Sengupta, M.; Johnson, M.; Jayaswal, R. K.; Morrissey, J. A. Copper stress induces a global stress response in Staphylococcus aureus and represses sae and agr expression and biofilm formation. *Appl. Environ. Microbiol.* **2010**, *76* (1), 150–160.
(41) Dridi, B.; Lupien, A.; Bergeron, M. G.; Leprohon, P.; Ouellette, M. Differences in antibiotic-induced oxidative stress responses between laboratory and clinical isolates of streptococcus pneumoniae. *Antimicrob. Agents Chemother.* **2015**, *59* (9), 5420–5426.
(42) Planet, P. J.; Diaz, L.; Kolokotronis, S.-O.; Narechania, A.; Reyes, J.; Xing, G.; Rincon, S.; Smith, H.; Panesso, D.; Ryan, C.; et al. Parallel Epidemics of Community-Associated Methicillin-Resistant Staphylococcus aureus USA300 Infection in North and South America. *J. Infect. Dis.* **2015**, *212* (12), 1874–1882.
(43) Herbert, S.; Ziebandt, A. K.; Ohlsen, K.; Schafer, T.; Hecker, M.; Albrecht, D.; Novick, R.; Gotz, F. Repair of Global Regulators in Staphylococcus aureus 8325 and Comparative Analysis with Other Clinical Isolates. *Infect. Immun.* **2010**, *78* (6), 2877–2889.
(44) Baker, L. F.; King, R. S.; Unrine, J. M.; Castellon, B. T.; Lowry, G. V.; Matson, C. W. Press or pulse exposures determine the environmental fate of cerium nanoparticles in

stream mesocosms. *Environ. Toxicol. Chem.* **2016**, *35* (5), 1213–1223.
(45) Mackevica, A.; Revilla, P.; Brinch, A.; Hansen, S. F.; Købler, C.; Mølhave, K.; Larsen, E. H.; Hungerbühler, K.; Ulrich, A.; Thomas, K. V.; et al. Current uses of nanomaterials in biocidal products and treated articles in the EU. *Environ. Sci. Nano* **2016**, *3* (5), 1195–1205.
(46) Tamayo, L.; Azócar, M.; Kogan, M.; Riveros, A.; Páez, M. Copper-polymer nanocomposites: An excellent and cost-effective biocide for use on antibacterial surfaces. *Mater. Sci. Eng. C* **2016**, *69*, 1391–1409.
(47) Ong, H. R.; Ramli, R.; Khan, M. M. R.; Yunus, R. M. The influence of CuO nanoparticle on non-edible rubber seed oil based alkyd resin preparation and its antimicrobial activity. *Prog. Org. Coatings* **2016**, *101*, 245–252.
(48) Parnia, F.; Yazdani, J.; Javaherzadeh, V.; Maleki Dizaj, S. Overview of Nanoparticle Coating of Dental Implants for Enhanced Osseointegration and Antimicrobial Purposes. *J. Pharm. Pharm. Sci.* **2017**, *20* (0), 148–160.
(49) Drudge, C. N.; Elliott, A. V. C.; Plach, J. M.; Ejim, L. J.; Wright, G. D.; Droppo, I. G.; Warren, L. A. Diversity of integron- and culture-associated antibiotic resistance genes in freshwater floc. *Appl. Environ. Microbiol.* **2012**, *78* (12), 4367–4372.
(50) Ji, X.; Shen, Q.; Liu, F.; Ma, J.; Xu, G.; Wang, Y.; Wu, M. Antibiotic resistance gene abundances associated with antibiotics and heavy metals in animal manures and agricultural soils adjacent to feedlots in Shanghai; China. *J. Hazard. Mater.* **2012**, *235–236*, 178–185.
(51) Farias, P.; Espírito Santo, C.; Branco, R.; Francisco, R.; Santos, S.; Hansen, L.; Sorensen, S.; Morais, P. V. Natural hot spots for gain of multiple resistances: arsenic and antibiotic resistances in heterotrophic, aerobic bacteria from marine hydrothermal vent fields. *Appl. Environ. Microbiol.* **2015**, *81* (7), 2534–2543.
(52) Knapp, C. W.; Callan, A. C.; Aitken, B.; Shearn, R.; Koenders, A.; Hinwood, A. Relationship between antibiotic resistance genes and metals in residential soil samples from Western Australia. *Environ. Sci. Pollut. Res. Int.* **2017**, *24* (3), 2484–2494.
(53) Seiler, C.; Berendonk, T. U. Heavy metal driven co-selection of antibiotic resistance in soil and water bodies impacted by agriculture and aquaculture. *Front. Microbiol.* **2012**, *3*, 399.
(54) Böckelmann, U.; Dörries, H.-H.; Ayuso-Gabella, M. N.; Salgot de Marçay, M.; Tandoi, V.; Levantesi, C.; Masciopinto, C.; Van Houtte, E.; Szewzyk, U.; Wintgens, T.; et al. Quantitative PCR monitoring of antibiotic resistance genes and bacterial pathogens in three European artificial groundwater recharge systems. *Appl. Environ. Microbiol.* **2009**, *75* (1), 154–163.
(55) Baker-Austin, C.; Wright, M. S.; Stepanauskas, R.; McArthur, J. V. Co-selection of antibiotic and metal resistance. *Trends Microbiol.* **2006**, *14* (4), 176–182.
(56) Li, L.-G.; Xia, Y.; Zhang, T. Co-occurrence of antibiotic and metal resistance genes revealed in complete genome collection. *ISME J.* **2017**, *11* (3), 651–662.
(57) Qiu, Z.; Yu, Y.; Chen, Z.; Jin, M.; Yang, D.; Zhao, Z.; Wang, J.; Shen, Z.; Wang, X.; Qian, D.; et al. Nanoalumina promotes the horizontal transfer of multiresistance genes mediated by plasmids across genera. *Proc. Natl. Acad. Sci.* **2012**, *109* (13), 4944–4949.
(58) Qiu, Z.; Shen, Z.; Qian, D.; Jin, M.; Yang, D.; Wang, J.; Zhang, B.; Yang, Z.; Chen, Z.; Wang, X.; et al. Effects of nano-TiO_2 on antibiotic resistance transfer mediated by RP4 plasmid. *Nanotoxicology* **2015**, *9* (7), 895–904.

(59) Matic, I.; Rayssiguier, C.; Radman, M. Interspecies gene exchange in bacteria: the role of SOS and mismatch repair systems in evolution of species. *Cell* **1995**, *80* (3), 507–515.
(60) Guo, M.-T.; Yuan, Q.-B.; Yang, J. Distinguishing Effects of Ultraviolet Exposure and Chlorination on the Horizontal Transfer of Antibiotic Resistance Genes in Municipal Wastewater. *Environ. Sci. Technol.* **2015**, *49* (9), 5771–5778.
(61) Zeng, X.; Ardeshna, D.; Lin, J. Heat Shock-Enhanced Conjugation Efficiency in Standard Campylobacter jejuni Strains. *Appl. Environ. Microbiol.* **2015**, *81* (13), 4546–4552.
(62) Frost, L. S.; Leplae, R.; Summers, A. O.; Toussaint, A. Mobile genetic elements: the agents of open source evolution. *Nat. Rev. Microbiol.* **2005**, *3* (9), 722–732.
(63) Wang, Z.; Gerstein, M.; Snyder, M. RNA-Seq: a revolutionary tool for transcriptomics. *Nat. Rev. Genet.* **2009**, *10* (1), 57–63.
(64) Goodwin, S.; McPherson, J. D.; McCombie, W. R. Coming of age: ten years of next-generation sequencing technologies. *Nat. Rev. Genet.* **2016**, *17* (6), 333–351.
(65) Cheng, K. J.; Costerton, J. W. Alkaline phosphatase activity of rumen bacteria. *Appl. Environ. Microbiol.* **1977**, *34* (5), 586–590.
(66) Yang, K.; Metcalf, W. W. A new activity for an old enzyme: Escherichia coli bacterial alkaline phosphatase is a phosphite-dependent hydrogenase. *Proc. Natl. Acad. Sci. U. S. A.* **2004**, *101* (21), 7919–7924.
(67) Peschel, A.; Otto, M. Phenol-soluble modulins and staphylococcal infection. *Nat. Rev. Microbiol.* **2013**, *11* (10), 12–14.
(68) Kornblum, J.; Kreiswirth, B.; Projan, S. J.; Ross, H.; Novick, R. P. No Title. In *Molecular Biology of the Staphylococci*; 1990; pp 373–402.
(69) Boles, B. R.; Horswill, A. R. Agr-mediated dispersal of Staphylococcus aureus biofilms. *PLoS Pathog.* **2008**, *4* (4), e1000052.
(70) Coelho, L. R.; Souza, R. R.; Ferreira, F. A.; Guimaraes, M. A.; Ferreira-Carvalho, B. T.; Figueiredo, A. M. S. agr RNAIII divergently regulates glucose-induced biofilm formation in clinical isolates of Staphylococcus aureus. *Microbiology* **2008**, *154* (11), 3480–3490.
(71) Yarwood, J. M.; Bartels, D. J.; Volper, E. M.; Greenberg, E. P. Quorum sensing in Staphylococcus aureus biofilms. *J. Bacteriol.* **2004**, *186* (6), 1838–1850.

APPENDIX A

Supporting Information for Chapter Two:

Impacts of pristine and transformed Ag and Cu engineered nanomaterials on surficial sediment microbial communities appear short-lived

A.1 SUPPLEMENTAL METHODS

A.1.A Nanoparticle synthesis. To 1.5 L of as-synthesized Ag^0 NPs prior to purification, 25 mL of 0.2 M thioacetamide (Sigma Aldrich) were added. The suspension was covered and stirred for 24 hours. As with the pristine NPs, multiple batches were combined, purified and concentrated by dialysis.

CuO NPs were stabilized and suspended as described in the main text, then 100 mL of 0.1 M Na_2S (Sigma Aldrich) were added directly to 900 mL of the CuO NP suspension under constant stirring and allowed to react for one week. To remove any excess Na_2S, the final product was centrifuged, decanted, washed with DI water and re-suspended three times, as described above.

A.1.B Sample processing. Surficial sediment (see below for sampling method) porewater was extracted by centrifugation of surficial sediment slurries for 5 minutes at 2,500 x *g*. The supernatant was deemed porewater.

A.1.C Background Cu concentration. The samples were acidified by adding concentrated HNO_3 and digested using EPA Method 3052 for microwave-assisted digestion (CEM MARS 5). Samples were filtered with 0.2 µm glass membrane filters and then diluted with deionized water to 5% acid content. Analysis by inductively coupled plasma mass spectrometry (ICP-MS) with an Agilent 7700 Series ICP-MS was used to determine the concentration of dissolved Cu in solution. A multi-element calibration standard was diluted with 5% HNO_3 to make the desired calibration standards.

A.1.D Nanoparticle characterization. The hydrodynamic diameter and electrophoretic mobility of the Ag and Cu NPs in 0.22µm-filtered mesocosm porewater were measured with a Malvern Zetasizer Nano at 10 mg/L of the NP. The Malvern Zetasizer Nano also reported the specific conductances of the suspensions. Prior to taking these measurements, the pH of the porewater was measured with a pH electrode (Fisher Scientific Accumet XL50).

Transmission electron microscopy (TEM) was used to determine NP primary particle sizes. One drop of diluted sample was applied to the Formvar side of a Carbon Type A Formvar-coated copper grid (Ted Pella) and allowed to evaporate. Images were taken using an FEI Tecnai G2 Twin Transmission Electron Microscope at an accelerating voltage of 160 kV.

A.1.E X-ray absorption spectroscopy. X-ray absorption spectroscopy (XAS) was used to determine metal speciation of Ag and Cu within surficial sediment samples. In preparation for XAS, sediments were freeze-dried and loaded into holders. Silver (25,514 eV) and copper (8,979 eV) K-edge absorption spectra were collected at Stanford Synchrotron Radiation Lightsource's (SSRL) beam lines 11-2 and 4-1, respectively. The spectra were compared with reference spectra of the initial materials and relevant metal species. Reference spectra were generated from the following model compounds: Ag^0 foil, Ag_2S NPs (this study), CuO NPs (this study), most sulfidized CuS NPs (from Ma et al.)[1] and Cu metal foil.

A.1.F Quantitative polymerase chain reaction (qPCR), amplicon library preparation, and DNA sequencing. qPCR tubes were composed of universal TaqMan master mix (Applied Biosystems), primers BAC 1369F (5' to 3': CGGTGAATACGTTCYCGG) and PROK 1492R (5' to 3': GGWTACCTTGTTACGACTT), probe TM1389F[2] (Fisher Scientific) and molecular biology grade water under thermal cycling conditions that have been described previously.[3] Per 20 µL reaction, 6.5 µL molecular biology grade H_2O, 1 µL each primer, 0.5 µL probe, 10 µL TaqMan master mix (Applied Biosystems) and 1 µL sample DNA.

PCR inhibition can afflict DNA extracted from environmental samples.[4] We subjected selected samples to testing for qPCR inhibition, including the 180 d Cu^{2+} sample. Neither addition of bovine serum albumin (BSA)[5] to the qPCR master mix at a final concentration of 20 ng/µL nor 1:10 dilution of extracted DNA in molecular biology grade H_2O prior to qPCR analysis[6] affected the number of gene copies measured.

For PCR of the V4 region of the 16S rRNA gene, each reaction consisted of 13 µL DreamTaq DNA master mix (ThermoScientific), 0.5 µL of 10 µM aliquots of both 515F (5' to 3': AATGATACGGCGACCACCGAGATCTACACTATGGTAATTGTGTGCCAGCMGCCGCG GTAA) and barcoded 806R (CAAGCAGAAGACGGCATACGAGATXXXXXXXXXXXX AGTCAGTCAG CC GGACTACHVGGGTWTCTAAT with Xs demarcating Golay barcode) primers,[7] 1 µL DNA and 10 µL molecular biology grade water. PCR was performed with a MyCycler thermal cycler (Bio-Rad) using the following conditions: 3 min initial denaturation at 96ºC; 30 cycles of 45 sec at 96ºC, 1 min at 50ºC and 1 min at 72ºC; a final extension of 10 min at 72ºC, and a final hold at 4ºC.

For PCR product purification, 1.3 times the PCR volume of AMPure bead solution, i.e. 32.5 µL, were used. Beads and PCRroducts were initially incubated for 15 min, with 10 sec vortexing and subsequent 3 sec centrifuging performed at 5 and 10 min of incubation. For both ethanol washes, freshly made 70% ethanol was mixed with the supernatant by pipetting. Eluent-DNA incubation occurred at 37ºC and followed the same 15-min vortexing and centrifuging protocol described above.

Immediately prior to sequencing, sample DNA was pooled to achieve 0.1 pmol of each. The pooled sample was diluted to 2 nM DNA with molecular biology grade water, denatured with 0.2 N NaOH, incubated at 95ºC for 2 min and cooled on an ice bath. The denatured pooled sample was further diluted to ~15 pM sample DNA using Illumina's HT1 buffer and supplemented with 0.625 pM PhiX DNA using a PhiX standard.

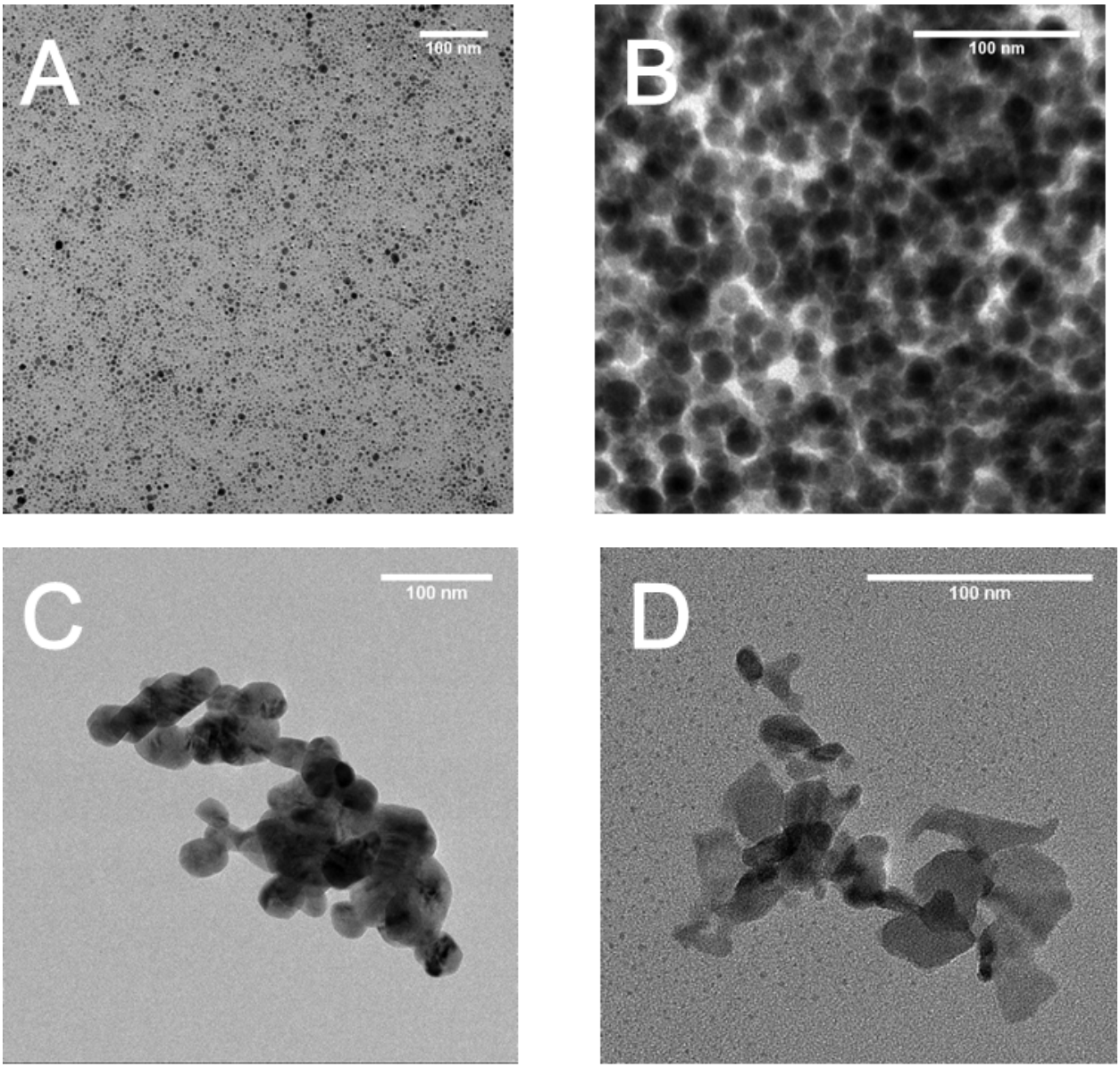

Figure A.1. ***TEM images of Ag^0 (A), Ag_2S (B), CuO (C) and CuS (D) ENMs.***

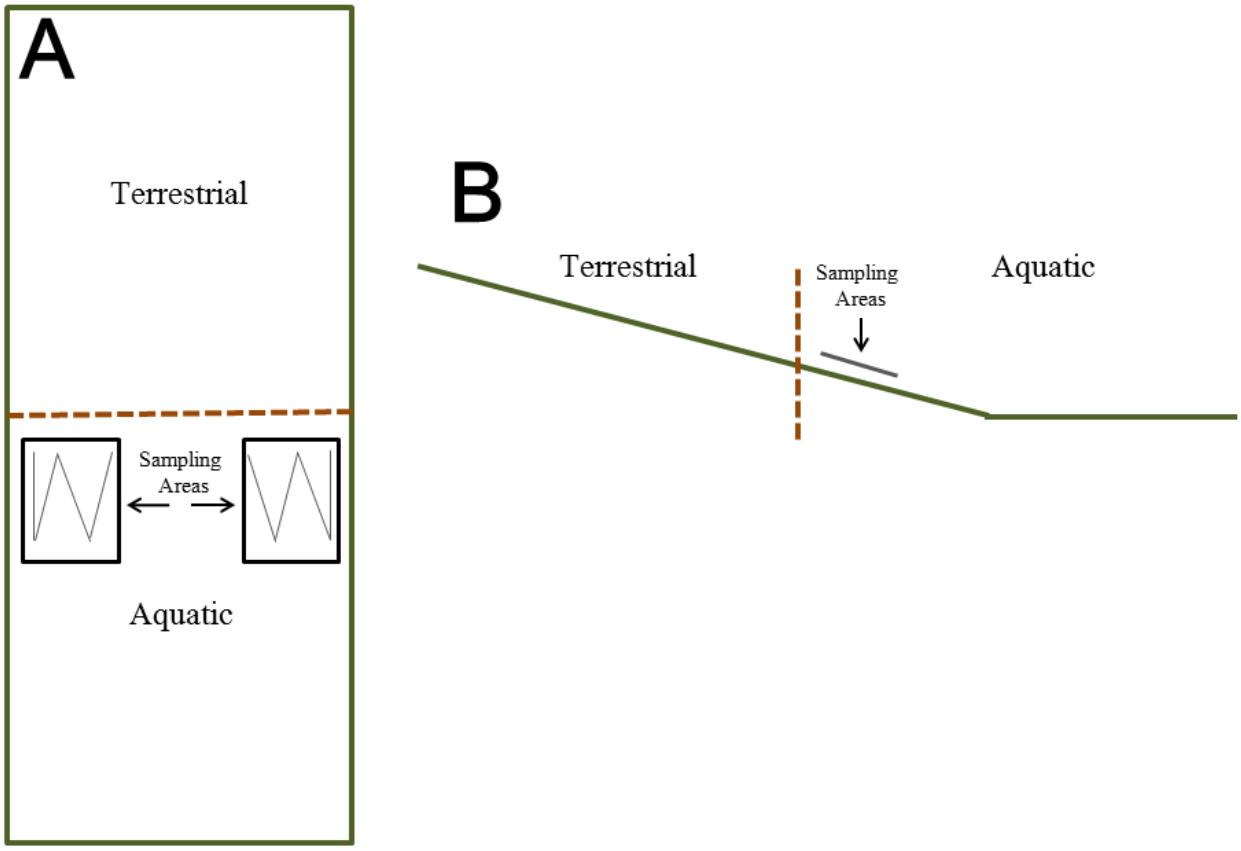

Figure A.2. ***Sampling areas depicted in aerial (A) and side views (B) of the mesocosms.*** *Sampling took place within the sloped portion of the aquatic half of the mesocosms. This area remained submerged for the entirety of the experiment. The tubing was gently pulled atop the surficial sediment in the form of a misshapen "W," generating 45 mL of sample. Surficial sediments were sampled in this area, because the sediment surface here was both visible and accessible to those conducting the sampling. The dashed brown line distinguishes the terrestrial and aquatic halves.*

A.2 RESULTS

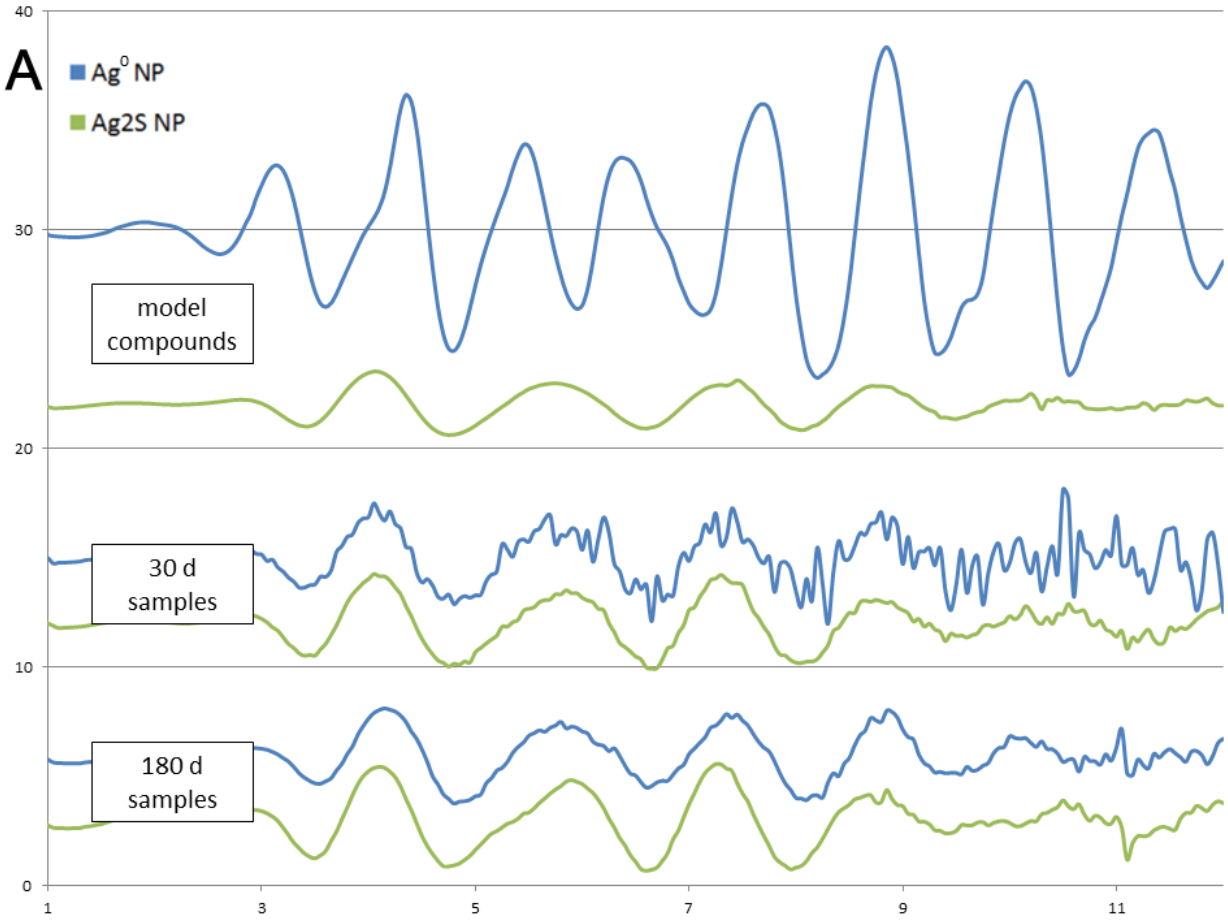
A
Ag0 NP
Ag2S NP
model compounds
30 d samples
180 d samples
40
30
20
10
0
1
3
5
7
9
11

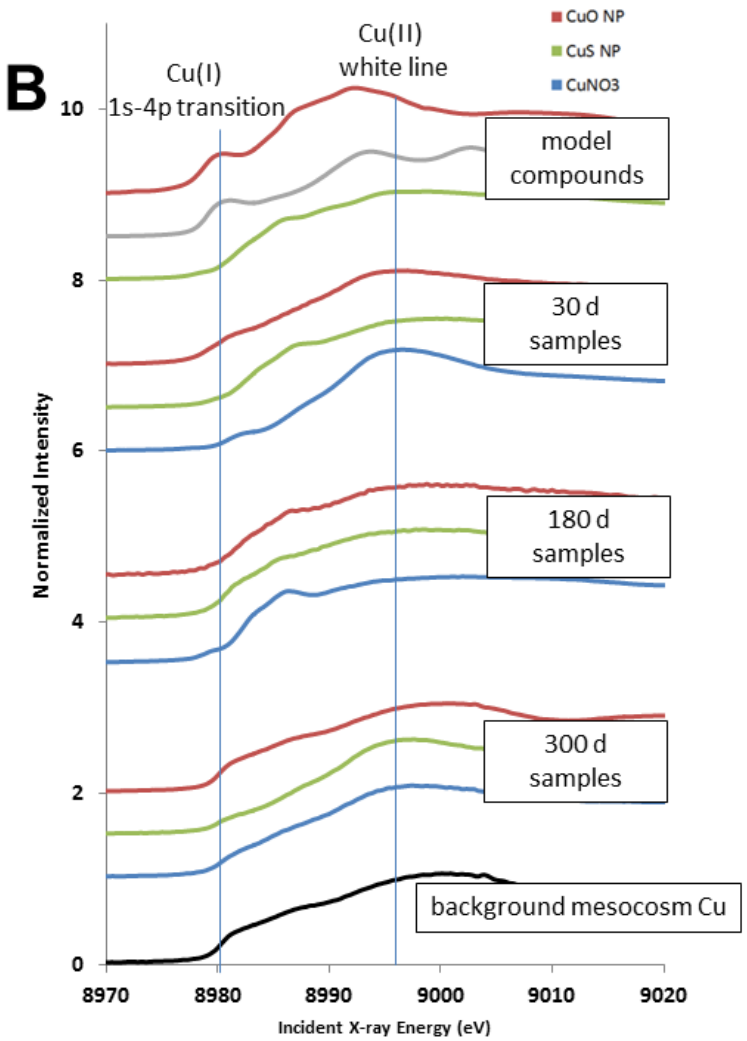

Figure A.3. ***X-ray absorption spectroscopy (XAS) spectra for Ag (A) and Cu (B) model compounds and mesocosm samples at one, six and nine months.*** *The grey model compound is Cu metal. Background mesocosm Cu was assessed in the* Ag_2S *180 d mesocosm.*

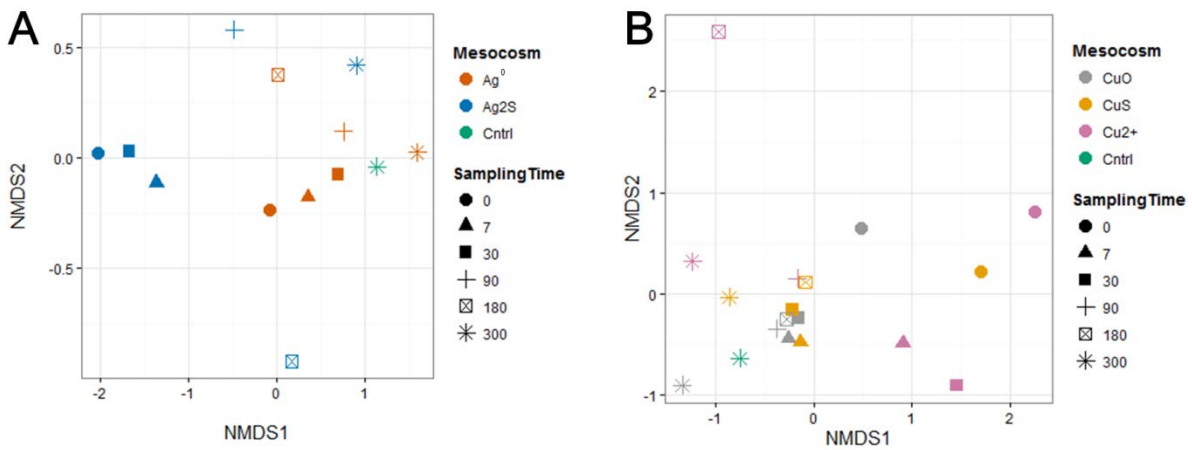

Figure A.4. ***NMDS plots of Ag- (A) and Cu-dosed (B) mesocosm OTU tables using the weighted Unifrac distance metric.*** *NMDS stresses were 0.072 for Ag and 0.052 for Cu.*

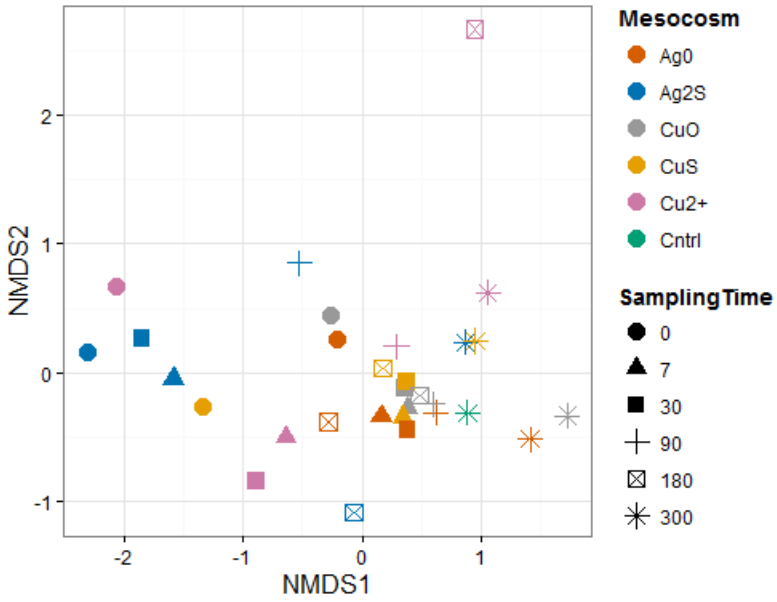

Figure A.5. ***NMDS plot of a combined Ag- and Cu-dosed mesocosm OTU table using the weighted Unifrac metric.*** *NMDS stress was 0.085.*

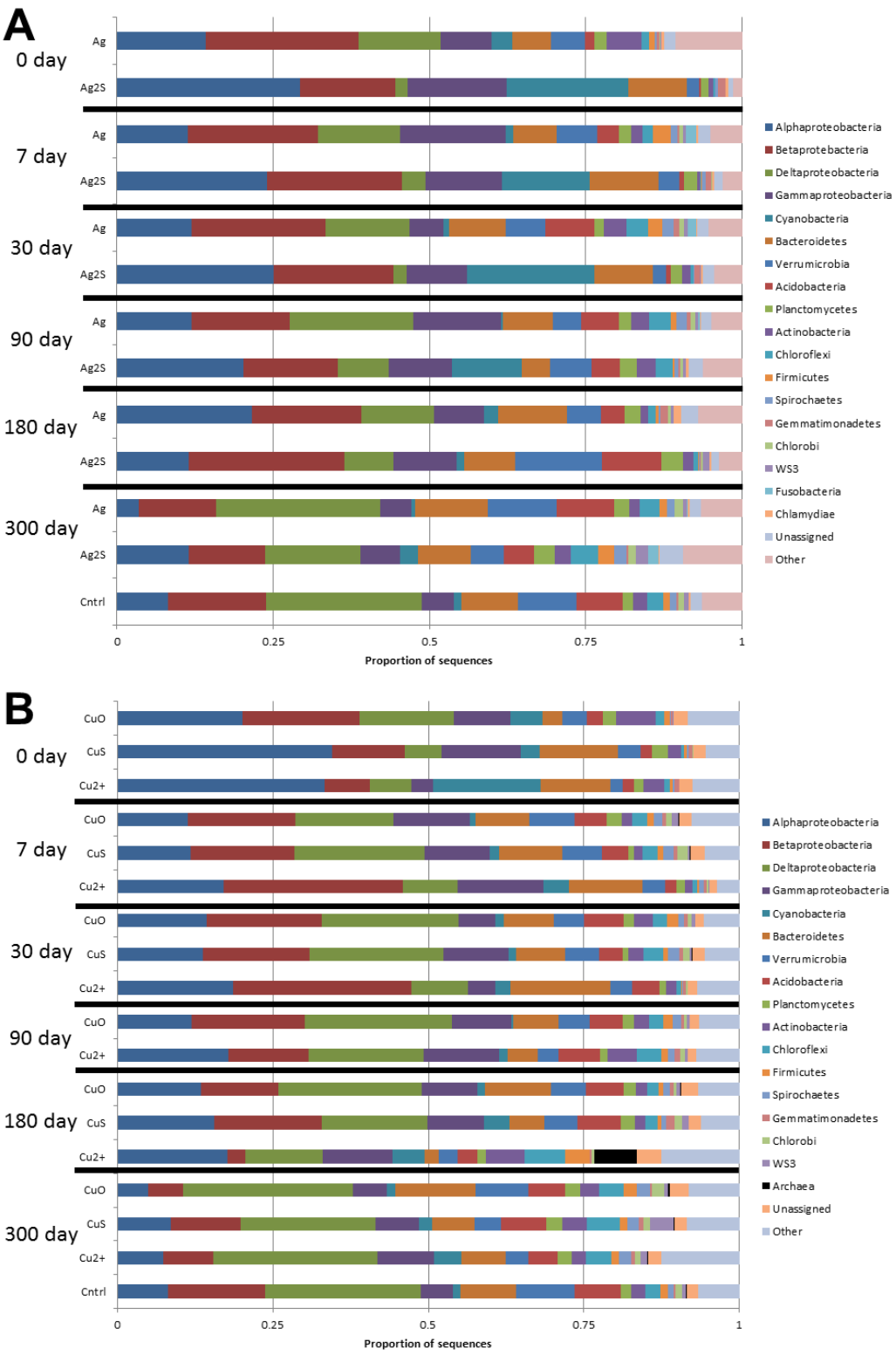

Figure A.6. ***Relative abundances of dominant taxa in Ag (A) and Cu (B) mesocosms.*** *Bacterial phylum* Proteobacteria *is broken down into its four most abundant classes. For Cu mesocosms only, kingdom* Archaea *sequences were among the dominant taxa, and for Ag mesocosms only, bacterial phyla* Chlamydiae *and* Fusobacteria *were among the dominant taxa.*

Table A.1. Nearest sequenced taxa indices (NSTI). *NSTI indicates how accurate PICRUSt-predicted metagenomes are expected to be. A lower NSTI indicates that a sample features OTUs that are more closely related to organisms with sequenced genomes.*

Sample	NSTI
t0Ag0	0.148
t0Ag2S	0.133
t0Cu2	0.131
t0CuO	0.144
t0CuS	0.147
t1Ag0	0.139
t1Ag2S	0.136
t1Cu2	0.111
t1CuO	0.144
t1CuS	0.137
t2Ag0	0.131
t2Ag2S	0.133
t2Cu2	0.114
t2CuO	0.124
t2CuS	0.126
t3Ag0	0.121
t3Ag2S	0.138
t3Cu2	0.131
t3CuO	0.123
t4Ag0	0.148
t4Ag2S	0.158
t4Cu2	0.158
t4CuO	0.141
t4CuS	0.153
t5Ag0	0.162
t5Ag2S	0.151
t5Cntrl	0.150
t5Cu2	0.157
t5CuO	0.163
t5CuS	0.163

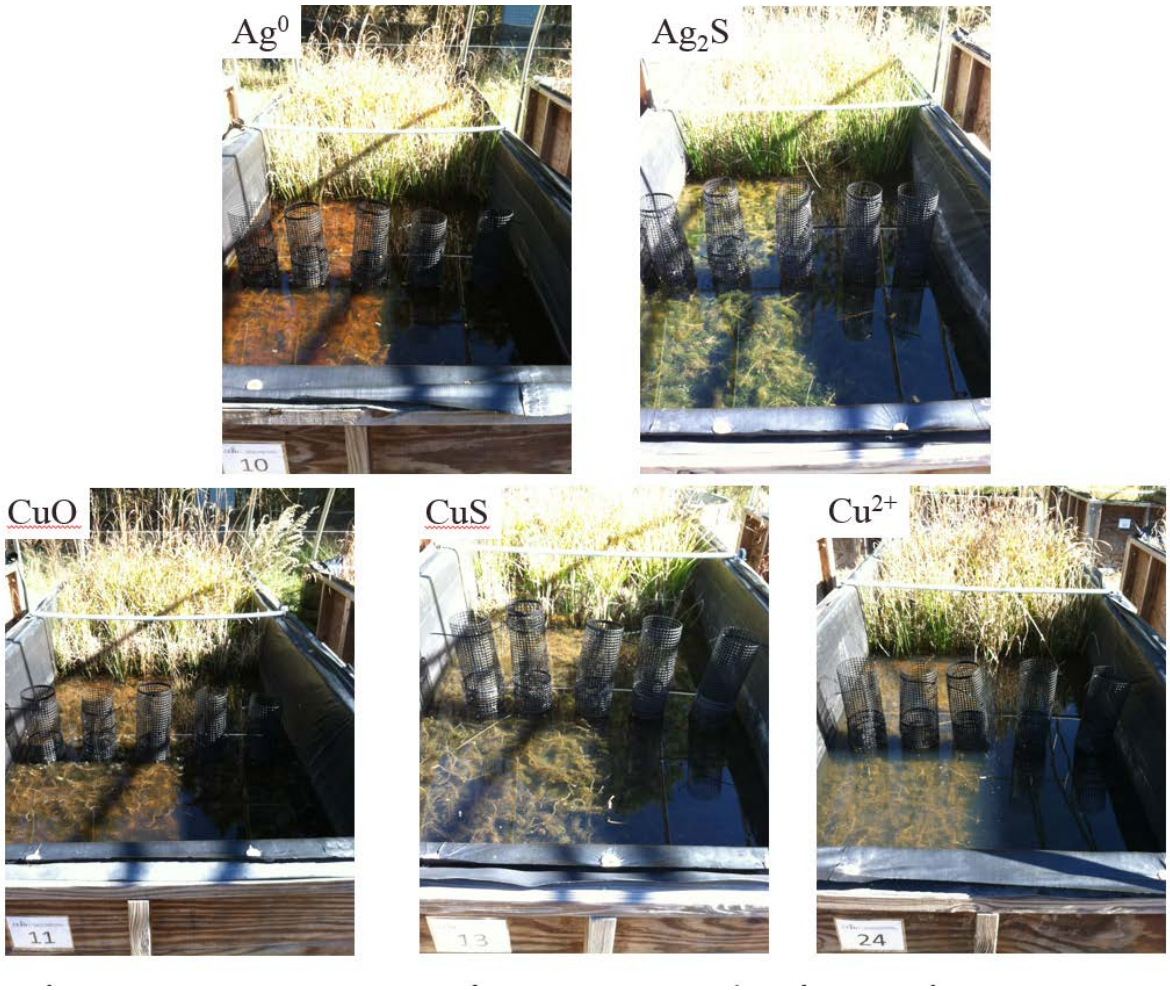

Figure A.7. ***Pictures of mesocosms at 30 d.*** *Differential effects of Ag^0 and Ag_2S NPs were observed on* Cyanobacteria *(depleted in Ag^0 and enriched or maintained in Ag_2S), especially at this time point. Notably, the different effect cannot be explained by the turbidity of the respective water columns.*

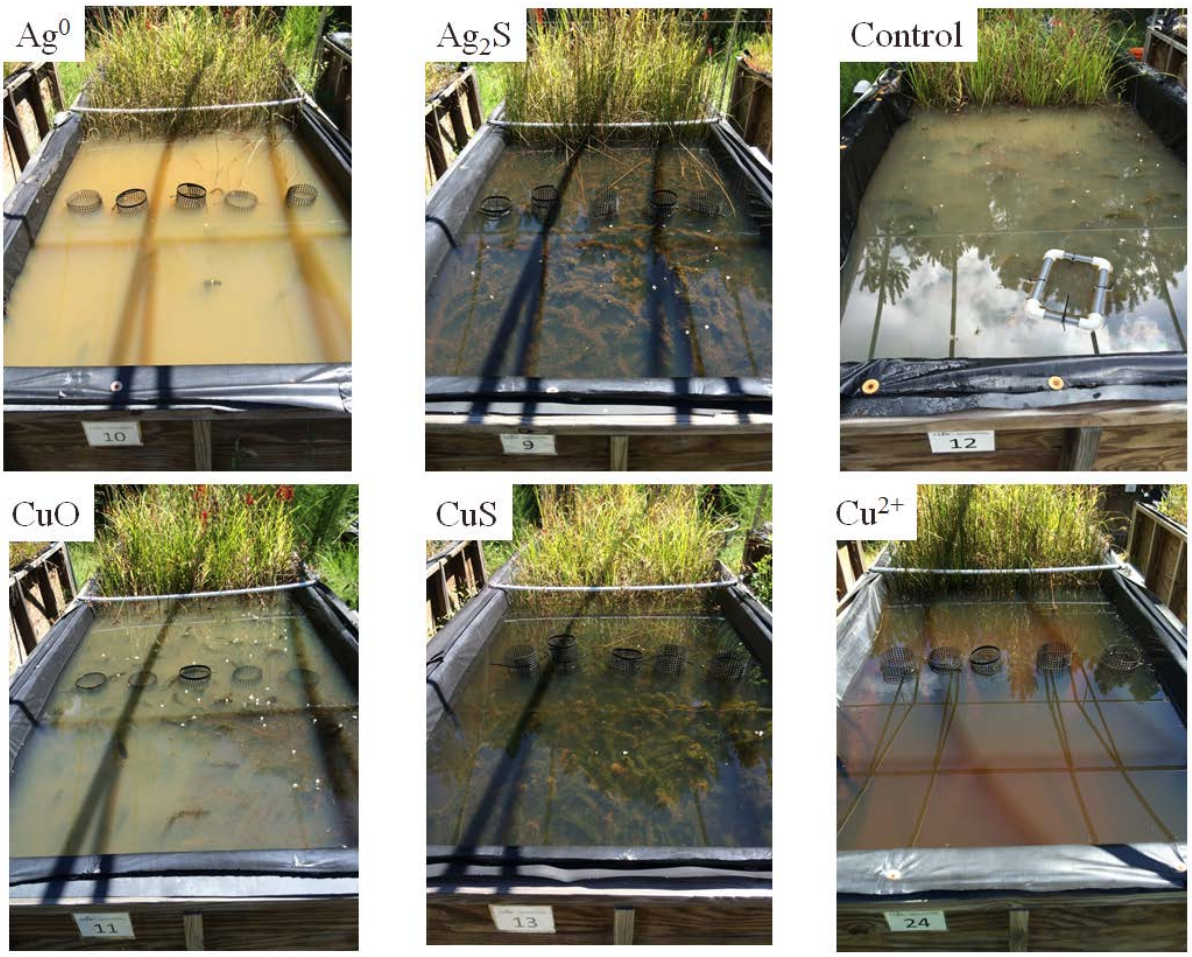

Figure A.8. ***Pictures of the five dosed mesocosms and control at 300 d.*** *Note the lack of aquatic plants in the Cu^{2+} mesocosm. The turbidity difference between Ag^0 and Ag_2S is also notable here. Despite the contrasting turbidities, neither differences in* Cyanobacteria *nor in annotated photosynthetic genes within 300 d predicted metagenomes were observed.*

A.3 REFERENCES FOR APPENDIX A

(1) Ma, R.; Stegemeier, J.; Levard, C.; Dale, J. G.; Noack, C. W.; Yang, T.; Brown, G. E.; Lowry, G. V. Sulfidation of copper oxide nanoparticles and properties of resulting copper sulfide. *Environ. Sci. Nano* **2014**, *1* (4), 347.

(2) Suzuki, M. T.; Taylor, L. T.; DeLong, E. F. Quantitative analysis of small-subunit rRNA genes in mixed microbial populations via 5'-nuclease assays. *Appl. Environ. Microbiol.* **2000**, *66* (11), 4605–4614.

(3) Murali Mohan, A.; Hartsock, A.; Bibby, K. J.; Hammack, R. W.; Vidic, R. D.; Gregory, K. B. Microbial community changes in hydraulic fracturing fluids and produced water from shale gas extraction. *Environ. Sci. Technol.* **2013**, *47* (22), 13141–13150.

(4) Schrader, C.; Schielke, A.; Ellerbroek, L.; Johne, R. PCR inhibitors - occurrence, properties and removal. *J. Appl. Microbiol.* **2012**, *113* (5), 1014–1026.

(5) Kreader, C. Relief of amplification inhibition in PCR with bovine serum albumin or T4 gene 32

protein. *Appl. Envir. Microbiol.* **1996**, *62* (3), 1102–1106.
(6) Cao, Y.; Griffith, J. F.; Dorevitch, S.; Weisberg, S. B. Effectiveness of qPCR permutations, internal controls and dilution as means for minimizing the impact of inhibition while measuring Enterococcus in environmental waters. *J. Appl. Microbiol.* **2012**, *113* (1), 66–75.
(7) Caporaso, J. G.; Lauber, C. L.; Walters, W. A.; Berg-Lyons, D.; Huntley, J.; Fierer, N.; Owens, S. M.; Betley, J.; Fraser, L.; Bauer, M.; et al. Ultra-high-throughput microbial community analysis on the Illumina HiSeq and MiSeq platforms. *ISME J.* **2012**, *6* (8), 1621–1624.

APPENDIX B

Supporting Information for Chapter Three:

Time-dependent bacterial transcriptional response to CuO nanoparticles differs from that of Cu^{2+} and provides insights into CuO nanoparticle toxicity mechanisms

B.1 SUPPLEMENTAL METHODS

B.1.A RNA extraction protocol in detail. Immediately following sampling, 2 mL RNAprotect was added to 1 mL of sample, vortexed on high, and allowed to incubate at room temperature for 10 min. The sample was then centrifuged for 10 min at 5000*g*. TE buffer with 1 mg/L lysozyme was added to the pellet, vortexed, and incubated for 10 min with shaking. Freshly made 2-mercaptoethanol-RLT buffer was added and vortexed, then 100% ethanol was added and mixed by pipetting before being transferred to a spin column and centrifuged. RW1 buffer was added and centrifuged through the spin column before on-column DNase 1 treatment according to the manufacturer's protocol. Freshly made RPE-ethanol was added to the spin column twice. Spin columns were transferred to a clean 1.5 mL tube and allowed to air dry for 5 min. RNA was eluted into 60 µL RNase-free 45ºC water that was divided into two 30 µL additions with 3 min incubation before centrifuging.

B.1.B Growth inhibition assays. Inhibition of E. coli growth by varying concentrations of CuO ENMs and Cu^{2+} was measured using 96-well plates and a microplate reader (SpectraMax, Molecular Devices, Sunnyvale, CA). Approximately 10^6 colony forming units (CFU) per mL were added to a 96-well plate containing serially diluted CuO NPs or Cu^{2+} in the growth medium. The plate was shaken at 160 rpm at 30ºC, and OD600 was measured at 0 hr and 24 hr. Growth was determined by subtracting the 0 hr reading from the 24 hr reading. Abiotic and undosed biotic controls were included alongside CuO NP and Cu^{2+} treatments, and eight wells were used per treatment or control condition. Stocks of Cu^{2+} were made from $Cu(NO_3)_2$ in ultrapure water. ICP-MS analysis (as described above) was used to ensure that nominal Cu concentrations agreed with analytical concentrations.

Both CuO NPs and Cu^{2+} demonstrated the expected dose response, with higher Cu concentrations leading to lower bacterial growth at 24 hr (**Figure S2**). As we had hypothesized, we measured a differential effect of CuO NPs and Cu^{2+} on *E. coli* growth. Cu^{2+} inhibited growth at ~1 ppm, while CuO NPs allowed growth out to ~20 mg/L Cu. Previous studies have also observed greater bacterial susceptibility to dissolved Cu than Cu ENMs.[1,2] The CuO NP data appear to show an increase in *E. coli* growth at low concentrations. This increase has been attributed to hormesis for exposures to Ag NPs.[3] However, follow up plating experiments showed that CFUs did not increase at the same low CuO NP concentrations (data not shown), suggesting that the low CuO NP concentration optical density increases were an artefact of the measurements.

B.1.C Discussion of CuO NP dosing concentration. We chose to dose at 100 mg/L (as Cu) CuO NPs to ensure that the NPs imposed a stress on the *E. coli*. This concentration has also been used in a previous study of CuO NP bacterial toxicity.[4] Inhibition assays with CuO NPs showed that 100 mg/L inhibited the growth of 10^6 *E. coli* CFU/mL. At the higher bacterial concentration needed for the transcriptional assays (5×10^7 CFU/mL) 100 mg/L CuO NPs provided a sublethal stress based on the observed increase in *rrsA* gene expression over time.

B.1.D Viability experiments. *E. coli* was grown and treated with Cu as described in the main text for HSI and transcriptional assays. All treatments were done in duplicate, including an

undosed control. After 30, 60, 100, 140, and 180 min of exposure, samples were vortexed to homogenize, and 100 µL samples of each sample was serially diluted. 50 µL of serially diluted samples were added to LB agar plates, again in duplicate. Plates were incubated at 37ºC, and CFUs were counted 24 hr later. Means and standard deviations were calculated at each time point.

B.1.E Oxidative stress probe protocol in detail. Cells were grown to early log phase growth as with the transcriptional response experiments. At OD ~ 0.2, cells were pelleted by centrifuging for 15 min at 8000*g*. While the cells were centrifuging, a 10 mM stock of CM-H2DCFDA (Molecular Probes, Life Technologies) was made by adding DMSO to a single CM-H2DCFDA tube in the dark. This 10 mM stock was diluted to 10 µM in pH 7.2 phosphate buffered saline (PBS). The cells were resuspended in the PBS containing the probe and allowed to incubate with gentle shaking for 30 min to allow for the probe to penetrate into the cells. The cells were then centrifuged and suspended back in an appropriate volume of growth medium for 5 x 10^7 CFU/mL. Treatments were added immediately. At 10, 60, and 180 min, samples were vortexed and 200 µL were withdrawn from each sample in triplicate and added to a 96 well plate. Fluorescence emitted at 517 nm was measured immediately on a microplate reader after excitation at 494 nm.

B.1.F Electron paramagnetic resonance (EPR) methods in detail. EPR was conducted using 5,5-dimethyl-1-pyrroline-N-oxide (DMPO) (Cayman Chemical, Ann Arbor, MI) as a radical spin trap. After 60 and 180 min Cu-exposed and undosed bacteria were incubated with 20 mM DMPO for 15 min at room temperature before being frozen with liquid N_2, where they were stored until EPR measurements were taken. Positive controls in H_2O and MMDM were generated by reacting 0.1 mM Fe^{2+}, 1 mM H_2O_2 and 20 mM DMPO in a glovebox (MBraun, Garching, Germany) filled with N_2 gas (O_2 < 0.5 ppm) for 5 min at room temperature, then were frozen in liquid N_2. Negative controls were generated by incubating 20 mM DMPO with abiotic MMDM, *E. coli* in MMDM, Cu^{2+} in MMDM, and CuO NPs in MMDM. X-band EPR spectra were measured on a Bruker Elexsys E-500 spectrometer (microwave frequency = 9.64 GHz, Billerica, MA) equipped with an Oxford ESP-910 cryostat (Abingdon, United Kingdom). All spectra were measured at 73 K with 0.3 mT modulation amplitude, 100 kHz modulation frequency. EPR spin quantification was done by comparing the double integration of an EPR signal with unknown concentration with the double integration of the EPR signal from a known concentration standard measured under the same measurement conditions. The spin standard used in this study is 1.2 mM Cu(II)-EDTA solution. EPR spectra were processed and plotted using SpinCount software.[5]

B.1.G EPR spectral interpretation. The DMPO treated samples included in this study exhibited three types of EPR-detectable signals. Two EPR signals were observed in all samples prepared in MMDM. The signal spreading across a wide magnetic field range (from 320 mT to 370 mT) is characteristic of Mn^{2+} (**Figure B.11**). The signal exhibiting a sharp g = 2 resonance belongs to certain organic radical with unknown origin (**Figures B.10g** and **B.10h**). The spin concentration quantification suggested that the Mn^{2+} ion signal was < 20 µM, and the organic radical signal was << 1 µM. In all Cu^{2+} or CuO NP dosed samples, a third EPR signal was

observed with various spin concentrations (**Figure B.10 a-f**), which was centered at g ~ 2 with a four-line splitting pattern. This EPR signal was reproduced (**Figures B.10i** and **B.10j**) in two positive control samples with the presence of DMPO under Fenton chemistry reaction conditions (see the experiment section for the details of sample preparation), suggesting that this signal belongs to a DMPO radical adduct formed in the presence of ·OH. The spectral analysis suggested that this four-line splitting EPR signal can be simulated by including a ^{14}N hyperfine coupling and ^{1}H hyperfine coupling interactions with hyperfine coupling constants of $A(^{14}N)$ = 60 MHz and $A(^{1}H)$ = 65 MHz (**Figure B.10j**). Although these parameters do not resemble the ones from the DMPO-OH radical adduct ($A(^{14}N) = A(^{1}H)$ = 40 MHz) that are expected to be generated from the spin trap experiment, these parameters are comparable to the ones from a DMPO radical adduct with carbon centered radicals ($A(^{14}N)$ = 45 MHz and $A(^{1}H)$ = 65 MHz).[6] DMSO was used as the solvent to prepare our DMPO stock solution. It has been reported that ·OH will activate DMSO to form a carbon centered radical (·CH_3), and further form the DMPO-CH_3 radical adduct.[6] Therefore, due to the presence of DMSO during our spin trap experiment, the DMPO-CH_3 radical adduct is observed in our systems.

Table B.1. ***Components in MMDM.*** *Ionic strength was estimated to be 0.485 using Visual Minteq (version 3.1) equilibrium modeling software.*

mM with pH 6.5 MDM + supplements	
K	103
PO4	94
NH4	15
SO4	171
Na	174
Mg	123
Mn	30
Cl	192
Fe	3.6
NO3	6.9
Ca	9.1
Zn	6.2
MoO4	0.41
SeO3	0.06
WO4	0.30
Ni	0.84

Table B.2. ***Alternative hypotheses for Mann-Whitney testing of gene expression data for comparisons made in this study.*** *H_1 refers to the value of the location shift, μ, between sample distributions of gene (x) expression at time (t) between treatments (y or undosed).*

Statistical comparison	Biological question	H_1
Treatment vs. control, *rrsA* expression only	Is bacterial growth negatively impacted by Cu exposures?	$\mu_{rrsA,t}^{y-undosed} < 0$
Treatment vs. control, all other genes	Does Cu exposure lead to differential expression of stress-response genes?	$\mu_{x,t}^{y-undosed} > 0$
Treatment vs. treatment, all genes	Does the mode of Cu exposure lead to differential expression of stress-response genes?	$\mu_{x,t}^{y_1-y_2} \neq 0$

B.2 RESULTS

Table B.3. ***Intensity means and polydispersity indices (PdI) of CuO NPs over time.***

Time [min]	Intensity mean [nm]	PdI
0	638 ± 150	0.356 ± 0.049
10	766 ± 81	0.402 ± 0.011
60	707 ± 160	0.422 ± 0.080
180	n/a	n/a

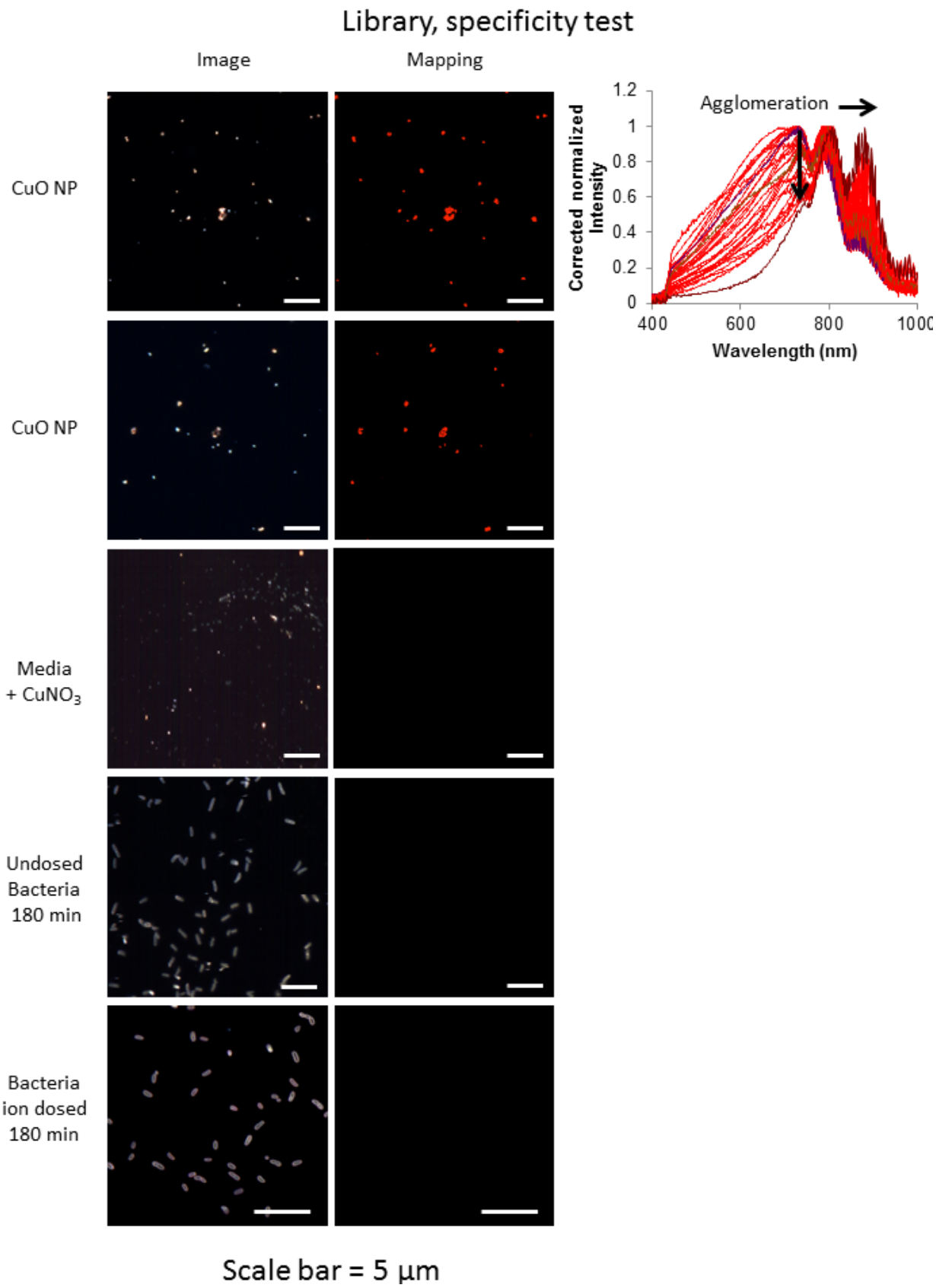

Figure B.1. ***Specificity tests of the CuO NP hyperspectral library signature.***

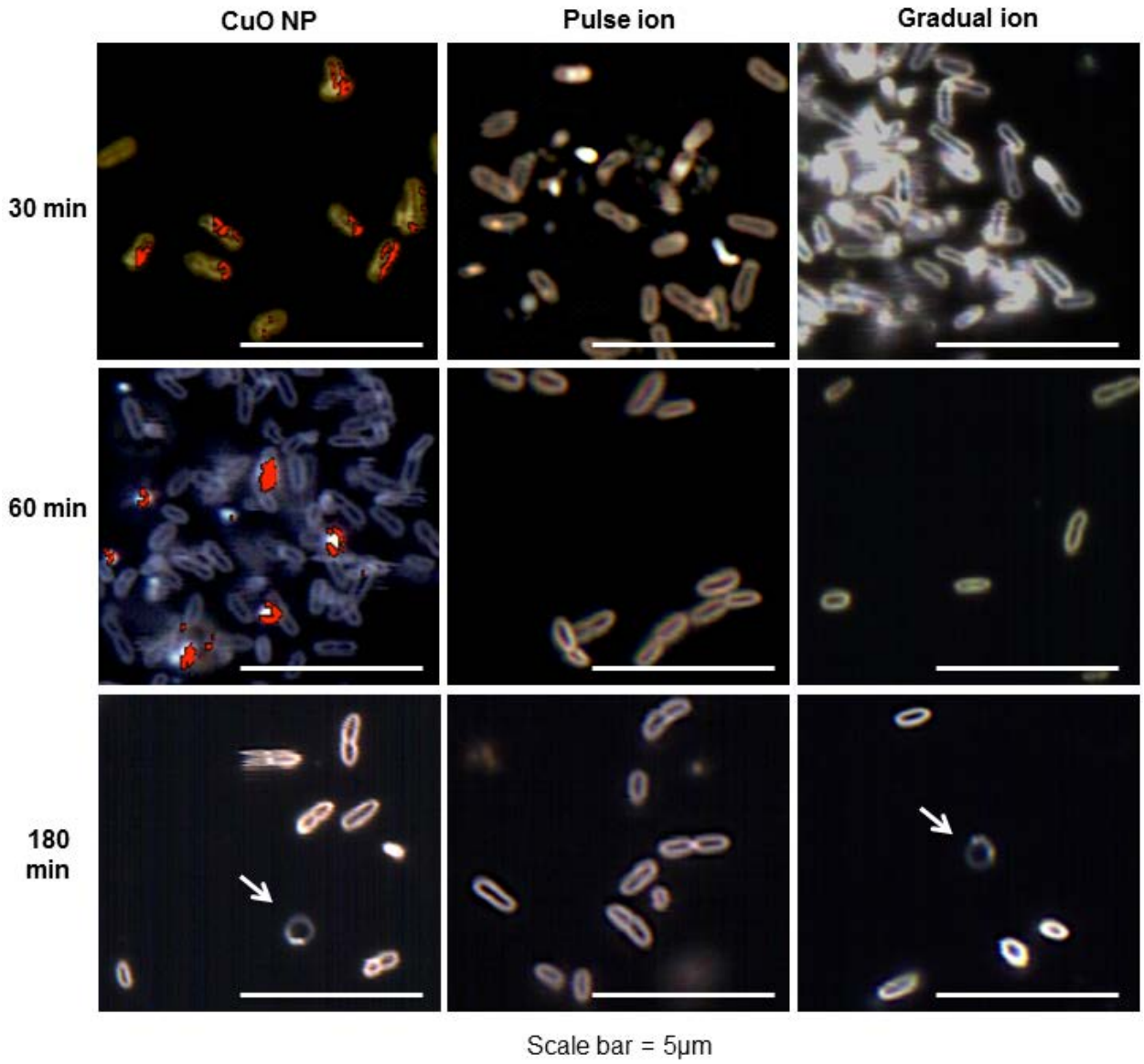

Figure B.2. ***HSI of all treatments at 30, 60, and 180 min.*** *Arrows point to OMVs detected at 180 min with NP and gradual ion treatment.*

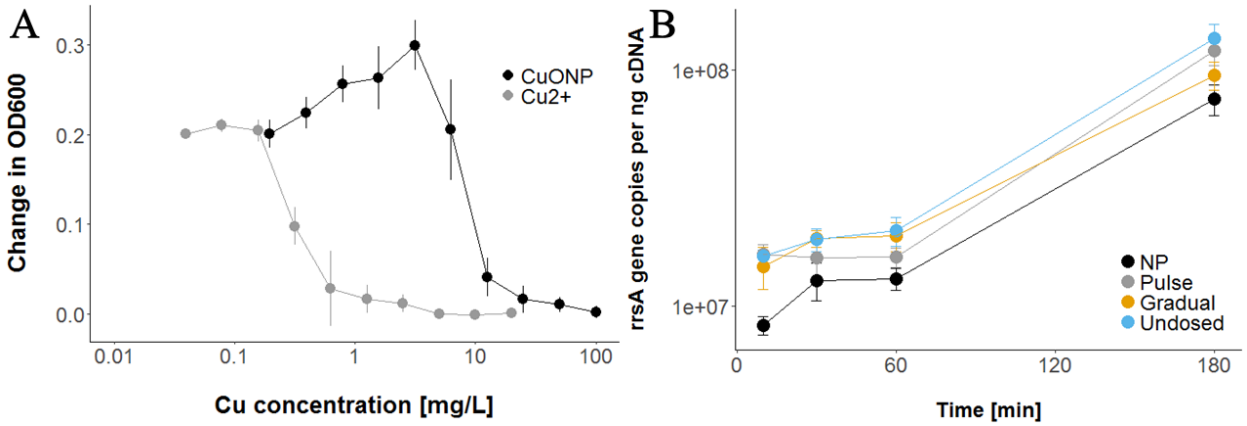

Figure B.3. E. coli *growth at various CuO NP and Cu^{2+} concentrations (as Cu) and housekeeping gene* (rrsA) *expression.* *(A) Growth was measured by change in optical density between 0 and 24 hr. (B)* rrsA *gene expression was statistically similar across treatments and showed at 180 min the enhanced expression that is characteristic of entering exponential growth.*

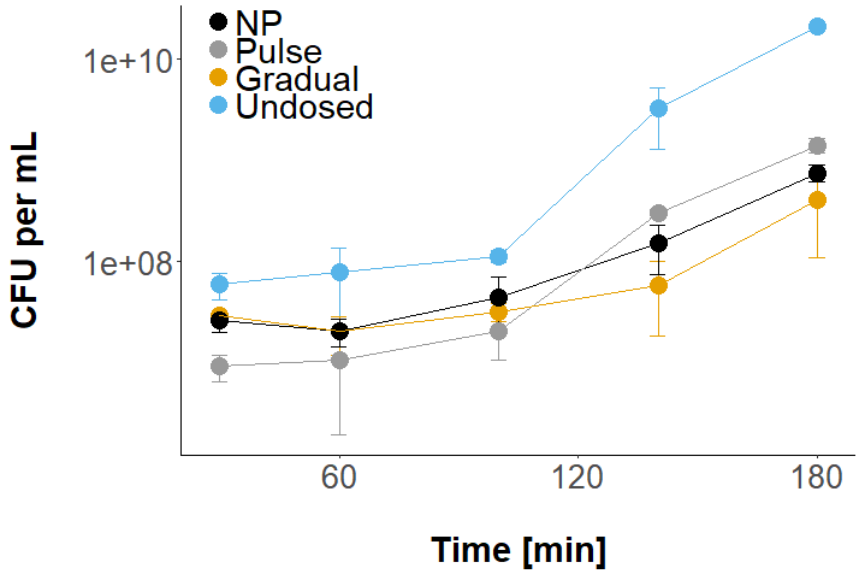

Figure B.4. *Treated and undosed* E. coli *viability over time.* *Results of time-resolved CFU experiment for all treatments on a y-axis log scale.*

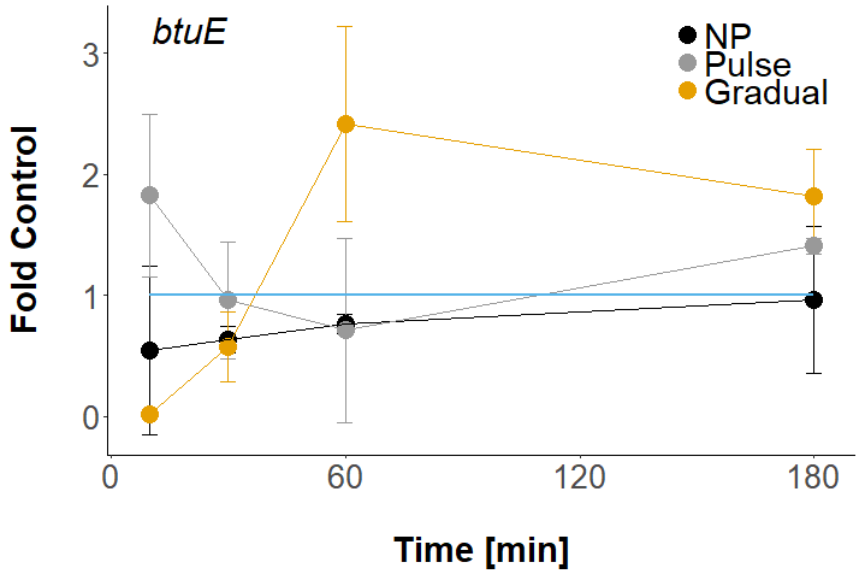

Figure B.5. ***Gene expression of*** **btuE** ***in response to Cu exposure.*** *Statistically significant differences were observed at 10 min. The blue horizontal line is fixed at one to represent the expression of the undosed control. Error bars represent one SD of triplicate samples.*

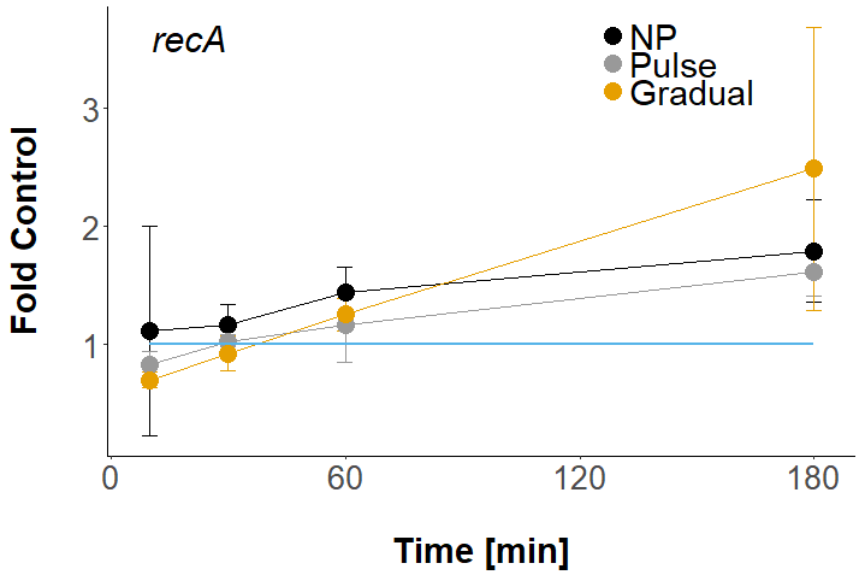

Figure B.6. ***Gene expression of*** **recA** ***in response to Cu exposure.*** *The blue horizontal line is fixed at one to represent the expression of the undosed control. Error bars represent one SD of triplicate samples.*

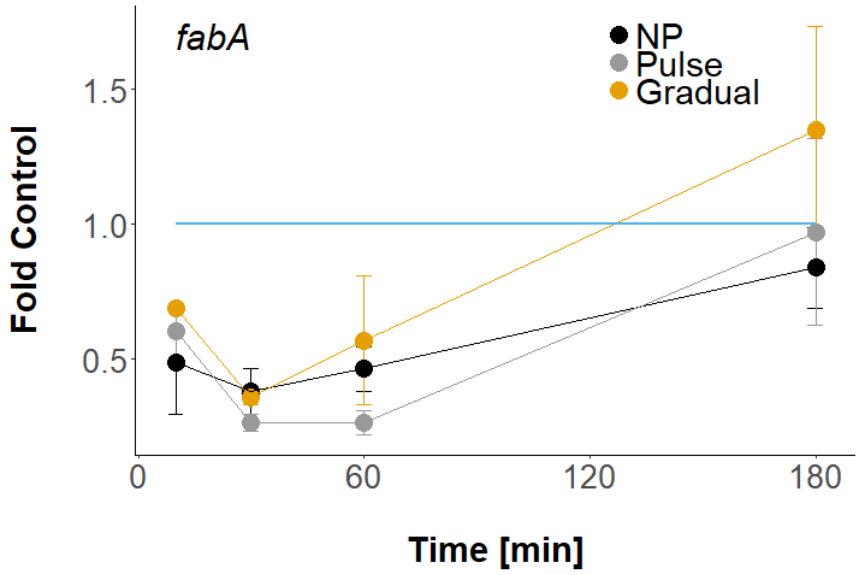

Figure B.7. ***Gene expression of*** **fabA** ***in response to Cu exposure.*** *Statistically significant differences were observed at 60 min. The blue horizontal line is fixed at one to represent the expression of the undosed control. Error bars represent one SD of triplicate samples.*

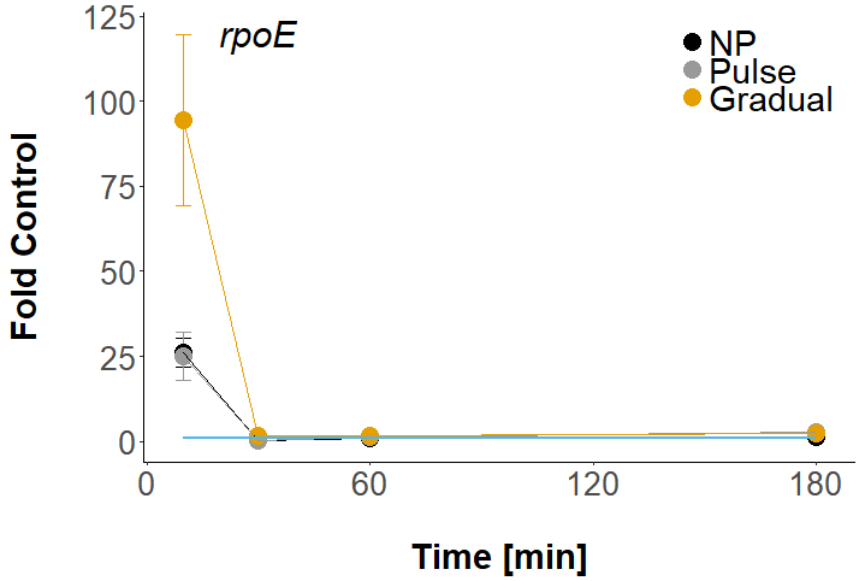

Figure B.8. ***Gene expression of*** **rpoE** ***in response to Cu exposure.*** *Statistically significant differences were observed at 30 min. The blue horizontal line is fixed at one to represent the expression of the undosed control. Error bars represent one SD of triplicate samples.*

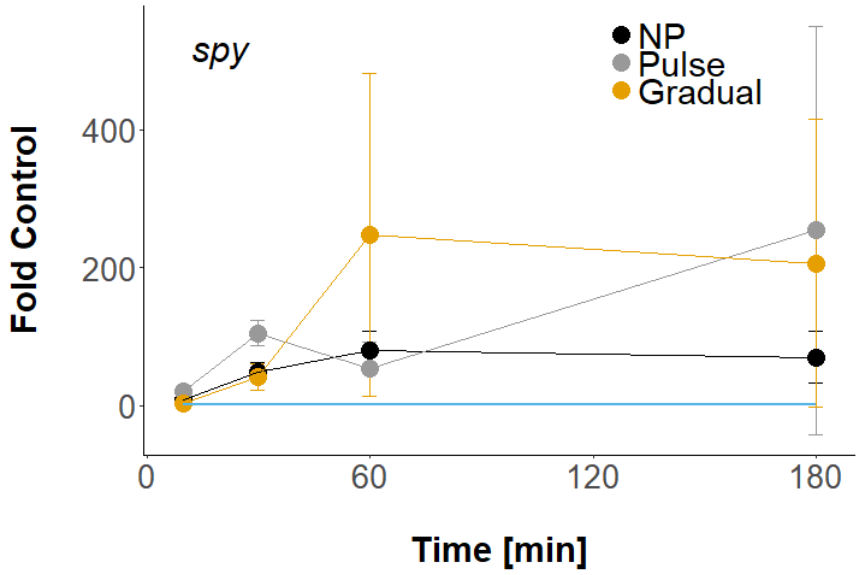

Figure B.9. ***Gene expression of*** **spy** ***in response to Cu exposure.*** *Statistically significant differences were observed at 30 min. The blue horizontal line is fixed at one to represent the expression of the undosed control. Error bars represent one SD of triplicate samples.*

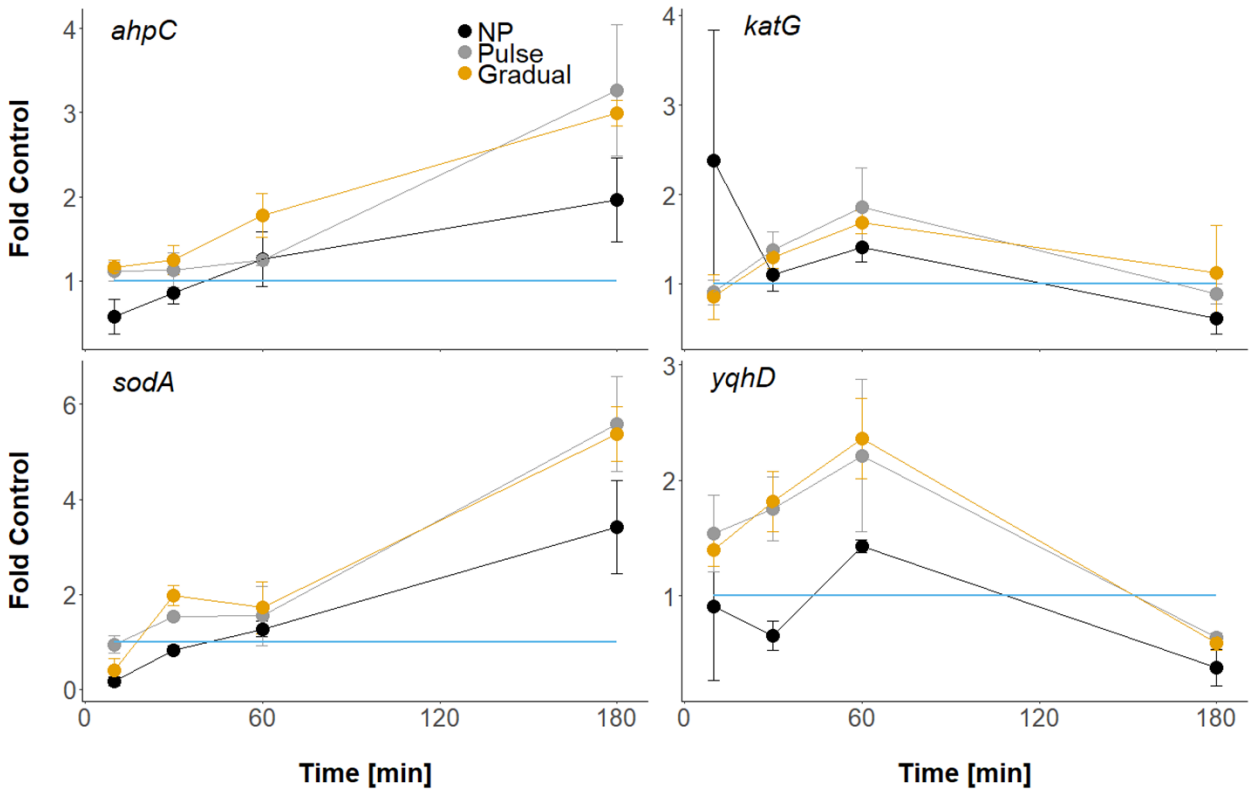

Figure B.10. ***Gene expression of four ROS-responsive genes in response to Cu exposure.*** *Details regarding each gene can be found in the main text. Statistically significant differences were observed for* ahpC *at 10 and 180 min; for* sodA *at 10, 30, and 180 min; and for* yqhD *at 30 and 60 min. The blue horizontal line is fixed at one to represent the expression of the undosed control. Error bars represent one SD of triplicate samples.*

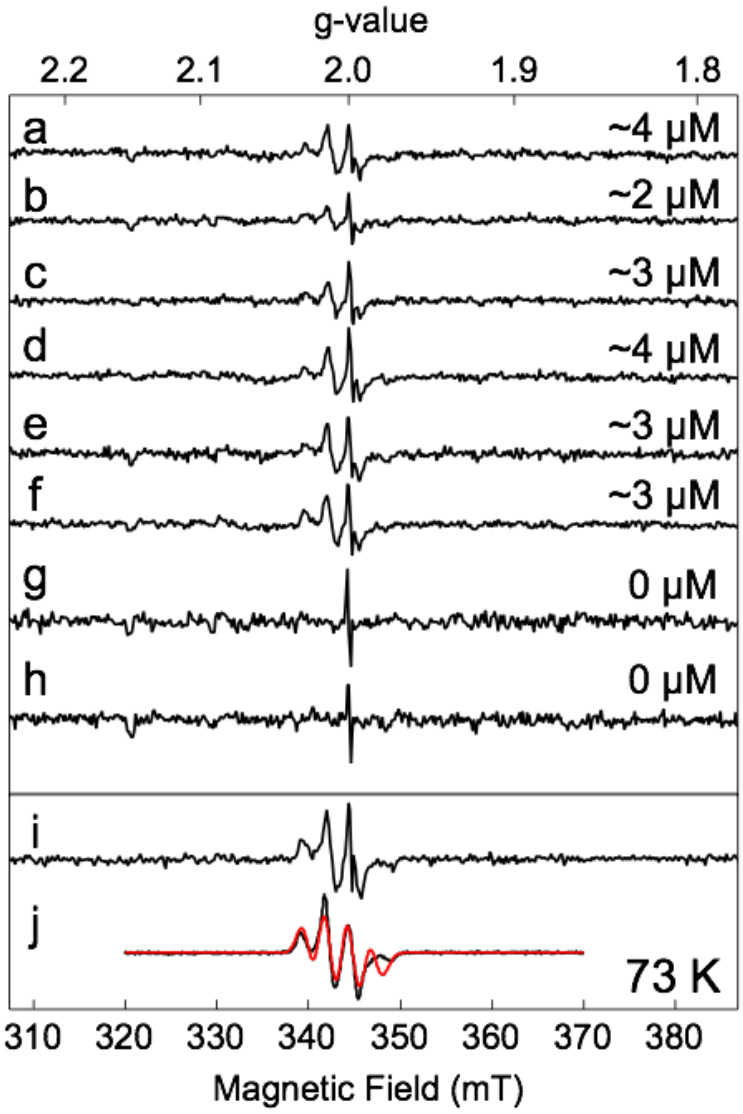

Figure B.11. ***X-band EPR spectra of various DMPO treated samples.*** *(a) Gradual Cu^{2+}-dosed bacteria grown to 180 min; (b) Gradual Cu^{2+}-dosed bacteria at 60 min; (c) pulse Cu^{2+}-dosed bacteria at 180 min; (d) CuO NP-dosed bacteria at 180 min; (e) Cu^{2+}-dosed MMDM; (f) CuO NP-dosed MMDM; (g) undosed bacteria at 180 min; (h) abiotic MMDM only; (i) positive control in MMDM; (j) positive control in H_2O (black) and the spectral simulation (red) using the following parameters: g = 2.005, $A(^{14}N)$ = 60 MHz, $A(^{1}H)$ = 65 MHz. The Mn^{2+} ion signal has been removed for each spectrum except for spectrum j, where no Mn^{2+} ion was present. The spin concentrations of the DMPO radical adduct in spectra (a) – (h) are indicated in the figure. Measurement conditions: microwave frequency, 9.64 GHz; microwave power, 20 uW; modulation amplitude, 0.3 mT; modulation frequency, 100 kHz; temperature, 73 K.*

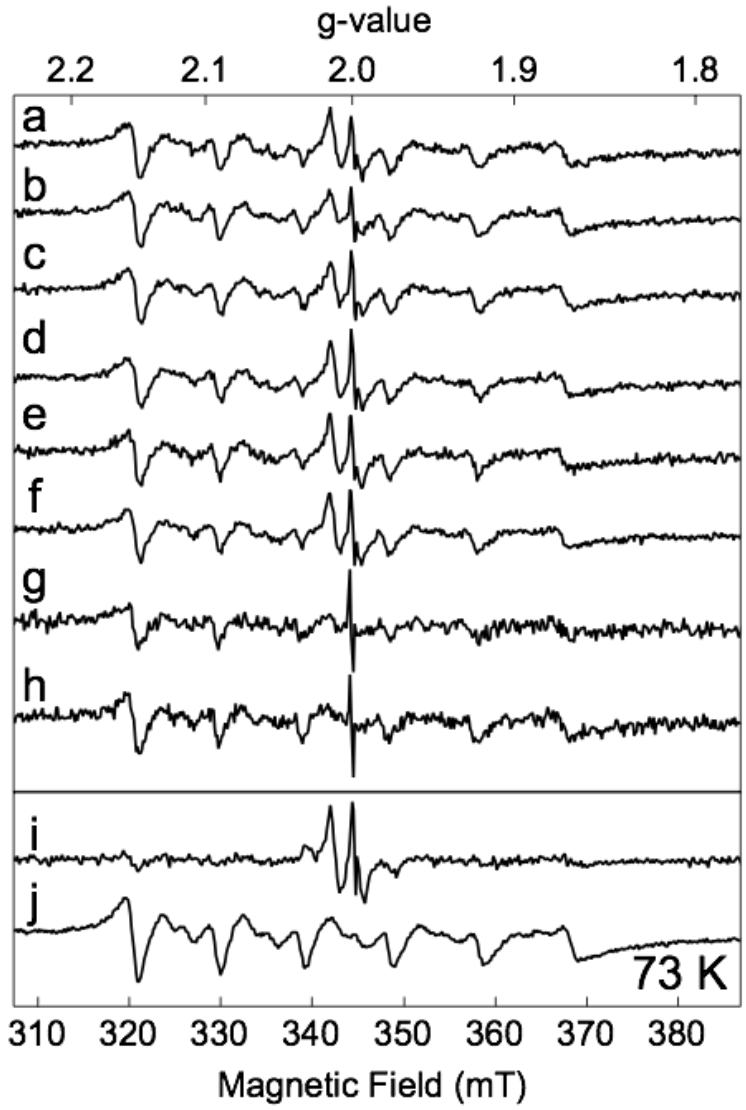

Figure B.12. ***Raw X-band EPR spectra of various DMPO treated samples without the removal of the Mn^{2+} ion EPR signal.*** *(a) Gradual Cu^{2+}-dosed bacteria at 180 min; (b) Gradual Cu^{2+}-dosed bacteria at 60 min; (c) pulse Cu^{2+}-dosed bacteria at 180 min; (d) CuO NP-dosed bacteria at 180 min; (e) Cu^{2+}-dosed MMDM; (f) CuO NP-dosed MMDM; (g) undosed bacteria at 180 min; (h) abiotic MMDM only; (i) positive control in MMDM; (j) the typical Mn^{2+} ion EPR spectrum measured in the MMDM only. Measurement conditions: microwave frequency, 9.64 GHz; microwave power, 20 uW (except for spectrum j, which was measured using 2 mW); modulation amplitude, 0.3 mT; modulation frequency, 100 kHz; temperature, 73 K.*

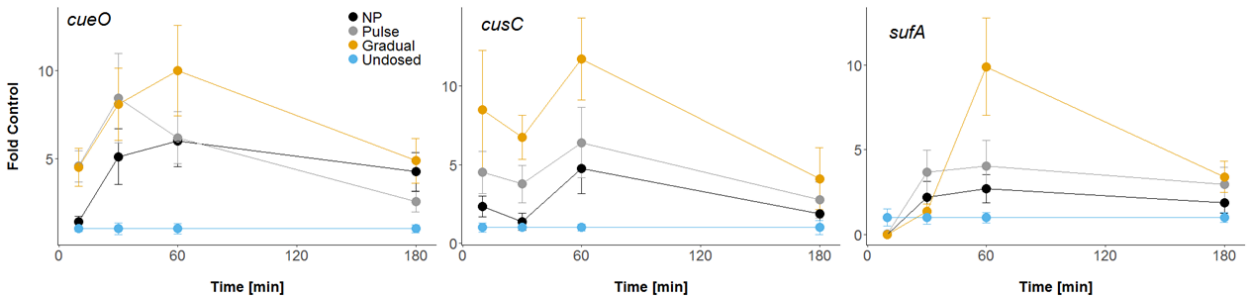

Figure B.13. ***Gene expression of Cu-responsive genes and* sufA *in response to Cu exposure.*** *Details regarding each gene can be found in the main text. Statistically significant differences were observed for* cueO *at 10 min, for* cusC *at all time points, and for* sufA *at 10 min.*

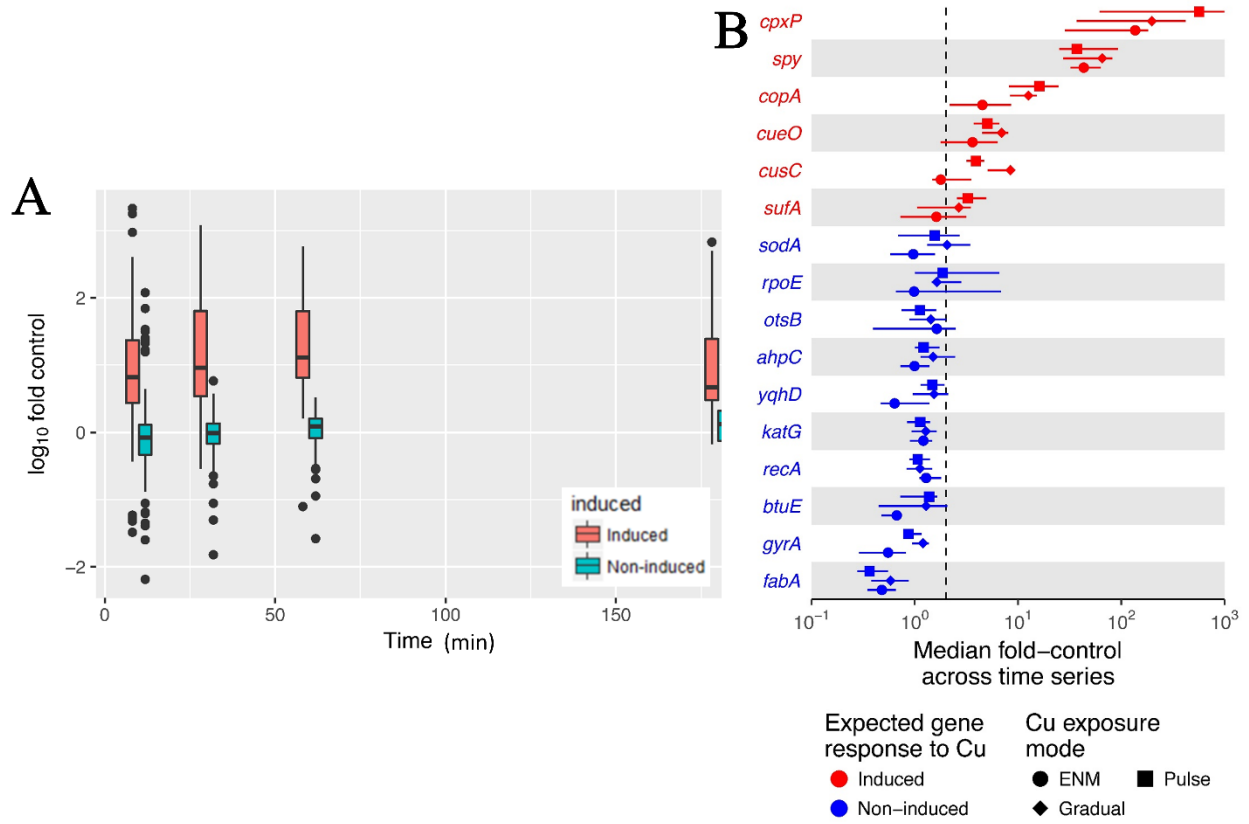

Figure B.14. ***Induction of induced versus non-induced genes.*** *Induced genes (*copA, cueO, cusC, sufA, cpxP, *and* spy*) demonstrate induction over the course of the experiment, but especially through 60 min, whereas non-induced genes do not (A). Median fold control over the whole time series distinguishes induced versus non-induced genes as well (B). The dashed line demarcates 2-fold control expression.*

B.3 References for Appendix B

1 C. Gunawan, W. Y. Teoh, C. P. Marquis and R. Amal, *ACS Nano*, 2011, 7214–7225.

2 C. Kaweeteerawat, C. H. Chang, K. R. Roy, R. Liu, R. Li, D. Toso, H. Fischer, A. Ivask, Z. Ji, J. I. Zink, Z. H. Zhou, G. F. Chanfreau, D. Telesca, Y. Cohen, P. A. Holden, A. E. Nel and H. A. Godwin, *ACS Nano*, 2015, **9**, 7215–7225.

3 Z. Xiu, Q. Zhang, H. Puppala, V. Colvin and P. Alvarez, *Nano Lett.*, 2012, 10–14.

4 G. Applerot, J. Lellouche, A. Lipovsky, Y. Nitzan, R. Lubart, A. Gedanken and E. Banin, *Small*, 2012, **8**, 3326–37.
5 D. T. Petasis and M. P. Hendrich, 2015, pp. 171–208.
6 G. R. Buettner, *Free Radic. Biol. Med.*, 1987, **3**, 259–303.

Supplemental statistical and computational methods

This section is meant to more thoroughly describe and divulge the computational methodologies utilized in the main text as well as provide additional insight into results where appropriate. Specifically, the text here will walk through the relevant steps in the analysis of gene expression data and oxidative-stress measured by fluorescence.

This section was written in R Markdown v1.5 using RStudio and contains all the relevant code necessary to reproduce the analysis presented in the manuscript.

Guide to computational methods

Analysis dependencies

The code makes extensive use of the packages `plyr`, `broom`,`magrittr`, `dplyr`, `tidyr`, and `ggplot2` (where the latter three packages are loaded as part of the `tidyverse` package) in addition to the functions present in the base `R` language. Therefore, these packages need to be installed by the `R` user in order to reproduce this analysis. Aside from plotting commands from `ggplot2` (which will be acknowledge with in-script comments: `# This is a comment`) and the pipe operator (`%>%`; loaded via the `dplyr` namespace, but part of the `magrittr` package), functions from external packages will be indicated by `package_name::function_name`. When these packages are attached *via* the `library()` function (as they are here), this syntax is technically redundant. However, this convention will still be used here to provide attribution to the appropriate source throughout.

```
## Uncomment these lines and execute in R if these packages are not already installed.
# install.packages('plyr')
# install.packages('broom')
# install.packages('tidyverse')
# install.packages('magrittr')

library(plyr)
library(broom)
library(tidyverse)
library(magrittr)
```

Analysis environment

The code given herein runs without errors under the following configuration; no assurances are made for backward or forward compatability of `R` versions or versions of the dependencies.

```
## R version 3.4.0 (2017-04-21)
## Platform: x86_64-apple-darwin15.6.0 (64-bit)
## Running under: OS X El Capitan 10.11.6
##
## Matrix products: default
## BLAS: /Library/Frameworks/R.framework/Versions/3.4/Resources/lib/libRblas.0.dylib
## LAPACK: /Library/Frameworks/R.framework/Versions/3.4/Resources/lib/libRlapack.dylib
##
## locale:
## [1] en_US.UTF-8/en_US.UTF-8/en_US.UTF-8/C/en_US.UTF-8/en_US.UTF-8
##
## attached base packages:
## [1] stats     graphics  grDevices utils     datasets  methods   base
```

```
##
## other attached packages:
##  [1] magrittr_1.5    dplyr_0.7.1     purrr_0.2.2.2   readr_1.1.1
##  [5] tidyr_0.6.3     tibble_1.3.3    ggplot2_2.2.1   tidyverse_1.1.1
##  [9] broom_0.4.2     plyr_1.8.4
##
## loaded via a namespace (and not attached):
##  [1] Rcpp_0.12.11     cellranger_1.1.0 compiler_3.4.0   bindr_0.1
##  [5] forcats_0.2.0    tools_3.4.0      digest_0.6.12    lubridate_1.6.0
##  [9] jsonlite_1.5     evaluate_0.10.1  nlme_3.1-131     gtable_0.2.0
## [13] lattice_0.20-35  pkgconfig_2.0.1  rlang_0.1.1      psych_1.7.5
## [17] yaml_2.1.14      parallel_3.4.0   haven_1.0.0      bindrcpp_0.2
## [21] xml2_1.1.1       httr_1.2.1       stringr_1.2.0    knitr_1.16
## [25] hms_0.3          rprojroot_1.2    grid_3.4.0       glue_1.1.1
## [29] R6_2.2.2         readxl_1.0.0     foreign_0.8-67   rmarkdown_1.6
## [33] modelr_0.1.0     reshape2_1.4.2   backports_1.1.0  scales_0.4.1
## [37] htmltools_0.3.6  rvest_0.3.2      assertthat_0.2.0 mnormt_1.5-5
## [41] colorspace_1.3-2 stringi_1.1.5    lazyeval_0.2.0   munsell_0.4.3
```

Gene expression data, quality control, and expression normalization

Gene expression data are stored in a CSV file accompanying this manuscript (first few rows shown below. The 16S rRNA gene, *rrsA*, was used as a housekeeping gene against which all other target genes were normalized. *rrsA* has been validated for this function before. The variables in this dataset are: `Treatment` (the mode of Cu exposure), `Time` (the duration of exposure in minutes), `Gene` (the target gene), and `Expression` (the expression of the target gene relative to *rrsA*). For `Treatment` the variable levels are: `Undosed` (the experimental control with no Cu exposure), `ENM` (the nano-Cu dosing), `Pulse` (immediate 100 mg/L dissolved Cu dosing), and `Gradual` (incremental dissolved Cu dosing to match observe ENM dissolution kinetics).

```
# add an identifier of the experimental replicates
gene_expression <- read.csv('gene-expression-time-series-UPDATED.csv') %>%
  dplyr::group_by(Treatment, Time, Gene) %>%
  dplyr::mutate(rep = 1:n()) %>%
  dplyr::ungroup()
dplyr::tbl_df(gene_expression)
```

```
## # A tibble: 799 x 5
##    Treatment  Time   Gene Expression   rep
##       <fctr> <int> <fctr>      <dbl> <int>
##  1       ENM    10   rrsA    4390000     1
##  2       ENM    10   rrsA    8000000     2
##  3       ENM    10   rrsA   12500000     3
##  4     Pulse    10   rrsA   16300000     1
##  5     Pulse    10   rrsA   17300000     2
##  6     Pulse    10   rrsA   16300000     3
##  7   Gradual    10   rrsA   14700000     1
##  8   Gradual    10   rrsA   14800000     2
##  9   Undosed    10   rrsA   14400000     1
## 10   Undosed    10   rrsA   17000000     2
## # ... with 789 more rows
```

As described in the main text, the relevant dependant variable in our analysis is the "fold-control" gene expression, that is the ratio of gene expression in a treatment sample relative to the expression of that gene in the control sample.

$$\text{Fold control}_{xy} = \frac{Expression_{x,y}/Expression_{rrsA,y}}{Expression_{x,Control}/Expression_{rrsA,Control}}$$

Because control samples were not explicitly paired to treatment samples, it is necessary to average $Expression_x$ across triplicates for normalization. However, inspection of the data showed some potential outlier data for one replicate at the $t = 10$ min. data point. An example of the undosed control data is shown below.

```
# Filter out undosed control samples to visualize gene expression
control <- dplyr::filter(gene_expression, Treatment == 'Undosed')

# These functions from ggplot2 package
control_plt <- ggplot(control, aes(x = Time,
                                   y = Expression,
                                   color = factor(rep))) +
  geom_point() +
  facet_wrap(~Gene, scales = 'free') +
  labs(title = 'Gene expression in undosed control samples')
print(control_plt)
```

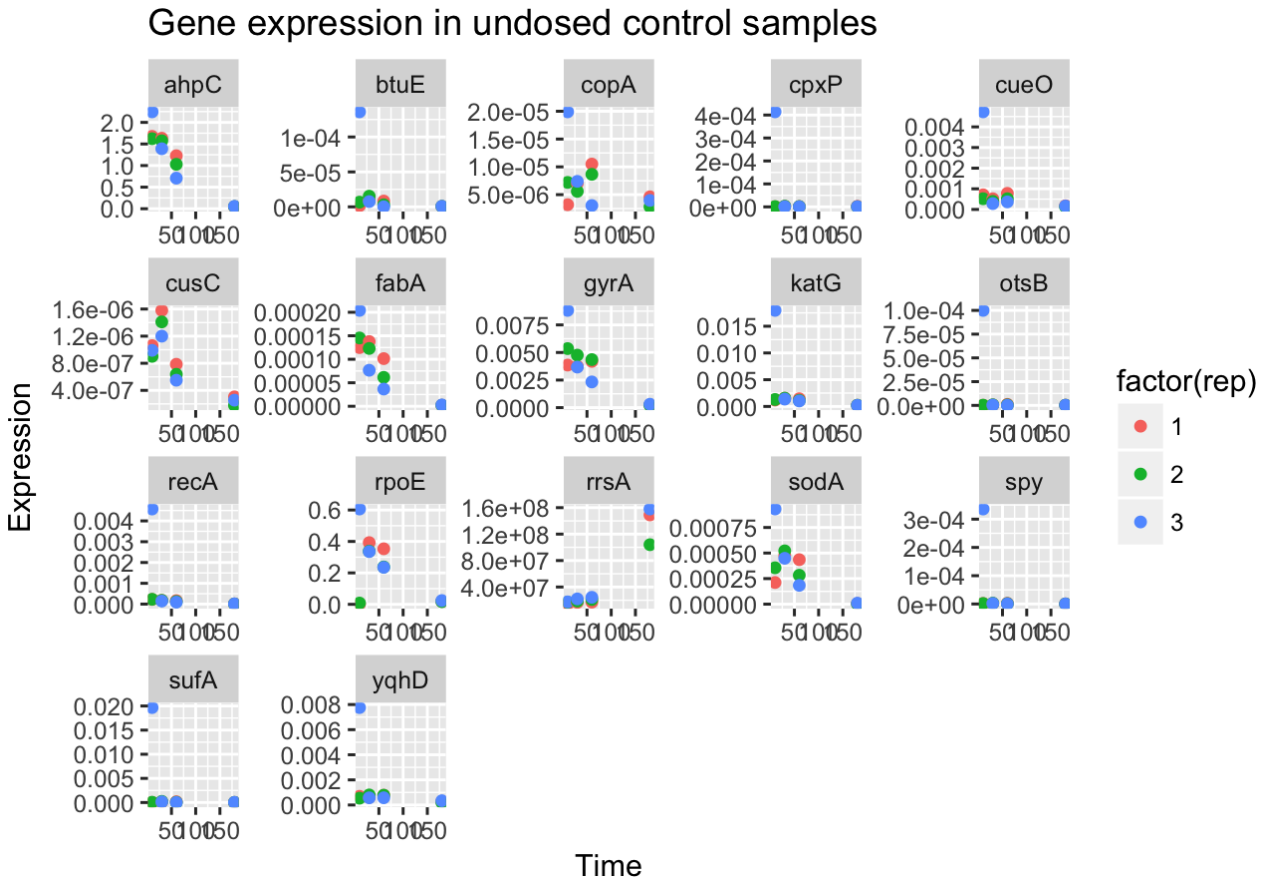

Closer examination of the dataset show that the third replicate at $t = 10$ minutes of the undosed sample produced the preponderance of extreme values in this dataset as measured by absolute deviation from the median of the replicates. As such, this data point was removed from the analysis discussed in the manuscript, however pieces of the analysis with and without that data point are included here.

$$\epsilon = \frac{|Expression_x - median(Expression_x)|}{median(Expression_x)}$$

```
# Add absolute deviation from the median for outlier identification
gene_expression %<>% dplyr::group_by(Treatment, Time, Gene) %>%
  dplyr::mutate(abs_dev = abs(Expression - median(Expression)) / median(Expression)) %>%
  dplyr::ungroup()

# arrange and display
gene_expression %>%
  dplyr::arrange(desc(abs_dev)) %>%
  dplyr::tbl_df()
```

```
## # A tibble: 799 x 6
##    Treatment  Time   Gene  Expression   rep   abs_dev
##       <fctr> <int> <fctr>       <dbl> <int>     <dbl>
##  1   Undosed    10   otsB 0.000100000     3 459.82949
##  2   Undosed    10   sufA 0.019673469     3 388.57364
##  3   Undosed    10   cpxP 0.000414000     3 344.00000
##  4   Undosed    10    spy 0.000336000     3 184.63536
##  5   Undosed    10   rpoE 0.606530612     3  73.74280
##  6       ENM    10   otsB 0.000002690     1  59.99773
##  7       ENM    10   sufA 0.000075000     1  44.18072
##  8       ENM    10   btuE 0.000006410     1  23.65385
##  9   Undosed    10   btuE 0.000136000     3  19.14815
## 10   Undosed    10   recA 0.004573526     3  18.79881
## # ... with 789 more rows
```

```
# Remove control replicate with anomalous data
gene_expression_clean <- gene_expression %>%
  filter(!(Treatment == 'Undosed' & rep == 3 & Time == 10))

control_plt_clean <- ggplot(filter(gene_expression_clean, Treatment == 'Undosed'),
                            aes(x = Time,
                                y = Expression,
                                color = factor(rep))) +
  geom_point() +
  facet_wrap(~Gene, scales = 'free') +
  labs(title = 'Gene expression in undosed control samples\nafter outlier removal')
print(control_plt_clean)
```

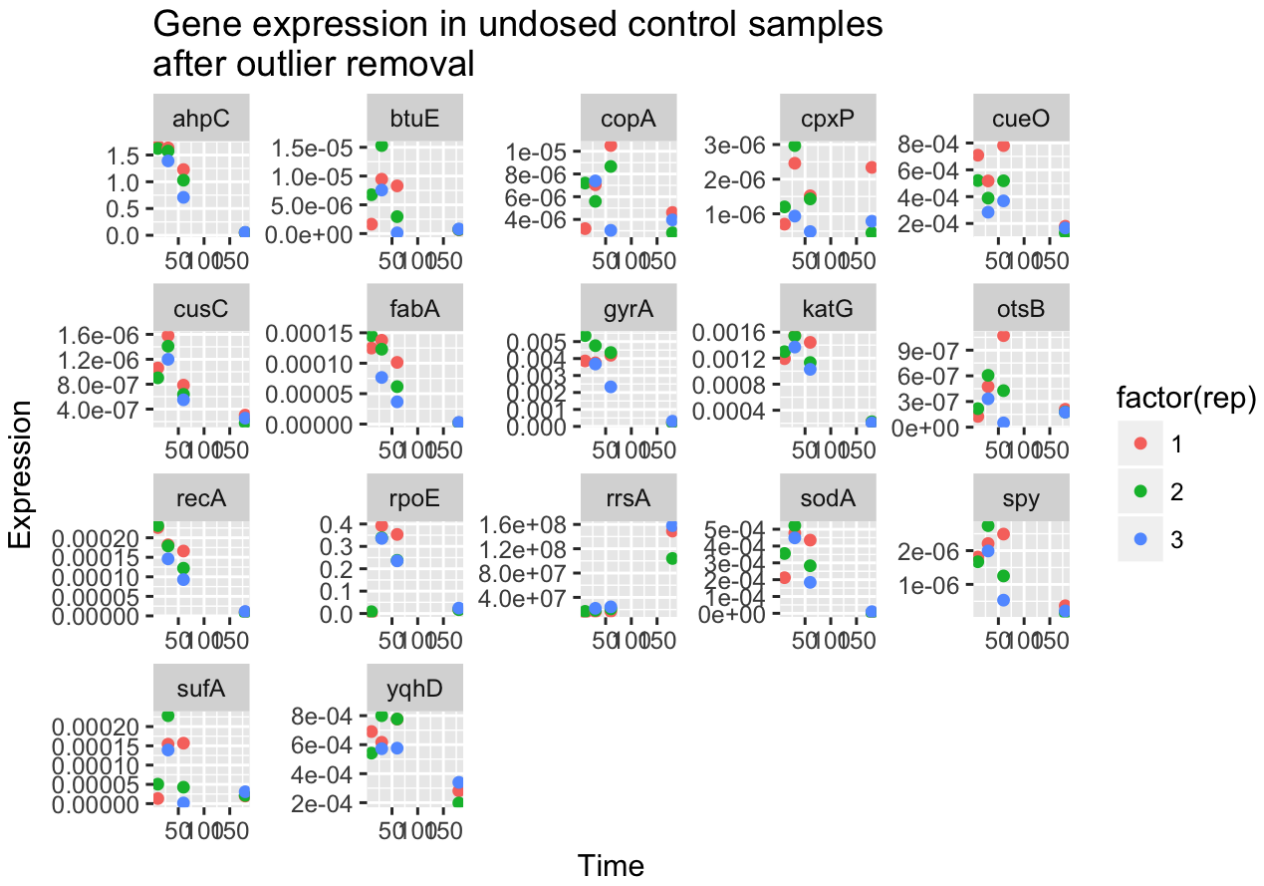

These control data were then averaged for each gene and time point for fold-control normalization of treatment data.

```
# Average over control replicates for determining fold control
control_av <- gene_expression_clean %>%
  dplyr::filter(Treatment == 'Undosed') %>%
  dplyr::group_by(Time, Gene) %>%
  dplyr::summarize(Expression = mean(Expression)) %>%
  dplyr::ungroup()

control_av_raw <- gene_expression_clean %>% # including anomalous data
  dplyr::filter(Treatment == 'Undosed') %>%
  dplyr::group_by(Time, Gene) %>%
  dplyr::summarize(Expression = mean(Expression)) %>%
  dplyr::ungroup()

# Add fold control calculation
treatment <- dplyr::filter(gene_expression_clean, Treatment != 'Undosed') %>%
  dplyr::left_join(control_av, by = c('Time','Gene'),
            suffix = c('.treat','.cont')) %>%
  dplyr::mutate(fold_control = Expression.treat/Expression.cont)

treatment_raw <- dplyr::filter(gene_expression, Treatment != 'Undosed') %>%
  dplyr::left_join(control_av, by = c('Time','Gene'),
            suffix = c('.treat','.cont')) %>%
  dplyr::mutate(fold_control = Expression.treat/Expression.cont)
```

Hypothesis testing of gene expression data

The first analysis we performed on the gene expression data sought to determine if ENM exposure was sublethal by examing fold changes in *rrsA* expression at each time point. This is can be done with a one-sided Mann-Whitney test:

$$H_0 : \mu_{ENM-Ctrl} = 0$$
$$H_1 : \mu_{ENM-Ctrl} < 0$$

```
# Establish sub-lethal Cu exposure using Mann-Whitney on raw
# expression of rrsA `alternative` set to "less" b.c. want one
# sided test if growth is significantly less in the treated
# samples
gene_expression_clean %>%
  dplyr::filter(Gene == 'rrsA') %>%
  dplyr::select(rep, Time, Treatment, Expression) %>%
  tidyr::spread(Treatment, Expression) %>%
  tidyr::gather(treatment, expression, ENM:Pulse) %>%
  dplyr::group_by(Time, treatment) %>%
  dplyr::do(
    broom::tidy(
      wilcox.test(x = .$expression, y = .$Undosed,
                  alternative = 'less', exact = T)
      )
    ) %>%
  dplyr::select(Time, treatment, p.value) %>%
  tidyr::spread(treatment, p.value)
```

```
## # A tibble: 4 x 4
## # Groups:   Time [4]
##    Time   ENM   Gradual     Pulse
## * <int> <dbl>     <dbl>     <dbl>
## 1    10  0.10 0.6666667 0.8128703
## 2    30  0.05 0.8000000 0.3500000
## 3    60  0.10 0.5000000 0.1000000
## 4   180  0.05 0.1000000 0.3500000
```

```
gene_expression %>% # including anomalous data
  dplyr::filter(Gene == 'rrsA') %>%
  dplyr::select(rep, Time, Treatment, Expression) %>%
  tidyr::spread(Treatment, Expression) %>%
  tidyr::gather(treatment, expression, ENM:Pulse) %>%
  dplyr::group_by(Time, treatment) %>%
  dplyr::do(
    broom::tidy(
      wilcox.test(x = .$expression, y = .$Undosed,
                  alternative = 'less', exact = T)
      )
    ) %>%
  dplyr::select(Time, treatment, p.value) %>%
  tidyr::spread(treatment, p.value)
```

```
## # A tibble: 4 x 4
```

```
## # Groups:   Time [4]
##    Time   ENM Gradual Pulse
## * <int> <dbl>   <dbl> <dbl>
## 1    10  0.05     0.4  0.50
## 2    30  0.05     0.8  0.35
## 3    60  0.10     0.5  0.10
## 4   180  0.05     0.1  0.35
```

```
ggplot(
  filter(gene_expression_clean, Gene == 'rrsA'),
  aes(x = Time, y = Expression, color = Treatment)
) +
  geom_point(position = position_dodge(5)) +
  labs(title = 'rrsA expression in treatment\nand control samples')
```

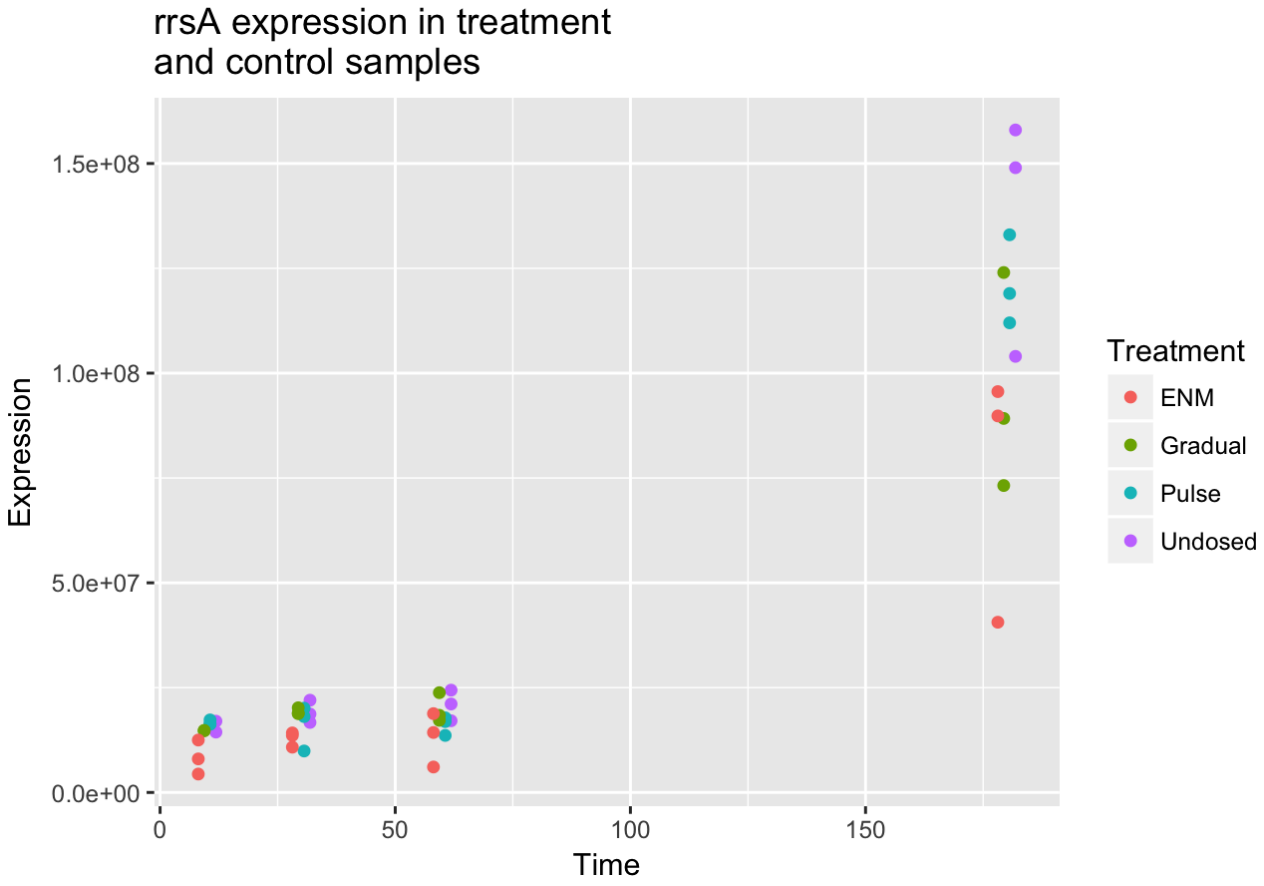

Next we sought to determine the genes identified in the literature as being Cu-induced exhibited differential expression between undosed and ENM dosed experiments. These genes were: *copA, cueO, cusC, cpxP, sufA,* and *spy.*

```
induced_genes <- c("copA", "cueO", "cusC","cpxP", "sufA", 'spy')

# Add identifier of Cu-induced genes
treatment %<>% dplyr::mutate(induced = ifelse(Gene %in% induced_genes,
                                              'Induced',
                                              'Non-induced'))

ggplot(filter(treatment, Treatment == 'ENM'),
```

```
      aes(x = Time, y = fold_control, color = induced)) +
  geom_hline(yintercept = 1, linetype = 2) +
  geom_point(alpha = 0.75) +
  facet_wrap(~Gene, scales = 'free')
```

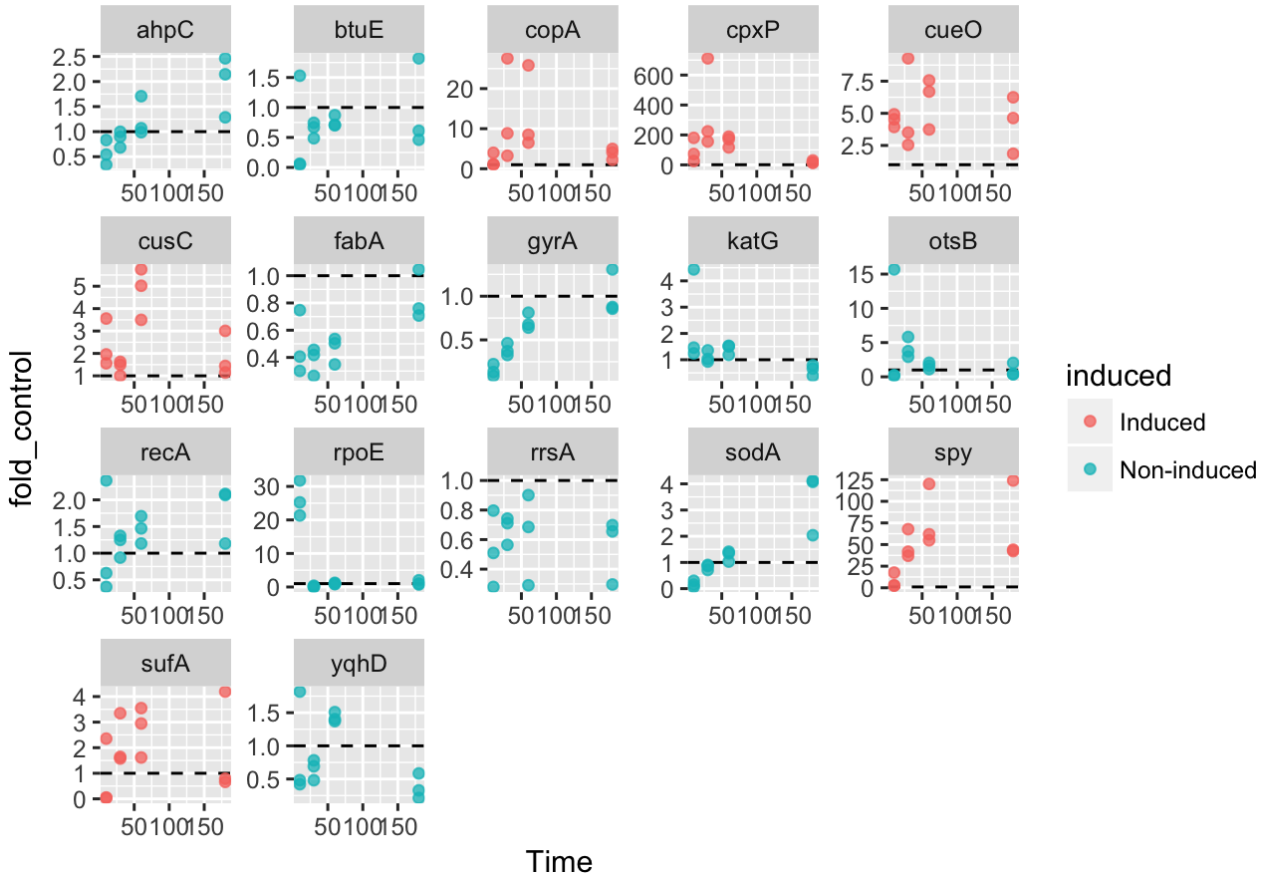


```
# `alternative` set to "greater" b.c. `Treatment` factor order is
# alphabetical (i.e. ENM is group 1, Undosed is group 2)
diff_expr <- gene_expression_clean %>%
  dplyr::filter(Gene != 'rrsA', Treatment %in% c('ENM','Undosed')) %>%
  dplyr::group_by(Gene, Time) %>%
  dplyr::do(
    broom::tidy(
      wilcox.test(.$Expression ~ .$Treatment, alternative = 'greater',
                  exact = T, conf.int = T)
    )
  ) %>%
  dplyr::mutate(p.value = round(p.value, 2)) %>%
  dplyr::select(Gene, Time, p.value)

diff_expr_raw <- gene_expression %>% # including anomalous data
  dplyr::filter(Gene != 'rrsA', Treatment %in% c('ENM','Undosed')) %>%
  dplyr::group_by(Gene, Time) %>%
  dplyr::do(
    broom::tidy(
      wilcox.test(.$Expression ~ .$Treatment, alternative = 'greater',
                  exact = T, conf.int = T)
```

```
    )
  ) %>%
  dplyr::mutate(p.value = round(p.value, 2)) %>%
  dplyr::select(Gene, Time, p.value)

# Combine statistical and practical data
comb_diff <- treatment %>%
  dplyr::filter(Treatment == 'ENM') %>%
  dplyr::group_by(Gene, Time) %>%
  dplyr::summarize(mu_fc = mean(fold_control)) %>%
  dplyr::ungroup() %>%
  dplyr::left_join(diff_expr, by = c('Gene','Time'))

comb_diff_raw <- treatment_raw %>% # including anomalous data
  dplyr::filter(Treatment == 'ENM') %>%
  dplyr::group_by(Gene, Time) %>%
  dplyr::summarize(mu_fc = mean(fold_control)) %>%
  dplyr::ungroup() %>%
  dplyr::left_join(diff_expr_raw, by = c('Gene','Time'))

# retain data meeting statistical and practical criterion
sig_diff <- comb_diff %>%
  dplyr::filter(p.value < 0.1, mu_fc > 2)

sig_diff_raw <- comb_diff_raw %>%
  dplyr::filter(p.value < 0.1, mu_fc > 2)

dplyr::tbl_df(sig_diff)
```

```
## # A tibble: 16 x 4
##      Gene  Time      mu_fc p.value
##    <fctr> <int>      <dbl>   <dbl>
##  1   copA    30  13.215177    0.05
##  2   copA    60  13.599099    0.05
##  3   copA   180   3.750658    0.05
##  4   cpxP    30 363.934004    0.05
##  5   cpxP    60 158.918243    0.05
##  6   cpxP   180  19.625384    0.05
##  7   cueO    30   5.109244    0.05
##  8   cueO    60   5.995792    0.05
##  9   cueO   180   4.245148    0.05
## 10   cusC    60   4.756592    0.05
## 11   otsB    30   4.168436    0.05
## 12   sodA   180   3.413932    0.05
## 13    spy    30  48.858934    0.05
## 14    spy    60  78.971683    0.05
## 15    spy   180  70.204082    0.05
## 16   sufA    30   2.188542    0.05
```

```
dplyr::tbl_df(sig_diff_raw)
```

```
## # A tibble: 17 x 4
##      Gene  Time      mu_fc p.value
##    <fctr> <int>      <dbl>   <dbl>
```

```
##  1   copA    30  13.215177    0.05
##  2   copA    60  13.599099    0.05
##  3   copA   180   3.750658    0.05
##  4   cpxP    30 363.934004    0.05
##  5   cpxP    60 158.918243    0.05
##  6   cpxP   180  19.625384    0.05
##  7   cueO    30   5.109244    0.05
##  8   cueO    60   5.995792    0.05
##  9   cueO   180   4.245148    0.05
## 10   cusC    10   2.358138    0.05
## 11   cusC    60   4.756592    0.05
## 12   otsB    30   4.168436    0.05
## 13   sodA   180   3.413932    0.05
## 14    spy    30  48.858934    0.05
## 15    spy    60  78.971683    0.05
## 16    spy   180  70.204082    0.05
## 17   sufA    30   2.188542    0.05
```

The genes which were found to be expressed significantly differently in the ENM-treated experiments compared to the undosed control ($p < 0.1$, Fold control$_{x,y} > 2$) were overwhelmingly in our expected list of Cu-induced genes (88% across all time points). Exclusion of the anomalous control replicate leads to no striking changes in the results of these analyses, only changing the statistical conclusion regarding *cusC* expression at $t = 10$ min.

Next, we investigated differences in gene-expression among modes of Cu exposure. This was done first through a Mann-Whitney test (two sided Wilcoxon test), between the pulse- and ENM Cu exposure modes.

```
# Mann-Whitney test for differences between ENM and Pulse Cu
# exposure modes on gene expression at each time point
treatment %>%
  filter(Treatment != 'Gradual') %>%
  group_by(Time, Gene) %>%
  do(
    tidy(
      wilcox.test(.$Expression.treat ~ .$Treatment, exact = T)
      )
    ) %>%
  ggplot(.,aes(x = Time, y = p.value)) +
    geom_hline(yintercept = 0.1) +
    geom_point() +
    facet_wrap(~Gene) +
    labs(title = 'P-value of Mann-Whitney\ntest between ENM and Pulse dosing schemes')
```

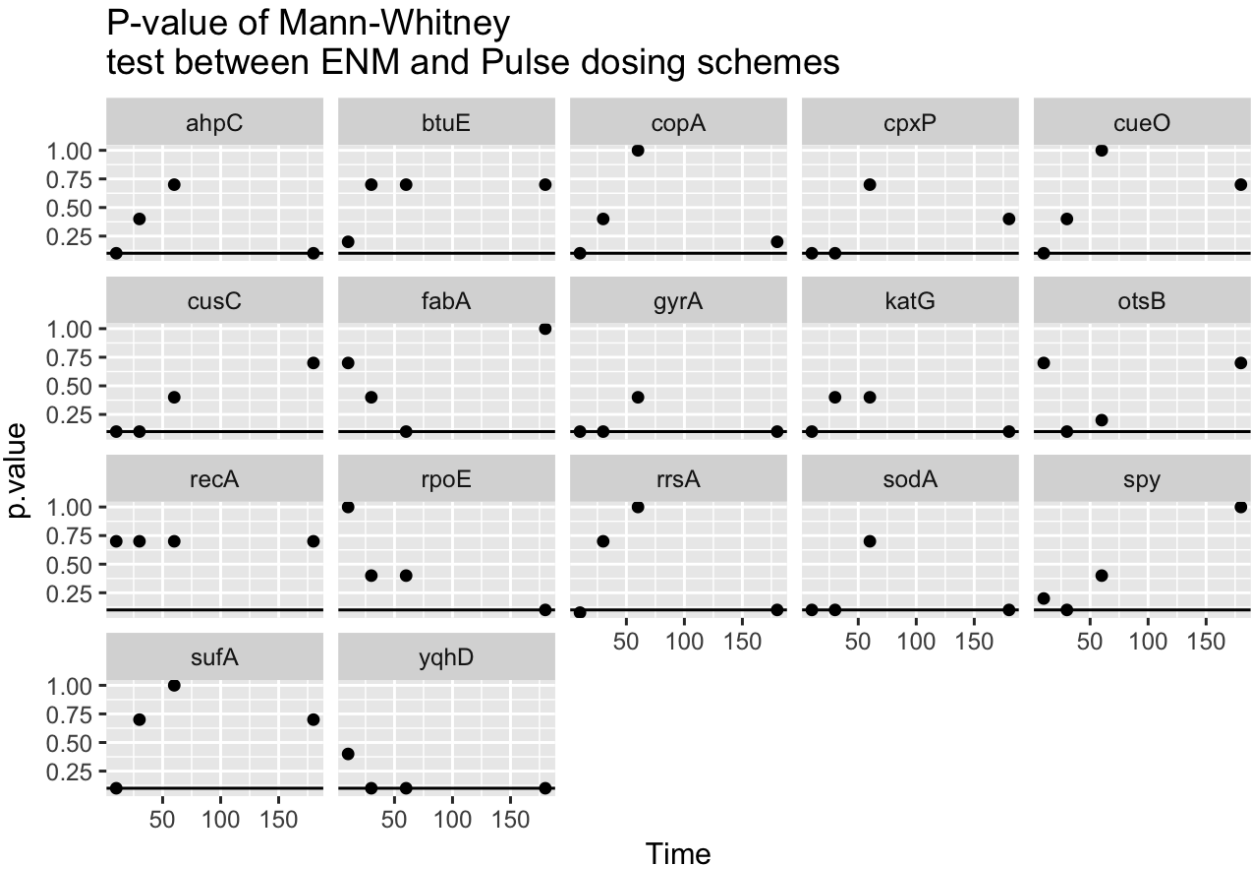

Next, a Kruskal-Wallis test, the non-parametric analog to one-way ANOVA, was used to test for differences among all three exposure modes. Results are visualized as fold control vs. time for the three Cu exposure modes, with markers dimmed for comparisons not meeting our statistical significance criteria, $\alpha \leq 0.1$.

```
# Kruskal-Wallis test for differences among Cu exposure modes
# on gene expression at each time point
kw_Cu_mode <- gene_expression_clean %>%
  dplyr::filter(Treatment != 'Undosed', Gene != 'rrsA') %>%
  dplyr::group_by(Time, Gene) %>%
  dplyr::do(
    broom::tidy(
      kruskal.test(.$Expression ~ .$Treatment)
    )
  ) %>%
  dplyr::select(Gene, Time, p.value) %>%
  mutate(sig = p.value <= 0.1)

treatment %<>% dplyr::filter(Gene != 'rrsA') %>%
  dplyr::left_join(kw_Cu_mode, by = c('Gene','Time'))

ggplot(treatment, aes(x = Time, y = fold_control,
                      color = Treatment,
                      shape = Treatment, alpha = sig)) +
  geom_point(size = 2, position = position_dodge(5)) +
  facet_wrap(~Gene, scales = 'free') +
  scale_alpha_manual(values = c(0.2,0.7)) +
  guides(alpha = F) +
```

```
  labs(title = paste0('Gene expression vs. time for Cu exposure ',
                      'modes\nwith indication of Kruskal-Wallis ',
                      'statistical significance'))
```

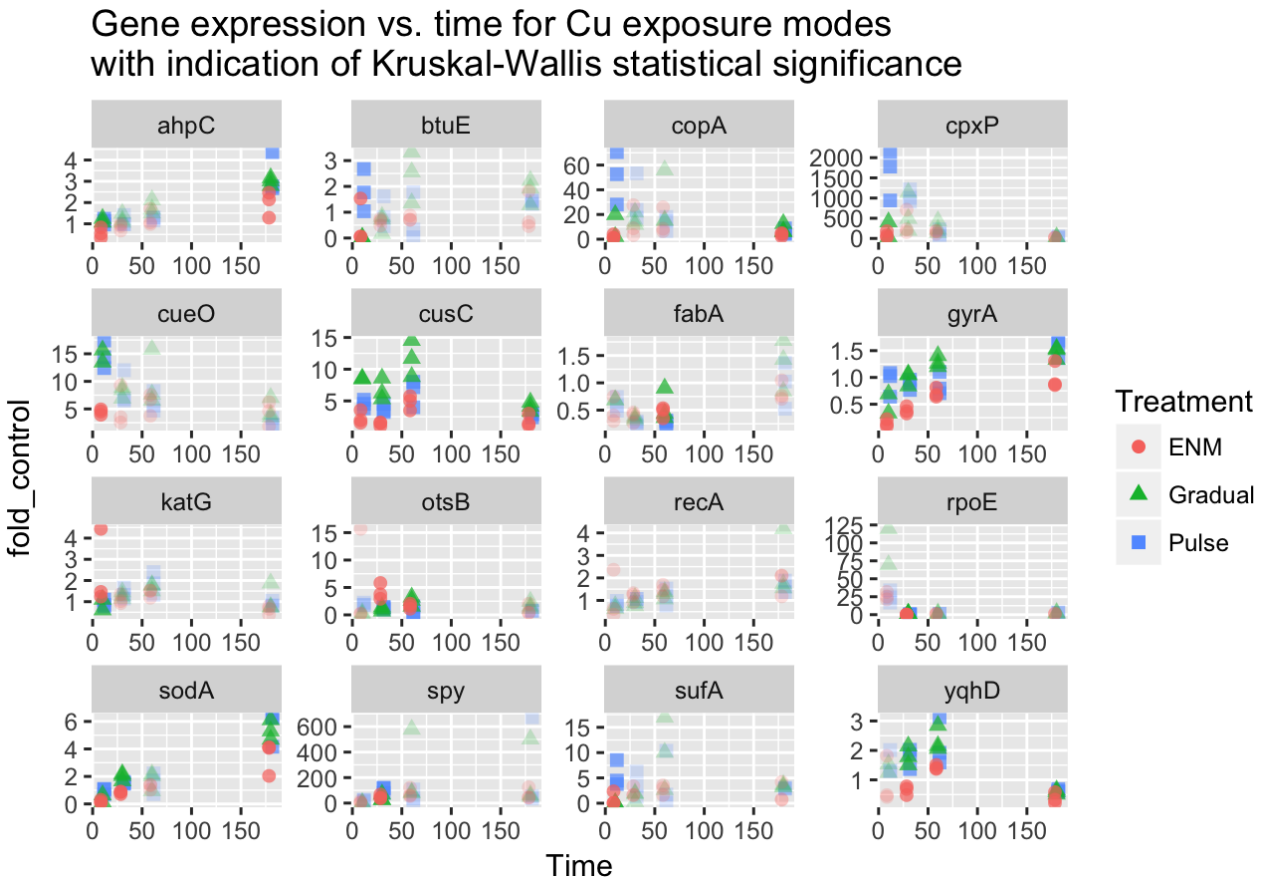

We further sought to explore differences among treatments on the temporal variation of gene expression in those genes that are specifically induced by Cu exposure. This is done by aggregating the fold-control data for all 6 induced genes for each treatment at each time point.

```
induced_data <- treatment %>%
  dplyr::filter(Gene %in% induced_genes)

ggplot(induced_data, aes(x = Time, y = fold_control,
                         group = interaction(Time, Treatment),
                         fill = Treatment)) +
  geom_boxplot() + scale_y_log10()
```

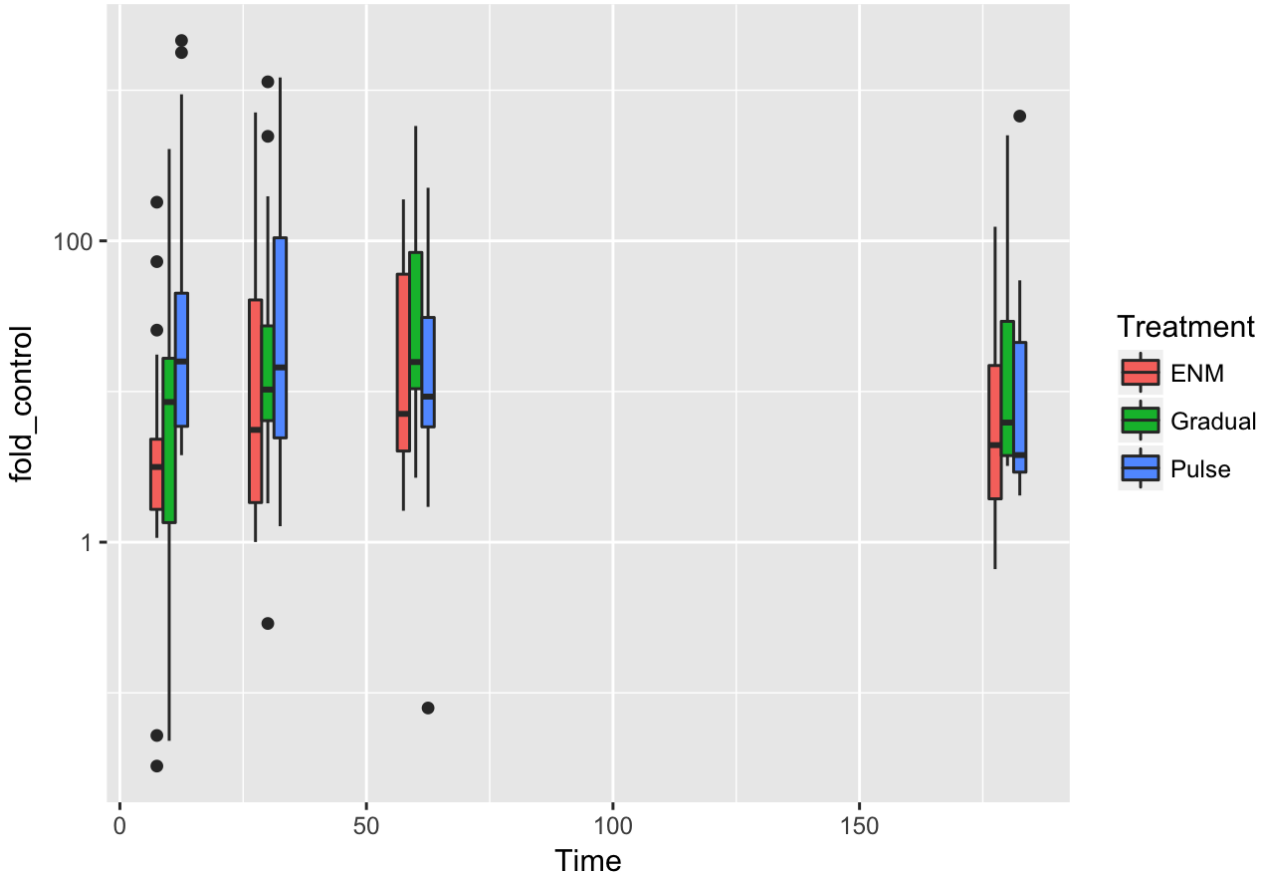


```
## Test across all treatments
induced_data %>%
  dplyr::group_by(Time) %>%
  dplyr::do(
    broom::tidy(
      kruskal.test(.$fold_control ~ .$Treatment)
    )
  ) %>%
  dplyr::select(Time, p.value)
```

```
## # A tibble: 4 x 2
## # Groups:   Time [4]
##    Time     p.value
##   <int>       <dbl>
## 1    10 0.008185893
## 2    30 0.419690420
## 3    60 0.137231904
## 4   180 0.269809611
```

```
## Test treatments pairwise against ENM dosing
dplyr::data_frame(vs_ENM = c('Gradual','Pulse')) %>%
  plyr::ddply(.(vs_ENM), function(df){
    induced_data %>%
      dplyr::filter(Treatment == 'ENM' | Treatment == df$vs_ENM) %>%
      group_by(Time) %>%
      dplyr::do(
        broom::tidy(
```

```
          wilcox.test(.$fold_control ~ .$Treatment, conf.int = T)
        )
      ) %>% ungroup() %>%
      dplyr::select(Time, p.value)
  }) %>%
  dplyr::group_by(Time) %>%
  dplyr::mutate(p.value = p.adjust(p.value)) %>%
  dplyr::tbl_df()
```

```
## # A tibble: 8 x 3
##    vs_ENM  Time    p.value
##     <chr> <int>      <dbl>
## 1 Gradual    10 0.43949181
## 2 Gradual    30 0.46187084
## 3 Gradual    60 0.15796743
## 4 Gradual   180 0.40543981
## 5   Pulse    10 0.00254904
## 6   Pulse    30 0.34157620
## 7   Pulse    60 0.81471992
## 8   Pulse   180 0.56277743
```

There is a strong difference among treatments at the 10 minute time point (deduced from Kruskal-Wallis), attributable to the large difference between the ENM and Pulse expressions at this time point (deduced from the post-hoc, Mann-Whitney test).

Further, it was our hypothesis that, temporally, the expression of genes in response to gradual ionic Cu exposure would be more similar to the expressive response to ENM exposure than in a pulse-dosing scenario. This comparison is made using time as a continuous variable, as opposed to a series of discrete tests as before. To test this hypothesis we choose to compare the similarity (overlap) of parameter estimates of a common model form for each treatment. However, since no biologically-relvant, parametric model is available for these data we chose to fit a linear model to the fold control data with time. In order to better meet the assumptions of a linear model (specifically observation independence, uncorrelated residuals), the fold-control data are first transformed to the "lag" (or difference vs. previous time), δ_ϕ.

$$\phi = \text{Fold control}_{xy}$$
$$\delta_\phi = \phi_i - \phi_{i-1}$$

These data are repeatedly bootstrapped to generate empirical distributions of the slope and intercept of a two parameter linear model:

$$\widehat{\delta_\phi} = \beta_1 \cdot t + \beta_0$$

We can then qualitatively assess the similarities among the treatments according to this model by comparing the extent of overlap between pairs of bootstrap parameter densities.[1]

```
## Transform fold-control data to lag
treat_lag <- treatment %>%
  dplyr::filter(induced == 'Induced') %>%
  dplyr::group_by(Treatment, Gene, rep) %>%
  dplyr::mutate(lag = c(NA, diff(fold_control))) %>%
```

[1]Inman, H. F., & Bradley Jr, E. L. (1989). The overlapping coefficient as a measure of agreement between probability distributions and point estimation of the overlap of two normal densities. *Communications in Statistics-Theory and Methods*, 18(10), 3851-3874.

```
    # NA values entered for t0 (lag not calculable), required to
    # maintain data vector dimensions.
  dplyr::select(Treatment:Gene, rep, fold_control, lag) %>%
  dplyr::ungroup() %>%
  dplyr::filter(!is.na(lag)) # Remove NA values

## Get point estimate of model parameters
point_est <- treat_lag %>%
  dplyr::group_by(Treatment) %>%
  dplyr::do(
    broom::tidy(
      lm(lag ~ Time, data = .)
    )
  ) %>%
  select(Treatment:estimate) %>% ungroup()


## Perform 1000 bootstrap estimates
## (NB: If rerunning this analysis, this may take some time)
boot_estimates <- data.frame(i = 1:1000) %>%
  plyr::ddply(.,.(i), function(df){
    # Create a bootstrap instance of the data by resampling
    # completely with replacement
    resamp <- treat_lag %>%
      dplyr::group_by(Treatment, Time) %>%
      dplyr::slice(sample(1:n(), replace = T))

    # Fit linear model and extract parameters
    resamp_lm <- resamp %>%
      dplyr::group_by(Treatment) %>%
      dplyr::do(
        broom::tidy(
          lm(lag ~ Time, data = .)
        )
      ) %>%
      dplyr::select(Treatment:estimate)

    return(resamp_lm)
  }) %>%
  dplyr::mutate(term = factor(term,
                       labels = c(bquote(beta[0]~" (Intercept)"),
                                  bquote(beta[1]~" (Slope)"))
                       ))

ggplot(boot_estimates,
       aes(x = estimate, fill = Treatment)) +
  stat_density(position = 'identity',alpha = 0.33, color = 'black') +
  facet_wrap(~term, scales = 'free', labeller = label_parsed) +
  scale_x_continuous('Parameter estimate') +
  scale_y_continuous('Kernel density') +
  guides(fill = guide_legend(override.aes = list(alpha = 1)))
```

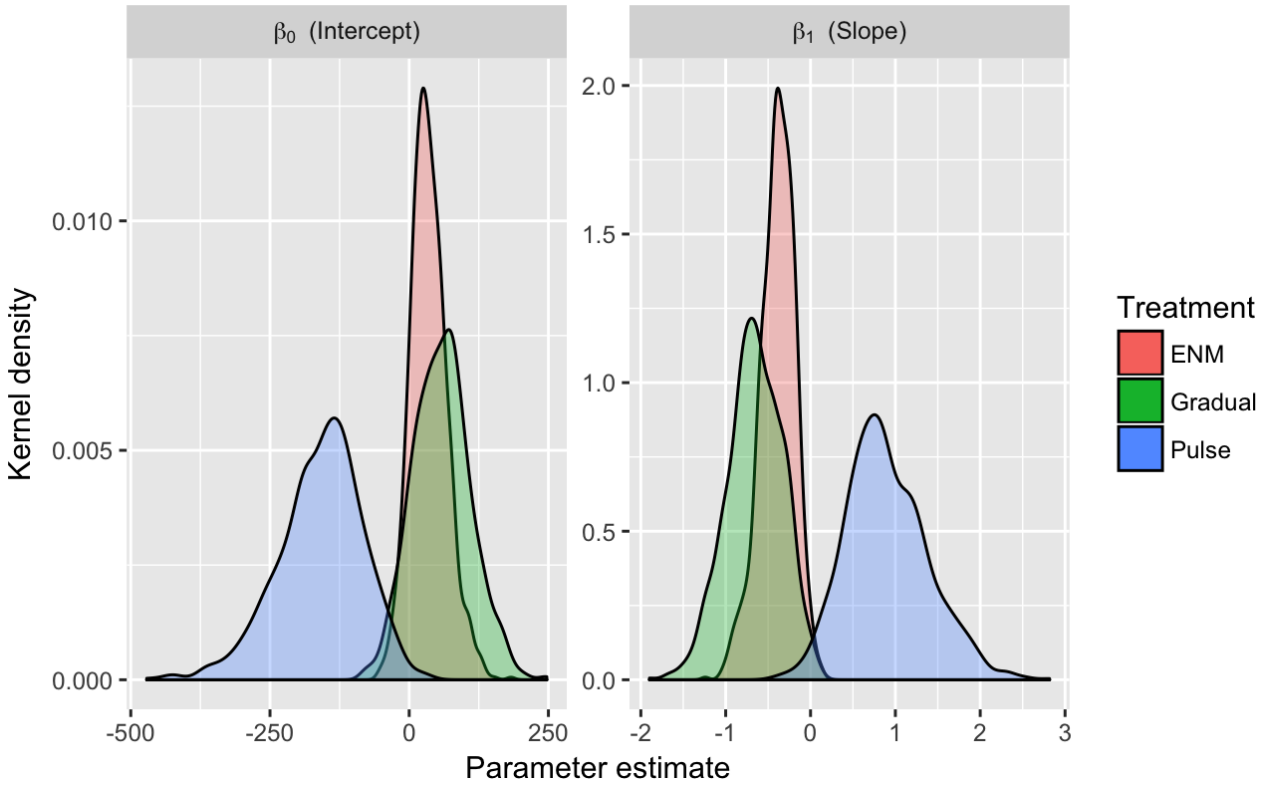

The higher degree of overlap between estimates of both parameters for ENM and Gradual (vs. Pulse), supports the stated hypothesis that the temporal response of gene expression in response to ionic copper exposure better represents that of ENM exposure than does a pulse exposure. However, our data show also that this means a mild practical difference at later time points, with early responses driving much of the overall difference.